# *Staphylococcus aureus*: the paths and crosstalks that lead to heme

Marco André Moras Videira

Dissertation presented to obtain the Ph.D degree in Biochemistry

Instituto de Tecnologia Química e Biológica António Xavier| Universidade Nova de Lisboa

Supervisor: Dr. Lígia M. Saraiva

Co-supervisor: Dr. Susana A. L. Lobo

**Oeiras, May 2018**

From left to right: Maria Arménia carrondo, Susana Lobo, Lígia Saraiva, Carlos Salgueiro, Marco Videira, Maria Salomé Gomes, Mariana Pinho, Arsénio Fialho.

14th of May 2018

Third Edition, May 2018

Molecular Mechanisms of Pathogen Resistance Laboratory

Instituto de Tecnologia Química e Biológica

Universidade Nova de Lisboa

2780-157 Portugal

# Acknowledgments

I would like to express my gratitude to the people that contributed to this work and made this thesis possible:

To my supervisor, Dr. Lígia Saraiva, for inviting me to apply for a PhD student grant and accepting me as member of her group. For her mentoring, constant support, motivation, advices and ideas. For her availability and for pointing the way when it was necessary. Thank you for the suggestions, critics and careful revision of this thesis. I also want to thank you for your friendship and making me a better person. Thank you very much.

To my co-supervisor, Susana Lobo, for her friendship, guidance and helpful brainstorms. For teaching me since the first day I arrived at the lab. And not less important for the many rides home when I was not coming to the lab by car! Thank you.

To my PhD Thesis Committee, Prof. Miguel Teixeira and Dr. Ana Melo, for accepting being part of the committee. For the availability for the meetings and for the discussions. A special thanks to Ana Melo for receiving me in her lab in my degree in biochemistry, showing me how to take my first steps in scientific research and for introducing me to Dr. Lígia Saraiva.

I want to thank Fábio Fernandes and Ana countinho, from Instituto Superior Técnico, for their collaboration in FLIM-FRET and fluorescent anisotropy experiments.

To Martin Warren and Dave Palmer for the collaboration in HPLC-MS experiments, for suggestions and experimental ideas and for the revision of the manuscripts.

To João Carita and Isabel Pacheco for their technical support.

I want to thank all the present and former members of our lab, Molecular Mechanisms of Pathogen Resistance, specially Lígia Nobre, Margarida Parente, João Monteiro, Liliana Silva, Sandra Carvalho, Joana Marques, Cátia Família and Patrícia Ferreira for your friendship, helpful discussions, for the laughs and for keeping the good environment in the lab throughout these years.

I also want to thank to ITQB for the facilities and for making fell a home.

To Fundação para a Ciência e Tecnologia (FCT) for the financial support and for awarding me a PhD grant (SFRH/BD/95912/2013).

À minha família pelo carinho e apoio constante ao longo destes anos. Principalmente aos meus pais porque me possibilitaram o meu desenvolvimento científico e pessoal.

Quero agradecer à Camila, minha mulher, pela ajuda preciosa que me deu! Pelo apoio e carinho constante mesmo nos momentos mais difíceis. Pelas discussões e paciência ao longo destes anos. Obrigado por me fazeres feliz!

*This thesis is dedicated to my parents and my wife*

# Thesis Publications

This dissertation is based on the following original publications, listed by chronological order:

Lobo SAL, Scott A, **Videira MAM**, Winpenny D, Gardner M, Palmer MJ, Schroeder S, Lawrence AD, Parkinson T, Warren MJ, Saraiva LM (2015) *Staphylococcus aureus* haem biosynthesis: characterisation of the enzymes involved in final steps of the pathway. *Mol Microbiol* 97(3):472–487.

**Videira MAM**, Lobo SAL, Silva LSO, Palmer DJ, Warren MJ, Prieto M, Coutinho A, Sousa FL, Fernandes F, and Saraiva LM (2018) *Staphylococcus aureus* haem biosynthesis and acquisition pathways are linked through haem monooxygenase IsdG. Submitted

**Manuscript in preparation, based on results presented in Chapter 6:**

**Videira MAM**, Família C, Lobo SAL and Saraiva LM (2018) Characterization of siroheme synthesis in *Staphylococcus aureus*.

**Publications not included in this thesis:**

Lobo SAL, **Videira, MAM**, Pacheco, I, Wass MN., Warren, MJ., Teixeira M, Matias PM & Saraiva, LM. (2017). *Desulfovibrio vulgaris* CbiKP cobaltochelatase: evolution of a haem binding protein orchestrated by the incorporation of two histidine residues. *Environ microbiol*, *19* (1), 106-118.

# Abstract

Tetrapyrroles are biological molecules widespread through all living organisms and necessary for fundamental cellular processes. Within the wide range of known tetrapyrroles, heme and siroheme are prosthetic groups in proteins responsible for important functions such as gas transport and storage, electron transport, cellular signaling, cellular detoxification as well as for reduction of sulfite and nitrite. Both molecules are synthesized from a last common tetrapyrrole precursor, namely uroporphyrinogen III, forming heme via four enzymatic steps know as the classical heme biosynthesis pathway and generating siroheme via an independent route. In some organisms such as sulfate and nitrate reducing bacteria, heme is alternatively synthesized through the siroheme-dependent pathway.

*S. aureus* is one of the leading causes of nosocomial infections and nowadays a major public health concern due to the increase in antibiotic resistant strains. During host invasion, *S. aureus* is exposed to different oxygen concentrations depending on the site of infection. When oxygen is available, *S. aureus* uses heme-dependent terminal oxidases for aerobic respiration. However, some locals of infection are oxygen-limited and in this case *S. aureus* has to use other substrates such as nitrate or nitrite as terminal electron acceptors of an anaerobic respiration chain, in which siroheme-containing enzymes are active. Also during infection, *S. aureus* uses the heme uptake system to scavenge heme from host hemoglobin and utilize it as iron source. In *S. aureus*, although the heme uptake system have been intensively studied, the knowledge on the biosynthesis of heme and siroheme remains incomplete. To better understand the metabolism that guarantees *S. aureus* survival during the infectious processes, this thesis elucidates the way *S. aureus* synthesizes these two tetrapyrroles. Herein, we

provide new insights into the heme metabolism of *S. aureus* through the comprehensive study of three topics: (i) the characterization of the heme biosynthesis pathway of *S. aureus* and its possible utilization as an antimicrobial target; (ii) clarification on how *S. aureus* is able to fine-tune the heme that is either synthesized *de novo* or acquired from the host; and (iii) characterization of the siroheme biosynthesis pathway of *S. aureus*.

The analysis of *S. aureus* genome revealed the presence of genes encoding putative enzymes involved in the late steps of heme biosynthesis pathway, namely HemE, HemN, HemY and HemH. The role of these enzymes in the heme biosynthesis pathway of *S. aureus* was addressed by overexpression, purification and characterization of the enzymes. The results have shown that in *S. aureus*, the coproporphyrinogen III produced by uroporphyrinogen III decarboxylase HemE is converted to coproporphyrin III by coproporphyrinogen III oxidase HemY, which is then used by coproporphyrin ferrochelatase HemH for iron insertion into the macrocycle, leading to the formation of iron-coproporphyrin III. A *S. aureus* strain deleted in *hemH* was constructed and shown to accumulate coproporphyrin III. It was demonstrated that HemY oxidizes coproporphyrinogen III with a specific activity of 24.6 $nmol.min^{-1}mg^{-1}$ and HemH inserts iron into coproporphyrin III with an activity of 815 $nmol.min^{-1}mg^{-1}$. It was shown that the last step of this pathway is the decarboxylation of iron-coproporphyrin III by the iron-coproporphyrin decarboxylase HemQ. This pathway represents a new transitional route between to previously described pathways, the classical and the siroheme-dependent pathways.

On the search for inhibitors of the pathway, HemY was shown to be impaired by derivatives of diphenyl-ether herbicides making this enzyme a promising candidate for drug discovery, which could be important for tackling the problem of antibiotic resistance.

The second part of the work addressed the link between the systems for heme uptake and heme biosynthesis of *S. aureus*. Both routes are known

to supply heme to *S. aureus*, and thus a regulation mechanism was hypothesized to occur to ensure heme homeostasis, so that the toxicity associated with elevated concentration of heme is avoided. To pursue this hypothesis, the late steps of *S. aureus* heme biosynthesis pathway were reconstituted in an *E. coli* strain unable to synthesize heme and also devoid of *S. aureus* heme oxygenases IsdG and IsdI. The results have shown that IsdG, but not IsdI, impairs the growth of the complemented *E. coli* strain by hampering heme synthesis. IsdG was shown to inhibit the ferrochelatase activity of HemH in a concentration dependent manner. It was shown by fluorescence anisotropy and also FLIM-FRET that IsdG interacts *in vitro* and *in vivo* with *S. aureus* HemH. It was also shown through RT-qPCR and flow cytometry that the cellular content of IsdG is higher in the presence of heme, which suggests that heme increases the content of IsdG promoting interaction with the ferrochelatase enzyme of the heme biosynthesis pathway which results in inhibition of the endogenous produced heme. Furthermore, an *in silico* analysis have revealed that one third of the genomes encoding heme biosynthesis pathway also contains a gene for an IsdG-type heme oxygenase. This analysis also revealed that IsdG homologues are normally encoded in genomes also containing HemH and/or HemQ. Altogether, this part of the work has demonstrated that bacteria are able to regulate heme homeostasis by linking the heme biosynthesis pathway and the heme uptake system through HemH and IsdG.

Upon infection of the host, *S. aureus* utilizes the siroheme-containing protein nitrite reductase to reduce nitrite, either using it as part of the respiratory chain to accept electrons when exposed to low oxygen environments or for the detoxification of nitrite produced by neighboring and host enzymes. Analysis of *S. aureus* genome showed that it contains three genes that may be involved in siroheme synthesis, which two were annotated as *cysG* in accordance to the siroheme synthase of *E. coli*. One *cysG* is located on the *nirBD* operon and the other *cysG* is separately localized in a

cluster downstream *cysJ*. The two gene products were overexpressed, the proteins purified, and *in vitro* and *in vivo* assays were performed to analyze their role in *S. aureus*. Enzymatic assays have shown that the protein encoded by the *cysG* gene downstream *nirBD* acts as uroporphyrinogen III methyltransferase (SirA), generating precorrin-2, and the protein encoded by the *cysG* gene downstream *cysJ* acts *as a* precorrin-2 dehydrogenase (SirC), which is able to produce sirohydrochlorin when incubated with precorrin-2 and $NAD^+$. Since one last step was missing and no apparent protein was present, a new search for a putative sirohydrochlorin ferrochelatase (SirB) was made. Blast analysis revealed the occurrence of a gene annotated as *nirR* which shares 25% sequence identity and 44% similarity to *B. megaterium* SirB. Following cloning and expression, the purified protein was shown to act as sirohydrochlorin ferrochelatase. Moreover, functional complementation experiments were performed, where *S. aureus* SirB in combination with SirA and SirC was able to complement an *E. coli* strain lacking *cysG* and thus unable to synthesize siroheme. Therefore, this protein constitutes the last step of the pathway that generates the final product siroheme. Altogether the siroheme pathway active in *S. aureus* was established for the first time.

To conclude, the results presented in this thesis contribute to a better understanding of the *S. aureus* physiology and metabolism, by elucidating the way in which the life dependent tetrapyrroles heme and siroheme are formed. Not less important, it was shown how *S. aureus* maintains the adequate levels of heme avoiding the excess of intracellular free toxic heme that would challenge the pathogen survival.

# Resumo

Os Tetrapirróis são moléculas biológicas presentes em todos os organismos vivos e necessários para processos celulares fundamentais. Entre os tetrapirróis mais conhecidos, o hemo e o sirohemo são grupos prostéticos de proteínas com funções importantes, tais como o transporte e armazenamento de gases, o transporte de eletrões, a sinalização celular, a desintoxicação celular e também a redução de sulfito e nitrito. As duas moléculas são sintetizadas a partir de um percursor final comum, o uroporfirinogénio III, onde a formação de hemo ocorre através de quatro reações enzimáticas pela via clássica de biossíntese de hemo e produzindo sirohemo através de uma via independente. Em alguns organismos como bactérias redutoras de sulfato e nitrato, a síntese do hemo ocorre através de uma via dependente de sirohemo.

*S. aureus* é uma das principais causas de infeções nosocomiais e atualmente, é considerado um grave problema de saúde pública devido ao aumento de estirpes resistentes aos antibióticos. Durante a infeção no hospedeiro, *S. aureus* está exposto a mudanças na concentração de oxigénio nos diferentes locais de infeção. Quando existe oxigénio disponível, *S. aureus* utiliza oxidases terminais dependentes de hemo para a respiração aeróbia. Contudo, alguns locais de infeção têm concentrações limitadas de oxigénio e neste caso *S. aureus* utiliza outros substratos, tais como o nitrato ou o nitrito, como aceitadores finais de eletrões numa cadeia respiratória anaeróbia, em que estão ativas enzimas que contêm sirohemo. Também durante a infeção, *S. aureus* recolhe hemo presente na hemoglobina do hospedeiro, através do sistema de aquisição do hemo, e utiliza-a como fonte de ferro. Embora o sistema de aquisição de hemo tenha sido intensamente estudado em *S. aureus*, o conhecimento acerca da síntese do hemo e

sirohemo é limitado. Para melhor compreender o metabolismo que permite a sobrevivência de *S. aureus* durante os processos de infeção, esta tese pretende elucidar as etapas essenciais para a síntese destes dois tetrapirróis em *S. aureus*. Nesta dissertação, apresentamos novas perspetivas sobre o metabolismo do hemo em *S. aureus* através do estudo abrangente de três tópicos: (i) a caracterização da via de biossíntese do hemo de *S. aureus* e a sua possível utilização como alvo antimicrobiano; (ii) a compreensão de como *S. aureus* equilibra o hemo que é sintetizado de novo ou adquirido através hospedeiro; e (iii) a caracterização da via de biossíntese de siroheme de *S. aureus*.

Através da análise do genoma de *S. aureus* verificou-se a presença de genes que codificam enzimas que poderão estar envolvidas nos passos tardios da via de biossíntese do hemo, nomeadamente a HemE, HemN, HemY e HemH. Determinou-se o papel destas enzimas na via de biossíntese do hemo de *S. aureus* através da sua sobreexpressão, purificação e caracterização. Os resultados mostraram que em *S. aureus*, o coproporfirinógenio III produzido pela uroporfirinogénio III descarboxilase HemE é convertido em coproporfirina III pela coproporfirinógenio III oxidase HemY, sendo posteriormente utilizado pela HemH para inserção de ferro no macrociclo, levando à formação de ferro-coproporfirina III. Foi construída uma estirpe de *S. aureus* mutante no gene *hemH* e mostrou-se que esta acumula coproporfirina III. Foi demonstrado que a HemY oxida o coproporfirinógeno III com uma atividade específica de 24,6 $nmol.min^{-1}mg^{-1}$ e a HemH insere ferro na coproporfirina III com uma atividade de 815 $nmol.min^{-1}mg^{-1}$. Mostrou-se também que o último passo é a descarboxilação de ferro-coproporfirina III pela ferro-coproporfirina descarboxilase HemQ. Esta via representa um novo caminho transicional entre duas vias de biossíntese do hemo descritas anteriormente, a via clássica e a dependente de sirohemo.

Através da pesquisa por inibidores para esta via, demonstrou-se que a HemY é inibida por derivados de herbicidas de difenil-éter que tornam esta enzima um candidato promissor para descoberta de fármacos, o que pode ser importante para enfrentar o problema da resistência a antibióticos.

Na segunda parte do trabalho, estudou-se a associação entre o sistema de aquisição de hemo e a via de biossíntese do hemo em *S. aureus*. As duas vias são conhecidas por fornecer hemo a *S. aureus*, e, portanto, colocou-se a hipótese de existir um mecanismo de regulação para garantir a homeostase do hemo, de modo a que a toxicidade associada às elevadas concentrações do hemo seja evitada. Para investigar esta hipótese, os últimos passos da via de biossíntese de hemo em *S. aureus* foi reconstituída numa estirpe de *E. coli* incapaz de sintetizar hemo, e em que também estão ausentes as oxigenases de hemo IsdG e IsdI de *S. aureus*. Os resultados mostraram que a IsdG, mas não a IsdI, prejudica o crescimento da estirpe de *E. coli* complementada, dificultando a síntese de hemo. Demonstrou-se que a IsdG inibe a atividade de ferroquelatase da HemH estando dependente da sua concentração. Mostrou-se por anisotropia de fluorescência e também por FLIM-FRET que a IsdG interage *in vitro* e *in vivo* com a HemH de *S. aureus*. Também se mostrou através de RT-qPCR e citometria de fluxo que o conteúdo celular de IsdG é maior na presença de hemo, o que sugere que o hemo aumenta o conteúdo de IsdG para promover a interação com a enzima ferroquelatase da via de biossíntese do hemo, resultando na inibição na produção endógena de hemo. Além disso, uma análise *in silico* revelou que um terço dos genomas que codificam a via de biossíntese do hemo também codificam uma oxigenase de hemo do tipo IsdG. Esta análise também revelou que homólogos da IsdG são normalmente codificados em genomas que também contêm HemH e / ou HemQ. Em conclusão, esta parte do trabalho demonstrou que as bactérias são capazes de regular a homeostase do hemo por ligação da via de

biossíntese do hemo e do sistema de aquisição de hemo através da HemH e da IsdG.

Após a infeção do hospedeiro, *S. aureus* utiliza a proteína reductase de nitrito, que contêm sirohemo, para reduzir nitrito, utilizando-a como parte da cadeia respiratória para aceitar eletrões quando em ambientes com baixo oxigénio ou para destoxificação de nitrito produzido por enzimas próximas ou do hospedeiro. Através da análise do genoma verificou-se que *S. aureus* contém três genes que podem estar envolvidos na síntese de sirohemo, sendo que dois destes genes estão anotados como *cysG* conforme a síntase de sirohemo de *E. coli*. Um dos genes *cysG* está localizado no operão *nirBD* enquanto que o outro gene *cysG* está localizado separadamente a jusante do gene *cysJ*. Os produtos dos dois genes foram sobreexpressos, as proteínas foram purificadas e foram efetuados ensaios *in vitro* e *in vivo* para analisar o seu papel em *S. aureus*. Através de ensaios enzimáticos mostrou-se que a proteína codificada pelo gene *cysG* a jusante do gene *nirBD* atua como uma uroporfirinogénio III metiltransferase (SirA), ao gerar precorrina-2 e o gene *cysG* a jusante *cysJ* atua como uma precorrina-2 desidrogenase (SirC), que é capaz de produzir sirohidroclorina quando incubada com precorrina-2 e $NAD^+$. Uma vez que faltava um passo para a produção de sirohemo e aparentemente nenhuma proteína foi encontrada, efetuou-se uma nova busca por uma proteína ferroquelatase de sirohydroclorina (SirB) hipotética. A análise Blast revelou a presença de um gene anotado como *nirR* que compartilha 25% de identidade e 44% de similaridade com a SirB de *B. megaterium*. Após a clonagem e expressão, mostrou-se que a proteína atua como uma ferroquelatase de sirohidroclorina. Além disso, foram feitas experiências de complementação funcional onde se demostrou que a SirB de *S. aureus* em combinação com a SirA e a SirC é capaz de complementar uma estirpe de *E. coli* sem *cysG* e, portanto, incapaz de sintetizar sirohemo. Portanto, esta proteína constituí o último passo da via que sintetiza o produto

final sirohemo. Em suma foi mostrado pela primeira vez uma via de síntese do sirohemo em *S. aureus*.

Para concluir, os resultados apresentados nesta tese contribuem para uma melhor compreensão da fisiologia e do metabolismo de *S. aureus*, elucidando o caminho pelos quais os tetrapirrois, hemo e o sirohemo são formados. Não menos importante, mostrou-se como *S. aureus* mantém níveis de hemo adequados evitando o excesso de hemo intracelular livre que pode comprometer a sobrevivência do patogénico.

# Abbreviations

δ-ALA - δ-aminolevulinic acid

ABM - antibiotic biosynthesis oxygenase

Ahb - Alternative heme biosynthesis

BHI - Brain Heart Infusion

CA-MRSA - Community-acquired MRSA

ChrA-ChrS - *Corynebacterium* heme response system

CO – Carbon monoxide

Copro III - Coproporphyrin III

Copro´gen III - Coprophyrinogen III

CPD - Coproporphyrin-dependent

CydAB - *bd*-type menaquinol oxidase

CysG - Siroheme synthase

DDSH – Didecarboxysiroheme

DMEM - Dulbecco's modified Eagle's medium

FAD- flavin adenine dinucleotide

FLIM-FRET - Lifetime imaging based Förster resonance energy transfer

FnrL - Fumarate nitrate reductase regulator

Fur - Ferric uptake regulator

$H_2O_2$- Hydrogen peroxide

HA-MRSA - Hospital-acquired MRSA

Hb- Hemoglobin

HMB- Hydroymethylbilane

HO- Heme oxygenase

HRMs -Heme regulatory motifs

HrrA-HrrS - heme response regulator

HrtAB - Heme-regulated transporter system

HssRS -Heme sensor system

Hts- Heme transport system

$IC_{50}$- half maximal inhibitory concentration

Isd - Iron-regulated surface determinant system

LB – Luria-Bertani

Lqo - L-lactate dehydrogenase

MpsABC - Membrane potential-generating system

MQ - Menaquinone

$MQH_2$ – Menaquinol

Mqo - Malate dehydrogenase

MRSA - Methicillin-resistant *Staphylococcus aureus*

MS – Mass spectrometry

NarGHI - Nitrate reductase

NDH2- Nicotinamide adenine dinucleotide NADH dehydrogenases type 2

NEAT - Near-Iron Transport

NirBD - Nitrite reductase

NreABC - Nitrogen regulation system

PBG – Porphobilinogen

Phu - *Pseudomonas* heme uptake

PPD - Protoporphyrin-dependent

Proto IX – Protoporphyrin IX

PrrA - photosynthetic response regulator

QoxABCD - $aa_3$/$ba_3$-type menaquinol oxidase

ROS -Reactive oxygen species

SCV - Small colony variants

SAM - S-adenosyl-L-methionine

Sdh - Succinate dehydrogenase

SHD - Siroheme-dependent

SUMT- Uroporphrinogen III methyltransferase

TIM - Triosephosphate Isomerase

TFA - Trifluoroacetic acid

TSA - Tryptic soy agar

TSB - Tryptic soy broth

Uro´gen III- Uroporphrinogen III

VISA - Vancomycin-intermediate *S. aureus*

VRSA - Vancomcyin-resistant *S. aureus*

# Table of Contents



## Introduction

**Chapter 3: Heme acquisition in prokaryotes**



# Results

**Chapter 4: *Staphylococcus aureus* heme biosynthesis characterisation of the enzymes involved in final steps of the pathways**

# Introduction

# Chapter 1

## *Staphylococcus aureus*

## 1.1 General Features

*Staphylococcus aureus* is one of the most important and well-studied species of the genus staphylococci. It was first isolated by Alexander Ogston in 1882 (1) and named *Staphylococcus* due to its appearance, a bunch of grapes, in Greek. In general, these bacteria grow in pairs, tetrads, short chains or clusters that can be visualized under the microscope (Fig 1.1). Later, in 1884, Rosenbach provided the first description of the *S. aureus* species (2, 3).

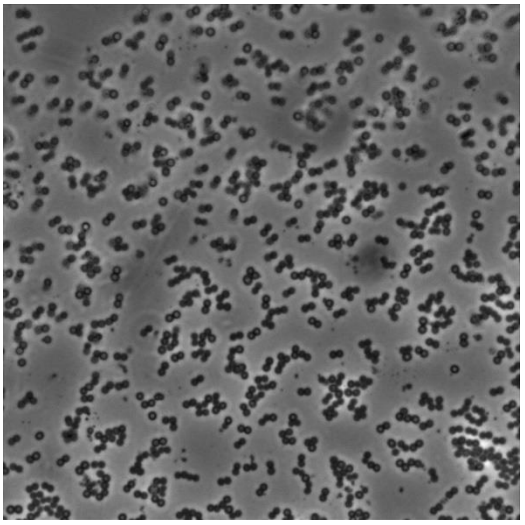

**Figure 1.1** Bright field microscope image of *S. aureus*.

*S. aureus* belong to the phylum Firmicutes and are Gram-positive round (cocci) bacteria, measuring around 1 µm diameter. These microorganisms are non-motile, non-spore-forming facultative anaerobes and coagulase and catalase positive (3). The production of coagulase enables *S. aureus* to clot blood plasma while the expression of catalase confers resistance to $H_2O_2$, which is detoxified to $H_2O$ and $O_2$. Catalase and coagulase tests are often used in clinics: catalase test is used to distinguish staphylococci from streptococci and coagulase test is employed to differentiate *S. aureus* from other coagulase-negative staphylococci (3–5).

*S. aureus* colonizes asymptomatically the anterior nares of approximately 30% of the human population (6, 7) and the throat (8). Although less frequent, also the skin, the perineum, the intestine, the axillae and vagina are sites of colonization (6, 9, 10). Human transmission of *S.*

*aureus* occurs by direct contact, contaminated surfaces and through the air (11, 12). Additionally, *S. aureus* also infects other mammals and birds (12).

## 1.2 Pathogenesis, clinical relevance and antibiotic resistance

*S. aureus* is a human commensal bacteria and the pathogenesis of infection is only initiated when the bacteria breaches the skin or tissue via a lesion (13). *S. aureus* contains several virulence factors that allow the microorganism to adhere and proliferate inside the host. Among the virulence factors identified so far, some examples of proteins required for innate immune evasion are, protein A, responsible for inhibiting phagocytosis through binding to the host IgG, fibronectin-binding proteins Fbp and clumping factor A ClfA, which are proteins involved in platelet activation and aggregation, and are responsible for protecting *S. aureus* against phagocytosis. Additionally, chemotaxis inhibitory protein of staphylococci, CHIPS, and extracellular adherence protein, Eap, inhibit the recruitment of neutrophils to the infection sites (14, 15, 16).

*S. aureus* also possesses several hemolysins, such as the alpha, beta, and gamma-hemolysins which are able to mediate lysis of red blood and white blood cells (15). Erythrocyte lysis releases hemoglobin that is captured by the iron-regulated surface determinant (Isd) system of *S. aureus*, removing heme, which is degraded by heme oxygenases to supply nutrient iron, an essential element during the infection process (16, 17). Bacterial heme-uptake systems and the Isd family of *S. aureus* will be described in detail in Chapter 3 of this dissertation.

*S. aureus* microorganism is currently a serious human threat and one of the main causes of nosocomial infections (14). Among the diseases caused by *S. aureus* are skin and soft tissue infections (folliculitis and impetigo), invasive diseases such as osteomyelitis, endocarditis,

bacteremia, pneumonia and toxin mediated diseases such as food poisoning and toxic shock syndrome (6, 10, 18). The occurrence of infections is strengthened by the ability of the bacteria to form biofilms, which allows *S. aureus* to adhere various surfaces and to resist antimicrobials.

Several *S. aureus* strains show resistance to antibiotics. The first emergence of drug resistant *S. aureus* strains was detected only one year after the introduction of penicillin in 1940 (19–21) (Fig 1.2). These strains harbored plasmids encoding penicillinase, a β-lactamase with the ability to destroy the β-lactam ring of penicillin (22). To overcome the penicillin resistance of *S. aureus* strains, a novel antibiotic, methicillin, was introduced. However, like for penicillin, resistant strains were identified only a few years later (23). The increase of hospital-acquired Methicillin-Resistant *Staphylococcus aureus* (HA-MRSA) infections led to the introduction of vancomycin. However, the frequent use of this antibiotic caused the appearance of the first vancomycin-intermediate *S. aureus* (VISA) resistant strains in 1997 (24), followed by the emergence of latter vancomycin-resistant *S. aureus* (VRSA) strains, that can cope with very high concentrations of vancomycin (25). Yet, vancomycin remains one of the first-line antibiotics to treat severe MRSA infections. More recently, linezolid, ceftaroline, and daptomycin have been utilized for the treatment of serious MRSA infections, which are used in combination with vancomycin or other β-lactams (26). Therefore the high increase of antibiotic resistance has been observed in the last years, which makes the pathogen one of major concerns in public health worldwide with a remarkable economic burden (27, 28).

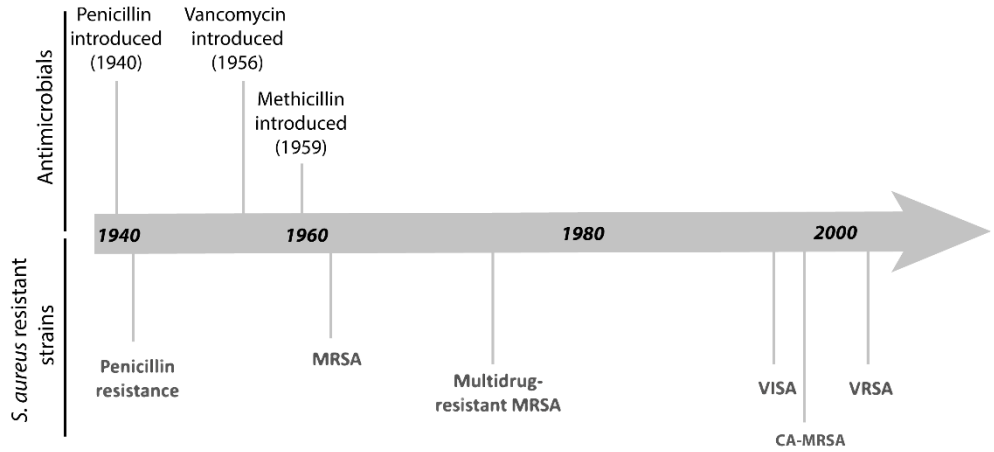


**Figure 1.2** Timeline of the emergence of antibiotic resistance in *S. aureus*. MRSA, community-associated methicillin-resistant *S. aureus*; VISA, vancomycin-intermediate *S. aureus*; VRSA, vancomycin-resistant *S. aureus*; CA-MRSA community-acquired methicillin-resistant *S. aureus*. Adapted from (22).

Currently, the strains that exhibit resistance to the whole β-lactam class of antibiotics are generally designated Methicillin-Resistant *Staphylococcus aureus* (MRSA) strains. The last years have shown a worldwide spread of MRSA present not only in the health care facilities, the so-called HA-MRSA, but also in the community (designated as the community-acquired MRSA (CA-MRSA)) (22). Although in general CA-MRSA strains are more virulent, they show susceptibility to several antibiotics, which suggests that these strains may be descendants strains of the HA-MRSA (22, 29). Nevertheless, an increase of HA-MRSA strains in the community have been reported (30).

In the latest report of the European Antimicrobial Resistance Surveillance Network (EARS-Net 2016), 10 out of 30 countries have MRSA percentages above 25%, while Portugal has approximately 44% (31). Despite the high prevalence of MRSA in Portugal, this percentage has been decreasing in the last years (31).

Hence, it is essential to understand the mechanisms that promote *S. aureus* survival, to discover novel therapeutic targets.



## 1.3 *S. aureus* metabolism

As above mentioned, *S. aureus* is a facultative anaerobic organism, which means it usually relies on oxygen respiration. However, these microorganisms can use alternative electron acceptors or grow by fermentation (3). Since *S. aureus* has the ability to invade niches with different oxygen concentrations, it is crucial for this organism to fine-tune the energy metabolism with the $O_2$ availability in these environments.

The $O_2$ dependent respiratory chain of *S. aureus* (Fig 1.3) comprises two nicotinamide adenine dinucleotide (NADH) dehydrogenases (NDH-2) type 2, (NdhC and NdhF) (32), menaquinones and a branched respiratory system harboring two or three types of oxygen reductases that are heme containing enzymes, namely, a *bd*-type menaquinol oxidase (CydAB), a heme-copper $aa_3$/$ba_3$-type menaquinol oxidase (QoxABCD), and a *bo*-type menaquinol oxidase (3). It also contains a F0F1-ATP synthase (AtpBEFHAGDC) but lacks the canonical complex I NADH: quinone oxidoreductase and a $Na^+$-translocating NADH:quinone oxidoreductase (3, 33). Instead, the respiratory chain of *S. aureus* has a MpsABC (membrane potential-generating system) linked to NDH-2 that is able to generate proton motive force similar to complex I (33). In this chain, electrons are transferred to menaquinones (MQ) generating reduced menaquinone, $MQH_2$, which transfer the electrons to the terminal oxidases $aa_3$ menaquinol oxidase (composed by cytochromes *b*-561 and *a*-602), *bo*-type menaquinol oxidase (composed by cytochromes *b*-555) or the cytochrome *bd* oxidase. Cytochrome *b*-552 is proposed to be linked to an $aa_3$-type menaquinol oxidase while cytochrome *b*-557 is suggested to be connected to the *bo*-type menaquinol oxidase (3, 34, 35). Electrons flow to these cytochromes before

passing to the terminal menaquinol oxidases, where $O_2$ is converted to $H_2O$ (34). Cytochromes *aa*$_3$ and *bo* are believed to act as proton pumps (36, 37), while cytochromes *aa3* and *bd* are suggested to support aerobic respiration (34, 38).

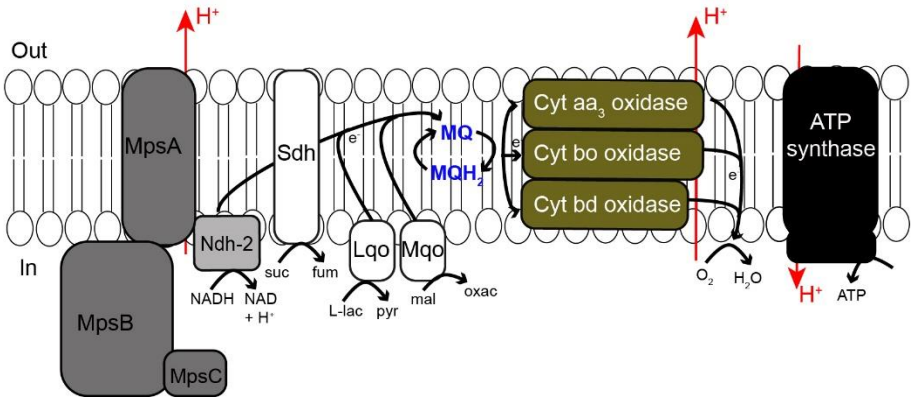


**Figure 1.3** Scheme of the respiratory chain of *S. aureus*. L-lactate (Lqo), succinate (Sdh) and malate (Mqo) dehydrogenases; Mps, membrane potential-generating system; suc, succinate; fum, fumarate; L-lac, L-lactate; pyr, pyruvate; mal, malate; oxac, oxaloacetate, MQ, menaquinone; $MQH_2$, menaquinol; NADH, nicotinamide adenine dinucleotide reduced; $NAD^+$, nicotinamide adenine dinucleotide oxidized; $H^+$, proton; out, outside and in, inside. Adapted from (33).

Due to the high number of heme containing enzymes, mutations in the biosynthesis of heme and menaquinones cofactors leads to impairment of the *S. aureus* growth, generating the so-called colony variants (SCV) that are persister cells (39). A detail description of the heme cofactors and their crucial role will be presented in Chapter 2.

To grow under anaerobic conditions, *S. aureus* utilizes nitrate or nitrite as electron terminal acceptors (40, 41). The genome of *S. aureus* contains a *nar* operon that encodes a nitrate reductase (NarGHI) that promotes the reduction of nitrate to nitrite using electrons provided by NADH (42) (Fig 1.4). The nitrite produced by NarGHI is converted to ammonia by the dissimilatory nitrite reductase (NirBD), encoded by *nirBD*, that also uses

NADH as electron donor (Fig 1.4) (3, 42). The *nir* operon has two additional genes, *nasF* (also annotated as *cysG*), proposed to be involved in the synthesis of siroheme and, *nirR,* that encodes a hypothetical protein with a so far unknown function, but which is speculated to control the *nir* promoter activity or to be involved in the synthesis of siroheme (3, 42). A detailed description of the synthesis of siroheme will be provided in the next chapter, section 2.4.

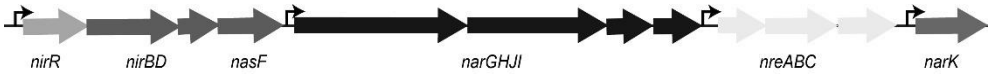


**Figure 1.4** Genetic map of the genes involved in nitrite and nitrate reduction in *S. aureus*. Putative promoters are indicated as angled arrows. Adapted from (42).

*S. aureus* also contains an oxygen-responsive nitrogen regulation system (NreABC), encoded by the gene cluster *nreABC* (Fig. 1.4) and positively regulates the expression of the nitrate and nitrite genes in cells exposed to oxygen (42, 43). In cells grown under anaerobic conditions in the presence of nitrate, deletion of this operon resulted in impairment of nitrate and nitrite reduction and consequently in a SCV growth phenotype (42). NreC also controls the expression of the nitrate transporter encoding gene *narK* (42). Moreover, when growing anaerobically in the presence of nitrate, *S. aureus* NreC downregulates fermentative genes, such as acetaldehyde dehydrogenase (*adhE*), L-lactate dehydrogenase (*lctE*) and alcohol dehydrogenase I (*adh1*) (42).

The importance of tetrapyrrole molecules, such as heme and siroheme and their associated proteins in the life-time of *S. aureus*, is patent in the processes mentioned above. Therefore, the *de novo* synthesis and acquisition pathways that provide these cofactors to *S. aureus* were studied under the scope of this dissertation and will be highlighted in the next chapters.

## 1.4 References


1. Ogston A (1882) *Micrococcus* Poisoning. *J Anat Physiol* 17(Pt 1):24–58.
2. Rosenbach FJ (1884) Mikroorganismen bei den Wundinfections-Krankheiten des Menschen. *Wiesbaden* Germany.
3. Götz F, Bannerman T, Schleifer K (2006) The Genera *Staphylococcus* and *Macrococcus*. *The Prokayotes*, pp 5–75.
4. Ruoff KL (2002) Miscellaneous catalase-negative, Gram-positive cocci: Emerging opportunists. *J Clin Microbiol* 40(4):1129–1133.
5. Goldstein J, Roberts JW (1982) Microtube coagulase test for detection of coagulase-positive staphylococci. *J Clin Microbiol* 15(5):848–851.
6. Wertheim HF, Melles DC, Vos MC, van Leeuwen W, van Belkum A, Verbrugh H a, Nouwen JL (2005) The role of nasal carriage in *Staphylococcus aureus* infections. *Lancet Infect Dis* 5(12):751–762.
7. Kuehnert MJ, Kruszon-Moran D, Hill HA, McQuillan G, McAllister SK, Fosheim G, McDougal LK, Chaitram J, Jensen B, Fridkin SK, Killgore G, Tenover FC (2006) Prevalence of *Staphylococcus aureus* nasal colonization in the United States, 2001-2002. *J Infect Dis* 197(2):172–179.
8. Nilsson P, Ripa T (2006) *Staphylococcus aureus* throat colonization is more frequent than colonization in the anterior nares. *J Clin Microbiol* 44(9):3334–3339.
9. Sollid JUE, Furberg AS, Hanssen AM, Johannessen M (2014) *Staphylococcus aureus*: Determinants of human carriage. *Infect Genet Evol* 21:531–541.
10. Mehraj J, Witte W, Akmatov MK, Layer F, Werner G, Krause G (2016) Epidemiology of *Staphylococcus aureus* Nasal Carriage Patterns in the Community. *Curr Top Microbiol Immunol* 398:55–87.
11. Miller LG, Diep BA (2008) Colonization, Fomites, and Virulence:

Rethinking the Pathogenesis of Community-Associated Methicillin-Resistant *Staphylococcus aureus* Infection. *Clin Infect Dis* 46(5):752–760.

12. Kamholz SL (2016) Human Emerging and Re-emerging Infections. *Clin Infect Dis* 63(5):713–714.
13. Foster TJ (2005) Immune evasion by staphylococci. *Nat Rev Microbiol* 3(12):948–58.
14. Liu GY (2009) Molecular Pathogenesis of *Staphylococcus aureus* Infection. *Pediatr Res* 65:71–77.
15. DeLeo F, Diep B, Otto M (2009) Host Defense and Pathogenesis in *Staphylococcus aureus* Infections. *Infect Dis Clin North Am* 23(1):17–34.
16. Foster TJ, Geoghegan JA, Ganesh VK, Höök M (2014) Adhesion, invasion and evasion: the many functions of the surface proteins of *Staphylococcus aureus*. *Nat Rev Microbiol* 12(1):49–62.
17. Reniere ML, Torres VJ, Skaar EP (2007) Intracellular metalloporphyrin metabolism in *Staphylococcus aureus*. *BioMetals* 20(3–4):333–345.
18. Gordon RJ, Lowy FD (2008) Pathogenesis of Methicillin-Resistant *Staphylococcus aureus* Infection. *Clin Infect Dis* 46(S5):S350–S359.
19. Abraham EP, Chain E (1940) An enzyme from bacteria able to destroy penicillin. *Nature* 146(3713):837–837.
20. Kirby WMM (1944) Extraction of a highly potent penicillin inactivator from penicillin resistant staphylococci. *Science* 99(2579):452–453.
21. Barber M, Rozwadowska-Dowzenko M (1948) Infection by penicillin-resistant staphylococci. *Lancet* 252(6530):641–644.
22. Chambers HF, Deleo FR (2009) Waves of resistance: *Staphylococcus aureus* in the antibiotic era. *Nat Rev Microbiol* 7(9):629–41.
23. Jevons MP (1961) “Celbenin”- Resistant staphylococci. *Br Med J* 1:124–125.
24. Hiramatsu K, Aritaka N, Hanaki H, Kawasaki S, Hosoda Y, Hori S,

Fukuchi Y, Kobayashi I (1997) Dissemination in Japanese hospitals of strains of *Staphylococcus aureus* heterogeneously resistant to vancomycin. *Lancet* 350(9092):1670–1673.

25. Weigel LM, Clewell DB, Gill SR, Clark NC, McDougal LK, Flannagan SE, Kolonay JF, Shetty J, Killgore GE, Tenover FC (2003) Genetic analysis of a high-level vancomycin-resistant isolate of *Staphylococcus aureus*. *Science* 302(5650):1569–71.
26. Bartash R, Nori P (2017) Beta-lactam combination therapy for the treatment of *Staphylococcus aureus* and <i>Enterococcus<i> species bacteremia: A summary and appraisal of the evidence. *Int J Infect Dis* 63:7–12.
27. Stewardson a J, Allignol a, Beyersmann J, Graves N, Schumacher M, Meyer R, Tacconelli E, Angelis G De (2011) The health and economic burden of bloodstream infections caused by antimicrobial-susceptible and non-susceptiblend 2011 : a multicentre retrospective cohort study. *Eurosurveillance* 21:1–12.
28. Lee BY, Singh A, David MZ, Bartsch SM, Slayton RB, Huang SS, Zimmer SM, Potter MA, Macal CM, Lauderdale DS, Miller LG, Daum RS (2013) The economic burden of community-associated methicillin-resistant *Staphylococcus aureus* (CA-MRSA). *Clin Microbiol Infect* 19(6):528–536.
29. Chambers HF (2001) The changing epidemiology of *Staphylococcus aureus*? *Emerg Infect Dis* 7(2):178–182.
30. Grundmann H, Schouls LM, Aanensen DM, Pluister GN, Tami A, Chlebowicz M, Glasner C, Sabat AJ, Weist K, Heuer O, Friedrich AW, on behalf of the ESCMID Study Group C (2014) The dynamic changes of dominant clones of *Staphylococcus aureus* causing bloodstream infections in the European region: Results of a second structured survey. *Eurosurveillance* 19(49):1–10.
31. European Centre for Disease Prevention and Control (2017)

Antimicrobial resistance surveillance in Europe 2016. Annual Report of the European Antimicrobial Resistance Surveillance Network (EARS-Net). *ECDC*:1–88.

32. Schurig-Briccio LA, Yano T, Rubin H, Gennis RB (2014) Characterization of the type 2 NADH:menaquinone oxidoreductases from *Staphylococcus aureus* and the bactericidal action of phenothiazines. *Biochim Biophys Acta - Bioenerg* 1837(7):954–963.
33. Mayer S, Steffen W, Steuber J, Götz F (2015) The *Staphylococcus aureus* nuoL-like protein MpsA contributes to the generation of membrane potential. *J Bacteriol* 197(5):794–806.
34. Taber HW, Morrison M (1964) Electron transport in staphylococci. Properties of a particle preparation from exponential phase *Staphylococcus aureus*. *Arch Biochem Biophys* 105:367–79.
35. Götz F, Mayer S (2013) Both terminal oxidases contribute to fitness and virulence during organ-specific *Staphylococcus aureus* colonization. *MBio* 4(6):4–6.
36. Thöny-Meyer L (1997) Biogenesis of respiratory cytochromes in bacteria. *Microbiol Mol Biol Rev* 61(3):337–76.
37. Tynecka Z, Szcześniak Z, Malm A, Los R (1999) Energy conservation in aerobically grown *Staphylococcus aureus*. *Res Microbiol* 150(8):555–566.
38. Hammer ND, Reniere ML, Cassat JE, Zhang Y, Hirsch AO, Hood MI, Skaar EP (2013) Two heme-dependent terminal oxidases power staphylococcus aureus organ-specific colonization of the vertebrate host. *MBio* 4(4):1–9.
39. Proctor RA, von Eiff C, Kahl BC, Becker K, McNamara P, Herrmann M, Peters G (2006) Small colony variants: a pathogenic form of bacteria that facilitates persistent and recurrent infections. *Nat Rev Microbiol* 4(4):295–305.
40. Burke KA, Lascelles J (1975) Nitrate reductase system in

*Staphylococcus aureus* wild type and mutants. *J Bacteriol* 123(1):308–316.

41. Somerville GA, Proctor RA (2009) At the crossroads of bacterial metabolism and virulence factor synthesis in staphylococci. *Microbiol Mol Biol Rev* 73(2):233–248.
42. Schlag S, Fuchs S, Nerz C, Gaupp R, Engelmann S, Liebeke M, Lalk M, Hecker M, Götz F (2008) Characterization of the oxygen-responsive NreABC regulon of *Staphylococcus aureus*. *J Bacteriol* 190(23):7847–7858.
43. Kamps A, Achebach S, Fedtke I, Unden G, Götz F (2004) Staphylococcal NreB: An O2-sensing histidine protein kinase with an O2-labile iron-sulphur cluster of the FNR type. *Mol Microbiol* 52(3):713–723.

# Chapter 2

## Tetrapyrrole biosynthesis in prokaryotes

## 2.1 Importance of tetrapyrroles

Tetrapyrroles are frequently called the pigments of life and include chlorophylls, coenzyme $F_{430}$, bilins, cobalamin (vitamin $B_{12}$), hemes and siroheme (1) (Fig 2.1).

Tetrapyrroles are molecules involved in many essential biological processes, such as DNA replication, cellular detoxification, metabolism, cell communication, respiration, signal transduction, reduction of nitrite and sulfite, and photosynthesis (2). These compounds derive all from a same universal common tetrapyrrole precursor, namely uroporphyrinogen III (uro´gen III), that is synthesized from δ-aminolaevulinic acid (δ-ALA) (detailed below). The tetrapyrrole structure is formed by four pyrrole aromatic rings often linked by methine groups, in linear (e.g., bilins) or cyclic arrangements (e.g., porphyrins). In the latter, the nitrogen atoms of each pyrrole ring face the center of the macrocycle, which allows the chelation of specific metal ions. Examples of chelated metal ions are: $Fe^{2+}$ in heme, siroheme and heme $d_1$; $Mg^{2+}$ in chlorophylls and bacteriochlorophylls; $Ni^{2+}$ in coenzyme $F_{430}$; and $Co^{2+}$ in cobalamin (1, 3).

Some porphyrins have clinical applications, such as for the treatment of tumors and infections. Porphyrins are light activated at specific wavelengths, transferring electrons to $O_2$ and generating reactive oxygen species (ROS) which are used to promote cell death (4).

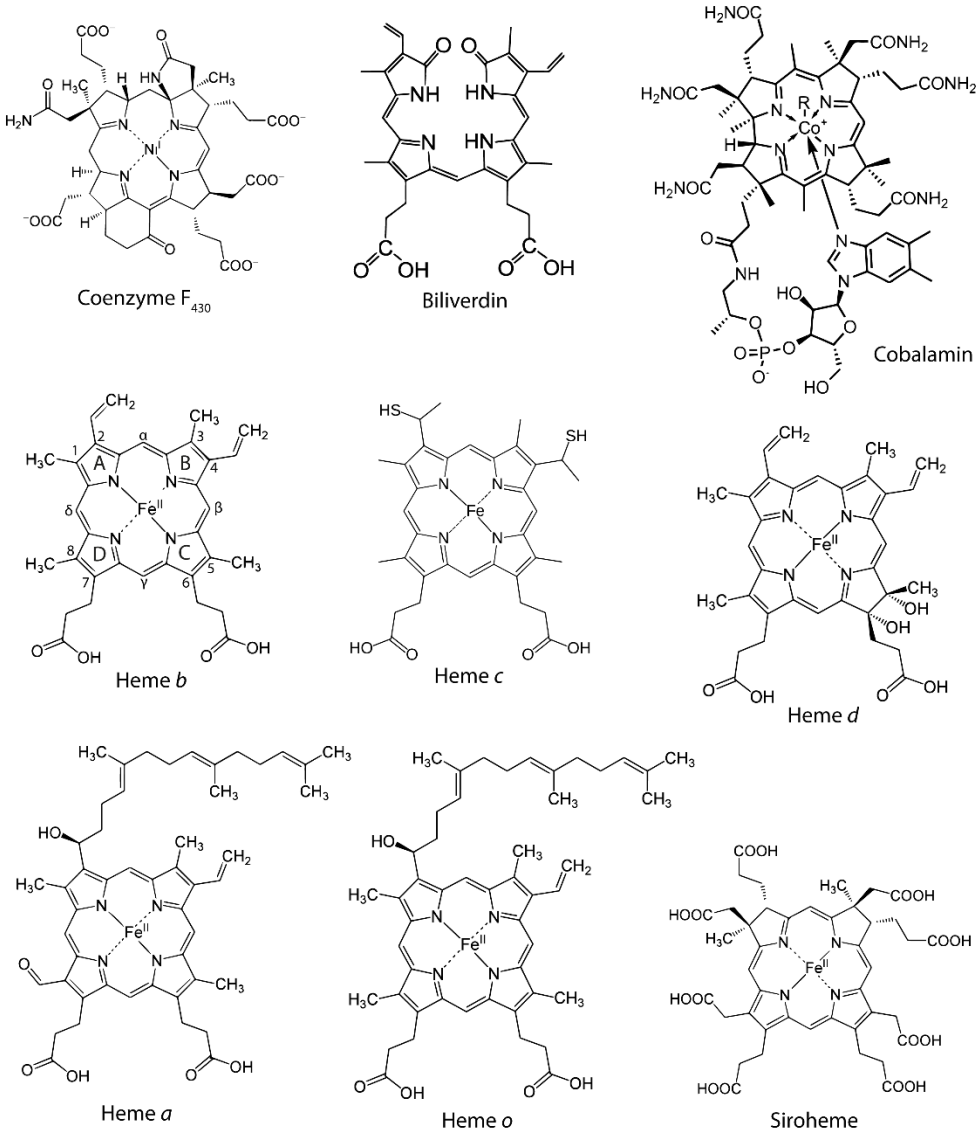


**Figure 2.1.** Examples of known tetrapyrroles. The rings A, B, C and D and carbons are indicated in heme *b* according to the Fisher nomenclature.

## 2.2 Heme

Heme is a hydrophobic molecule and the prosthetic group of numerous proteins involved in crucial life associated processes. One of the best acknowledged function is the storage and transport diatomic gases in hemoglobin and myoglobin (5). Other important roles of heme are for example: i) electron conservation and transfer throughout the respiratory chain in heme containing cytochromes to promote the synthesis of cellular energy (6); ii) catalytic purposes namely in detoxification enzymes such as catalases and peroxidases that reduce $H_2O_2$ to $H_2O$ (7), and in cytochrome P450, that catalyzes the oxidation of organic substrates (8); iii) gas sensors, as observed for the CO-sensing CooA transcription factor (9), and as demonstrated for DosS and DosT sensory kinases of *Mycobacterium tuberculosis* (10); iv) regulation of transcription, translation, protein translocation and protein assembly through the interactions with Heme Regulatory Motifs (HRMs), which are short motifs constituted of cysteine-proline sequences (11).

The iron coordinated to the porphyrin moiety allows heme to function as an electron donor or acceptor due to the change between $Fe^{2+}$ and $Fe^{3+}$ redox states. Iron is coordinated by the nitrogen atoms of each pyrrole ring and can be further coordinated by up to two axial ligands to yield a five or six-coordinated heme, respectively (1). The axial ligands are usually histidine, cysteine or methionine from the polypeptide chain. Five-coordinated hemes are generally present in proteins with catalytic, gas sensor and transporter functions as it allows the coordination of a substrate molecule, while six-coordinated hemes are usually present in electron transfer proteins (1, 12). Several types of heme are found in organisms (Hemes *a*, *b*, *c*, *d* and *o*) (Fig 2.1), being the more common one heme *b*, which is also the precursor of all other types of hemes. Heme *b* is characterized by the presence of vinyl groups attached to rings A and B,

propionic acid groups in rings C and D, and four methyl groups distributed one per ring. Heme *a* and *o* are very similar between them, as heme *o* is an intermediary compound of the heme *a* synthesis from heme *b* (1). In heme *a* and heme *o*, the vinyl group of ring A is substituted by an isoprenoid side chain; however, in position 8 heme *a* contains a formyl group, while a methyl group is present in heme *o* (Fig 2.1). In heme *c*, the vinyl groups of rings A and B are substituted by thioether bridges that covalently bound to the apoprotein through cysteines (Fig 2.1). The more significant modifications are present in heme *d*, where two additional hydroxyl groups are observed in ring C (Fig 2.1), and the hydroxyl and propionate side groups in carbon 6 can form a lactone (1, 13). These types of hemes are usually present in bacterial respiratory proteins (1). Other less common forms of heme are heme *l,* heme *m* and heme *s*. Heme *l* is found in mammalian lactoperoxidases, heme *m* in mammalian neutrophil enzyme myeloperoxidase while heme *s* is present in marine worm hemoglobins (1).

Although heme has a high biological importance, the intracellular heme content has to be tightly regulated as high levels of free heme are highly reactive and toxic to the cells, for instance causing the formation of ROS, which damage DNA, lipids and proteins (14). Due to its hydrophobic properties, heme has the ability to intercalate into lipid membranes promoting the oxidation of membrane components that leads to cell lysis and death (5, 15). Additionally, heme mediates degradation of proteins to small peptide fragments and is also a strong pro-inflammatory agent (5, 15).

Heme toxicity is well studied in mammalian cells and is estimated that the physiological concentration of free heme ranges from 0.03 to 1 μM (16) and concentrations above 10 μM (16), produce ROS. In mammals the possible causes for accumulation of intracellular free heme are, the increase of heme synthesis, the accumulation of extracellular heme, deficient heme oxygenase activity, impaired heme incorporation in apo-proteins and enhanced hemeprotein degradation (5). Mammals avoid heme toxicity by

degradation of the free heme via heme oxygenase or by means of other proteins such as reduced glutathione and NADPH–cytochrome P-450 reductase (15). Additionally, heme content is controlled by heme binding proteins such as hemopexin, albumin, haptoglobin, and heme-binding protein (HBP23), all of which form non-toxic heme complexes (15). In mammals, other mechanisms for regulation of intracellular heme content consists in the regulation of heme synthesis and in extracellular heme trafficking (5).



In bacteria, the effects of heme toxicity are generally more pronounced in Gram-positive than in Gram-negative bacteria (17, 18). The growth of *S. aureus* is slightly inhibited at concentrations above 5 µM of hemin (19). *Staphylococcus epidermidis* seems to tolerate higher concentrations of hemin as concentrations above 10 µM are necessary for reduced growth (20). *Pseudomonas aeruginosa* and *E. coli* can cope with 150 µM of hemin without growth impairment (17). Nevertheless, the number of studies on mechanisms of heme toxicity to bacteria are limited. In *S. aureus* and *E. coli*, heme was shown to cause DNA damage (21). Also for *S. aureus*, hemin was reported to induce ion fluxes in a light-independent mode, hence causing oxidative damage (22). Additionally, free iron released during heme degradation promotes bacterial cell damage through the production of hydroxyl free radicals (Fenton chemistry) (18). It was recently demonstrated for *S. aureus* that, when heme is in excess, heme molecules accumulate in bacterial membranes, that by interaction with oxygen and membrane menaquinones generate superoxide radicals (23).

Bacteria have also evolved mechanisms to prevent heme toxicity that comprise heme efflux pumps, heme sequestration proteins and heme degrading proteins. Numerous Gram-positive bacteria encode a heme-regulated transporter system (HrtAB), an efflux pump that was shown in *S. aureus* to act in combination with the heme sensor system HssRS. High levels of heme are recognized by HssRS that activates the HrtAB heme

export activity (19, 24). Orthologues of this efflux system were found in Gram-positive bacteria such as *Bacillus anthracis*, *Lactococcus lactis*, *Corynebacterium diphtheriae* and *Streptococcus agalactiae* (25–28). Alternatively to the heme efflux systems mentioned above, Gram-negative bacteria rely on heme sequestration proteins to face heme toxicity. Examples of these proteins are *Yersinia enterocolitica* HemS (29), *Pseudomonas aeruginosa* PhuS (30), *Escherichia coli* O157:H7 ChuS (31), *Yersenia pestis* HmuS (32) and *Shigella dysenteriae* ShuS (33). Interestingly, some of these proteins are also considered part of the heme uptake systems operating in Gram-negatives.

### 2.2.1 Heme biosynthesis

In bacteria, heme is either synthesized endogenously or captured from the environment by heme uptake systems. Almost every living organism is capable of synthetizing heme; however, bacteria such as those of the genera *Dehalococcoides* and *Thermotoga* are not able to produce heme. Furthermore, *Enterococcus faecalis,* lactic acid bacteria*, Bartonella hensaela*, *Haemophilus influenzaea* and some *Streptococcus* species although possessing hemeproteins apparently do not contain heme biosynthesis related genes (14, 34).

For organisms that produce endogenously heme and/or other tetrapyrroles, its synthesis starts with the formation of the universal tetrapyrrole precursor δ-aminolevulinic acid (δ-ALA) (Fig 2.2) (1, 3, 34–36). So far, two distinct pathways are known for the synthesis of δ-ALA: i) the Shemin or C4 pathway, where succinyl-coenzyme A and glycine are condensed to δ-ALA with the action of Ala synthase encoded by *hemA* (3, 34, 37). This route is present in metazoans, fungi and alphaproteobacteria; ii) the C5-pathway, that although discovered latter it is likely to be the more ancient route, and which uses charged glutamyl-tRNA for the production of

δ-ALA in a two-step reaction (3, 34, 37). Glutamyl-tRNA is converted into glutamate-1-semialdehyde by glutamyl-tRNA reductase (HemA or GtrR) which is then converted into δ-ALA by glutamate-1-semialdehyde-2,1-aminomutase encoded by the *hemL* gene (3, 34, 37). The C5-pathway occurs in most bacteria, plants and archaea. The only organisms known to have the two pathways for the synthesis of δ-ALA are *Euglena gracilis* and *Chromobacterium violaceum* (34).



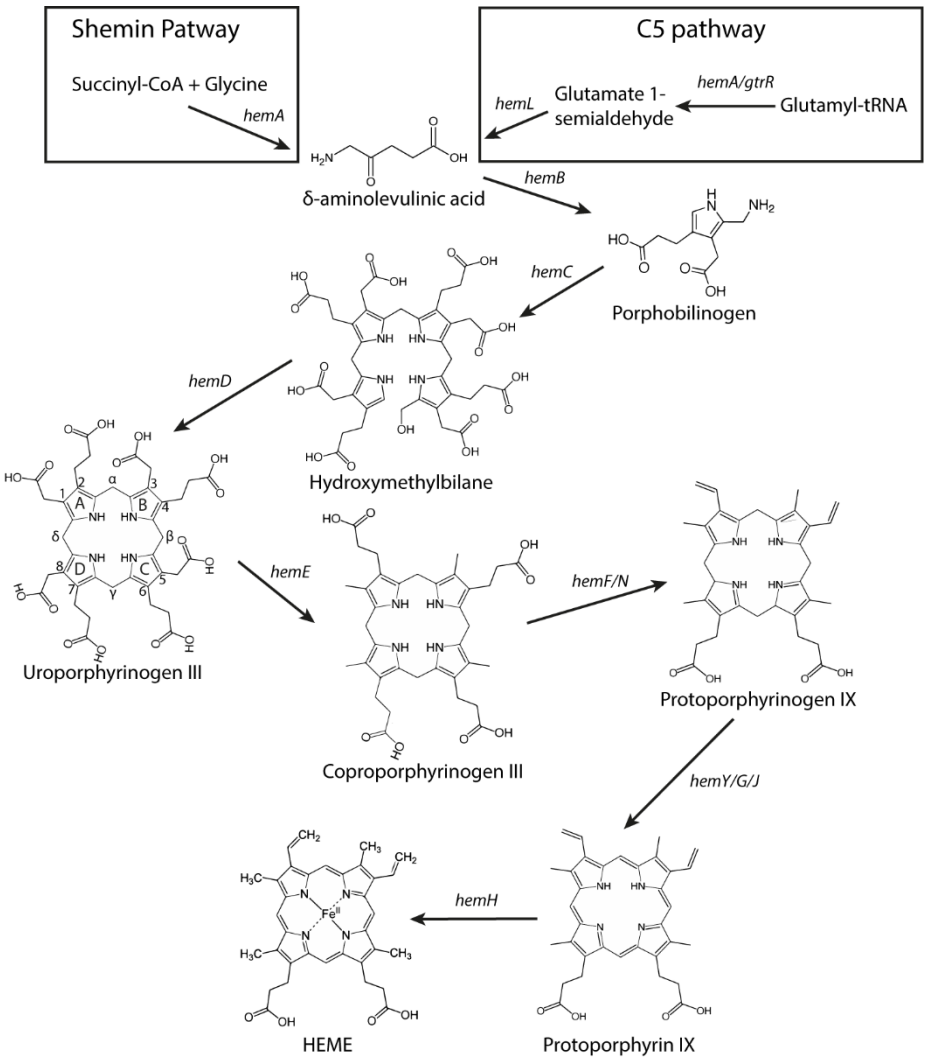


**Figure 2.2** Scheme of the steps of the biosynthesis of heme *b* via the classical pathway, also known as the protoporphyrin-dependent pathway. The rings A, B, C and D and carbons are indicated in uro´gen III according to Fisher nomenclature. Adapted from (3).

Following the generation of δ-ALA, the porphobilinogen synthase enzyme (HemB) promotes the condensation of two molecules of δ-ALA to produce porphobilinogen (PBG) (3, 34).

The next enzymatic step involves the deamination and assembly of four porphobilinogen molecules to yield hydroxymethylbilane, which is performed by hydroxymethylbilane (HMB) synthase (HemC). This enzyme deaminates PBG and promotes the assembly of the four deaminated porphobilinogen molecules into a linear complex (HMB) (3, 34). HMB spontaneously cyclizes to generate uroporphyrinogen I, a non-physiological compound (37). Therefore, HMB is converted into uro´gen III by cyclization and inversion of the acetate and propionate groups of the D pyrrole ring in the presence of uroporphyrinogen III synthase (HemD) (Fig 2.2) (3, 34).

As mentioned in section 2.1, uro´gen III is the last common precursor of all known tetrapyrroles and until this step, all enzymatic reactions from δ-ALA to uro´gen III are highly conserved in organisms that synthesize these pigments. In the classical pathway, following the generation of uro´gen III four extra enzymatic reactions are necessary to catalyze its conversion to the final product heme *b* (Fig 2.2).

For many years, the classical pathway was considered as conserved in all heme producing organisms. However, a second type of route, named alternative heme biosynthetic pathway was revealed and broke that dogma (38). This new route proceeds via the methylation of uro´gen III through the generation of siroheme. The pathway has been proposed to precede the classical pathway since it utilizes intermediates, such as siroheme, that are more ancient than heme, and because the reactions take place under anaerobic conditions (34). The alternative heme biosynthetic pathway is widespread in archaea, denitrifying and sulphate-reducing bacteria (34, 38).

More recently a third route for the synthesis of heme has been reported to be present mostly in Firmicutes and Actinobacteria (39). This pathway, termed transitional pathway, branches from uro´gen III and contains coproporphyrin III as a new intermediate (39). This novel heme biosynthetic pathway was shown in this thesis to be active in *S. aureus* as described in chapter 4 of the results section.

Very recently, in 2017 (34), these pathways were renamed as protoporphyrin-dependent (PPD), siroheme-dependent (SHD) pathway and coproporphyrin-dependent (CPD) pathway, respectively, as well as the enzymes involved. However, in this dissertation the enzyme names will be referred according to the classical nomenclature since this still remains the one that is most used.



*Protoporphyrin-dependent (PPD) pathway*

The synthesis of heme *b* through the PPD route (previously known as classical heme pathway (Fig 2.2) converts uro´gen III to coprophyrinogen III (copro´gen III) by the decarboxylation of the acetic acid side chains of each pyrrole ring, generating methyl groups, in a reaction that is catalyzed by uro´gen III decarboxylase enzyme (HemE) (3, 34). Bacterial HemE enzymes are homodimers with subunits of 40 kDa and with no apparent associated cofactor (34).

In the next step, the propionate groups of rings A and B of copro´gen III are oxidatively decarboxylated to vinyl groups, yielding protoporphyrinogen IX (proto´gen IX) in a step catalyzed by coproporphyrinogen III decarboxylase. Depending on the oxygen dependence, two family of enzymes catalyze the reaction: the oxygen-dependent HemF (copro´gen III decarboxylase) and the oxygen-independent HemN (copro´gen III dehydrogenase). HemF is typically a homodimer that requires $O_2$ as a terminal electron acceptor, with the concomitant formation

of $CO_2$ and $H_2O_2$ (40, 41). HemN is a monomeric protein which harbors a [4Fe-4S] cluster and a S-adenosyl-L-methionine (SAM) molecule (42).

In the penultimate step of the pathway, proto´gen IX is oxidized to protoporphyrin IX in a reaction that involves six electrons. As in the previous step, the reaction may be performed by an oxygen-dependent or an oxygen-independent enzyme. The oxygen-dependent proto´gen IX oxidase, HemY, is a homodimer protein containing flavin adenine dinucleotide (FAD) that, like HemF, utilizes $O_2$ as terminal electron acceptor. The oxidation of proto´gen IX by HemY uses FAD and involves three $O_2$ molecules generating three $H_2O_2$ molecules (34). The oxygen-independent HemG was first reported in *E. coli* and is a 21 kDa protein (35). Contrarily to HemY, HemG feeds electrons to the respiratory chain, anticipating the use of several electron acceptors (43). HemG is mostly present in γ-proteobacteria while HemY occurs in eukaryotes and prokaryotes (34, 44). In 2010, a new proto´gen oxidase was identified in α-proteobacteria and δ-proteobacteria and named HemJ, but its full characterization remains to be done (44, 45).

The final step of heme biosynthesis consists in the insertion of iron into protoporphyrin IX to form protoheme, which is commonly designated as heme *b* (Fig 2.2). This reaction is catalyzed by protoporphyrin ferrochelatase (HemH), a well characterized enzyme that was reported to be a membrane-bound protein in eukaryotes and several prokaryotes, but that is a soluble monomer in Gram-positive bacteria, such as *B. subtilis* (46–48). Furthermore, protoporphyrin ferrochelatases may contain an iron-sulfur cluster bound to C-terminal region of the protein, which occurs mainly in eukaryotes, but has also been reported for some bacteria, such as, *Mycobacterium tuberculosis*, *Bdellovibrio bacteriovorus*, *Caulobacter crescentus* and *Myxococcus xanthus* (47, 49). Apart from protoporphyrin, ferrochelatases may use a wide range of substrates such as, mesoporphyrin, deuteroporphyrin and protoporphyrin, and promote the insertion of other cations like $Co^{2+}$, $Zn^{2+}$ and $Mn^{2+}$ (34, 35, 46). Interestingly, in murine and

yeast ferrochelatases, the chelation of metal ions other than iron such as $Cu^{2+}$, $Zn^{2+}$, $Co^{2+}$ and $Ni^{2+}$ promotes substrate inhibition (50).

*Siroheme-dependent (SHD) pathway*

For the formation of heme through the SHD pathway (previously known as alternative heme biosynthetic pathway), uro´gen III is first converted to siroheme via precorrin-2 and sirohydrochlorin in three consecutive reactions involving the siroheme synthase CysG (Figure 2.3) (1, 51). Siroheme is then converted to 12,18-didecarboxysiroheme by the decarboxylation of the acetic acid side chains in rings C and D to methyl groups, in a step involving the alternative heme biosynthesis proteins AhbA and AhbB (38, 52, 53) (Fig 2.3). Both proteins form a heterodimeric complex with a mass of 40 kDa named siroheme decarboxylase complex (52). The next step involves the elimination of the acetic acid residues of rings A and B, generating Fe-coproporphyrin III, also known as coproheme, which is catalyzed by AhbC in a SAM-dependent reaction (38, 53) (Fig 2.3). In the last step, the two propionate side chains of rings A and B of Fe-coproporphyrin III are oxidative decarboxylated into vinyl groups forming the final product, heme *b*. This reaction is promoted by AhbD (38, 54) (Fig 2.3) and is also SAM-dependent. In *D. vulgaris*, AhbD was shown to be a monomeric cytoplasmic protein that harbors two iron-sulfur clusters (54).

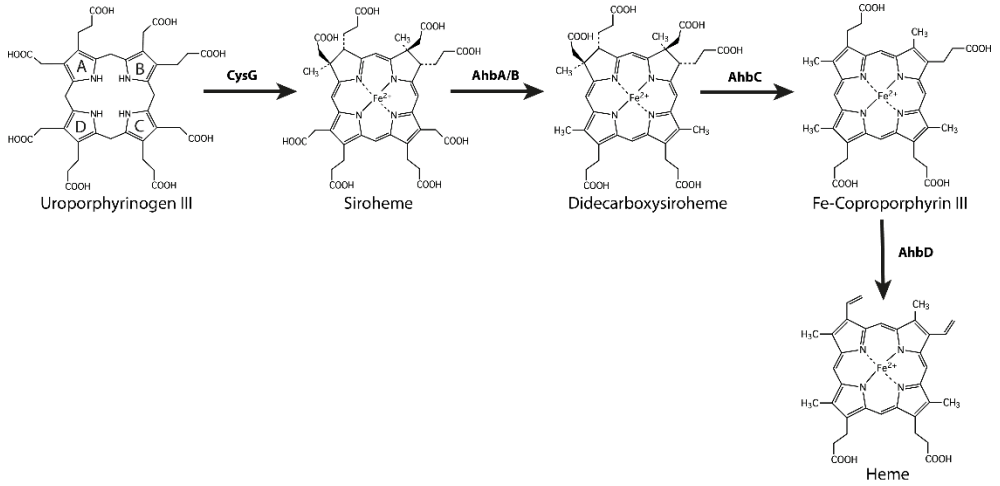


**Figure 2.3** Steps required for the synthesis of heme *b* via the siroheme-dependent pathway. Adapted from (38).

### 2.2.2 Regulation of heme biosynthesis

In several biosynthetic pathways, substrates and products may have an active role in the regulatory process. In heme biosynthesis the best known regulatory process involves the control of the first step by its final end product, heme. In *Salmonella* species and *E. coli*, heme binds to HemA promoting its degradation by proteases, which impairs the heme biosynthesis (55) and excess of cellular heme levels is avoided. In *Corynebacterium diphtheriae*, high concentrations of heme leads to repression of the *hemA* promoter by the *Corynebacterium* heme response system (ChrA-ChrS) and the heme response regulator (HrrA-HrrS). These two-component regulatory systems also activate the transcription of the *hmuO* gene, which encodes a heme oxygenase enzyme (56, 57). Furthermore, when heme levels are elevated, HrrA represses the transcription of *hemE* and *hemH* (57).

In *Acidithiobacillus ferrooxidans*, addition of δ-ALA substrate to cells increases heme levels, decreasing the Glu-tRNA synthetase activity and the levels of Glu-tRNA reductase (58).

Iron is a limiting nutrient for the heme biosynthesis pathway as it is required by ferrochelatases for insertion into porphyrins. Therefore, it also plays a regulatory role. So far, the best studied system is the iron response regulator (Irr), which is present in *Alphaproteobacteria* (59). Irr is a repressor of the *hemA* and *hemB* genes. Under iron replete conditions, ferrochelatase binds Irr while producing heme. Consequently, the heme produced by ferrochelatase binds Irr, promoting its degradation. On the other hand, when iron concentrations are low, Irr does not bind to ferrochelatase remaining active to repress *hemA* and *hemB*, which impairs the formation of toxic porphyrin intermediates (60, 61).

As previous mentioned, some of the heme biosynthetic enzymes utilize $O_2$ as substrate, namely copro´gen III decarboxylase (HemF) and proto´gen IX oxidase (HemY). However, in other organisms these steps are done by oxygen-independent enzymes such as copro´gen III dehydrogenase (HemN) and proto´gen IX dehydrogenase (HemG).

In *Rhodobacter sphaeroides or Rhodobacter capsulatus*, the oxygen-sensing regulator FnrL (fumarate nitrate reductase regulator) binds to the *hemA* promoters and induces the synthesis δ-ALA under anaerobic conditions (62, 63). Also, in response to $O_2$ tensions, the photosynthetic response regulator (PrrA) binds to the *hemA* promoter activating its transcription under aerobic and anaerobic growth conditions (64).

In *P. aeruginosa hemA*, *hemN* and *hemF* are regulated by the oxygen sensor protein Anr and the redox regulator Dnr (65, 66). While both Anr and Dnr are required for the anaerobic induction of *hemF* and *HemN*, only Anr is necessary for the aerobic expression of *hemN* (65).

Under low oxygen conditions, the two-component regulatory system FixLJ of *Bradyrhizobium japonicum* controls positively the *hemA*, *hemB*, *hemN* genes by activating the $FixK_2$ regulator (67, 68).

In *B. subtilis*, the *hemHYE* operon was found to be induced in a *fnr* mutant strain grown under anaerobic growth conditions (69). Also, oxidation

of the peroxide response regulator PerR by $H_2O_2$ is responsible for the de-repression of *hemAXCBL*, which increases heme biosynthesis (70).

In *E. coli*, $H_2O_2$ activates the peroxide-sensing transcriptional activator, OxyR, which induces the expression of *hemH* and *hemF* (71).

## 2.3 Siroheme biosynthesis

Siroheme is an iron containing tetrapyrrole used as cofactor in sulfite and nitrite reductases in plants, fungi and prokaryotes (1, 51). It works with a [4Fe-4S] cluster in sulfite and nitrite reductases to perform the six-electron reduction of sulfite or nitrite to sulfide and ammonia, respectively (51). Siroheme is an isobacteriochlorin with the same chemical groups of its precursor uro´gen III but with two additional methyl groups attached to carbons 1 and 3 of rings A and B, respectively (Fig 2.4). It is synthesized from uro´gen III in three enzymatic steps. The first enzymatic step consists in the bis-methylation of uro´gen III to yield precorrin-2, followed by oxidation to sirohydrochlorin. In the final step there is the insertion of ferrous iron into sirohydrochlorin to generate siroheme (Fig 2.4).

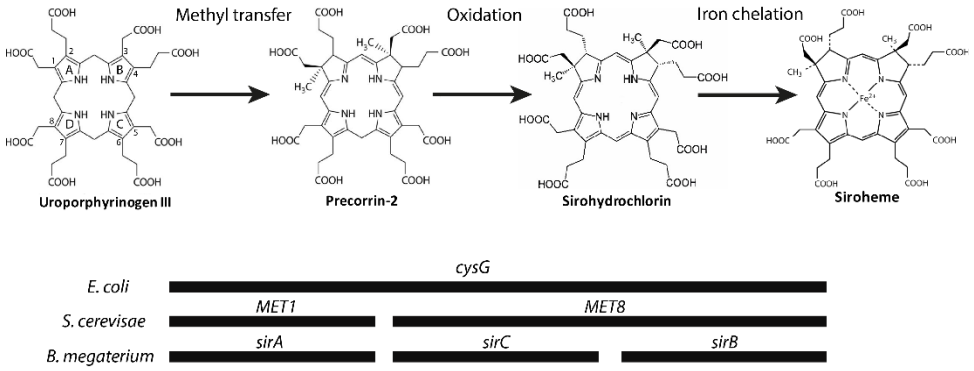


**Figure 2.4** Steps involved in the siroheme biosynthesis. Adapted from (72).

Until now, few genes were identified as involved in the synthesis of siroheme and, depending on the organism, the products of one, two or three genes are required to complete the three enzymatic reactions for the synthesis of siroheme from uro´gen III (Fig 2.4).

In *E. coli*, only one gene, *cysG*, was described to be involved in the three steps required for this synthesis (73, 74), as its mutation generates cells with no nitrite reductase activity (75). The *cysG* gene encodes a 457-amino acid protein that was named siroheme synthase (CysG) (74). *E. coli* CysG has a C-terminal part ($CysG^A$) that provides the protein a SAM-dependent uroporphyrinogen III methyltransferase (SUMT) activity, *i.e.*, promotes the SAM-dependent methylation of carbons 1 and 3 of uroporphyrinogen III into precorrin-2 (76). The N-terminal part of *E. coli* CysG ($CysG^B$) catalyzes the $NAD^+$-dependent dehydrogenation of precorrin-2 into sirohydrochlorin and insertion of iron to yield siroheme (73). Similarly, *Salmonella enterica* also encodes a multifunctional homodimeric protein CysG with two structurally independent modules (77). The C-terminal part has a similar topology to SUMT, and the N-terminal part contains a $NAD^+$-binding Rossman fold and a phosphoserine, which acts as a regulatory residue between the synthesis of siroheme and cobalamin (77).

In yeast, two genes are required for the synthesis of siroheme, *MET1* and *MET8* (78). Met1p, the product of *MET1* is a 526-amino acid protein whose C-terminal region shares a high degree amino acid sequence similarity with the C-terminus of *E. coli* CysG and other SUMT proteins, displaying SUMT activity (78, 79). *MET8* encodes a protein with 274 residues (Met8p) that shares amino acid sequence similarity with the N-terminal region of *E. coli* CysG and exhibits $NAD^+$-dependent precorrin-2 dehydrogenase and sirohydrochlorin chelatase activities (78–80).

In *Bacillus megaterium*, three different enzymes named SirA, SirB and SirC, are required to synthesize siroheme, and the correspondent genes are organized in a operon (81, 82). SirA shares high amino acid sequence

similarity to the C-terminal part of *E. coli* CysG, and has SUMT activity (82). SirB shows amino acid similarity with *B. megaterium* CbiX, a cobaltochelatase involved in the synthesis of cobalamin (81). SirB was shown to have sirohydrochlorin ferrochelatase activity both in *in vitro* and *in vivo* experiments (81, 82). SirC carries precorrin-2 dehydrogenase activity and the protein shares amino acid sequence similarity with the *E. coli* $CysG^B$ and *S. cerevisiae* Met8p (82, 72).

The sulfate reducer *D. vulgaris* also encodes a functional SirC that shares sequence identity with *E. coli* $CysG^B$ and has $NAD^+$-dependent precorrin-2 dehydrogenase activity (83). Additionally, in *D. vulgaris* the SUMT activity is performed by CobA/HemD, a bi-functional enzyme that has uro´gen III synthase activity (83). This bacterium encodes two chelatases, $CbiK^C$ and $CbiK^P$ that have sirohydrochlorin ferro and cobalto-chelatase activities (84).

Furthermore, it was shown recently, in a scientific publication in which I am the first co-author, that *D. vulgaris* $CbiK^P$ is a periplasmic protein that can bind two additional heme groups within the tetramer, through His103 in $\Delta28CbiK^P$ (85). Also, two residues were identified as essential for the sirohydrochlorin ferrochelatase activity, namely His154 and His216 in $\Delta28CbiK^P$ (85). The periplasmic localization and the ability to bind more heme groups indicate that *D. vulgaris* $CbiK^P$ may function as a heme transporter (85).

In plants, siroheme is synthesized in plastids. The three consecutive steps for its synthesis in *Arabidopsis thaliana* are carried out by an uro´gen III methyltransferase (UPM1p) and a sirohydrochlorin ferrochelatase (SirB) (86). However, no precorrin-2 dehydrogenase has been described so far (87). UPM1p is synthesized in the cytosol and contains an N-terminal transit peptide that is cleaved after plastid translocation (88). SirB is located in the plastid, and the mature form of the enzyme contains 150 amino acid.

Interestingly, *A. thaliana* SirB contains an iron-sulfur cluster which is not required for sirohydrochlorin ferrochelatase activity (86, 87).

The siroheme synthesis of *S. aureus* will be presented in the results section (Chapter 6).

## 2.4 References


1. Warren MJ, Smith AG (2009) *Tetrapyrroles: Birth, Life and Death* (Springer New York, New York, NY).
2. Schlicke H, Richter A, Rothbart M, Brzezowski P, Hedtke B, Grimm B (2015) Function of Tetrapyrroles, Regulation of Tetrapyrrole Metabolism and Methods for Analyses of Tetrapyrroles. *Procedia Chem* 14:171–175.
3. Heinemann IU, Jahn M, Jahn D (2008) The biochemistry of heme biosynthesis. *Arch Biochem Biophys* 474(2):238–251.
4. Kou J, Dou D, Yang L (2017) Porphyrin photosensitizers in photodynamic therapy and its applications. *Oncotarget* 8(46):81591–81603.
5. Chiabrando D, Vinchi F, Fiorito V, Mercurio S, Tolosano E (2014) Heme in pathophysiology: A matter of scavenging, metabolism and trafficking across cell membranes. *Front Pharmacol* 5(April):1–24.
6. Thöny-Meyer L (1997) Biogenesis of respiratory cytochromes in bacteria. *Microbiol Mol Biol Rev* 61(3):337–76.
7. Benson DR, Rivera M (2013) Heme uptake and metabolism in bacteria. *Metal Ions in Life Sciences*, pp 279–332.
8. Guengerich FP (2007) Mechanisms of cytochrome P450 substrate oxidation: MiniReview. *J Biochem Mol Toxicol* 21(4):163–168.
9. Vos MH (2008) Ultrafast dynamics of ligands within heme proteins. *Biochim Biophys Acta* 1777(1):15–31.
10. Sivaramakrishnan S, De Montellano PRO (2013) The DosS-

DosT/DosR mycobacterial sensor system. *Biosensors* 3(3):259–282.

11. Mense SM, Zhang L (2006) Heme : a versatile signaling molecule controlling the activities of diverse regulators ranging from transcription factors to MAP kinases. 681–692.
12. Vicente M da GH, Smith KM (2001) Haem structure and function. *Encyclopedia of Life Sciences* (John Wiley & Sons, Ltd, Chichester, UK), pp 1–8.
13. Murshudov GN, Grebenko AI, Barynin V, Dauter Z, Wilson KS, Vainshtein BK, Melik-Adamyan W, Bravo J, Ferran JM, Ferrer JC, Switala J, Loewen PC, Fita I (1996) Structure of the heme d of Penicillium vitale and Escherichia coli catalases. *J Biol Chem* 271(15):8863–8868.
14. Choby JE, Skaar EP (2016) Heme synthesis and acquisition in bacterial pathogens. *J Mol Biol*:16–18.
15. Kumar S, Bandyopadhyay U (2005) Free heme toxicity and its detoxification systems in human. *Toxicol Lett* 157(3):175–188.
16. Sassa S (2004) Why heme needs to be degraded to iron, biliverdin IXα, and carbon monoxide? *Antioxid Redox Signal* 6(5):819–824.
17. Nitzan Y, Ladan H, Malik Z (1987) Growth-inhibitory effect of hemin on staphylococci. *Curr Microbiol* 14(5):279–284.
18. Anzaldi LL, Skaar EP (2010) Overcoming the heme paradox: heme toxicity and tolerance in bacterial pathogens. *Infect Immun* 78(12):4977–4989.
19. Torres VJ, Stauff DL, Pishchany G, Bezbradica JS, Gordy LE, Iturregui J, Anderson KL, Dunman PM, Joyce S, Skaar EP (2007) A *Staphylococcus aureus* regulatory system that responds to host heme and modulates virulence. *Cell Host Microbe* 1(2):109–19.
20. Juarez-Verdayes M a, Gonzalez-Uribe PM, Peralta H, Rodriguez-Martinez S, Jan-Roblero J, Escamilla-Hernandez R, Cancino-Diaz ME, Cancino-Diaz JC (2012) Detection of hssS, hssR, hrtA, and hrtB

genes and their expression by hemin in *Staphylococcus epidermidis*. *CanJMicrobiol* 58:1063–1072.

21. Nir U, Ladan H, Malik Z, Nitzan Y (1991) In vivo effects of porphyrins on bacterial DNA. *J Photochem Photobiol B Biol* 11(3–4):295–306.
22. Ladan H, Nitzan Y, Malik Z (1993) The antibacterial activity of haemin compared with cobalt, zinc and magnesium protoporphyrin and its effect on potassium loss and ultrastructure of *Staphylococcus aureus*. *FEMS Microbiol Lett* 112(2):173–177.
23. Wakeman CA, Hammer ND, Stauff DL, Attia AS, Anzaldi LL, Dikalov SI, Calcutt MW, Skaar EP (2012) Menaquinone biosynthesis potentiates haem toxicity in *Staphylococcus aureus*. *Mol Microbiol* 86(6):1376–1392.
24. Wakeman CA, Stauff DL, Zhang Y, Skaar EP (2014) Differential activation of *Staphylococcus aureus* heme detoxification machinery by heme analogues. *J Bacteriol* 196(7):1335–1342.
25. Bibb LA, Schmitt MP (2010) The ABC transporter HrtAB confers resistance to hemin toxicity and is regulated in a hemin-dependent manner by the ChrAS two-component system in *Corynebacterium diphtheriae*. *J Bacteriol* 192(18):4606–4617.
26. Pedersen MB, Garrigues C, Tuphile K, Brun C, Vido K, Bennedsen M, Møllgaard H, Gaudu P, Gruss A (2008) Impact of aeration and heme-activated respiration on *Lactococcus lactis* gene expression: Identification of a heme-responsive operon. *J Bacteriol* 190(14):4903–4911.
27. Fernandez A, Lechardeur D, Derré-Bobillot A, Couvé E, Gaudu P, Gruss A (2010) Two coregulated efflux transporters modulate intracellular heme and protoporphyrin IX availability in *Streptococcus agalactiae*. *PLoS Pathog* 6(4):e1000860.
28. Stauff DL, Skaar EP (2009) *Bacillus anthracis* HssRS signalling to HrtAB regulates haem resistance during infection. *Mol Microbiol*

72(3):763–778.

29. Stojiljkovic I, Hantke K (1994) Transport of haemin across the cytoplasmic membrane through a haemin-specific peripiasmic binding-protein- dependent transport system in *Yersinia enterocolitica*. *Mol Microbiol* 13(4):719–732.
30. Lansky IB, Lukat-Rodgers GS, Block D, Rodgers KR, Ratliff M, Wilks A (2006) The cytoplasmic heme-binding protein (PhuS) from the heme uptake system of *Pseudomonas aeruginosa* is an intracellular heme-trafficking protein to the δ-regioselective heme oxygenase. *J Biol Chem* 281(19):13652–13662.
31. Suits MDL, Pal GP, Nakatsu K, Matte A, Cygler M, Jia Z (2005) Identification of an *Escherichia coli* O157:H7 heme oxygenase with tandem functional repeats. *Proc Natl Acad Sci U S A* 102(47):16955–16960.
32. Thompson JM, Jones H a, Perry RD (1999) Molecular characterization of the hemin uptake locus (hmu) from *Yersinia pestis* and analysis of hmu mutants for hemin and hemoprotein utilization. *Infect Immun* 67(8):3879–92.
33. Wyckoff EE, Lopreato GF, Tipton KA, Payne SM (2005) *Shigella dysenteriae* ShuS promotes utilization of heme as an iron source and protects against heme toxicity. *J Bacteriol* 187(16):5658–5664.
34. Dailey HA, Dailey TA, Gerdes S, Jahn D, Jahn M, O'Brian MR, Warren MJ (2017) Prokaryotic heme biosynthesis: multiple pathways to a common essential product. *Microbiol Mol Biol Rev* 81(1):e00048-16.
35. Layer G, Jahn D, Deery E, Lawrence AD, Warren MJ (2010) Biosynthesis of heme and vitamin B12. *Compr Nat Prod II*:445–499.
36. Lobo SAL, Warren MJ, Saraiva LM (2012) Sulfate-reducing bacteria reveal a new branch of tetrapyrrole metabolism. *Adv Microb Physiol* 61:267–295.
37. Layer G, Reichelt J, Jahn D, Heinz DW (2010) Structure and function

of enzymes in heme biosynthesis. *Protein Sci* 19(6):1137–61.

38. Bali S, Lawrence AD, Lobo SA, Saraiva LM, Golding BT, Palmer DJ, Howard MJ, Ferguson SJ, Warren MJ (2011) Molecular hijacking of siroheme for the synthesis of heme and d1 heme. *Proc Natl Acad Sci U S A* 108(45):18260–5.
39. Dailey HA, Gerdes S, Dailey TA, Burch JS, Phillips JD (2015) Noncanonical coproporphyrin-dependent bacterial heme biosynthesis pathway that does not use protoporphyrin. *Proc Natl Acad Sci U S A* 112(7):2210–5.
40. Macieira S, Martins BM, Huber R (2003) Oxygen-dependent coproporphyrinogen-III oxidase from *Escherichia coli*: one-step purication and biochemical characterisation. *FEMS Microbiol Lett* 226:31–37.
41. Lash TD (2005) The enigma of coproporphyrinogen oxidase : How does this unusual enzyme carry out oxidative decarboxylations to afford vinyl groups ? *Bioorganic Med Chem Lett* 15:4506–4509.
42. Layer, G. Katrin, G. T. Teschner, V. Schünemann, D. Breckau, A. Masoumi, M. Jahn, Heathcote, P. , Trautwein, A. X. , Jahn D (2005) Radical S-adenosylmethionine enzyme coproporphyrinogen III oxidase HemN: functional features of the [4Fe-4S] cluster and the two bound S-adenosyl-L-methionines. *J Biol Chem* 280(32):29038–29046.
43. Möbius K, Arias-Cartin R, Breckau D, Hännig AL, Riedmann K, Biedendieck R, Schröder S, Becher D, Magalon A, Moser J, others (2010) Heme biosynthesis is coupled to electron transport chains for energy generation. *Proc Natl Acad Sci* 107(23):10436–10441.
44. Kobayashi K, Masuda T, Tajima N, Wada H, Sato N (2014) Molecular phylogeny and intricate evolutionary history of the three isofunctional enzymes involved in the oxidation of protoporphyrinogen IX. *Genome Biol Evol* 6(8):2141–2155.

45. Kato K, Tanaka R, Sano S, Tanaka A, Hosaka H (2010) Identification of a gene essential for protoporphyrinogen IX oxidase activity in the cyanobacterium *Synechocystis* sp. PCC6803. *Proc Natl Acad Sci* 107(38):16649–16654.
46. Dailey HA, Dailey TA, Wu C-K, Medlock AE, Rose JP, Wang K-F (2000) Ferrochelatase at the millennium: structures, mechanisms and [2Fe-2S] clusters. *Cell Mol Life Sci* 57(13):1909–1926.
47. Dailey TA, Dailey HA (2002) Identification of [2Fe-2S] clusters in microbial ferrochelatases. *J Bacteriol* 184(9):2460–2464.
48. Al-Karadaghi S, Hansson M, Nikonov S, Jönsson B, Hederstedt L (1997) Crystal structure of ferrochelatase: the terminal enzyme in heme biosynthesis. *Structure* 5(11):1501–1510.
49. Shepherd M, Dailey TA, Dailey HA (2006) A new class of [2Fe-2S]-cluster-containing protoporphyrin (IX) ferrochelatases. *Biochem J* 397(1):47.
50. Hunter G a., Sampson MP, Ferreira GC (2008) Metal ion substrate inhibition of ferrochelatase. *J Biol Chem* 283(35):23685–23691.
51. Layer G, Warren MJ (2012) Biosynthesis of Siroheme, Cofactor 430 and Heme *d1*. *Handbook of Porphyrin Science*, pp 111–138.
52. Palmer DJ, Schroeder S, Lawrence AD, Deery E, Lobo SA, Saraiva LM, Mclean KJ, Munro AW, Ferguson SJ, Pickersgill RW, Brown DG, Warren MJ (2014) The structure, function and properties of sirohaem decarboxylase - an enzyme with structural homology to a transcription factor family that is part of the alternative haem biosynthesis pathway. *Mol Microbiol* 93(2):247–261.
53. Kühner M, Haufschildt K, Neumann A, Storbeck S, Streif J, Layer G (2014) The alternative route to heme in the methanogenic archaeon *Methanosarcina barkeri*. *Archaea* 2014.
54. Lobo SAL, Lawrence AD, Romão C V., Warren MJ, Teixeira M, Saraiva LM (2014) Characterisation of *Desulfovibrio vulgaris* haem b

synthase, a radical SAM family member. *Biochim Biophys Acta - Proteins Proteomics* 1844(7):1238–1247.

55. Wang LY, Brown L, Elliott M, Elliott T (1997) Regulation of heme biosynthesis in *Salmonella typhimurium*: Activity of glutamyl-tRNA reductase (HemA) is greatly elevated during heme limitation by a mechanism which increases abundance of the protein. *J Bacteriol* 179(9):2907–2914.
56. Bibb LA, Kunkle CA, Schmitt MP (2007) The ChrA-ChrS and HrrA-HrrS signal transduction systems are required for activation of the *hmuO* promoter and repression of the *hemA* promoter in *Corynebacterium diphtheriae*. *Infect Immun* 75(5):2421–2431.
57. Frunzke J, Gätgens C, Brocker M, Bott M (2011) Control of heme homeostasis in *Corynebacterium glutamicum* by the two-component system HrrSA. *J Bacteriol* 193(5):1212–1221.
58. Levicán G, Katz A, de Armas M, Núñez H, Orellana O (2007) Regulation of a glutamyl-tRNA synthetase by the heme status. *Proc Natl Acad Sci U S A* 104(9):3135–3140.
59. O'Brian MR (2015) Perception and homeostatic control of iron in the rhizobia and related bacteria. *Annu Rev Microbiol* 69(1):229–245.
60. Qi Z, O'Brian MR (2002) Interaction between the bacterial iron response regulator and ferrochelatase mediates genetic control of heme biosynthesis. *Mol Cell* 9(1):155–162.
61. Hamza I, Chauhan S, Hassett R, O'Brian MR (1998) The bacterial Irr protein is required for coordination of heme biosynthesis with iron availability. *J Biol Chem* 273(34):21669–21674.
62. Zeilstra-ryalls JH, Kaplan S (1995) Aerobic and anaerobic regulation in *Rhodobacter sphaeroides* 2.4.1: the role of the *fnrL* Gene. 177(6):1496–1503.
63. Ranson-Olson B, Zeilstra-Ryalls JH (2008) Regulation of the *Rhodobacter sphaeroides* 2.4.1 *hemA* Gene by PrrA and FnrL. *J*

*Bacteriol* 190(20):6769–6778.

64. Ranson-Olson B, Jones DF, Donohue TJ, Zeilstra-Ryalls JH (2006) In vitro and in vivo analysis of the role of PrrA in *Rhodobacter sphaeroides* 2.4.1 *hemA* gene expression. *J Bacteriol* 188(9):3208–3218.
65. Rompf A, Hungerer C, Hoffmann T, Lindenmeyer M, Römling U, Groß U, Doss MO, Arai H, Igarashi Y, Jahn D (1998) Regulation of *Pseudomonas aeruginosa hemF* and *hemN* by the dual action of the redox response regulators Anr and Dnr. *Mol Microbiol* 29(4):985–997.
66. Krieger R, Rompf A, Schobert M, Jahn D (2002) The *Pseudomonas aeruginosa hemA* promoter is regulated by Anr, Dnr, NarL and Integration Host Factor. *Mol Genet Genomics* 267(3):409–417.
67. Page KM, Guerinot ML (1995) Oxygen control of the *Bradyrhizobium japonicum hemA* gene. *J Bacteriol* 177(14):3979–3984.
68. Nellen-Anthamatten D, Rossi P (1998) *Bradyrhizobium japonicum* FixK2, a crucial distributor in the FixLJ-dependent regulatory cascade for control of genes inducible by low oxygen Levels. *J Bacteriol* 180(19):5251–5255.
69. Ye RW, Tao W, Bedzyk L, Young T, Chen M, Li L (2000) Global gene expression profiles of *Bacillus subtilis* grown under anaerobic conditions. *J Bacteriol* 182(16):4458–65.
70. Chen L, Keramati L, Helmann JD (1995) Coordinate regulation of *Bacillus subtilis* peroxide stress genes by hydrogen peroxide and metal ions. *Proc Natl Acad Sci U S A* 92(18):8190–4.
71. Mancini S, Imlay J a. (2015) The induction of two biosynthetic enzymes helps *Escherichia coli* sustain heme synthesis and activate catalase during hydrogen peroxide stress. *Mol Microbiol* 96(4):744–63.
72. Schubert HL, Rose RS, Leech HK, Brindley AA, Hill CP, Rigby SEJ, Warren MJ (2008) Structure and function of SirC from *Bacillus*

*megaterium*: a metal-binding precorrin-2 dehydrogenase. *Biochem J* 415(2):257–63.

73. Spencer JB, Stolowich NJ, Roessner CA, Scott AI (1993) The *Escherichia coli* cysG gene encodes the multifunctional protein, siroheme synthase. *FEBS Lett* 335(1):57–60.
74. Warren MJ, Bolt EL, Roessner CA, Scott AI, Spencert JB, Woodcock SC (1994) Gene dissection demonstrates that the *Escherichia coli cysG* gene encodes a multifunctional protein. *Biochem J* 302:837–844.
75. Cole JA, Newman BM, White P (1980) Biochemical and genetic characterization of *nirB* mutants of *Escherichia coli* K12 pleiotropically defective in nitrite and sulphite reduction. *J Gen Microbiol* 120(2):475–483.
76. Warren MJ, Roessner CA, Santander PJ, Scott AI (1990) The *Escherichia coli cysG* gene encodes S-adenosylmethionine-dependent uroporphyrinogen III methylase. *Biochem J* 265(3):725–729.
77. Stroupe ME, Leech HK, Daniels DS, Warren MJ, Getzoff ED (2003) CysG structure reveals tetrapyrrole-binding features and novel regulation of siroheme biosynthesis. *Nat Struct Biol* 10(12):1064–73.
78. Hansen J, Muldbjerg M, Chérest H, Surdin-Kerjan Y (1997) Siroheme biosynthesis in *Saccharomyces cerevisiae* requires the products of both the *MET1* and *MET8* genes. *FEBS Lett* 401(1):20–24.
79. Raux E, McVeigh T, Peters SE, Leustek T, Warren MJ (1999) The role of *Saccharomyces cerevisiae* Met1p and Met8p in sirohaem and cobalamin biosynthesis. *Biochem J* 338 ( Pt 3:701–708.
80. Schubert HL, Raux E, Brindley AA, Leech HK, Wilson KS, Hill CP, Warren MJ (2002) The structure of *Saccharomyces cerevisiae* Met8p, a bifunctional dehydrogenase and ferrochelatase. *EMBO J* 21(9):2068–2075.

81. Leech HK, Raux-Deery E, Heathcote P, Warren MJ (2002) Production of cobalamin and sirohaem in *Bacillus megaterium*: an investigation into the role of the branchpoint chelatases sirohydrochlorin ferrochelatase (SirB) and sirohydrochlorin cobalt chelatase (CbiX). *Biochem Soc Trans* 30:610–613.
82. Raux E, Leech HK, Beck R, Schubert HL, Santander PJ, Roessner CA, Scott AI, Martens JH, Jahn D, Thermesr C, Rambach A, Warren MJ (2003) Identification and functional analysis of enzymes required for precorrin-2 dehydrogenation and metal ion insertion in the biosynthesis of sirohaem and cobalamin in *Bacillus megaterium*. *Biochem J* 370:505–516.
83. Lobo SAL, Brindley A, Warren MJ, Saraiva LM (2009) Functional characterization of the early steps of tetrapyrrole biosynthesis and modification in *Desulfovibrio vulgaris* Hildenborough. *Biochem J* 420(2).
84. Lobo SAL, Brindley AA, Romão C V., Leech HK, Warren MJ, Saraiva LM (2008) Two distinct roles for two functional cobaltochelatases (CbiK) in *Desulfovibrio vulgaris* Hildenborough. *Biochemistry* 47(21):5851–5857.
85. Lobo SAL, Videira MAM, Pacheco I, Wass MN, Warren MJ, Teixeira M, Matias PM, Romão C V., Saraiva LM (2017) *Desulfovibrio vulgaris* CbiK P cobaltochelatase: evolution of a haem binding protein orchestrated by the incorporation of two histidine residues. *Environ Microbiol* 19(1):106–118.
86. Raux-Deery E, Leech HK, Nakrieko KA, McLean KJ, Munro AW, Heathcote P, Rigby SEJ, Smith AG, Warren MJ (2005) Identification and characterization of the terminal enzyme of siroheme biosynthesis from *Arabidopsis thaliana*: A plastid-located sirohydrochlorin ferrochelatase containing A 2Fe-2S center. *J Biol Chem* 280(6):4713–4721.

87. Saha K, Webb ME, Rigby SEJ, Leech HK, Warren MJ, Smith AG (2012) Characterization of the evolutionarily conserved iron–sulfur cluster of sirohydrochlorin ferrochelatase from *Arabidopsis thaliana*. *Biochem J* 444(2):227–237.

88. Leustek T, Smith M, Murillo M, Singh DP, Smith AG, Woodcock SC, Awan SJ, Warren MJ (1997) Siroheme biosynthesis in higher plants. Analysis of an S-adenosyl-L-methionine-dependent uroporphyrinogen III methyltransferase from *Arabidopsis thaliana*. *J Biol Chem* 272(5):2744–52.

# Chapter 3

## Heme acquisition in prokaryotes

## 3.1 Heme uptake systems

Iron is an essential nutrient for almost all organisms, including bacteria, that in general, require iron for growth and virulence (1, 2). However, bacteria do not easily access the iron host as: i) Under physiological conditions, iron is in an insoluble form; ii) free iron is toxic to cells and therefore its amount in host cells is low; iii) iron is sequestered to limit iron acquisition by pathogenic bacteria as a defense mechanism, a phenomenon called nutritional immunity or iron withholding defense system (1, 3–5). Therefore, iron in the host is bound to proteins such as lactoferrin, transferrin and ferritin. In particular, the most abundant source of iron is found in hemeproteins (e.g. hemoglobin and myoglobin) (4–6). To access heme, the majority of bacterial pathogens produce hemolysins that lyse erythrocytes and release heme from hemoglobin. Heme is then captured by bacterial heme uptake systems and utililized as iron source or directly incorporated into heme containing enzymes where it acts as a cofactor, processes that are important for bacterial pathogenesis (3, 7, 8).

Several heme uptake systems are active in Gram-positive and Gram-negative bacteria and they all share a similar strategy for the import and degradation of heme. First, a set of surface receptor proteins recognize and bind heme and/or heme-containing proteins. Free heme is then transferred to inner-membrane transporters and translocated into the cytoplasm where it is used as a whole or is degraded by heme oxygenases to release its iron which is used as nutrient. However, heme uptake systems differ between Gram-negative and Gram-positive bacteria due to the presence of the outer membrane in Gram-negative bacteria, that constitutes an additional barrier for the transport of heme to the intracellular compartment.

### 3.1.1 Gram-negative heme uptake systems

The heme uptake systems of Gram-negative bacteria are well characterized and include two categories: those that bind heme or hemeproteins directly, and those that use extracellular secreted hemophores to bind hemeproteins (6). Both systems require the coupling of cytoplasmic membrane proton motive force and TonB–like proteins to transport heme across the outer membrane (3, 6).

*Direct heme uptake systems*

The direct heme uptake systems can be found in several Gram-negative bacteria such as the Hem system present in *Yersinia enterocolitica* (9, 10) and *Serratia marcescens* (11), the Chu system of *E. coli* (12), the Hmu system in *Yersinia pestis* (13) and *Porphyromonas gingivalis* (14), and the Shu system described in *Shigella dysenteriae* (15).

One of the better characterized direct heme uptake system is that of *Pseudomonas aeruginosa. Pseudomonas* heme uptake (Phu) system (Fig 3.1) is a non-hemophore heme uptake system that involves: i) an outer membrane receptor (PhuR), that is responsible for the binding of heme and heme-containing proteins; ii) a periplasmic heme transport protein (PhuT) that uses a TonB-dependent process to pass heme into the periplasm; iii) an inner membrane ABC transporter (PhuUVW) that transfers heme from the periplasmic space to the cytoplasm passing it to the cytoplasmic protein PhuS (2, 3); iv) a heme trafficking protein PhuS, that transfers heme to the *P. aeruginosa* heme oxygenase HemO, also called PigA (16) (Fig 3.1). The promotors of *phuR* and *phuSTUVW* were shown to be repressed by the ferric uptake regulator (Fur) under iron-replete conditions (17).

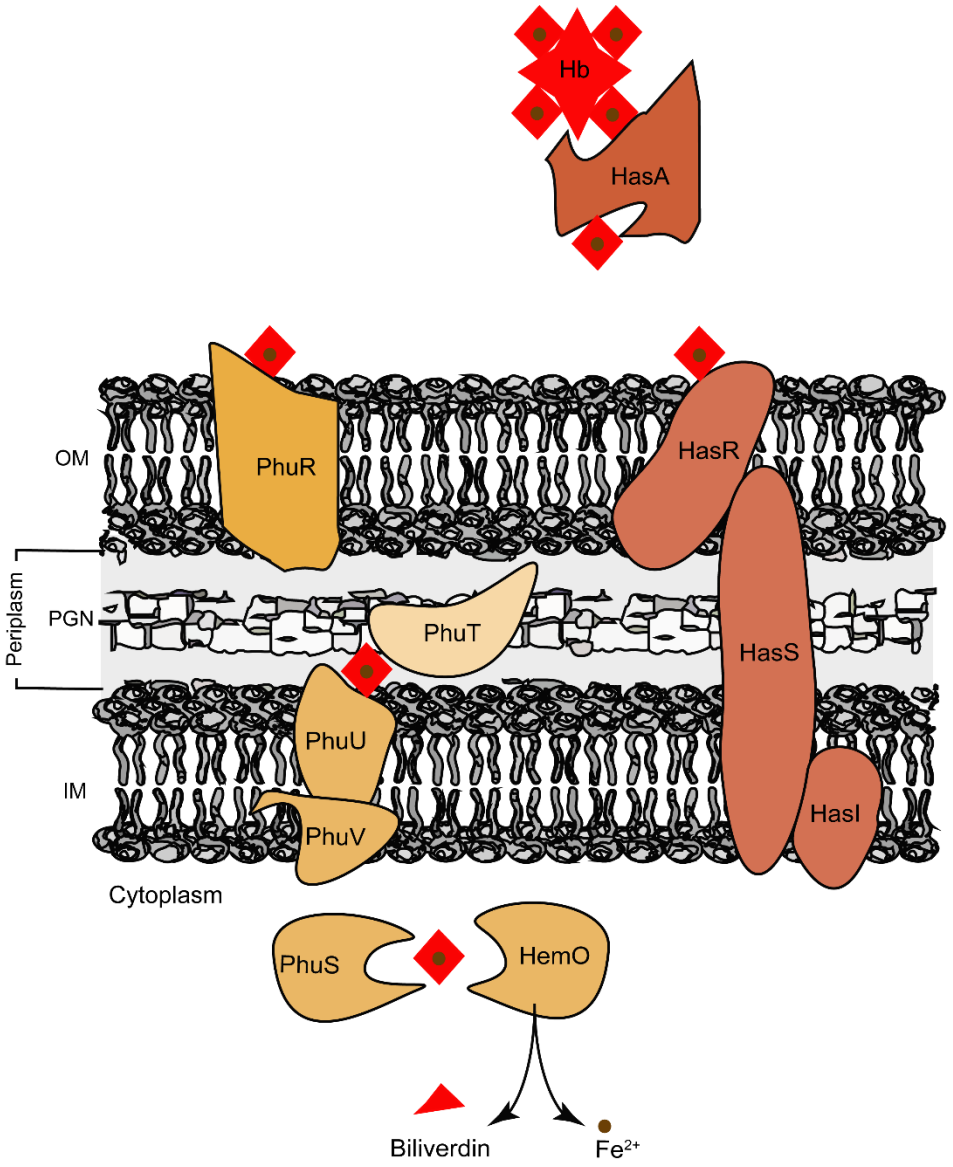


**Figure 3.1** Heme uptake system of *P. aeruginosa*. Direct heme uptake system via the Phu system and hemophore-mediated heme uptake via Has. Orthologue systems are present in other Gram-negative bacteria. Adapted from (3).

*Neisseria meningitidis* also imports heme through a direct heme uptake system using the hemoglobin receptor HmbR and the hemoglobin-haptoglobin utilization receptor HpuAB. The latter is a bipartite two-component receptor system which can be considered a third heme uptake system of Gram-negative bacteria. HpuAB is constituted by the lipoprotein HpuA, and the TonB-dependent transport protein HpuB (2, 18, 19). HpuAB acquires heme from hemoglobin and hemoglobin-haptoglobin complexes, while HmbR can only extract heme from hemoglobin (19, 20). Once heme is translocated into the cytoplasm is degraded by HemO to give iron (21). A Fur box is located upstream the promoter regions of *hmbR* and *hpuAB* genes, indicating that genes are regulated by Fur (3, 18).

*Haemophilus influenza* encodes a variety of heme uptake systems (22). The direct heme uptake by *H. influenza* involves the hemoglobin–haptoglobin binding proteins HgpA, HgpB, and HgpC that incorporate heme from hemoglobin-haptoglobin complexes (23–25), of which HgpB was shown to be the most efficient one (22). Additionally, *H. influenzae* expresses heme binding lipoprotein HpbA which is considered to be a periplasmic heme transporter protein (26). *Haemophilus influenza* lacks all proteins involved in heme biosynthesis except HemH, and thus it requires external heme for aerobic growth (27).

*Hemophore-mediated heme uptake system*

In Gram-negative bacteria, two hemophore-mediated heme uptake systems were identified so far, namely the heme acquisition system Has and the heme–hemopexin utilization HxuCBA. The Has system was characterized in *S. marcescens* (28), *P. aeruginosa* (29) (Fig 3.1), *Pseudomonas fluorescens* (30), and *Y. pestis* (31). In this system, hemophores such as HasA pick up free heme or, instead, extract heme from hemoglobin transferring it to the TonB-dependent outer-membrane receptor,

HasR (2, 32). However, HasR can also take up free heme without the need of a hemophore binding protein (33). Indeed, HasR activates a signaling cascade between the sigma factor HasI and anti-sigma factor HasS controlling the expression of *hasAR* which is dependent on the abundance of extracellular heme (32, 34). In *S. marcescens*, heme is transported across the membrane through HasR in a HasB dependent manner (35). Contrarily, *P. aeruginosa* does not encode a HasB homolog and thus utilizes a non-specific TonB-like protein or cytoplasmic and periplasmic components of the Phu system (32) (Fig 3.1).

A second hemophore-mediated heme uptake system was described in *H. influenza*, namely HxuCBA (36). Alternatively to the direct heme uptake system, *H. influenza* uses the HxuCBA system to acquire free heme and heme-hemopexin (36, 37). The hemophore HxuA is secreted by the HxuB and HxuC is the TonB-dependent transporter that imports heme to the periplasm (36). Additionally, HxuC can also utilize heme from heme–albumin (37).



### 3.1.2 Gram-positive heme uptake systems

The absence of outer membrane in Gram-positive bacteria precludes the necessity to utilize TonB-dependent transporters for heme import. Instead, the heme acquisition system of Gram-positive bacteria is equipped with surface receptors proteins for the binding of heme or hemeproteins, in some bacteria secreted hemophores, and ABC transporters for the transport of heme across the cytoplasmic membrane. The best characterized heme uptake system of Gram-positive organisms is the Isd system of *S. aureus* (Fig 3.2). *S. aureus* secretes hemolysins that lyse red blood cells, releasing hemoglobin (38). The surface exposed proteins IsdA, IsdB and IsdH bind free heme, hemoglobin and hemoglobin complexes (such as haptoglobin-hemoglobin), respectively (3). Upon removal of heme from hemoglobin by

IsdB and IsdA, the later transfers heme directly to the cell wall-anchored protein IsdC (38, 39). IsdH, IsdA, IsdB and IsdC are covalently anchored to peptidoglycan by sortases, namely sortase A surface expose IsdA/B/H and sortase B specifically buries IsdC into the cell wall (40, 41). IsdA, IsdH, IsdB and IsdC bind heme and hemeproteins through conserved Near-Iron Transport (NEAT) domains, which are 125 amino acid residues in an eight-stranded β-sandwich fold with a large hydrophobic heme-binding pocket (42). IsdC transfers heme to the membrane transporter IsdDEF which passes heme into the cytoplasm (38). After import, heme is incorporated into hemeproteins or degraded by IsdG or IsdI for the release of iron (43). The operons encoding the *S. aureus isd* acquisition system are regulated by Fur, that in environments with high concentration of iron represses *isdA*, *isdB*, *isdCDEFsrtBisdG*, and *isdI* (38). *S. aureus* mutants lacking genes of the *isd* system are defective in pathogenesis, demonstrating the importance of this system in this organism (44–47). However, this remains a controversial issue as IsdABH was reported in a mouse septic arthritis model to not contribute for the virulence of *S. aureus* (48).

In addition to the IsdDEF membrane transporter, *S. aureus* also utilizes the heme transport system (*htsABC)* for heme-iron acquisition across the membrane. This system encodes an ABC transporter permease, also regulated by Fur, and contributes to the pathogenecity of *S. aureus* (49).

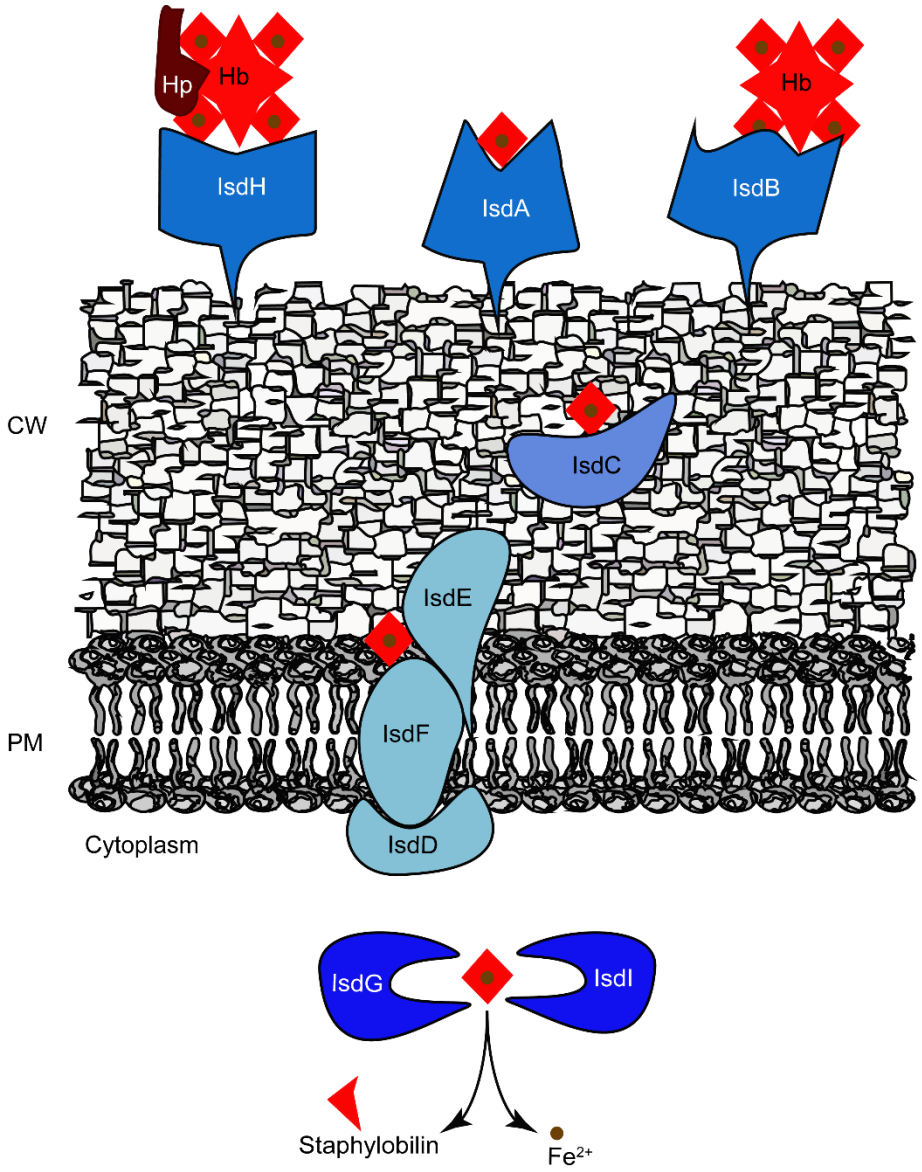


**Figure 3.2** Isd heme uptake system of *S. aureus*. Similar systems are present in other Gram-positive bacteria. Adapted from (3).

*Bacillus anthracis* also encodes an Isd system (50). Although the Isd system of *B. anthracis* is very similar to that of *S. aureus*, *B. anthracis* encodes two extra secreted hemophores, IsdX1 and IsdX2, which were the first hemophores identified in Gram-positive bacteria (51).

Other heme uptake systems are present in Gram-positive bacteria such as, the hemin uptake system HmuTUV, heme-transport associated HtaABC, ChtABC/CirA of *Corynebacterium diphterae* (52–54), Sia in *Streptococcus pyogenes* (55), and Isd of *Listeria monocytogenes* (56).

### 3.2 Heme oxygenases

Heme oxygenases (HO) are ubiquitous proteins that were firstly described in mammals for the protection of cells against the toxic effect of free heme (2). In bacteria, heme oxygenases are primarily responsible for the last step of the heme uptake system, which consists in the degradation of heme for the release of iron (2, 5, 57). However, some bacterial heme oxygenases were also shown to be implicated in relieving heme toxicity (58, 59). The bacterial heme oxygenases can be sub-divided in two classes: canonical heme oxygenases and non-canonical heme oxygenases. Canonical heme oxygenases use three oxygen molecules for the conversion of heme to α-biliverdin with the concomitant release of carbon monoxide (CO) and iron (60) while non-canonical enzymes although use oxygen in the reaction, the protein binding cause ruffling distortions in the heme molecule leading to the formation of new products (61) (Fig 3.3). Although canonical heme oxygenases are monomeric proteins that adopt an α-helical structural, non-canonical heme oxygenases adopt a ferredoxin-like α/β-sandwich fold (62).

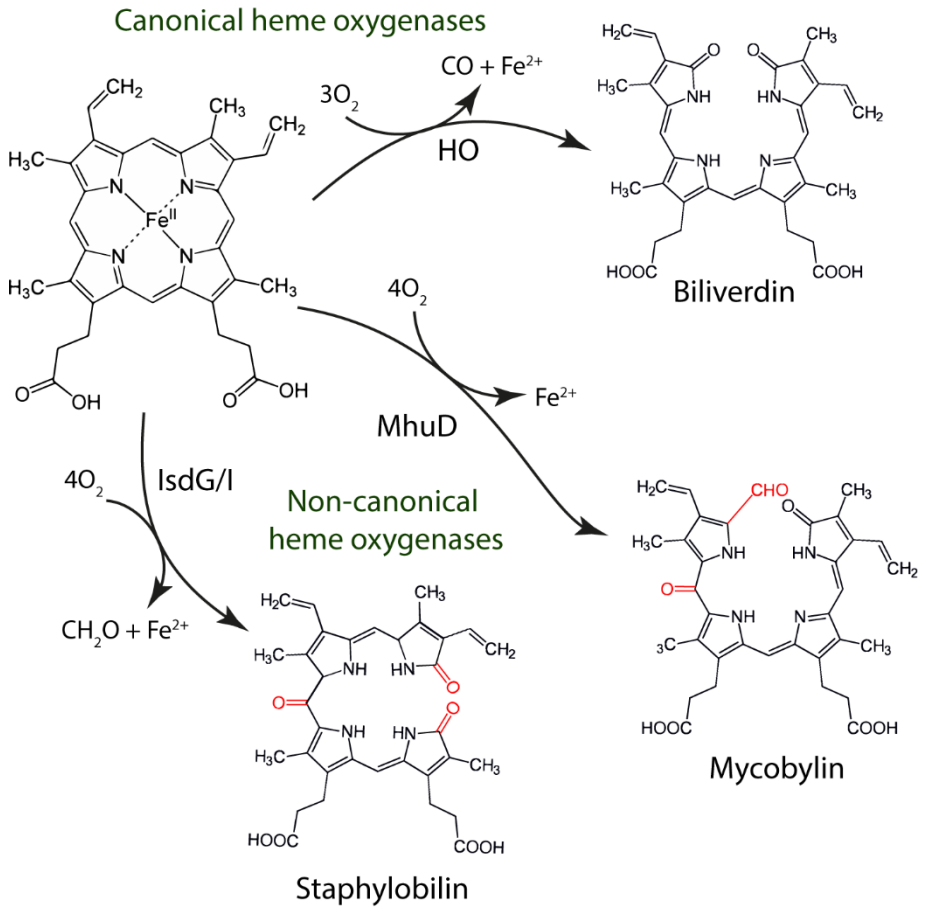


**Figure 3.3** Heme degradation products of canonical and non-canonical heme oxygenases. Adapted from (62).

The first canonical bacterial heme oxygenase was characterized in 1998, in *C. diphtheriae*, namely HmuO (63). Canonical heme oxygenases are monomeric proteins that adopt an α-helical structural fold as shown for HmuO of *C. diphtheriae* (Fig 3.4). As mentioned in the last chapter, HmuO is activated by the ChrA-ChrS and the HrrA-HrrS two-component systems when high levels of heme are present (64) and similar to Fur, *hmuO* is also controlled by the diphtheria toxin repressor protein DtxR (63).

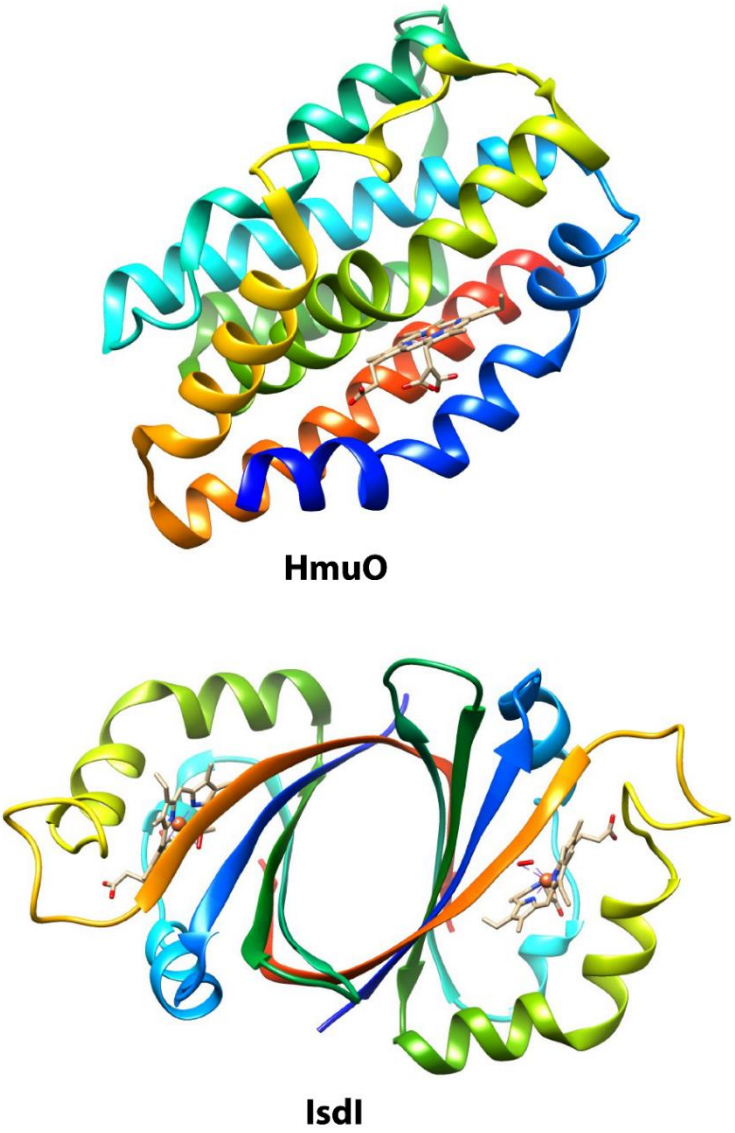


**Figure 3.4** Structure of HmuO (PDB 1IW0) from C. diphtheriae and IsdI (PDB 3LGN) from *S. aureus*. HmuO has an overall α-helical structural fold, characteristic of the HO family of HOs. IsdI adopts a ferredoxin-like α/β-sandwich fold, which is present in the IsdG-type of HO. The proteins are represented in ribbon format with heme bound molecules in stick format. The representation was done in UCSF Chimera.

Other examples of bacterial pathogens encoding canonical heme oxygenases include *N. meningitidis* (59), *Campylobacter jejuni* (65) and *P. aeruginosa* (66, 67). The last encodes HemO, which is an uncommon canonical heme oxygenase since it produces unusual β-biliverdin and δ-biliverdin isomers (66). Additionally, *P. aeruginosa* encodes another heme oxygenase, BphO, that produces the usual α-biliverdin (67).

Non-canonical heme oxygenases were first identified in *S. aureus* (43). *S. aureus* encodes two heme oxygenases, IsdG and IsdI, that were shown *in vitro* to bind and degrade heme to a mixture of β-oxo-δ-bilirubin and δ-oxo-β-bilirubin, named staphylobilin (68). Interestingly, the cleavage of heme by these enzymes liberates formaldehyde instead of CO like in the canonical heme oxygenases (69) (Fig 3.3). The IruO reductase serves as electron donor for heme degradation in *S. aureus* (70). Moreover, the concentration of IsdG and IsdI enzymes are regulated by iron and heme (43, 44). While both enzymes are expressed under iron-deplete conditions through a process regulated by Fur, only IsdG is targeted for degradation in the absence of heme (44). This process occurs through an amino acid motif that forms a flexible loop in the IsdG structure, which is absence from the sequence of IsdI (71). Unlike canonical heme oxyenases, IsdG and IsdI are homodimeric proteins with each monomer adopting a ferredoxin-like α/β-sandwich (Fig 3.4).

IsdG homologs are present in Gram-positive pathogens such as in *B. anthracis* (58) and *S. lugdunensis* (72). Another IsdG-like heme oxygenase, is the MhuD of *Mycobacterium tuberculosis* that converts heme into mycobilin and iron retaining the α-meso carbon as an aldehyde without releasing CO or formaldehyde (73) (Fig 3.3). Although *L. monocytogenes* Isd (74) and *B. subtilis* HmoB (75) are considered IsdG-like proteins, instead of homodimers, they are monomeric proteins that adopt a similar ferredoxin-like structure (74, 76). *B. subtilis* also encodes another heme oxygenase, namely HmoA, which gene is repressed by Fur in contrast to HmoB, and

phylogenetic analysis have shown to cluster separately from HmoB and other IsdG-like proteins (75).

An enzyme that does not fit in either canonical or non-canonical heme oxygenases is the ChuW of *E. coli*, a more recently discovered radical SAM enzyme that degrades heme to anaerobilin without using $O_2$ (77).

### 3.3 References


1. Weinberg ED (2009) Iron availability and infection. *Biochim Biophys Acta - Gen Subj* 1790(7):600–605.
2. Tong Y, Guo M (2009) Bacterial heme-transport proteins and their heme-coordination modes. *Arch Biochem Biophys* 481(1):1–15.
3. Choby JE, Skaar EP (2016) Heme synthesis and acquisition in bacterial pathogens. *J Mol Biol*:16–18.
4. Runyen-Janecky LJ (2013) Role and regulation of heme iron acquisition in Gram-negative pathogens. *Front Cell Infect Microbiol* 3:55.
5. Sheldon JR, Heinrichs DE (2015) Recent developments in understanding the iron acquisition strategies of gram positive pathogens. *FEMS Microbiol Rev* 39(4):592–630.
6. Huang W, Wilks A (2017) Extracellular heme uptake and the challenge of bacterial cell membranes. *Annu Rev Biochem* 86(April):799–823.
7. Reniere ML, Torres VJ, Skaar EP (2007) Intracellular metalloporphyrin metabolism in *Staphylococcus aureus*. *BioMetals* 20(3–4):333–345.
8. Benson DR, Rivera M (2013) Heme Uptake and Metabolism in Bacteria. *Metal Ions in Life Sciences*, pp 279–332.
9. Stojiljkovic I, Hantke K (1992) Hemin uptake system of *Yersinia enterocolitica*: similarities with other TonB-dependent systems in gram-negative bacteria. *EMBO J* 11(12):4359–4367.
10. Stojiljkovic I, Hantke K (1994) Transport of haemin across the

cytoplasmic membrane through a haemin-specific peripiasmic binding-protein- dependent transport system in *Yersinia enterocolitica*. *Mol Microbiol* 13(4):719–732.

11. Benevides-Matos N, Biville F (2010) The Hem and Has haem uptake systems in *Serratia marcescens*. *Microbiology* 156(6):1749–1757.
12. Torres a G, Payne SM (1997) Haem iron-transport system in enterohaemorrhagic *Escherichia coli* O157:H7. *Mol Microbiol* 23(4):825–833.
13. Hornung JM, Jones HA, Perry RD (1996) The *hmu* locus of *Yersinia pestis* is essential for utilization of free haemin and haem-protein complexes as iron sources. *Mol Microbiol* 20(4):725–739.
14. Olczak T, Simpson W, Liu X, Genco CA (2005) Iron and heme utilization in *Porphyromonas gingivalis*. *FEMS Microbiol Rev* 29(1):119–144.
15. Eakanunkul S, Lukat-Rodgers GS, Sumithran S, Ghosh A, Rodgers KR, Dawson JH, Wilks A (2005) Characterization of the periplasmic heme-binding protein ShuT from the heme uptake system of *Shigella dysenteriae*. *Biochemistry* 44(39):13179–13191.
16. Lansky IB, Lukat-Rodgers GS, Block D, Rodgers KR, Ratliff M, Wilks A (2006) The cytoplasmic heme-binding protein (PhuS) from the heme uptake system of *Pseudomonas aeruginosa* is an intracellular heme-trafficking protein to the δ-regioselective heme oxygenase. *J Biol Chem* 281(19):13652–13662.
17. Ochsner UA, Johnson Z, Vasil ML (2000) Genetics and regulation of two distinct haem-uptake systems, *phu* and *has*, in *Pseudomonas aeruginosa*. *Microbiology* 146(1):185–198.
18. Lewis L a, Gray E, Wang YP, Roe B a, Dyer DW (1997) Molecular characterization of *hpuAB*, the haemoglobin-haptoglobin-utilization operon of *Neisseria meningitidis*. *Mol Microbiol* 23(4):737–749.
19. Lewis LA, Sung MH, Gipson M, Hartman K, Dyer DW (1998) Transport

of intact porphyrin by HpuAB, the hemoglobin-haptoglobin utilization system of *Neisseria meningitidis*. *J Bacteriol* 180(22):6043–6047.

20. Stojijkovic I, Hwa V, de Saint Martin L, O'Gaora P, Nassif X, Heffron F, So M (1995) The *Neisseria meningitidis* haemoglobin receptor: its role in iron utilization and virulence. *Mol Microbiol* 15(3):531–541.
21. Zhu W, Wilks A, Stojiljkovic I (2000) Degradation of heme in gram-negative bacteria: the product of the *hemO* gene of *Neisseriae* is a heme oxygenase. *J Bacteriol* 182(23):6783–6790.
22. Morton DJ, VanWagoner TM, Seale TW, Whitby PW, Stull TL (2006) Differential utilization by *Haemophilus influenzae* of haemoglobin complexed to the three human haptoglobin phenotypes. *FEMS Immunol Med Microbiol* 46(3):426–432.
23. Jin H, Ren Z, Pozsgay JM, Elkins C, Whitby PW, Morton DJ, Stull TL (1996) Cloning of a DNA fragment encoding a heme-repressible hemoglobin-binding outer membrane protein from *Haemophilus influenzae*. *Infect Immun* 64(8):3134–3141.
24. Ren Z, Jin H, Morton DJ, Stull TL (1998) *hgpB*, a gene encoding a second *Haemophilus influenzae* hemoglobin-and hemoglobin-haptoglobin-binding protein. *Infect Immun* 66(10):4733–4741.
25. Morton DJ, Whitby PW, Jin H, Ren Z, Stull TL (1999) Effect of Multiple Mutations in the Hemoglobin-and Hemoglobin-Haptoglobin-Binding Proteins, HgpA, HgpB, and HgpC, of *Haemophilus influenzae* Type b. *Infect Immun* 67(6):2729–2739.
26. Morton DJ, Madore LL, Smith A, VanWagoner TM, Seale TW, Whitby PW, Stull TL (2005) The heme-binding lipoprotein (HbpA) of *Haemophilus influenzae*: Role in heme utilization. *FEMS Microbiol Lett* 253(2):193–199.
27. Panek H, O'Brian MR (2002) A whole genome view of prokaryotic haem biosynthesis. *Microbiology* 148(8):2273–2282.
28. Letoffe S, Ghigo JM, Wandersman C (1994) Iron acquisition from

heme and hemoglobin by a *Serratia marcescens* extracellular protein. *Proc Natl Acad Sci* 91(21):9876–9880.

29. Létoffé S, Redeker V, Wandersman C (1998) Isolation and characterization of an extracellular haem-binding protein from *Pseudomonas aeruginosa* that shares function and sequence similarities with the *Serratia marcescens* HasA haemophore. *Mol Microbiol* 28(6):1223–1234.
30. Idei A, Kawai E, Akatsuka H, Omori K (1999) Cloning and characterization of the *Pseudomonas fluorescens* ATP-binding cassette exporter, HasDEF, for the heme acquisition protein HasA. *J Bacteriol* 181(24):7545–51.
31. Rossi M, Fetherston JD, Létoffé S, Carniel E, Perry RD, Ghigo J (2001) Identification and Characterization of the Hemophore-Dependent Heme Acquisition System of *Yersinia pestis*. *Society* 69(11):6707–6717.
32. Smith AD, Wilks A (2015) Differential contributions of the outer membrane receptors PhuR and HasR to heme acquisition in *Pseudomonas aeruginosa*. *J Biol Chem* 290(12):7756–7766.
33. Létoffé S, Delepelaire P, Wandersman C (2004) Free and hemophore-bound heme acquisitions through the outer membrane receptor HasR have different requirements for the TonB-ExbB-ExbD complex. *J Bacteriol* 186(13):4067–4074.
34. Biville F, Cwerman H, Létoffé S, Rossi MS, Drouet V, Ghigo JM, Wandersman C (2004) Haemophore-mediated signalling in *Serratia marcescens*: A new mode of regulation for an extra cytoplasmic function (ECF) sigma factor involved in haem acquisition. *Mol Microbiol* 53(4):1267–1277.
35. Benevides-Matos N, Wandersman C, Biville F (2008) HasB, the *Serratia marcescens* TonB paralog, is specific to HasR. *J Bacteriol* 190(1):21–27.

36. Cope LD, Yogev R, Muller-Eberhard U, Hansen EJ (1995) A gene cluster involved in the utilization of both free heme and heme:hemopexin by *Haemophilus influenzae* type b. *J Bacteriol* 177(10):2644–53.
37. Morton DJ, Seale TW, Madore LL, VanWagoner TM, Whitby PW, Stull TL (2007) The haem-haemopexin utilization gene cluster (*hxuCBA*) as a virulence factor of *Haemophilus influenzae*. *Microbiology* 153(1):215–224.
38. Mazmanian SK, Skaar EP, Gaspar AH, Humayun M, Gornicki P, Jelenska J, Joachmiak A, Missiakas DM, Schneewind O (2003) Passage of heme-iron across the envelope of *Staphylococcus aureus*. *Science* 299(5608):906–9.
39. Liu M, Tanaka WN, Zhu H, Xie G, Dooley DM, Lei B (2008) Direct hemin transfer from IsdA to IsdC in the iron-regulated surface determinant (Isd) heme acquisition system of *Staphylococcus aureus*. *J Biol Chem* 283(11):6668–6676.
40. Mazmanian SK, Liu G, Ton-That H, Schneewind O (1999) *Staphylococcus aureus* sortase, an enzyme that anchors surface proteins to the cell wall. *Science* 285(5428):760–763.
41. Mazmanian SK, Ton-That H, Su K, Schneewind O (2002) An iron-regulated sortase anchors a class of surface protein during *Staphylococcus aureus* pathogenesis. *Proc Natl Acad Sci* 99(4):2293–2298.
42. Grigg JC, Vermeiren CL, Heinrichs DE, Murphy MEP (2007) Haem recognition by a *Staphylococcus aureus* NEAT domain. *Mol Microbiol* 63(1):139–149.
43. Skaar EP, Gaspar AH, Schneewind O (2004) IsdG and IsdI, heme-degrading enzymes in the cytoplasm of *Staphylococcus aureus*. *J Biol Chem* 279(1):436–443.
44. Reniere ML, Skaar EP (2008) *Staphylococcus aureus* haem

oxygenases are differentially regulated by iron and haem. *Mol Microbiol* 69(5):1304–1315.

45. Torres VJ, Pishchany G, Humayun M, Schneewind O, Skaar EP (2006) *Staphylococcus aureus* IsdB is a hemoglobin receptor required for heme iron utilization. *J Bacteriol* 188(24):8421–8429.
46. Cheng AG, Kim HK, Burts ML, Krausz T, Schneewind O, Missiakas DM (2009) Genetic requirements for *Staphylococcus aureus* abscess formation and persistence in host tissues. *FASEB J* 23(10):3393–3404.
47. Clarke SR, Mohamed R, Bian L, Routh AF, Kokai-Kun JF, Mond JJ, Tarkowski A, Foster SJ (2007) The *Staphylococcus aureus* surface protein IsdA mediates resistance to innate defenses of human skin. *Cell Host Microbe* 1(3):199–212.
48. Hurd AF, Garcia-Lara J, Rauter Y, Cartron M, Mohamed R, Foster SJ (2012) The iron-regulated surface proteins IsdA, IsdB, and IsdH are not required for heme iron utilization in *Staphylococcus aureus*. *FEMS Microbiol Lett* 329(1):93–100.
49. Skaar EP, Humayun M, Bae T, DeBord KL, Schneewind O (2004) Iron-source preference of *Staphylococcus aureus* infections. *Science* 305(5690):1626–8.
50. Fabian M, Solomaha E, Olson JS, Maresso AW (2009) Heme transfer to the bacterial cell envelope occurs via a secreted hemophore in the Gram-positive pathogen *Bacillus anthracis*. *J Biol Chem* 284(46):32138–32146.
51. Maresso AW, Garufi G, Schneewind O (2008) *Bacillus anthracis* secretes proteins that mediate heme acquisition from hemoglobin. *PLoS Pathog* 4(8):e1000132.
52. Drazek ES, Hammack CA, Schmitt MP (2000) *Corynebacterium diphtheriae* genes required for acquisition of iron from haemin and haemoglobin are homologous to ABC haemin transporters. *Mol*

*Microbiol* 36(1):68–84.

53. Allen CE, Schmitt MP (2009) HtaA is an iron-regulated hemin binding protein involved in the utilization of heme iron in *Corynebacterium diphtheria*. *J Bacteriol* 191(8):2638–2648.
54. Allen CE, Burgos JM, Schmitt MP (2013) Analysis of novel iron-regulated, surface-anchored hemin-binding proteins in *Corynebacterium diphtheriae*. *J Bacteriol* 195(12):2852–2863.
55. Sook BR, Block DR, Sumithran S, Montañez GE, Rodgers KR, Dawson JH, Eichenbaum Z, Dixon DW (2008) Characterization of SiaA, a streptococcal heme-binding protein associated with a heme ABC transport system. *Biochemistry* 47(8):2678–2688.
56. Jin B, Newton SMC, Shao Y, Jiang X, Charbit A, Klebba PE (2006) Iron acquisition systems for ferric hydroxamates, haemin and haemoglobin in *Listeria monocytogenes*. *Mol Microbiol* 59(4):1185–98.
57. Wilks A, Heinzl G (2014) Heme oxygenation and the widening paradigm of heme degradation. *Arch Biochem Biophys* 544:87–95.
58. Skaar EP, Gaspar AH, Schneewind O (2006) *Bacillus anthracis* IsdG, a heme-degrading monooxygenase. *J Bacteriol* 188(3):1071–80.
59. Zhu W, Hunt DJ, Richardson AR, Stojiljkovic I (2000) Use of heme compounds as iron sources by pathogenic Neisseriae requires the product of the *hemO* gene. *J Bacteriol* 182(2):439–47.
60. Wilks A (2002) Heme oxygenase: evolution, structure, and mechanism. *Antioxid Redox Signal* 4(4):603–14.
61. Graves AB, Horak EH, Liptak MD, Murphy ME, Wolinski K, Copeland TD, Waugh DS, Eastman MA, Rivera M (2016) Dynamic ruffling distortion of the heme substrate in non-canonical heme oxygenase enzymes. *Dalt Trans* 45(24):10058–10067.
62. Wilks A, Ikeda-Saito M (2014) Heme utilization by pathogenic bacteria: not all pathways lead to biliverdin. *Acc Chem Res*

47(8):2291–8.

63. Wilks A, Schmitt MP (1998) Expression and characterization of a heme oxygenase (HmuO) from *Corynebacterium diphtheriae*. *J Biol Chem* 273(2):837–841.

64. Bibb LA, Kunkle CA, Schmitt MP (2007) The ChrA-ChrS and HrrA-HrrS signal transduction systems are required for activation of the *hmuO* promoter and repression of the *hemA* promoter in *Corynebacterium diphtheriae*. *Infect Immun* 75(5):2421–2431.

65. Ridley KA, Rock JD, Li Y, Ketley JM (2006) Heme utilization in *Campylobacter jejuni*. *J Bacteriol* 188(22):7862–7875.

66. Ratliff M, Zhu W, Deshmukh R, Wilks A, Stojiljkovic I (2001) Homologues of neisserial heme oxygenase in Gram-negative bacteria: degradation of heme by the product of the *pigA* gene of *Pseudomonas aeruginosa*. *J Bacteriol* 183(21):6394–6403.

67. Wegele R, Tasler R, Zeng Y, Rivera M, Frankeinberg-Dinkel N (2004) The heme oxygenase(s)-phytochrome system of *Pseudomonas aeruginosa*. *J Biol Chem* 279(44):45791–45802.

68. Reniere ML, Ukpabi GN, Harry SR, Stec DF, Krull R, Wright DW, Bachmann BO, Murphy ME, Skaar EP (2010) The IsdG-family of haem oxygenases degrades haem to a novel chromophore. *Mol Microbiol* 75(6):1529–1538.

69. Matsui T, Nambu S, Ono Y, Goulding CW, Tsumoto K, Ikeda-Saito M (2013) Heme degradation by *Staphylococcus aureus* IsdG and IsdI liberates formaldehyde rather than carbon monoxide. *Biochemistry* 52(18):3025–3027.

70. Loutet SA, Kobylarz MJ, Chau CHT, Murphy MEP (2013) IruO is a reductase for heme degradation by IsdI and IsdG proteins in *Staphylococcus aureus*. *J Biol Chem* 288(36):25749–25759.

71. Reniere ML, Haley KP, Skaar EP (2011) The flexible loop of *Staphylococcus aureus* IsdG is required for its degradation in the

absence of heme. *Biochemistry* 50(31):6730–7.

72. Haley KP, Janson EM, Heilbronner S, Foster TJ, Skaar EP (2011) *Staphylococcus lugdunensis* IsdG liberates iron from host heme. *J Bacteriol* 193(18):4749–4757.
73. Nambu S, Matsui T, Goulding CW, Takahashi S, Ikeda-Saito M (2013) A new way to degrade heme: the *Mycobacterium tuberculosis* enzyme MhuD catalyzes heme degradation without generating CO. *J Biol Chem* 288(14):10101–9.
74. Duong T, Park K, Kim T, Kang SW, Hahn MJ, Hwang HY, Kim KK (2014) Structural and functional characterization of an Isd-type haem-degradation enzyme from *Listeria monocytogenes*. *Acta Crystallogr Sect D Biol Crystallogr* 70(3):615–626.
75. Gaballa A, Helmann JD (2011) *Bacillus subtilis* Fur represses one of two paralogous haem-degrading monooxygenases. *Microbiology* 157:3221–3231.
76. Park S, Choi S, Choe J (2012) *Bacillus subtilis* HmoB is a heme oxygenase with a novel structure. *BMB Rep* 45(4):239–41.
77. LaMattina JW, Nix DB, Lanzilotta WN (2016) Radical new paradigm for heme degradation in *Escherichia coli* O157:H7. *Proc Natl Acad Sci* 113(43):12138–12143.

# Results

# Chapter 4

## *Staphylococcus aureus* heme biosynthesis: characterization of the enzymes involved in final steps of the pathway

**This chapter was published in:**

Lobo SAL, Scott A, **Videira MAM**, Winpenny D, Gardner M, Palmer MJ, Schroeder S, Lawrence AD, Parkinson T, Warren MJ, Saraiva LM (2015) *Staphylococcus aureus* haem biosynthesis: characterisation of the enzymes involved in final steps of the pathway. *Mol Microbiol* 97(3):472–487.

MAMV is co-autor in this publication. MAMV performed a large number of the experiments, which included cloning procedures and protein production and purification, enzymatic activities of HemH and HemQ and *S. aureus* metabolite profile analysis. MAMV also interpeted the data and wrote the manuscript.

## 4.1. Summary

Heme is a life supporting molecule that is ubiquitous in all major kingdoms. In *Staphylococcus aureus*, the importance of heme is highlighted by the presence of systems both for the exogenous acquisition and endogenous synthesis of this prosthetic group. In this work, we show that in *S. aureus* the formation of heme involves the conversion of coproporphyrinogen III into coproporphyrin III by coproporphyrin synthase HemY, insertion of iron into coproporphyrin III via ferrochelatase HemH, and oxidative decarboxylation of Fe-coproporphyrin III into protoheme IX by Fe-coproporphyrin oxidase/dehydrogenase HemQ. Together, this route represents a transitional pathway between the classic pathway and the more recently acknowledged alternative biosynthesis machinery. The role of the heme biosynthetic pathway in the survival of the bacterium was investigated by testing for inhibitors of HemY. Analogues of acifluorfen are shown to inhibit the flavin-containing HemY, highlighting that this as a suitable target for the development of drugs against *S. aureus*. Moreover, the presence of this transitional pathway for heme biosynthesis within many Gram-positive pathogenic bacteria suggests that this route has the potential not only for the design of antimicrobials but also for the selective discrimination between bacteria operating different routes to the biosynthesis of heme.



## 4.2. Introduction

Heme is a remarkably versatile prosthetic group that is found in all kingdoms of life. It is an iron-containing modified tetrapyrrole (porphyrin), which belongs to the same family of compounds as the chlorophylls, corrins (vitamin $B_{12}$) and siroheme (1). Although some organisms, such as *Caenorhabditis elegans,* salvage heme from their environment (2) most organisms are able to synthesise the molecule *de novo*. Indeed, until

recently, it was largely accepted that heme is biosynthesized along a “classic” pathway, via four steps from the first common tetrapyrrole macrocyclic precursor uroporphyrinogen III (uro’gen III). These steps involve the selective decarboxylation of a number of the peripheral carboxylic acid side chains, macrocyclic ring oxidation and insertion of iron (Figure 4.1) (3).

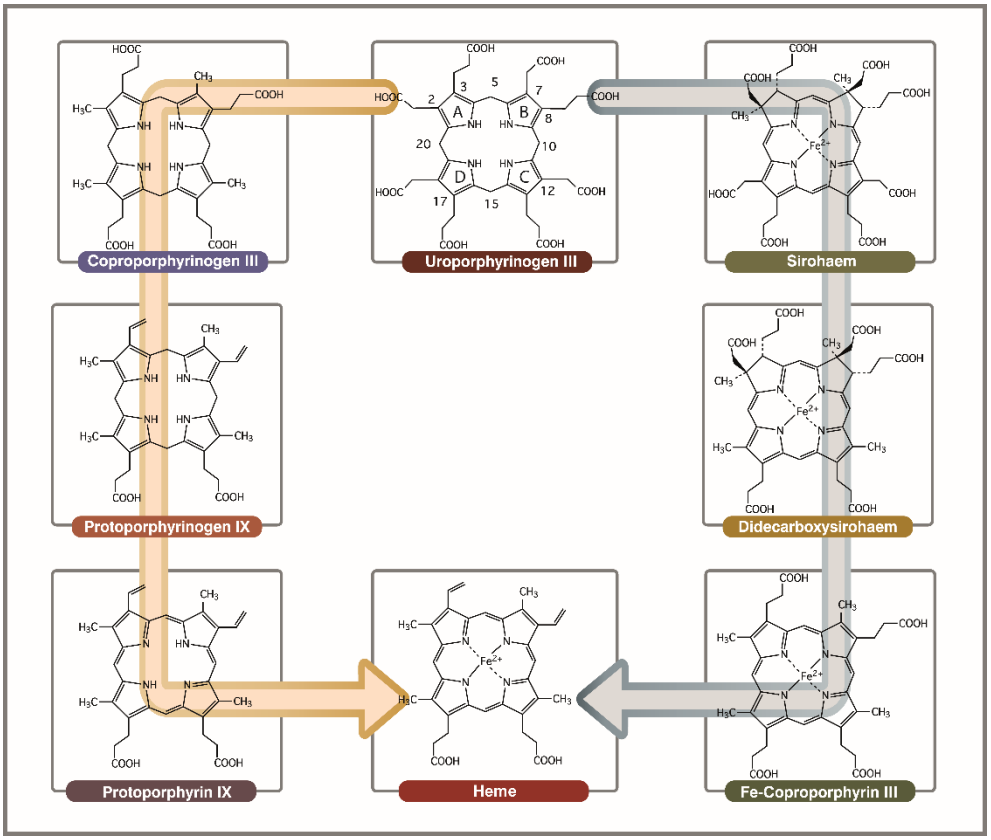


**Figure 4.1** Transformation of uro’gen III into heme via the classic and alternative heme biosynthetic pathways. The classic pathway proceeds via copro’gen III, proto’gen IX and protoporphyrin IX (highlighted with the orange arrow) whereas the alternative pathway proceeds via siroheme, didecarboxysiroheme and Fe-coproporphyrin III (highlighted with the green arrow).

The heme biosynthetic pathway is initiated by the formation of 5-aminolevulinic acid, the precursor of all naturally occurring tetrapyrroles, which is subsequently transformed into the first macrocyclic intermediate uro'gen III in three enzymatic steps that are catalyzed by HemB, C and D (3). Uro'gen III represents the first major branch point in the formation of modified tetrapyrroles from where the synthesis of molecules such as cobalamin and siroheme diverge from the synthesis of heme. For the classic heme pathway, all four acetic acid side chains of uro'gen III undergo decarboxylation, generating methyl groups, in a reaction catalyzed by the cofactor-free uro'gen decarboxylase (4). The product of this reaction, coproporphyrinogen III (copro'gen III), is transformed into protoporphyrinogen IX (proto´gen IX) by the oxidative decarboxylation of the two propionic acid side chains attached to rings A and B of the substrate by an enzyme called copro'gen oxidase (HemF) (5). Proto'gen IX is converted into protoporphyrin IX by the removal of six protons and six electrons in a reaction catalyzed by proto'gen oxidase (HemY), which requires FAD as cofactor (6, 7). Finally, protoheme IX is synthesized by the insertion of ferrous iron into the macrocyclic core of the maturing prosthetic group, a reaction catalyzed by protoporphyrin IX ferrochelatase (HemH) (8).

Some of the steps described for the classic pathway, in particular those involving HemF and HemY, are oxygen-dependent and, therefore, are only operative under aerobic conditions (5–7). Anaerobic versions of these enzymes which are oxygen independent are also found and hence many bacteria, for instance, have HemN as an anaerobic substitute for HemF, which employs S-adenosyl-L-methionine (SAM) as a radical to mediate decarboxylation via dehydrogenation of the substrate (9). Similarly, many bacteria utilize non-homologous isofunctional equivalents for HemY, such as HemJ, that works under aerobiosis (10, 11) and HemG that possesses proto´gen oxidase activity in aerobic or anaerobic conditions (12, 13). Thus, the classic heme synthesis pathway is able to operate under different

oxygenated conditions yielding the same intermediates via the engagement of orthologous enzymes.

Recently, we demonstrated that heme can be also made from siroheme (Figure 4.1), the prosthetic group of sulphite and nitrite reductases, through a pathway that is operative in sulphate reducing bacteria and archaea (14–16). In this “alternative heme biosynthesis” (Ahb) pathway, siroheme undergoes a *bis*-decarboxylation to give didecarboxysiroheme (DDSH) in a reaction mediated by siroheme decarboxylase (AhbA-B) (17). DDSH is subsequently converted into Fe-coproporphyrin III in a radical SAM mediated process via AhbC, which oversees the removal of the two acetic acid side chains attached to rings A and B of the substrate (14). The last step involves another radical SAM enzyme (AhbD) that is analogous to the HemN reaction in that it catalyses the oxidative decarboxylation of the two propionic acid side chains attached to C3 and C8 (Figure 4.1) via a dehydrogenation process that yields vinyl side chains, i.e. it converts Fe-coproporphyrin III to protoheme IX (18).

In an attempt to characterize the heme biosynthetic pathway in the pathogen *Staphylococcus aureus* with a view to screening for potential antibiotics, we identified a number of issues that challenged the idea that *S. aureus* makes heme via the classic pathway. An analysis of the *S. aureus* genome revealed the presence of genes encoding orthologues of canonical enzymes such as HemE, HemN, HemY and HemH. However, our initial characterisation of HemY demonstrated that this enzyme oxidizes copro’gen III in preference to proto’gen IX and, similarly, HemH preferably uses coproporphyrin III over protoporphyrin IX for iron insertion, a set of results that are shown herein. Moreover, recently, insightful research from Dailey and colleagues has demonstrated that some bacteria operate a pathway that combines aspects of the classic and the alternative pathways (19). They reported that copro’gen is oxidized to coproporphyrin, into which iron is then inserted to give Fe-coproporphyrin prior to the final step involving the

synthesis of the vinyl side chains in a reaction catalyzed by the pentameric enzyme HemQ (19, 20). In this work, we demonstrate that this “transitional” pathway, intermediary between the classic and alternative pathways, operates in *S. aureus* and we provide a detailed characterization of the enzymes involved. We have also attempted to exploit the biochemical differences found within the *S. aureus* heme biosynthetic pathway by screening for inhibitors of the HemY enzyme.

## 4.3. Materials and Methods

### Gene cloning and complementation assays

Genes were amplified by means of PCR standard reactions using the oligonucleotides presented in Table S4.1 (Supplementary data). Plasmids used in this work are shown in Table 4.1. All recombinant plasmids were sequenced and the integrity of the inserted DNA sequences was confirmed. *E. coli hemF* gene was amplified using as template the pCalhemF plasmid (21) (kind gift from Prof. Dieter Jahn, Technical University Braunschweig, Germany), and subsequently subcloned into previously digested NdeI and ScaI pET-14b (Novagen). *B. subtilis hemH* was amplified from genomic DNA of *B. subtilis* strain 168 (kind gift from Dr. Adriano Henriques, ITQB, Portugal) and inserted into pET-23b. *S. aureus hemE, hemY, hemQ and hemH* genes were amplified from the *S. aureus* NCTC 8325 genomic DNA and cloned separately into pET-23b and pET-28a vectors (Novagen).

**Table 4.1.** Plasmids used in this study.

| Recombinant vector | Restriction sites | Organism | Reference |
|---|---|---|---|
| pET-14b-*BmhemC* | - | *B. megaterium* | (22) |
| pET-14b-*DvhemC* | - | *D. vulgaris* | (23) |
| pET-14b-*DvhemD*$^{d}$ | - | *D. vulgaris* | (23) |
| pET-14b-*BmhemD* | - | *B. megaterium* | (22) |
| pET-14b-*HhemE HUROD* (S19F mutant) | - | Human | Gift from Dr. Sarah Woodcock |
| pET-23b-*SahemE* | NheI/HindIII | *S. aureus* | This study |
| pET-14b-*EchemF* | NdeI/ScaI | *E. coli* | This study |
| pET-23b-*SahemH* | NheI/HindIII | *S. aureus* | This study |
| pET-23b-*BshemH* | NheI/XhoI | *B. subtilis* | This study |
| pET-28a-*SahemY* | NdeI/HindIII | *S. aureus* | This study |
| pET-23b-*SahemQ* | NheI/HindIII | *S. aureus* | This study |
| pET-23b-*SahemHY* | - | *S. aureus* | This study |
| pET-23b-*SahemHQ* | - | *S. aureus* | This study |
| pET-23b-*SahemHQY* | - | *S. aureus* | This study |
| pCAL*hemF* | - | *E. coli* | (21) |

For the complementation assays, the *E. coli* ferrochelatase mutant (Δ*hemH*) (kind gift from Prof. Mark O´Brian State University of New York at Buffalo, NY, USA) (24) was used together with plasmids pET-23b harbouring combinations of *S. aureus hemY*, *hemQ* and *hemH* genes that were prepared by the link and lock method, which allows the consecutive cloning of genes with the reuse of the same restriction enzyme sites (25). Plasmids pET-23b, pET-23b-*SahemH*, pET-23b-*SahemQ*, pET-23b-*SahemHY,* pET-23b-*SahemHQ* and pET-23b-*SahemHQY* were transformed separately into chemically competent *E. coli* Δ*hemH* cells which were plated onto Luria Bertani (LB) agar containing ampicillin (100 μg.ml$^{-1}$) and hemin (10 μg.ml$^{-1}$), and incubated overnight, at 37 °C; the resultant colonies were streaked onto LB-antibiotic agar plates in the presence and absence of hemin to test for their viability.

**Production and purification of recombinant proteins**

BL21$^{STAR}$ DE3 pLysS (Novagen) cells were transformed separately with each recombinant plasmid and grown in LB medium, at 37 °C, to an $OD_{600}$ of 0.6. At this OD, 0.4 mM isopropyl β-D-1-thiogalactopyranoside (IPTG) was added and cells were grown for an extra 16–20 h, at 20 °C. For cells harbouring pET-23b-*SahemH* and pET-23b-*BshemH*, 8 mg.ml$^{-1}$ of iron in the form of $FeSO_4$ was added to the medium at the time of induction. Cells were harvested by centrifugation (11323 x*g*, 10 min) and pellets were resuspended in the appropriated lysis buffer. Cells expressing separately the Human HemE, *E. coli* HemF, *B. megaterium* HemC and HemD proteins were resuspended in 20 mM Tris-HCl pH 8, supplemented with 500 mM NaCl and 5 mM imidazole. The buffer used for cells harbouring the *S. aureus* HemY protein consisted of 50 mM Tris-HCl pH 8 (buffer A) with 50 mM NaCl, 10 % glycerol, 5 mM imidazole and 1 % Triton X-100. In this later case, prior to cell breakage, the suspension was incubated with 0.02 % benzonase, at room temperature, for a sufficient time to observe a significant decline of the solution´s viscosity.

Cell pellets were then lysed by sonication on ice-water slurry at 60 % amplitude, for 3 min and using 30 second bursts to allow for cooling. Insoluble material was removed by centrifugation at ~30000 *xg,* for 15 min, and at 4 °C. Each supernatant was loaded separately into a $Ni^{2+}$ Sepharose column (GE Healthcare), and the column was washed with the respective lysis buffer (without Triton X-100, in the case of *S. aureus* HemY) to which was added 5 and 50 mM imidazole. Proteins were eluted by applying a 400 mM imidazole containing lysis buffer and judged pure by SDS gel electrophoresis. Purified protein was buffer exchanged in a PD-10 column (GE Healthcare) loaded with buffer A with 150 mM NaCl, 20 % glycerol and 5 mM DTT. For the Human HemY, the buffer also contained 0.02 % Tween-20.

The purification of proteins from the BL21$^{STAR}$ DE3 pLysS cells expressing *S. aureus* HemE, HemQ, HemH *and B. subtilis* HemH required slightly different conditions. In this case, the harvested cells were resuspended in buffer A and disrupted by passing three times through a French Press, at 900 Psi, followed by centrifugation at ~30000 *xg*, for 30 min. Each supernatant was loaded onto a 3 ml $Ni^{2+}$ Sepharose column (GE Healthcare), previously equilibrated in buffer A plus 400 mM NaCl and 10 mM imidazole. A step gradient of imidazole in buffer A was applied and the proteins were eluted at 250 mM imidazole, concentrated in an Amicon Stirred Ultrafiltration Cell using a 10 kDa membrane (Millipore), and submitted to buffer exchange by means of a PD10 column (GE Healthcare) that used buffer A as running buffer.

In all cases, protein purity was evaluated by SDS-PAGE and the protein concentration was determined by the Pierce Bicinchoninc acid Protein Assay (Thermo Scientific) using Sigma protein standards. Protein molecular mass and quaternary structures were determined by passage through a Superdex 200 10/300GL column (GE, Healthcare), equilibrated with 50 mM sodium phosphate pH 7 buffer containing 150 mM NaCl and using protein standards from Sigma.

**Identification of HemY cofactors**

For protein ligand identification, samples were heat denatured in a heating block for 10 min and centrifuged at 12100 *xg,* for 5 min. The samples (50 µl) were injected into an ACE 5AQ column (dimensions 2.1 x 150 mm) connected to an Agilent 1100 HPLC with a flow rate of 1 $ml.min^{-1}$. Using as aqueous phase 0.1 % trifluoroacetic acid (TFA) (A) and as organic phase acetonitrile (B), the following elution gradient was applied: 20 % B for 10 min, linear gradient up to 50 % B during 20 min, linear gradient up to 100 % B for 10 min, 100 % B for 10 min and final re-equilibration to 20 % B, for 5 min.

Electrospray mass spectrometry (MS) was performed using in a Bruker microTOF-QII.

**Construction of *S. aureus hemH and hemQ* mutants**

*S. aureus* Newman *hemH* and *hemQ* non-polar mutants were constructed according to a method previously described (26). Briefly, the sequence upstream of the *hemH* (or *hemQ*) gene was amplified using two pairs of oligonucleotides HemHMutA/HemHMutB (HemQMutA/HemQMutB) and HemHMutC/HemHMutD (HemQMutC/HemQMutD) (Table S4.1, Supplementary data), which amplify DNA fragments located upstream (fragment A/B) and downstream (fragment C/D) of the *hemH* gene, respectively. Oligonucleotides HemHMutA (HemQMutA) and HemHMutD (HemQMutD) contained restriction sites for SacI and SalI, respectively and oligonucleotide HemHMutC (HemQMutC) contained a 5´ overhang sequence complementary to the 3´ of oligonucleotide HemHMutB (HemQMutB). Fragments A/B and C/D served as templates in a Splicing by Overlap Extension PCR reaction together with HemHMutA (HemQMutA) and HemHMutD (HemQMutD) oligonuleotides. The resultant A/D-PCR product was digested with SacI and SalI restriction enzymes, ligated to SacI-SalI linearized pIMAY vector, and transformed into *E. coli* DC10B (pIMAY and *E. coli* DC10B were a kind gift from the laboratory of T. J. Foster, Trinity College Dublin, Ireland). After confirming by sequencing the integrity of the final DNA fragment, the recombinant plasmid was electroporated into competent *S. aureus* Newman, and cells were plated onto trypic soy agar (TSA) supplemented with chloramphenicol 10 $\mu g.ml^{-1}$, and grown overnight at 28 °C. Single colonies were homogenized in 200 µl trypic soy broth (TSB), and the cell suspensions were diluted up to $10^{-3}$ fold. Each dilution was plated onto brain heart infusion agar (BHIA) supplemented with chloramphenicol 10 $\mu g.ml^{-1}$ (Cm10) and incubated overnight, at 37 °C, for the chromosomal

integration of pIMAY. Colony PCR analysis using oligonucleotides for the MCS site of pIMAY (Table S4.1, Supplementary data) allowed confirming the absence of extra plasmid DNA. Selected colonies were further checked by PCR for plasmid integration and localization using oligonucleotides HemHOutF/HemHMutA (HemQOutF/HemQMutA) and HemHOutF/HemHMutD (HemQOutF/HemQMutD). Plasmid excision from the genome was achieved by streaking overnight cultures onto TSA plus 10 $\mu g.ml^{-1}$ hemin (He10), and overnight incubation at 28 °C. Cells were then re-platted onto TSA containing 1 $\mu g.ml^{-1}$ anhydrotetracycline (ATc) and He10 and incubated for 2 days, at 28 °C. Large colonies were patched onto TSA plus ATc and He10, and TSA plus Cm10 and He10, and incubated overnight, at 37 °C. For identification of the clones containing the *hemH (*or *hemQ)* mutation, Cm10 sensitive colonies were screened by PCR using oligonucleotides HemHOutF (HemQOutF) and HemHOutR (HemQOutR) (Table S4.1, Supplementary data).

The absence of *hemH* or *hemQ* genes in *S. aureus* cells was also confirmed by gene expression analysis. Total RNA was extracted, using the High Pure RNA Isolation Kit (Roche), from *S. aureus hemH* and *hemQ* mutant cells previously grown in TSB medium containing He10, to an $OD_{600}$ of 1.5. RNA samples were purified from contaminant DNA by treatment with Ambion®TURBO DNA-*free*™ DNase kit (Life Technologies). cDNA was synthesized from the DNA-free RNA using the Transcriptor High Fidelity cDNA Synthesis Kit (Roche), and used as template in a PCR reaction done in the presence of oligonucleotides SaHemMutHF/SaHemMutHR, in the case of *hemH* mutant and SaHemMutQF/SaHemMutQR for the *hemQ* mutant (Table S4.1, Supplementary data).

**Activity assays**

Porphobilinogen, coproporphyrin III, Fe-coproporphyrin III, hemin and protoporphyrin IX were purchased from Frontier Scientific. In these assays, freshly prepared enzymes were used. All experiments, except when otherwise indicated, were done under anaerobic conditions in Coy model A-2463 and Belle Technology anaerobic chambers. Porphyrins were resolved by HPLC-MS on an Ace 5 AQ column attached to an Agilent 1100 series HPLC equipped with a diode array detector and coupled to a micrOTOF-Q II (Bruker) mass spectrometer, using the indicated solvents and gradients. Porphyrins were detected by their spectral absorbance at 390 and 400 nm. Unless otherwise indicated, reactions were done in buffer A loaded in magnetically stirred quartz cuvettes and recorded in a Shimadzu UV-1800 spectrophotometer, at room temperature. Kinetic parameters were obtained by plotting the substrate concentration against rate, and using a non-linear regression to determine $V_{max}$ and $K_M$ by fitting the data to the Michaelis-Menten equation in GraphPad Prism (GraphPad Software, La Jolla California USA). For the determination of the kinetic parameters of *S. aureus* and *B. subtilis* HemH coproporphyrin III ferrochelatase data were fitted more accurately when using a substrate inhibition equation ($\text{Activity} = \frac{Vmax}{1+\frac{Km}{[\text{Fe}]}+\frac{[\text{Fe}]}{Ki}}$) in GraphPad Prism.

*HemE from* S. aureus

A linked protein assay was used to test the *S. aureus* HemE activity. To this end, HemC and HemD$^{d}$ from *D. vulgaris* were first expressed and purified according to a previously described procedure (23). Enzymatic reactions were done by mixing 20 µg *S. aureus* HemE, 70 µg *D. vulgaris* HemC, 620 µg *D. vulgaris* HemD$^{d}$ with 1.3 mg porphobilinogen in a 2.5 ml final volume of buffer A supplemented with 150 mM NaCl, 20 % glycerol and 5 mM DTT. Control reactions were performed under the same conditions, but

omitting *S. aureus* HemE from the mixture. All reactions were incubated overnight, and the formation of uro´gen III and copro´gen III was evaluated by UV-visible spectroscopy and HPLC-MS analysis. Prior to the spectroscopic analysis, reactions were oxidized by addition of HCl to a final concentration of 0.1 M HCl. Samples for HPLC-MS analysis were first treated with 0.6 M HCl and centrifuged at 10500 *xg,* for 10 min, to remove the protein precipitates. Products separation was achieved by applying a binary gradient, at a flow rate of 0.2 $ml.min^{-1}$, composed by 0.1 % TFA (solvent A) and acetonitrile (solvent B). The column was first equilibrated with 20 % solvent B and after sample injection the concentration of solvent B was increased up to 100 % during 50 min.

*HemY from* S. aureus

For the HemY activity assays, copro´gen III and proto´gen IX substrates were produced enzymatically as follows. Copro´gen III was made by mixing 50 µg HemC, 50 µg HemD (both from *B. megaterium*), 100 µg HemE (Human) and 200 µM porphobilinogen in a final volume of 200 µl buffer A supplemented with 50 mM NaCl, 20 % glycerol and 5 mM DTT. Proto´gen IX was generated in reactions that contained all of the above indicated proteins plus 50 µg HemF (*E. coli*) and 0.2 % Tween 20. Reaction mixtures were incubated, at 37 °C, for 50 min to allow the reaction to reach completion. The newly synthesised substrate was used immediately before depletion by auto-oxidation. An aliquot was retained and treated with 1 M HCl and production of the appropriate substrate was analyzed by quantitative HPLC-MS. Samples (3 µl) were separated on a Waters Acquity UPLCT BEH C18 1.7 µm column, in a Waters Acquity UPLC apparatus using a flow rate of 0.4 $ml.min^{-1}$. The aqueous phase consisted in 0.1 % formic acid (A) and the organic phase contained 0.1 % formic acid in methyl cyanide (B). The following gradient was applied: 2 % B for 1.7 min; a linear gradient up to 98

% of 0.1 % B during 7 min; 98 % B for 1.7 min, and re-equilibration to 2 % B for 3.5 min.

HemY activity was measured aerobically in a Tecan Ultra or Fluorostar Optima plate reader (BMG Laboratories) using a 400 nm excitation filter and either a 615 nm or 620 nm emission filter. Reactions were done in black 96-well plates (Thermo-Matrix or Brand) with a final volume of 100 µl reaction buffer A with 13 nM HemY, 0-3 µM copro´gen III or proto´gen IX, 150 mM NaCl, 20 % glycerol and 5 mM DTT. When using the proto´gen IX substrate, 0.2 % Tween 20 was added to the buffer. The fluorescence increase was monitored for 20 min, at 37 °C. The relative fluorescence units were converted into concentration by interpolation of a calibration curve obtained with coproporphyrin III and protoporphyrin IX standards. The initial rate was calculated from the linear region of the graph. Due to the high auto-oxidation rate of the substrate, the background reaction was always subtracted from the rate of the enzyme reaction.

*HemH from* S. aureus *and* B. subtilis

The protoporphyrin IX stock solution was prepared by addition to the compound (1-3 mg) of 1-3 drops of 25 % $NH_4OH$, 500 µl Triton X-100 and 4.5 ml water, and its concentration was determined spectrophotometrically in 2.6 M HCl at 408 nm (ε= 297 $mM^{-1}cm^{-1}$). The coproporphyrin III stock solution was prepared as described for protoporphyrin IX, but with no Triton X-100 addition, and its concentration was determined spectrophotometrically in 0.1 M HCl by following the 548 nm absorbance band (ε= 16.8 $mM^{-1}cm^{-1}$).

The *S. aureus* HemH protoporphyrin IX ferrochelatase specific activity was measured by following the decrease in absorbance of protoporphyrin IX, at 408 nm. Enzymatic reaction mixtures contained 240 µg *S. aureus* HemH, 10 µM protoporphyrin IX and 0-150 µM iron in the form of $(NH_4)_2Fe(SO_4)_2$ in 1 ml final volume of buffer A.

The coproporphyrin III ferrochelatase specific activity of *S. aureus* and *B. subtilis* HemH was measured by following the absorbance decrease at 392 nm and using an extinction coefficient of 115 $mM^{-1}cm^{-1}$, which was determined in this work. The reaction contained 0.5-10 µg *S. aureus* HemH or 0.5-32 µg *B. subtilis* HemH, 10 µM coproporphyrin III and 0-12 µM of iron in 1 ml final volume of buffer A.

The ability of *S. aureus* HemH to insert iron into coproporphyrin III was also analyzed by HPLC. The reaction mixture contained *S. aureus* HemH (80 µg), coproporphyrin III (5 µM), iron (14 µM) in 0.5 ml buffer A, and the control reaction was prepared similarly but with no addition of the enzyme. After a 5 min incubation period, 0.6 M HCl was added to all reaction mixtures and all samples were centrifuged at 10500 *xg*, for 10 min. The tetrapyrrole products were separated by HPLC using 0.1 % TFA as solvent A and acetonitrile as solvent B, at a flow rate of 0.2 $ml.min^{-1}$; the column was first equilibrated with 20 % solvent B, followed by a linear gradient up to 50 % B (10 min), gradient up to 70 % B (10 min), gradient up to 100 % B (5 min) and washed with 100 % B for 5 min.

*HemQ from* S. aureus

Reaction mixtures containing *S. aureus* HemQ (0.5-1 mg), Fe-coproporphyrin III (15 µM) and $H_2O_2$ (1-5 molar equivalents) were prepared in 0.5 ml buffer A, and incubated for 5-30 min, and stopped by the addition of 0.6 M HCl. The precipitated protein was removed by centrifugation at 10500 *xg*, for 10 min. Samples were resolved by HPLC using 0.1 % TFA as solvent A and acetonitrile as solvent B, at a flow rate of 0.2 $ml.min^{-1}$. The column was firstly equilibrated with 20 % solvent B and the following conditions were used: linear gradient up to 50 % B (10 min), gradient up to 100 % B (17 min) and 100 % B for 8 min. Next, the masses of the several products were determined by HPLC-MS.

### Inhibition assays of *S. aureus* HemY

The inhibitors used in this work (Table S4.2, Supplementary data) were stored and serialised in 100 % DMSO, and the final concentration of DMSO in the assays was kept at 3 %. $IC_{50}$ values, i.e. the concentration required for 50 % inhibition, were determined in reactions containing 6.5 nM HemY, 60 nM copro´gen III and by varying the concentration of the inhibitors between 1.5 pM and 3 mM. Controls samples were run in the absence of the inhibitor to measure the 100 % response (reaction without enzyme) and 0 % response (for reactions performed in the presence of enzyme and substrate).

Enzyme activity was measured using a fluorescence plate reader assay under conditions similar to those described above for the *S. aureus* HemY activity assays. Fluorescence increase was monitored for 20 min and the initial rate calculated by linear regression; data were normalised using the 100 % and 0 % response control wells. $IC_{50}$ values were calculated by fitting the data to a four parameter logistic equation in GraphPad Prism (GraphPad Software, La Jolla California USA) and $K_i$ was estimated from the $IC_{50}$ using the Cheng-Prusoff equation $K_i=IC_{50}/(1+[S]/K_M)$ based on the assumption that all the inhibitors were competitive.



### *S. aureus m*etabolite profile analysis

Overnight cultures of *S. aureus* wild type and Δ*hemH* grown in TSB medium were inoculated 1:10 in fresh medium and cultured for another 8 h, at 37 °C. Cells were then diluted in 200 ml TSB, to an $OD_{600}$ of 0.1, and left to grow overnight at the same temperature. Cells collected by centrifugation were resuspended in 2 ml of 20 mM potassium phosphate pH 7.6 (buffer B),

and washed twice with the same buffer. Aliquots of 0.5 ml of the cell suspensions were incubated with lysostaphin from Sigma (1 $mg.ml^{-1}$, 100 µl) for 45 min, at 37 °C, after which the volume was adjusted with buffer B to a final volume of 1 ml. Cells were disrupted by passage into a French Press at 900 Psi, and centrifuged at ~11000 *xg*, for 15 min. Protein content of the cell-free lysates was quantified in a Nanodrop ND-2000C (Thermo Scientific). Cell-free lysates of *S. aureus* wild type and Δ*hemH* with the same protein concentration were prepared in buffer B (300 µl) and treated, at room temperature, with 0.6 M HCl, for 10 min. The precipitated proteins were removed by centrifugation at 10500 *xg,* for 10 min, and the extracted porphyrins were analyzed by HPLC-MS, using a binary gradient with 0.1 % TFA as solvent A and acetonitrile as solvent B, at a flow rate of 0.2 $ml.min^{-1}$. The column was first equilibrated with 20 % solvent B and after sample injection the concentration of solvent B was increased to 100 %. The total duration of each run was 50 min.

**Homology-based modeling of HemY**

The homology model of *S. aureus* HemY was created using an internal software package MoViT (Pfizer Inc.). The *B. subtilis* HemY crystal structure that shares 47.5 % sequence identity with *S. aureus* HemY was used as a template (PDB: 3I6D) (27). FAD and acifluorfen were docked with PyMOL by simple superimposition of the *B. subtilis* crystal structure with the homology model and merging the ligand and homology model coordinates into a single file. To assess the potential binding interactions of the novel inhibitors, the acifluorfen molecule was edited in PyMOL using the Build command to generate structures resembling the inhibitors.

## 4.4. Results

The *S. aureus* heme biosynthetic pathway was analyzed by studying the enzymes involved in the transformation of uro'gen III into protoheme IX, which was achieved by assaying their enzymatic activity and identifying the tetrapyrrole intermediates formed along the biosynthetic route.

### *S. aureus* uroporphyrinogen III decarboxylase HemE

The ability of the recombinant *S. aureus* uro´gen III decarboxylase HemE to convert uro´gen III into copro´gen III was investigated. The substrate, uro'gen III, was synthesised from porphobilinogen using the heme synthesis enzymes HemC and HemD$^{d}$ from *D. vulgaris* (23). Addition of *S. aureus* HemE to the reaction mixture of HemC and HemD$^{d}$ led to the formation of copro´gen III, as shown by UV-visible spectroscopy and HPLC-MS (Figure 4.2). Collectively, these results demonstrate that the *S. aureus* HemE is functional as uro´gen III decarboxylase.



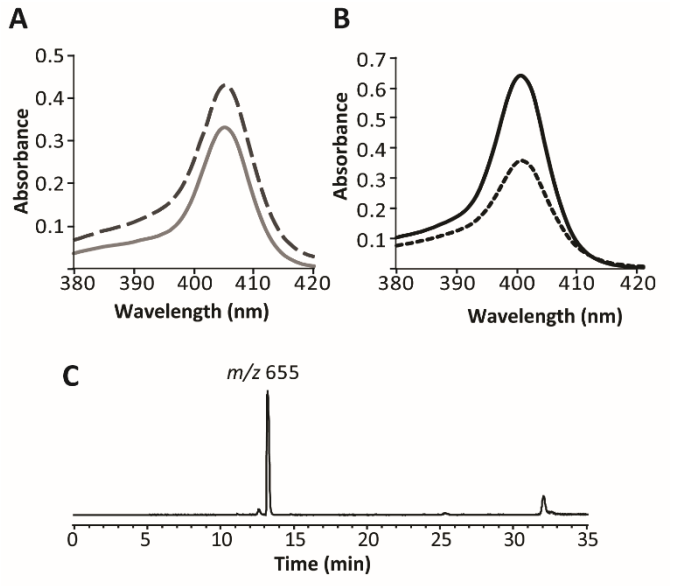


**Figure 4.2.** Analysis of the reaction product of *S. aureus* HemE. A. UV-visible spectra of the uroporphyrin III standard (filled line) and the oxidized form of the reaction product of *D. vulgaris*

HemC and HemD$^{d}$ (dotted line) dissolved in 0.1 M HCl. B. UV-visible spectra of the coproporphyrin III standard (filled line) and oxidized reaction product of *S. aureus* HemE (dotted line), in 0.1 M HCl. C. HPLC-MS extracted-ion chromatogram (EIC) of the reaction of *S. aureus* HemE at the expected *m/z* for coproporphyrin III, the oxidized form of copro´gen III, with the corresponding mass spectrum showing an *m/z* of 655.

### *S. aureus* coproporphyrinogen III oxidase HemY

The *S. aureus hemY* was cloned into pET-28a and transformed into *E. coli* for protein production. Cells expressing HemY exhibited a slight reddish colour whilst the supernatant had a pink coloration. This observation suggested that overproduction of *S. aureus* HemY leads to the accumulation of a porphyrin, some of which is excreted into the culture medium (7). After purification by immobilised metal affinity chromatography, the recombinant HemY was found to be yellow in colour, indicating the presence of a bound flavin. However, the UV-visible spectrum of the purified HemY failed to show the expected characteristics for a flavin, with maxima at 360 nm and 450 nm. Instead, a broad peak at 400 nm was observed, which may be due to the binding of porphyrin to HemY. Nevertheless, the presence of flavin could not be ruled out due to the broad peak at 400 nm that may mask the flavin spectrum. To investigate this possibility, HemY was denatured to allow the release of any bound material, and the supernatant was analyzed by HPLC-MS (Figure 4.3). Two compounds were detected: the first eluted at 5 min and had an absorbance spectrum typical of a flavin with peaks at 360 nm and 450 nm and *m/z* of 786, which corresponds to a FAD molecule (Figure 4.3A-B). The second compound, eluted at 15 min, had an absorbance peak at 400 nm and *m/z* of 653 (Figure 4.3C-D). This *m/z* value does not correspond to any known tetrapyrrole but it is only two units lower than the expected *m/z* of coproporphyrin III (655). It was concluded that the recombinant HemY is a

flavoprotein that also binds a tetrapyrrole molecule, and may therefore represent an enzyme-product complex.

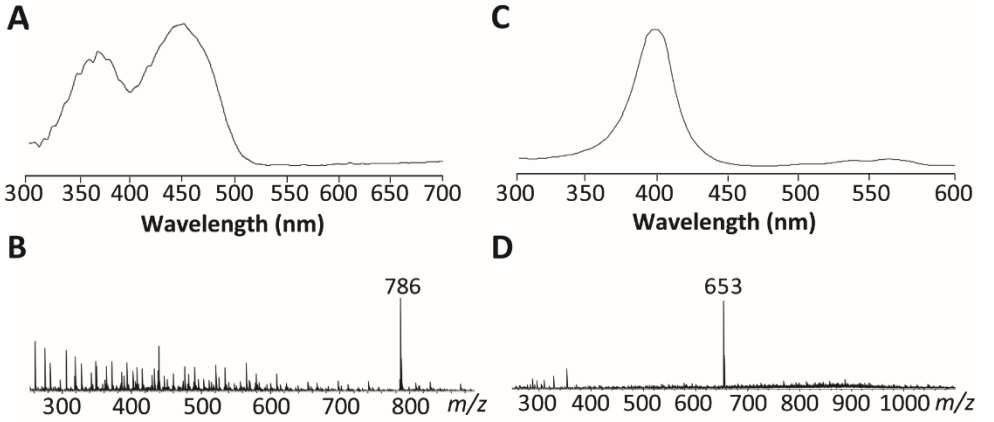


**Figure 4.3.** Analysis of the ligands bound to HemY. Recombinant, purified *S. aureus* HemY was heat-denatured and the supernatant was run on HPLC-MS to identify bound chromophores. A. Absorption spectra for the eluate at 5 min. The maxima at 360 nm and 450 nm are consistent with the presence of a flavin. B. The mass spectrum of the material identified in A. showing an *m/z* of 786, which corresponds to the molecular mass of FAD.C. Absorption spectra for the ligand eluting at 15 min. The absorption maximum at 400 nm suggests that the material is a porphyrin. D. The mass spectrum of the material identified in C showing an *m/z* of 653. The mass is close to the expected *m/z* of coproporphyrin (655).



The enzymatic activity of HemY for proto´gen IX was measured with a fluorescence plate reader assay, as described in the Materials and Methods. Due to the high auto-oxidation rate of porphyrinogen, the background reaction rate was measured and subtracted from the rate of the enzyme catalyzed reaction. Unexpectedly, no activity could be detected above the background rate when proto´gen IX was used as a substrate in concentrations up to 5 µM, even in the presence of the detergent Tween-20. In contrast, when copro´gen III was supplied, a significant porphyrinogen oxidase activity was detected that was dependent on the enzyme concentration. Incubation of copro'gen III with HemY resulted only in the

formation of coproporphyrin III, as confirmed by mass spectrometry (*m/z* 655), which negated the unlikely possibility that HemY may be able to convert coproporphyrin III into protoporphyrin IX. The kinetic parameters of HemY for coproporphyrin III synthase activity were as follows: maximal specific activity of 24.6 ± 0.7 nmol.min$^{-1}$mg$^{-1}$, $k_{cat}$ of 1.33 ± 0.04 min$^{-1}$ and $K_M$ of 0.31 ± 0.01 μM. Reactions performed in the presence of Tween-20 led to an approximate 4-fold increase in $K_M$, but did not alter the $V_{max}$ value. Thus, while *S. aureus* HemY can oxidise copro´gen III to coproporphyrin III it is unable to oxidise proto´gen IX to protoporphyrin IX.

### *S. aureus* coproporphyrin III ferrochelatase

The recombinant *S. aureus* HemH specific activity for iron insertion into protoporphyrin IX was determined to be 10.1 ± 0.1 nmol.min$^{-1}$mg$^{-1}$. The dependence of the activity of HemH on iron concentration was obtained by non-linear regression to a Michaelis-Menten equation, which resulted in the determination of $k_{cat}$ as 15.3 ± 0.6 min$^{-1}$ and a $K_M$ for iron of 52 ± 5 μM (Figure 4.4A).

As *S. aureus* HemY proved to oxidise copro´gen III, but not proto'gen IX, to the corresponding porphyrin, we therefore tested whether the *S. aureus* ferrochelatase, HemH, could use coproporphyrin III as substrate for metal chelation. The ability of *S. aureus* HemH to insert iron into coproporphyrin III was initially examined by incubating HemH with coproporphyrin III and iron, and analysing the products of the reaction by HPLC (Figure 4.5). While the control reaction, which contained all the components except HemH, gave only a single peak corresponding to the substrate, coproporphyrin III (Figure 4.5B), and addition of HemH led to the complete conversion of coproporphyrin III into Fe-coproporphyrin III (Figure 4.5B). To obtain the kinetic parameters of HemH for the iron insertion into coproporphyrin III, the

consumption of coproporphyrin III was determined by following the decrease of the Soret band at 392 nm. Analysis of these data revealed that *S. aureus* HemH inserts iron into coproporphyrin III with a specific activity of 815 ± 30 $nmol.min^{-1}mg^{-1}$, a $k_{cat}$ of 165 ± 54 $min^{-1}$ and an apparent $K_M$ for iron of 0.6 ± 0.1 μM. Since the activity of *S. aureus* HemH was inhibited by iron concentrations higher than 0.8 μM, the data was fitted with a substrate inhibition equation (see Materials and Methods) which allowed the determination of an apparent substrate binding inhibitory constant ($K_i$) of 0.8 ± 0.2 μM (Figure 4.4B).

For comparison purposes, the ability of the Gram-positive bacterium *B. subtilis* HemH to insert iron into coproporphyrin III was evaluated. This enzyme also catalyses the metallation of coproporphyrin with a specific activity of 110 ± 7 $nmol.min^{-1}mg^{-1}$, an apparent $K_M$ of 0.15 ± 0.03 μM and a $k_{cat}$ of 78 ± 9 $min^{-1}$. As with the *S. aureus* enzyme, the *B. subtilis* HemH kinetic data were fitted more accurately using a substrate inhibition equation with a $K_i$ of 2.8 ± 0.5 μM (Figure 4.4C).

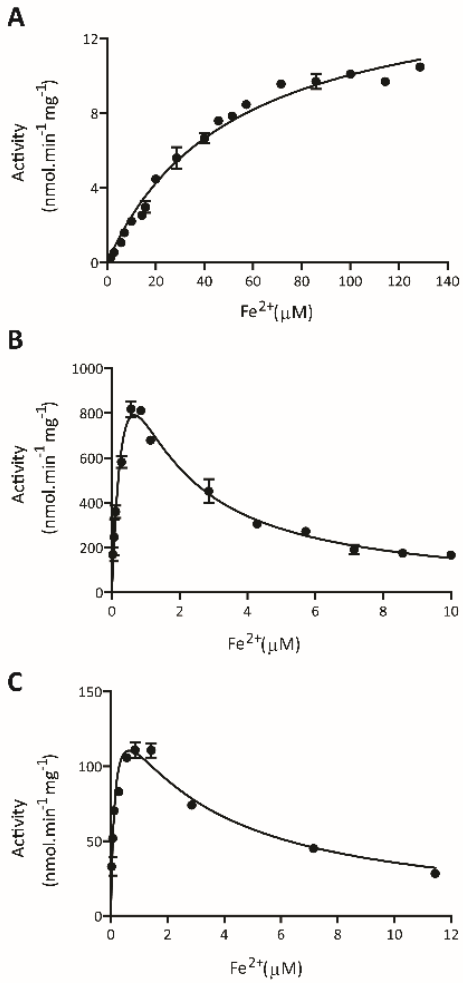


**Figure 4.4.** Activity profiles of *S. aureus* and *B. subtilis* HemH ferrochelatases for different porphyrin substrates and dependence on iron concentration. A. *S. aureus* HemH activity with protoporphyrin IX and iron (1 - 140 μM); data were fitted to the Michaelis-Menten equation, which provided a $k_{cat}$ of 15.3 ± 0.6 $min^{-1}$ and a $K_M$ for iron of 52 ± 5 μM. B. *S. aureus* HemH activity profile with coproporphyrin III and iron (0.02 - 10 μM); data were fitted with a substrate inhibition equation and the following parameters were determined: $k_{cat}$ of 165 ± 54 $min^{-1}$, $K_M$ of 0.6 ± 0.1 μM and a $K_i$ of 0.8 ± 0.2 μM. C. *B. subtilis* HemH activity using coproporphyrin III and iron (0.02 - 12 μM); data were fitted with a substrate inhibition equation from which a $k_{cat}$ of 78 ± 9 $min^{-1}$, $K_M$ of 0.15 ± 0.03 μM and $K_i$ of 2.8 ± 0.5 μM were calculated.

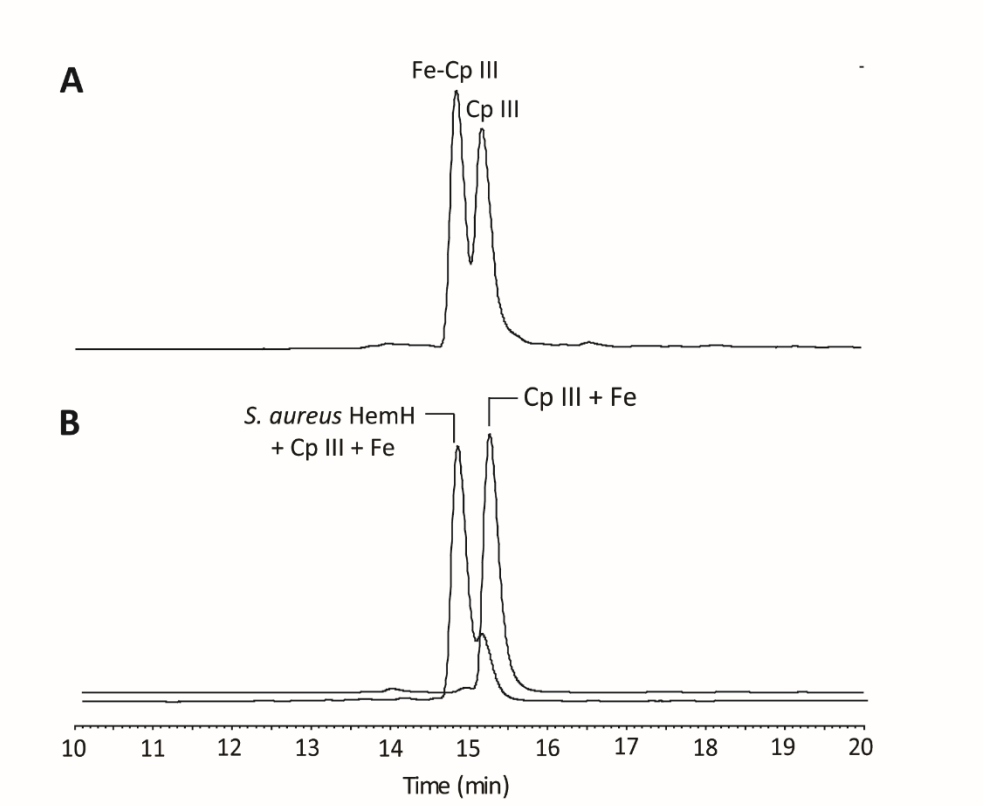


**Figure 4.5.** Conversion of coproporphyrin III into Fe-coproporphyrin III by *S. aureus* HemH. A. HPLC chromatogram of coproporphyrin III (Cp III) and Fe-coproporphyrin III (Fe-Cp III) standards, at 390 and 400 nm. B. HPLC chromatogram of the reaction product of *S. aureus* HemH using iron and coproporphyrin III as substrates (*S. aureus* HemH + Cp III + Fe), and of the control reaction done in the presence of all components except HemH (Cp III + Fe).



### *S. aureus* Fe-coproporphyrin III oxidase/dehydrogenase

Taking into account the substrate preferences of *S. aureus* HemY and HemH, the ability of HemQ to convert Fe-coproporphyrin III, the product of *S. aureus* HemH, into protoheme IX was investigated. The *S. aureus hemQ* was cloned into pET23b and the recombinant protein was purified from suitably transformed *E. coli* cells by immobilised metal affinity

chromatography. In assays with Fe-coproporphyrin III, and in the absence of any electron acceptor, the recombinant *S. aureus* HemQ converted only a very minor proportion (around 1 %) of Fe-coproporphyrin III into protoheme IX (Figure 4.6A). However, a significant increase in protoheme IX synthesis activity was observed upon the addition of the strong oxidizer $H_2O_2$ (Figure 4.6B-D). Reactions performed in the presence of one molar equivalent of $H_2O_2$ led to the formation of significant amounts of protoheme IX as well as the generation of the mono-vinyl intermediate (Figure 4.6B). The complete conversion of Fe-coproporphyrin III into protoheme IX by HemQ was achieved by the addition of 5 molar equivalents of $H_2O_2$ (Figure 4.6D).

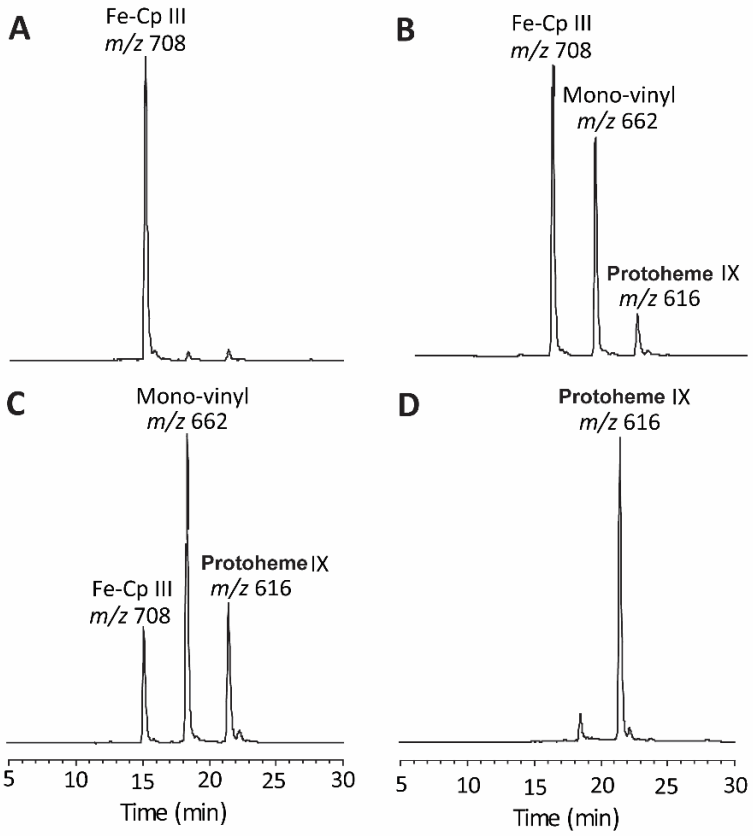


**Figure 4.6.** Conversion of Fe-coproporphyrin III into protoheme IX by *S. aureus* HemQ. HPLC chromatograms of the reaction products of *S. aureus* HemQ recorded at 390 nm. The reactions were incubated for 5 minutes. The mass spectrum showed several *m/z* values: 708 for the peak eluting at ~15 min consistent with Fe-coproporphyrin III (Fe-Cp III); 662 for the peak eluting at ~18 min corresponding to the mass of the mono-vinyl intermediate; and 616 at ~21 min for protoheme IX. A. Incubation of HemQ with Fe-Cp III. B. Incubation of HemQ with Fe-Cp III in the presence of one molar equivalent of $H_2O_2$ leading to the appearance of the mono-vinyl intermediate and of the final product protoheme IX. C. Products of the reaction of HemQ achieved as in B but with the addition of 4 molar equivalents of $H_2O_2$, were a decrease in Fe-Cp III and increase of the mono-vinyl and protoheme IX peaks can be observed. D. Products of the reaction of HemQ achieved as in B, but with the addition of 5 molar equivalents of $H_2O_2$. In this reaction, the full conversion of Fe-Cp III into protoheme IX was observed.

Previous reports indicated that *S. aureus* HemQ binds exogenous hemin (20, 28). In agreement, incubation of the *E. coli* supernatant containing overexpressed *S. aureus* HemQ with hemin, prior to purification of the protein on a nickel-column, yielded protein with 1 mol of protoheme IX/HemQ pentamer. This complex exhibited a typical protoheme IX-bound UV-visible spectrum (Figure S4.1, Supplementary data). To examine whether the bound prosthetic group modifies the protein activity, the hemin-loaded HemQ was incubated with Fe-coproporphyrin III in the presence and in the absence of $H_2O_2$, and the reaction products analyzed. Since under these conditions it is not possible to differentiate between protoheme IX formed during the reaction from that released from hemin-bound HemQ, the consumption of Fe-coproporphyrin III was monitored. The amount of Fe-coproporphyrin III remaining in the reaction mixture after incubation with HemQ or with hemin-loaded HemQ was found to be similar (Figure S4.2, Supplementary data). These results indicate that the presence of a heme cofactor bound to the enzyme does not seem to modify the biochemical and enzymatic properties of HemQ, in agreement with what was previously observed for the *Mycobacterium tuberculosis* HemQ (19).

### *S. aureus hemH* mutant generate small colony variants

We observed that *S. aureus* Δ*hemH* colonies grow poorly on tryptic soy agar (TSA) plates when compared to the wild type strain, forming the so-called small colony variants (SCVs) (29), and that the wild type phenotype was rescued by supplementation with exogenous hemin (Figure S4.3, Supplementary data). Tetrapyrrole intermediates of Δ*hemH* and parental strains were analyzed in cultures grown aerobically by means of HPLC-MS (Figure 4.7). In contrast to the wild type, Δ*hemH* accumulated coproporphyrin III (*m*/*z* = 655), which is consistent with a heme biosynthetic pathway of *S.*

*aureus* that proceeds via the coproporphyrin III and Fe-coproporphyrin III intermediates.

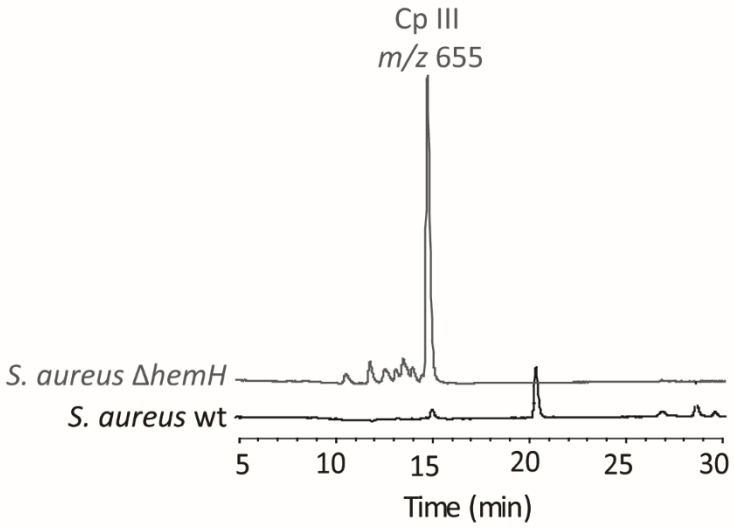


**Figure 4.7.** Porphyrin metabolite profile of *S. aureus* wild type and Δ*hemH strains*. HPLC-MS traces, recorded at 400 nm, of cell free extracts of *S. aureus* wild type (lower line) and Δ*hemH* (upper line), where the accumulation of coproporphyrin III (Cp III) in the Δ*hemH* mutant is observed.



## Complementation of the *E. coli* Δ*hemH* mutant strain with *S. aureus* heme synthesis enzymes

The data above showed that the *in vitro* formation of heme in *S. aureus* from uro´gen III involves HemQ, HemY and HemH. To analyse the *in vivo* function of these gene products, complementation assays were performed in the background of the *E. coli* Δ*hemH* mutant using combinations of *S. aureus hemH*, *hemY* and *hemQ* genes (Table 4.1). The data demonstrated that the genetic deficiency of the *E. coli* Δ*hemH* mutant

is only overcome when the three genes are expressed simultaneously (Table 4.2). Similar results were obtained for other Gram-positives bacteria (28).

Together, these data are consistent with HemY, HemH and HemQ acting as a copro'gen III oxidase, coproporphyrin III ferrochelatase, and Fe-coproporphyrin III oxidase/dehydrogenase, respectively, along a transitional route that is intermediary between the classic and alternative pathways.

**Table 4.2.** Complementation of the *E. coli* Δ*hemH* with plasmids expressing *S. aureus* HemH, HemY and HemQ. *E. coli* Δ*hemH* cells harbouring the recombinant plasmids were streaked onto LB-antibiotic agar plates in the absence and presence of hemin (10 μg.ml$^{-1}$) to test for their viability. (+) represents growth and (-) represents absence of growth.

| Recombinant plasmids | LB agar plus hemin | LB agar |
|---|---|---|
| pET-23b | + | - |
| pET-23b-*SahemH* | + | - |
| pET-23b-*SahemY* | + | - |
| pET-23b-*SahemQ* | + | - |
| pET-23b-*SahemHQ* | + | - |
| pET-23b-*SahemHY* | + | - |
| pET-23b-*SahemHYQ* | + | + |

## Inhibitor studies of *S. aureus* HemY

*S. aureus* HemH contains no cofactor and the binding of protoheme IX to HemQ does not relate to the protein's function. In contrast, HemY is a flavin containing enzyme whose function may be impaired by ligation to small molecules. Hence, in an attempt to find inhibitors of *S. aureus* flavin-containing HemY, a search was made of Pfizer's chemical library based on analogues of the commercially available diphenyl-ether herbicides. These herbicides are known to be potent inhibitors of proto'gen oxidases from a range of sources including human (30, 31), yeast (32) and bacterial species (33). Herein, the selection of the compounds was made by taking consideration of their structural similarity compared to the diphenyl-ether herbicides and the legal restrictions against their use in drug screening. In

total, 52 compounds were selected for screening, and their potency was evaluated by measuring the $IC_{50}$ values at substrate concentrations below the $K_M$, which allows the optimisation to sensitivity for competitive inhibitors such as diphenyl-ether herbicides (30, 32, 34, 35). For comparison purposes, screening also included acifluorfen, a known diphenyl-ether herbicide. For all compounds the $K_i$ was calculated using the Cheng-Prusoff equation on the assumption that all the inhibitors were competitive. Tables 4.3 and S4.2 (in Supplementary data) show the structures and inhibition data for a selection of the compounds screened. Acifluorfen gave a $K_i$ value of 77.1 µM revealing a weak inhibitory activity. Although, the majority of the Pfizer compounds gave little or no inhibition, nine compounds were more effective than acifluorfen. In particular, three compounds had $K_i$ values <5 µM and the lowest $K_i$ was observed for CP-027216 (Table 4.3).

**Table 4.3.** $IC_{50}$ data for selected screening hits. Log $IC_{50}$ values are the mean of two experiments. $K_i$ values were calculated using the Cheng-Prusoff equation based on the assumption that the inhibitors are competitive.

| Compound Name | Chemical Structure | Mean Log $IC_{50}$ (M) | Calculated $K_i$ (µM) | Mean Hill Coefficient |
|---|---|---|---|---|
| CP-027216 | 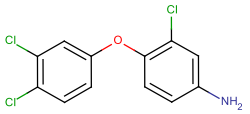 | -5.36±0.04 | 3.6 | 1.2 |
| MCP-77212 (Oxyfluorfen) | 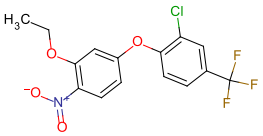 | -5.31±0.02 | 4.1 | 1.1 |
| CP-143375 | 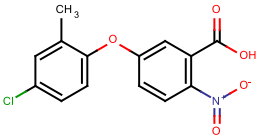 | -5.30±0.42 | 4.2 | 0.8 |
| Acifluorfen | 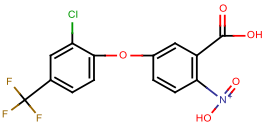 | -4.03±0.07 | 77.1 | 0.7 |

To determine the structure of *S. aureus* HemY and understand how the inhibitor and substrate interact with the protein, attempts were made to grow protein crystals for X-ray diffraction. However, this was unsuccessful despite a considerable effort. Therefore, a homology model was made using the *B. subtilis* HemY crystal structure (3I6D) as template (27) (Figure 4.8A), as it shares the highest sequence identity to *S. aureus* HemY among the 3D structures deposited in the PDB to date. In particular, all residues proposed to be involved in substrate binding and catalysis in the *B. subtilis* enzyme (27) are conserved in the homology model (Figure S4.4, Supplementary data).

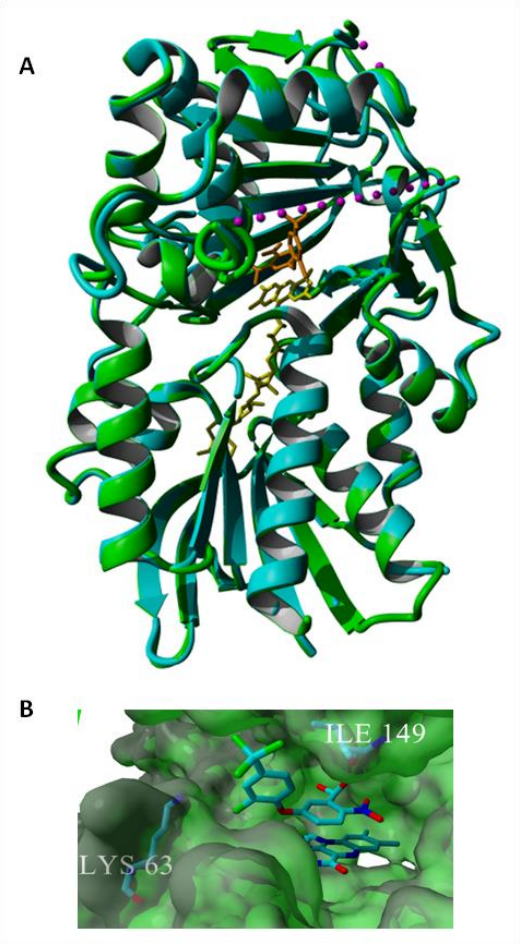


**Figure 4.8.** *S. aureus* HemY homology modelling. A. The homology model of *S. aureus* HemY was predicted using the MoViT molecular modelling tool (Pfizer, Inc.) (coloured in cyan). *B. subtilis* HemY crystal structure was used as template (3I6D) (coloured in light green). The FAD molecule is represented in yellow and the acifluorfen inhibitor in orange. The purple beads represent the "missing" residues from the crystal structure, which are not modelled. This picture was generated using YASARA View. The two structures were superimposed using MUSTANG align. The RMSD is 0.224 and the identity 47.5 %. B. Acifluorfen binding at the active site of *S. aureus* HemY model. Acifluorfen and FAD were positioned into the active site by alignment with the *B. subtilis* HemY structure (316D). Acifluorfen is held in place by a charge-dipole interaction between Lys63 and the chlorine, a hydrogen bond between the backbone oxygen of Ile149 and the carboxylic acid, hydrophobic interactions with Ile149 and pi stacking between the phenyl ring and FAD.

The herbicide acifluorfen and FAD cofactor were placed into the active site of the *S. aureus* homology model by structural alignment with the *B. subtilis* crystal structure which contains both ligands bound (3I6D) (Figure 4.8B). The model predicts the aromatic-aromatic interaction between the nitrophenyl ring of acifluorfen and the isoalloxazine ring of FAD, the hydrophobic interaction with Ile149 (*S. aureus* numbering) and the hydrogen bond between the carboxy group, and the main chain oxygen on Ile149 and the dipole-charge interaction between chorine and Lys63.

Structural comparison suggests that compounds with an oxyethyl group in the *ortho* position of the nitrophenyl ring and a *meta* chlorine in the trichlorophenyl ring (CP-027216) exhibited higher potency (Tables 4.3 and S4.2, Supplementary data). While for the first, the inhibitory effect may be due to the possible fitting of the oxyethyl group into a hydrophobic pocket of HemY, the second result suggests that the chlorine group strongly interacts with HemY.

## 4.5. Discussion

We have detailed and characterized the *S. aureus* enzymes involved in the transformation of uro'gen III into heme and shown that this organism operates a pathway that is distinct from both the "classical" and "alternative" routes. This route represents a transitional pathway that shares copro'gen III and Fe-coproporphyrin III intermediates of the classic and alternative pathways, respectively (Figure 4.9). During the course of our research Dailey et corworkers (19) highlighted that many Gram-positive bacteria appear to operate this transitional heme biosynthesis pathway although their experiments were carried out with enzymes from several organisms. This report represents the first demonstration that this pathway operates fully in *S. aureus.* The first step in the conversion of uro'gen III into heme involves the decarboxylation of the four acetic acid side chains of uro'gen III to give

copro'gen III in a reaction catalyzed by uro'gen III decarboxylase, HemE. The next step is catalyzed by HemY, an enzyme that co-purifies with FAD together with a tetrapyrrole that is likely to be coproporphyrin III. To avoid confusion, we suggest that HemY is termed coproporphyrin synthase, rather than copro'gen oxidase, since the latter is also an oxidative decarboxylase of the classic heme pathway. The kinetic parameters of the *S. aureus* coproporphyrin III synthase activity are similar to the previously reported for *B. subtilis* HemY ($K_M$ 0.56 μM, specific activity 7 nmol.min$^{-1}$mg$^{-1}$) (6) (Table S4.3, Supplementary data). The *S. aureus* HemH inserts iron into protoporphyrin IX with a $k_{cat}$ in the same order of magnitude as described for other bacterial ferrochelatases (36). However, considerably higher $k_{cat}$ values and lower $K_M$ values were found for iron insertion into coproporphyrin III, clearly indicating a much stronger preference for coproporphyrin III as the substrate. These results are similar to those obtained by us for *B. subtilis* HemH and recently reported by others (19). Altogether, these data help highlight the role of coproporphyrin III as an intermediate in the heme synthesis pathway of Gram-positive bacteria.

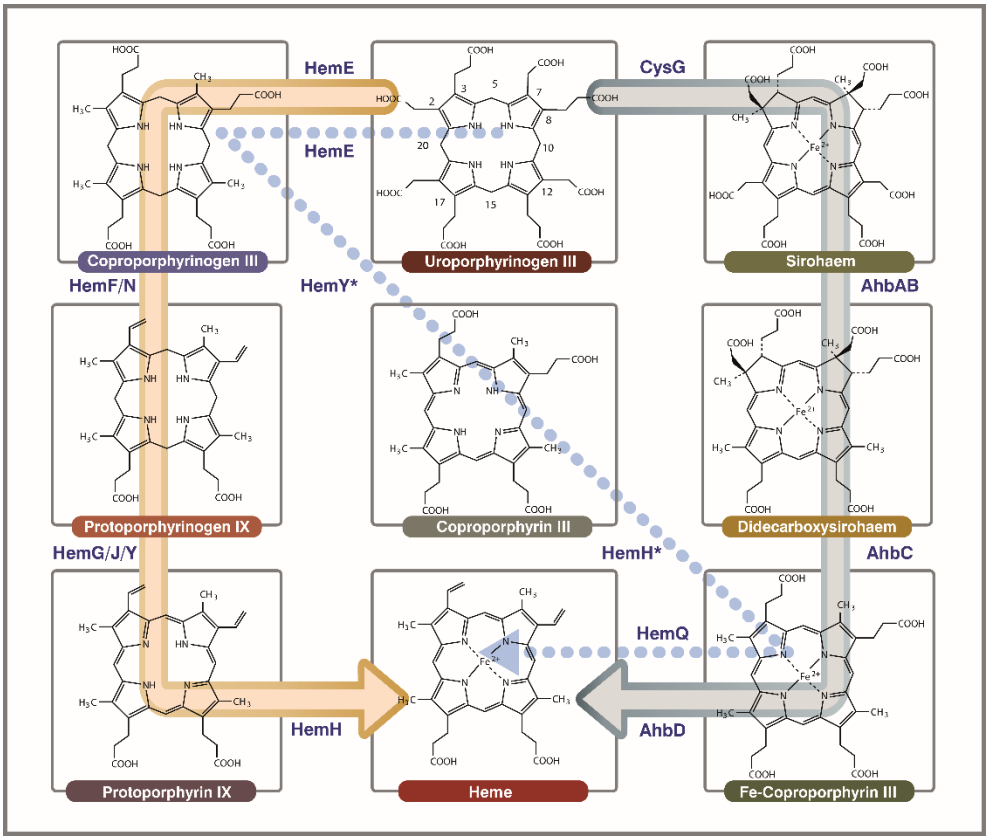


**Figure 4.9.** Diagrammatic representation of the relationship between the classic, transitional and alternative heme biosynthetic pathways. The classic pathway is highlighted in orange, the alternative pathway in green and the transitional pathway in blue. The transitional pathway shares copro'gen III as a substrate with the classic pathway and Fe-coproporphyrin III with the alternative pathway. The enzymes associated with each stage of the transformation are highlighted. HemY* and HemH* denote enzymes that use copro'gen and coproporphyrin as substrates, respectively.

In this work, *S. aureus,* HemQ was shown to promote the sequential decarboxylation of the two propionates attached to the C3 and C8 of Fe-coproporphyrin III to yield protoheme IX, the final product of the pathway. These results fully agree with those recently reported by Dailey and co-

workers (19), although it remains to be determined whether the enzyme is an oxidase or a dehydrogenase.

Interestingly, little primary sequence similarity is shared between HemQ and AhbD, which is a SAM-radical protoheme IX synthase enzyme that is active in the alternative heme pathway (18). The conversion of Fe-coproporphyrin III into protoheme IX by the *S. aureus* HemQ, which involves the formation of a mono-vinyl intermediate, is fully achieved upon the addition of $H_2O_2$ that is most probably required as an electron acceptor (19). Although, it has been speculated that HemQ would contribute to lowering the intracellular content of reactive oxygen species (28), the *hemQ* mutant strain showed no increased in susceptibility to this type of stress (Figure S4.5, Supplementary data). Hence, it remains to be established whether $H_2O_2$ is the true physiological electron acceptor of HemQ.

The *S. aureus* genome also encodes a HemN like protein, which we hypothesised that could convert coproporphyrin III into protoporphyrin IX since in other microorganisms it transforms copro´gen III into proto´gen IX. We overproduced *S. aureus* HemN but could find no activity for this protein in any of our assays. Hence, it is likely that HemN plays some other role, perhaps in heme trafficking as it has been suggested for HemN-like proteins in other organisms (19). Since many proteins annotated in bacterial genomes as “HemN” are not true radical SAM copro´gen III oxidases (19, 37), the possibility that the *S. aureus hemN* gene is unrelated to heme synthesis should be considered.

As a unique coproporphyrin synthase in Gram-positive pathogens, HemY represents a candidate for inhibitor compounds, especially the derivatives of diphenyl-ether herbicides that have been previously proved to target protoporphyrin synthases in plants (38). Our results indicate that *S. aureus* HemY shares with *B. subtilis* HemY the resistance to acifluorfen, with a $K_i$ for acifluorfen in the 30 - 200 µM range (7, 27, 39–41), whereas the Human PPOX exhibits a $K_i$ for acifluorfen of 0.53 µM (42) (Table S4.4,

Supplementary data). Interestingly, from 52 analogues of diphenyl-ether herbicides, 9 are ~20 times more potent than acifluorfen including the commercial herbicide oxyfluorfen herein named MCP-77212. Of the tested compounds, CP-027216 was found to be the best inhibitor ($K_i$ of 3.6 μM) albeit in concentrations much higher than those determined for the herbicides against HemY from plants (34).

We have therefore proved that *S. aureus* HemY is sensitive to a number of acifluorfen analogues, which have the potential to be developed further. Moreover, as there is no homolog of HemQ in humans (28) and that *S. aureus* HemH acts upon coproporphyrin III rather than protoporphyrin IX, these two proteins make plausible targets for novel antimicrobial agents, which are essential due to the alarming increase in drug resistance amongst pathogens. Furthermore, as this transitional pathway is restricted to many Gram-positive bacteria it raises the possibility that the pathway can not only be explored for its potential as an antimicrobial drug target but also that it can be used for selective therapy to differentiate between Gram-positive and Gram-negative pathogens.

### 4.6. Acknowledgements

The work was funded by PTDC/BBB-BQB/0937/2012 and by grants SRFH/BPD/63944/2009 (SALL) and SFRH/BD/95912/2013 (MAMV), all funded by Fundação para a Ciência e Tecnologia (FCT, Portugal). We thank Mafalda Figueiredo for technical support.

## 4.7. References


1. Battersby AR (2000) Tetrapyrroles: the pigments of life. *Nat Prod Rep* 17(6):507–26.
2. Rao AU, Carta LK, Lesuisse E, Hamza I (2005) Lack of heme synthesis in a free-living eukaryote. *Proc Natl Acad Sci U S A* 102:4270–4275.
3. Heinemann IU, Jahn M, Jahn D (2008) The biochemistry of heme biosynthesis. *Arch Biochem Biophys* 474(2):238–251.
4. Elder GH, Roberts AG (1995) Uroporphyrinogen decarboxylase. *J Bioenerg Biomembr* 27(2):207–14.
5. Xu K, Elliott T (1993) An oxygen-dependent coproporphyrinogen oxidase encoded by the hemF gene of *Salmonella typhimurium*. *J Bacteriol* 175(16):4990–4999.
6. Hansson M, Hederstedt L (1994) *Bacillus subtilis* HemY is a peripheral membrane protein essential for protoheme IX synthesis which can oxidize coproporphyrinogen III and protoporphyrinogen IX. *J Bacteriol* 176(19):5962–5970.
7. Dailey TA, Meissner P, Dailey HA (1994) Expression of a cloned protoporphyrinogen oxidase. *J Biol Chem* 269(2):813–815.
8. Dailey H a (2002) Terminal steps of haem biosynthesis. *Biochem Soc Trans* 30(4):590–595.
9. Layer, G. Katrin, G. T. Teschner, V. Schünemann, D. Breckau, A. Masoumi, M. Jahn, Heathcote, P. , Trautwein, A. X. , Jahn D (2005) Radical S-adenosylmethionine enzyme coproporphyrinogen III oxidase HemN: functional features of the [4Fe-4S] cluster and the two bound S-adenosyl-L-methionines. *J Biol Chem* 280(32):29038–29046.
10. Kato K, Tanaka R, Sano S, Tanaka A, Hosaka H (2010) Identification of a gene essential for protoporphyrinogen IX oxidase activity in the

cyanobacterium Synechocystis sp. PCC6803. *Proc Natl Acad Sci U S A* 107(38):16649–16654.

11. Boynton TO, Gerdes S, Craven SH, Neidle EL, Phillips JD, Dailey HA (2011) Discovery of a gene involved in a third bacterial protoporphyrinogen oxidase activity through comparative genomic analysis and functional complementation. *Appl Environ Microbiol* 77(14):4795–4801.
12. Möbius K, Arias-Cartin R, Breckau D, Hännig AL, Riedmann K, Biedendieck R, Schröder S, Becher D, Magalon A, Moser J, others (2010) Heme biosynthesis is coupled to electron transport chains for energy generation. *Proc Natl Acad Sci* 107(23):10436–10441.
13. Boynton TO, Daugherty LE, Dailey TA, Dailey HA (2009) Identification of *Escherichia coli* HemG as a novel, menadione-dependent flavodoxin with protoporphyrinogen oxidase activity. *Biochemistry* 48(29):6705–6711.
14. Bali S, Lawrence AD, Lobo SA, Saraiva LM, Golding BT, Palmer DJ, Howard MJ, Ferguson SJ, Warren MJ (2011) Molecular hijacking of siroheme for the synthesis of heme and d1 heme. *Proc Natl Acad Sci U S A* 108(45):18260–5.
15. Lobo SAL, Warren MJ, Saraiva LM (2012) Sulfate-Reducing Bacteria Reveal a New Branch of Tetrapyrrole Metabolism. *Adv Microb Physiol* 61:267–295.
16. Kühner M, Haufschildt K, Neumann A, Storbeck S, Streif J, Layer G (2014) The alternative route to heme in the methanogenic archaeon methanosarcina barkeri. *Archaea* 2014. doi:10.1155/2014/327637.
17. Palmer DJ, Schroeder S, Lawrence AD, Deery E, Lobo SA, Saraiva LM, Mclean KJ, Munro AW, Ferguson SJ, Pickersgill RW, Brown DG, Warren MJ (2014) The structure, function and properties of sirohaem decarboxylase - an enzyme with structural homology to a transcription factor family that is part of the alternative haem biosynthesis pathway.

*Mol Microbiol* 93(2):247–261.

18. Lobo SAL, Lawrence AD, Romão C V., Warren MJ, Teixeira M, Saraiva LM (2014) Characterisation of Desulfovibrio vulgaris haem b synthase, a radical SAM family member. *Biochim Biophys Acta - Proteins Proteomics* 1844(7):1238–1247.
19. Dailey HA, Gerdes S, Dailey TA, Burch JS, Phillips JD (2015) Noncanonical coproporphyrin-dependent bacterial heme biosynthesis pathway that does not use protoporphyrin. *Proc Natl Acad Sci U S A* 112(7):2210–5.
20. Mayfield J a., Hammer ND, Kurker RC, Chen TK, Ojha S, Skaar EP, DuBois JL (2013) The chlorite dismutase (HemQ) from Staphylococcus aureus has a redox-sensitive heme and is associated with the small colony variant phenotype. *J Biol Chem* 288(32):23488–23504.
21. Breckau D, Mahlitz E, Sauerwald A, Layer G, Jahn D (2003) Oxygen-dependent coproporphyrinogen III oxidase (HemF) from *Escherichia coli* is stimulated by manganese. *J Biol Chem* 278(47):46625–46631.
22. Raux E, Leech HK, Beck R, Schubert HL, Santander PJ, Roessner CA, Scott AI, Martens JH, Jahn D, Thermesr C, Rambach A, Warren MJ (2003) Identification and functional analysis of enzymes required for precorrin-2 dehydrogenation and metal ion insertion in the biosynthesis of sirohaem and cobalamin in *Bacillus megaterium*. *Biochem J* 370:505–516.
23. Lobo SAL, Brindley A, Warren MJ, Saraiva LM (2009) Functional characterization of the early steps of tetrapyrrole biosynthesis and modification in Desulfovibrio vulgaris Hildenborough. *Biochem J* 420(2).
24. Frustaci JM, O'Brian MR (1993) The Escherichia coli visA gene encodes ferrochelatase, the final enzyme of the heme biosynthetic pathway. *J Bacteriol* 175(7):2154–2156.

25. McGoldrick HM, Roessner CA, Raux E, Lawrence AD, McLean KJ, Munro AW, Santabarbara S, Rigby SEJ, Heathcote P, Scott AI, Warren MJ (2005) Identification and characterization of a novel vitamin B12 (cobalamin) biosynthetic enzyme (CobZ) from Rhodobacter capsulatus, containing flavin, heme, and Fe-S cofactors. *J Biol Chem* 280(2):1086–1094.
26. Monk IR, Shah IM, Xu M (2012) Transforming the Untransformable : Application of direct transformation to manipulate genetically *Staphylococcus aureus* and Staphylococcus epidermidis. *MBio* 3(2):e00277-11.
27. Qin X, Sun L, Wen X, Yang X, Tan Y, Jin H, Cao Q, Zhou W, Xi Z, Shen Y (2010) Structural insight into unique properties of protoporphyrinogen oxidase from *Bacillus subtilis*. *J Struct Biol* 170(1):76–82.
28. Dailey T, Boynton T, Albetel A, Gerdes S, Johnson M, Dailey H (2010) Discovery and Characterization of HemQ: An essential heme biosynthetic pathway component. *J Biol Chem* 285(34):25978–25986.
29. von Eiff C, Heilmann C, Proctor RA, Woltz C, Peters G, Götz F (1997) A site-directed Staphylococcus aureus hemB mutant is a small-colony variant which persists intracellularly. *J Bacteriol* 179(15):4706–12.
30. Corrigall A V, Hift RJ, Adams PA, Kirsch RE (1994) Inhibition of mammalian protoporphyrinogen oxidase by acifluorfen. *Biochem Mol Biol Int* 34(6):1283–9.
31. Dailey TA, Dailey HA (1996) Human protoporphyrinogen oxidase: Expression, purification, and characterization of the cloned enzyme. *Protein Sci* 5:98–105.
32. Camadro JM, Thome F, Brouillet N, Labbe P (1994) Purification and Properties of Protoporphyrinogen Oxidase from the Yeast *Saccharomyces cerevisiae*: Mitochondrial location and evidence for a precursor form of the protein. *J Biol Chem* 269(51):32085–32091.

33. Dailey HA, Dailey TA (1996) Protoporphyrinogen oxidase of *Myxococcus xanthus*: Expression, purification, and characterization of the cloned enzyme. *J Biol Chem* 271(15):8714–8718.
34. Camadro JM, Matringe M, Scalla R, Labbe P (1991) Kinetic studies on protoporphyrinogen oxidase inhibition by diphenyl ether herbicides. *Biochem J* 277:17–21.
35. Jeong E, Houn T, Kuk Y, Kim ES, Chandru HK, Baik M, Back K, Guh JO, Han O (2003) A point mutation of valine-311 to methionine in *Bacillus subtilis* protoporphyrinogen oxidase does not greatly increase resistance to the diphenyl ether herbicide oxyfluorfen. *Bioorg Chem* 31(5):389–397.
36. Shepherd M, Dailey TA, Dailey HA (2006) A new class of [2Fe-2S]-cluster-containing protoporphyrin (IX) ferrochelatases. *Biochem J* 397(1):47.
37. Sofia HJ, Chen G, Hetzler BG, Reyes-Spindola JF, Miller NE (2001) Radical SAM, a novel protein superfamily linking unresolved steps in familiar biosynthetic pathways with radical mechanisms: functional characterization using new analysis and information visualization methods. *Nucleic Acids Res* 29(5):1097–1106.
38. Matringe M, Camadro JM, Labbe P, Scalla R (1989) Protoporphyrinogen oxidase as a molecular target for diphenyl ether herbicides. *Biochem J* 260(1):231–235.
39. Corrigall A V., Siziba KB, Maneli MH, Shephard EG, Ziman M, Dailey TA, Dailey HA, Kirsch RE, Meissner PN (1998) Purification of and kinetic studies on a cloned protoporphyrinogen oxidase from the aerobic bacterium *Bacillus subtilis*. *Arch Biochem Biophys* 358(2):251–256.
40. Tan Y, Sun L, Xi Z, Yang GF, Jiang DQ, Yan XP, Yang X, Li HY (2008) A capillary electrophoresis assay for recombinant *Bacillus subtilis* protoporphyrinogen oxidase. *Anal Biochem* 383(2):200–204.

41. Sun L, Wen X, Tan Y, Li H, Yang X, Zhao Y, Wang B, Cao Q, Niu C, Xi Z (2009) Site-directed mutagenesis and computational study of the Y366 active site in *Bacillus subtilis* protoporphyrinogen oxidase. *Amino Acids* 37(3):523–530.
42. Shepherd M, Dailey HA (2005) A continuous fluorimetric assay for protoporphyrinogen oxidase by monitoring porphyrin accumulation. *Anal Biochem* 344(1):115–121.

## 4.8. Supplementary data

**Table S4.1.** Oligonucleotides used in this work

| Name | Oligonucleotide sequence (5´- 3´) |
|---|---|
| *Cloning* | |
| SaHemE_F | CGAGCTAGCCACCACCACCACCACCACATGGTGCATAATAAAAAC |
| SaHemE_R | CTCAAGCTTAAAACTAGTTTATCTTTGTGTATATGTGTGTAC |
| SaHemH_F | CATGCTAGCCACCACCACCACCACCACATGACTAAAAAAATGGG |
| SaHemH_R | CTCAAGCTTCTTACTAGTTTAAAATATAGACTTGATTTCATC |
| BsHemH_F | GTGGCTAGCATGAGTAGAAAGAAAATGG |
| BsHemH_R | CTCTCGAGACGTCCTAATTTTTTTAATACGAC |
| SaHemY_F | GCGTGAAACCATATGACTAAATC |
| SaHemY_R | CAAAAAAAGCTTAACCTTTGTCTC |
| SaHemQ_F | GATGCTAGCCACCACCACCACCACCACATGAGTCAAGCAGCCG |
| SaHemQ_R | CATAAGCTTACCACTAGTTTAAGAAATCGCAAAGAATTGATC |
| *Construction of S. aureus hemH and hemQ mutants* | |
| HemHMutA | CCATTAGAGCTCATTGGTGTCG |
| HemHMutB | CCTTCCTTTAAATGAATTATCTTTC |
| HemHMutC | TAATTCATTTAAAGGAAGGGCGTGAAACGTTGTGACTAAATC |
| HemHMutD | GTTGCAACAGTCGACCTATCCATC |
| HemHOutF | CGGAGTTGTGCGCTTATGTAAC |
| HemHOutR | CCATCATGGGTATTTTCAATGTC |
| SaHemHMutF | CACCACATTATTCTTCATTTTCAG |
| SaHemHMutR | GCCGAAACAACTAATACCGTG |
| HemQMutA | CACCTGGAGCTCTTTTCTCAGC |
| HemQMutB | TCATAAAGCAAAGGGGTAACG |
| HemQMutC | TTACCCCTTTGCTTTATGAGGTTTAAGCTTGGAATTTTTCGT |

**Table S4.1.** continued

| Name | Oligonucleotide sequence (5´- 3´) |
|---|---|
| *Construction of S. aureus hemH and hemQ mutants* | |
| HemHMutD | GTTGCAACAGTCGACCTATCCATC |
| HemHOutF | CGGAGTTGTGCGCTTATGTAAC |
| HemHOutR | CCATCATGGGTATTTTCAATGTC |
| SaHemHMutF | CACCACATTATTCTTCATTTTCAG |
| SaHemHMutR | GCCGAAACAACTAATACCGTG |
| HemQMutA | CACCTGGAGCTCTTTTCTCAGC |
| HemQMutB | TCATAAAGCAAAGGGGTAACG |
| HemQMutC | TTACCCCTTTGCTTTATGAGGTTTAAGCTTGGAATTTTTCGT |

**Table S4.2.** *IC50* data for selected screening hits

| Compound Name | Chemical Structure | Mean Log *IC50* (M) (error as 95 % confidence interval of mean) | 95 % Confidence interval of fit to graph | *Ki* (μM) | Mean Hill Coefficient | Maximum inhibition (%) |
|---|---|---|---|---|---|---|
| CP-027216 | 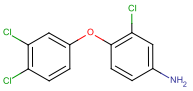 | -5.36±0.04 | -5.6 to -5.1 | 3.6 | 1.2 | 100 |
| MCP-77212 (Oxyfluorfen) | 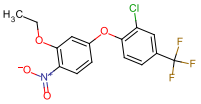 | -5.31±0.02 | -5.5 to -5.2 | 4.1 | 1.1 | 100 |
| CP-143375 | 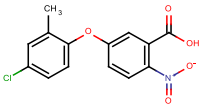 | -5.30±0.42 | -5.7 to -4.8 | 4.2 | 0.8 | 100 |
| CP-143382 | 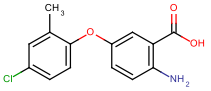 | -5.02±0.16 | -5.2 to -4.9 | 8 | 0.9 | 100 |
| CP-227449 | 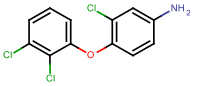 | -5.02±0.21 | -5.1 to -4.9 | 8 | 1 | 100 |
| MCP-173310 | 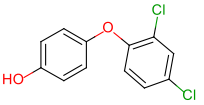 | -4.68±0.10 | -5.1 to -4.3 | 17.3 | 0.9 | 100 |
| 0604988 | 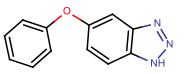 | -4.46±0.14 | -4.8 to -4.2 | 29.2 | 0.8 | 100 |
| Acifluorfen | 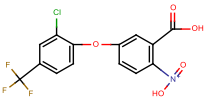 | -4.03±0.07 | -4.5 to -3.5 | 77.1 | 0.7 | 100 |
| CP-021292 | 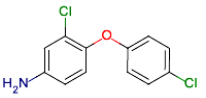 | -3.91±0.02 | -4 to -3.8 | 101.8 | 5.54 | 100 |
| UK-140415 | 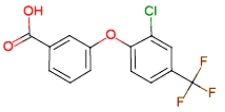 | -4.08±0.13 | -4.5 to -3.7 | 68.6 | 0.60 | 100 |

**Table S4.3.** Comparison of *S. aureus* HemY kinetics with HemY from other organisms

| Enzyme | $K_M$ (μM) | $V_{max}$ ($min^{-1}$) | Substrate | Reference |
|---|---|---|---|---|
| *S. aureus* HemY | 0.3 | 1.3 | copro'gen III | This work |
| *P. acnes* HemY | 19 | 3 | proto'gen IX | (1) |
| *P. acnes* HemY+HemQ | 10.1 | 19.8 | proto'gen IX | (1) |
| *B. subtilis* HemY | 0.56 | 0.358 | copro'gen III | (2) |
| *B. subtilis* HemY | 0.95 | 0.0435 | proto'gen IX | (2) |

**Table S4.4.** *Ki* data for acifluorfen of bacterial HemY and Human PPOX

| | $K_i$ **Acifluorfen** (μM) | Reference |
|---|---|---|
| *S. aureus* HemY | 77.1 | This work |
| Human PPOX | 0.53 | (3) |
| *B. subtilis* HemY | 32.9 - 193.6 | (4–8) |

## Homology modeling of *S. aureus* HemY

Docking of acifluorfen into the homology model shows that all the interactions previously reported for the *B. subtilis* enzyme are conserved (7). These are the aromatic-aromatic interaction between the nitrophenyl ring of acifluorfen and the isoalloxazine ring of FAD, the hydrophobic interaction with Ile149 (*S. aureus* numbering), the hydrogen bond between the carboxy group and the main chain oxygen on Ile149, and the dipole-charge interaction between chorine and Lys63. The nitro group on acifluorfen projects towards the active site entrance and does not interact with the protein. Removal of this nitro group (UK 140415) caused no significant alteration on the inhibition effect.

The herbicide oxyfluorfen (MCP-77212) substitutes the carboxy group of acifluorfen for an oxyethyl group and has a $K_i$ approximately 19 times lower than acifluorfen. As the modelled position for acifluorfen does not provide room to accommodate the extra bulk, oxyfluorfen must bind elsewhere in the active site.

Compared to acifluorfen, CP-143375 substitutes the *meta* chlorine for a methyl group and the *para* trifluorocarbon for a single chlorine. This results in an 18-fold decrease in $K_i$. As there are no residues close enough to form interactions with these groups the molecule probably binds in a different position to acifluorfen. CP-143382 substitutes the nitro group of CP-143375 for an amino group with no significant change in the activity.

CP-027216 caused the strongest inhibition. The substituents differ significantly from acifluorfen and therefore the compound probably binds in a different position. Removal of the *meta* chlorine from the trichlorophenyl ring leads to a 28-fold increase in $K_i$ (CP-021292) showing the importance of this substituent for binding. Conversely the *para* chlorine does not seem to be important as moving it from the *para* to *ortho* position (CP-227449) had no significant effect on the activity.



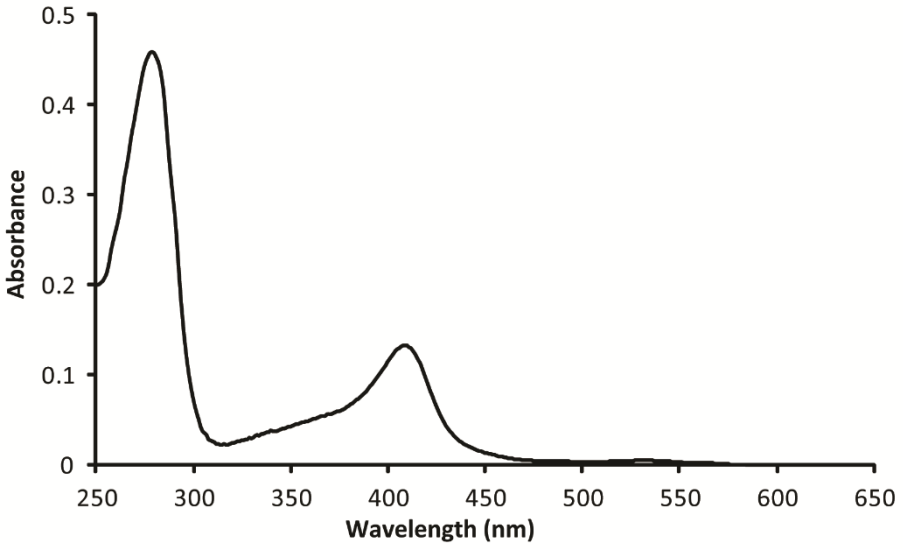


**Figure S4.1.** UV-visible spectrum of the purified *S. aureus* hemin-loaded HemQ.

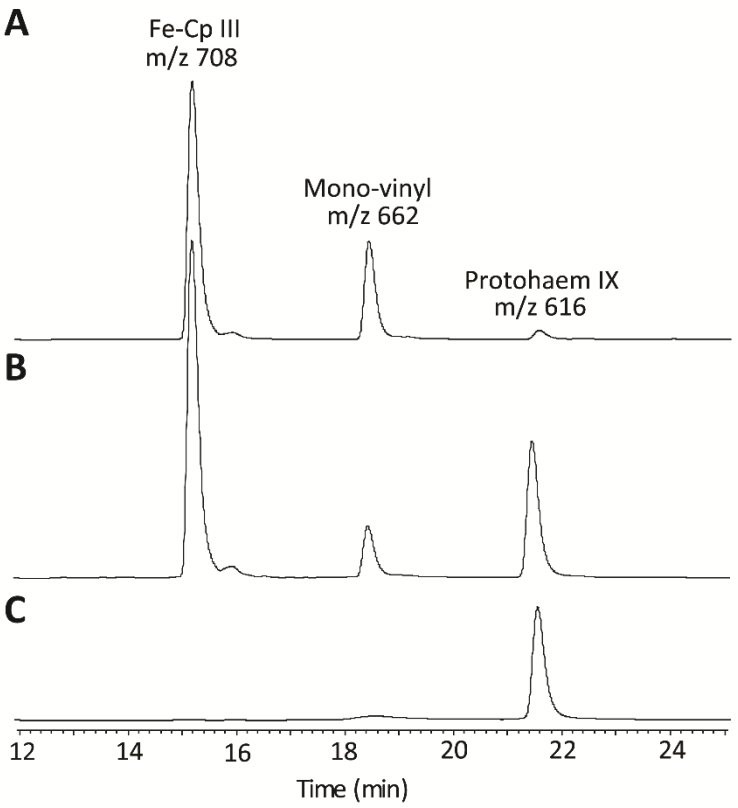


**Figure S4.2.** Conversion of Fe-coproporphyrin III (Fe-Cp III) into protoheme IX by *S. aureus* HemQ and hemin-loaded HemQ. HPLC chromatograms, recorded at 400 nm, of HemQ and hemin-HemQ reaction products (A and B) and of the hemin-loaded HemQ (C), after treatment with HCl. A. Incubation of HemQ (0.5 mg) with Fe-Cp III (15 μM). B. Incubation of hemin-loaded HemQ (0.5 mg) with Fe-Cp III (15 μM). C. Hemin-loaded HemQ (0.5 mg).

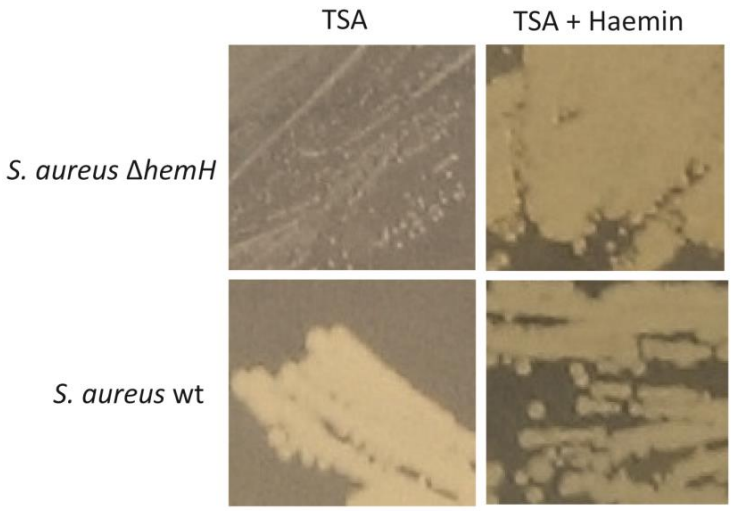


**Figure S4.3.** *S. aureus* Δ*hemH* forms small colony variants that revert to the wild type phenotype upon addition of exogenous hemin.

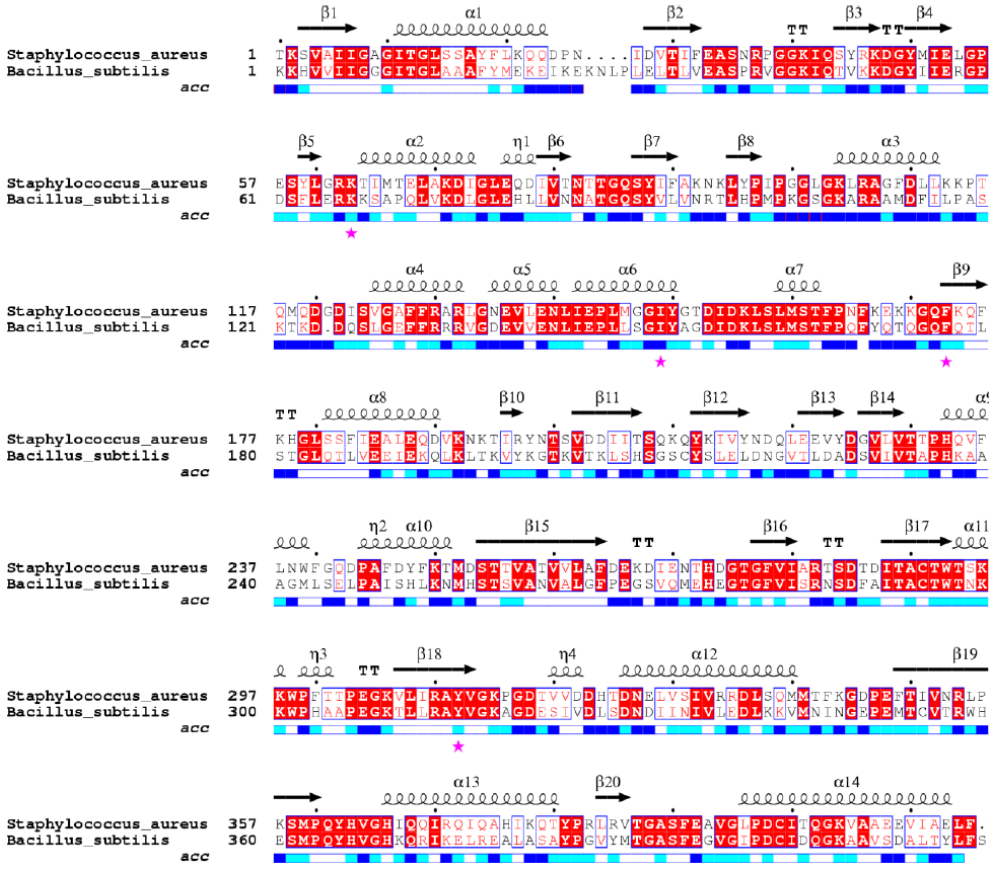


**Figure S4.4.** Structure based sequence alignment of *B.subtilis* HemY and *S.aureus* HemY**.** *S. aureus* HemY homology model was aligned with the *B. subtilis* HemY crystal structure (3I6D) in PyMol and the alignment exported to ESPript (http://espript.ibCp.fr/ESPript/ESPript/). The pink stars show the residues which were suggested to be involved in substrate binding in the *B. subtilis* enzyme and that are conserved in *S. aureus* HemY. The bottom line depicts the relative accessibility (*Acc*) of each residue. White identifies buried residues (*Acc* <0.1), cyan is intermediate (0.1 ≤ *Acc* ≤*0.4*), blue is accessible (0.1 ≤ *Acc* ≤*1.0*) and blue with red border is *Acc* >1.0.

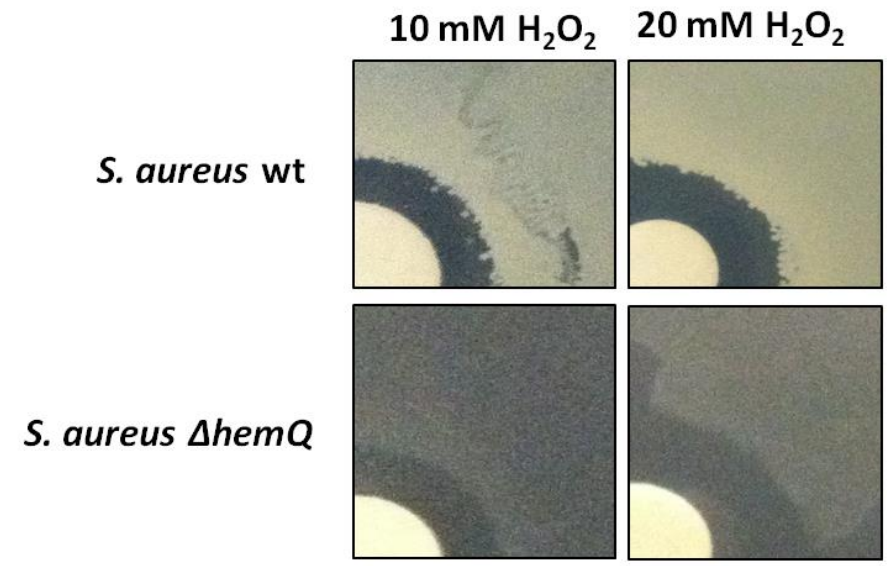


**Figure S4.5.** Sensitivity of *S. aureus* wild type and Δ*hemQ*, to $H_2O_2$ assessed by disk diffusion assays. Cell suspensions prepared in phosphate saline buffer were spread on TSA plates. Discs of 10-mm containing 10 or 20 mM $H_2O_2$ were placed on top of the cell layer and the plates were incubated over night at 37 ˚C.



## Supplementary References

1. Dailey T, Boynton T, Albetel A, Gerdes S, Johnson M, Dailey H (2010) Discovery and Characterization of HemQ: An essential heme biosynthetic pathway component. *J Biol Chem* 285(34):25978–25986.
2. Hansson M, Hederstedt L (1994) *Bacillus subtilis* HemY is a peripheral membrane protein essential for protoheme IX synthesis which can oxidize coproporphyrinogen III and protoporphyrinogen IX. *J Bacteriol* 176(19):5962–5970.
3. Shepherd M, Dailey HA (2005) A continuous fluorimetric assay for protoporphyrinogen oxidase by monitoring porphyrin accumulation. *Anal Biochem* 344(1):115–121.

4. Dailey TA, Meissner P, Dailey HA (1994) Expression of a cloned protoporphyrinogen oxidase. *J Biol Chem* 269(2):813–815.
5. Corrigall A V., Siziba KB, Maneli MH, Shephard EG, Ziman M, Dailey TA, Dailey HA, Kirsch RE, Meissner PN (1998) Purification of and kinetic studies on a cloned protoporphyrinogen oxidase from the aerobic bacterium *Bacillus subtilis*. *Arch Biochem Biophys* 358(2):251–256.
6. Tan Y, Sun L, Xi Z, Yang G-F, Jiang D-Q, Yan X-P, Yang X, Li H-Y (2008) A capillary electrophoresis assay for recombinant Bacillus subtilis protoporphyrinogen oxidase. *Anal Biochem* 383(2):200–204.
7. Qin X, Sun L, Wen X, Yang X, Tan Y, Jin H, Cao Q, Zhou W, Xi Z, Shen Y (2010) Structural insight into unique properties of protoporphyrinogen oxidase from *Bacillus subtilis*. *J Struct Biol* 170(1):76–82.
8. Sun L, Wen X, Tan Y, Li H, Yang X, Zhao Y, Wang B, Cao Q, Niu C, Xi Z (2009) Site-directed mutagenesis and computational study of the Y366 active site in *Bacillus subtilis* protoporphyrinogen oxidase. *Amino Acids* 37(3):523–530.

# Chapter 5

## *Staphylococcus aureus* heme biosynthesis and acquisition pathways are linked through heme oxygenase IsdG

**This chapter was submitted to a scientific journal with peer-review and awaits publication:**

**Videira MAM**, Lobo SAL, Silva LSO, Palmer DJ, Warren MJ, Prieto M, Coutinho A, Sousa FL, Fernandes F, and Saraiva LM (2018) Staphylococcus aureus haem monooxygenase IsdG links the haem biosynthesis and acquisition pathways. Submitted

MAMV designed the research, interpreted the data, performed all experiments with the exception of heme quantification assays, HPLC-MS and genomic analysis, and wrote the paper.

## 5.1. Summary

Heme is an essential cofactor in central metabolic pathways in the vast majority of living systems. Most prokaryotes encode a heme biosynthesis pathway often coexists with a heme uptake system. However, how prokaryotes balance the heme requirements with toxicity associated with free heme remains unclear. Here, using the model pathogen *Staphylococcus aureus*, we show that IsdG, one of two heme oxygenase enzymes in the heme uptake system, inhibits the formation of heme by the heme biosynthesis pathway. More specifically, we show that IsdG decreases the activity of ferrochelatase, a key enzyme of the heme biosynthesis pathway, and that the two proteins interact both *in vitro* and *in vivo*. Further, a bioinformatics analysis reveals that a significant number of heme biosynthesis pathway containing organisms possess an IsdG-homologue and that those with both heme biosynthesis pathway and uptake systems have at least two heme oxygenases. We conclude that IsdG-like proteins control intracellular heme levels by coupling heme uptake with heme synthesis. IsdG thus, represents a novel target for the treatment of *S. aureus* infections.



## 5.2. Introduction

In all forms of life, the ability to perform redox reactions is crucial, often requiring compounds with metal centers and cofactors that are evolutionarily ancient. Heme is an iron-based redox center that is widely distributed in living organisms and which permits an extensive range of proteins and enzymes to function in essential cellular processes such as aerobic and anaerobic respiration, detoxification, microRNA processing and regulation of gene expression (1). Heme is obtained by either *de novo* synthesis (via heme biosynthesis pathways) or by uptake from the environment. Several pathogens uptake heme from their host's hemoglobin,

which upon degradation serves as a source of iron to satisfy the nutritional needs of the pathogen (1, 2). Furthermore, a large number of microorganisms combine pathways for the endogenous production of heme with complex heme uptake systems.

Prokaryotes utilize one of three distinct heme biosynthesis pathways, all of which have common early steps that lead to the intermediate uroporphyrinogen III (Fig. 5.1). Thereafter, the three distinct routes are referred to as the protoporphyrin, siroheme and coproporphyrin branches, reflecting intermediates that are unique to each pathway, and the genes involved were recently renamed (3). The protoporphyrin dependent branch (PPD), previously known as classic pathway, operates in many Gram-negative bacteria. This pathway involves the decarboxylation of uroporphyrinogen III to coproporphyrinogen III by HemE (now UroD), followed by decarboxylation to protoporphyrinogen IX by HemN/HemF (now CgdH/CgdC) and then oxidation to protoporphyrin IX by HemY/HemG (now PgoX/PgdH1) prior to metal insertion by ferrochelatase HemH (now PpfC) to give protoheme (3, 4). The siroheme dependent branch, originally named the alternative heme biosynthesis pathway Ahb, is active in sulphate-reducing proteobacteria and archaea, transforms uroporphyrinogen III to protoheme via siroheme in an oxygen-independent process requiring four-enzymatic steps involving the enzymes AhbA-D (5, 6). The most recently discovered branch, namely the coproporphyrin dependent pathway (CPD), is active in several Gram-positive organisms including *S. aureus* (7). This pathway involves the conversion of uroporphyrinogen III to coproporphyrinogen III by HemE (now UroD) and subsequent oxidation to coproporphyrin III by HemY (now CgoX). Insertion of iron into coproporphyrin III to make coproheme is mediated by HemH (now CpfC), and the final step involves the decarboxylation of coproheme to protoheme by HemQ (now ChdC) (7, 8). The mechanisms of heme biosynthesis in prokaryotes vary widely (3) and control over the pathway has been reported to be regulated by iron, oxygen,

reactive oxygen species and by its final product heme (1, 3). In the case of the latter, the binding of heme to HemA (now GtrR), the first enzyme of the pathway, is thought to control the system via a feedback inhibition mechanism (1, 9, 10).

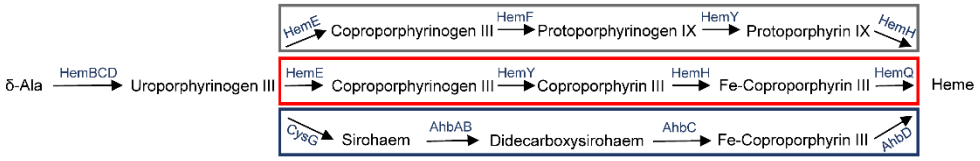


**Figure 5.1.** Three different heme biosynthesis pathways that diverge from uroporphyrin III. The enzymes in the three pathways are conserved between aminolaevulinic acid (δ-Ala) and uroporphyrinogen III. The protoporphyrin dependent (or classical) pathway is boxed in grey and converts uroporphyrinogen III into heme using protoporphyrin as an intermediate. The coproporphyrin dependent pathway is represented in red and the siroheme dependent pathway (alternative heme biosynthesis pathway) highlighted in blue.

The most common heme acquisition system in Gram-positive pathogens is the iron-regulated surface determinant (Isd). *S. aureus* also contains an additional heme transport system (Hts) that, like the Isd proteins, was first described in this bacterium (11, 12). The Isd system includes the cell wall-anchored proteins IsdA, IsdB, IsdC and IsdH, as well as the heme-binding protein and permease components IsdD, IsdE, and IsdF, and the transmembrane ABC transporter HtsABC (11, 12). Once heme is transported into the cytoplasm, it is either degraded by the heme oxygenases IsdG and IsdI to release iron (13), or becomes bound to membrane-associated proteins to act as a cofactor in, for example, electron transport (14). *S. aureus* also possesses the heme regulated transporter (HrtAB), an efflux pump that protects cells from heme toxicity (15).

*S. aureus* is clinically significant as it is responsible for a large number of human infections including respiratory, urogenital, skin burn-associated and systemic infections (16). It is also a widely studied Gram-positive pathogen and the paradigm for the CPD pathway operating alongside a

heme acquisition system. Genes encoding enzymes of the CPD pathway are organized into two operons in *S. aureus*, *hemAXCDB* and *hemEHY*, whereas *hemQ* is isolated elsewhere in the genome (7). The *S. aureus* heme acquisition system is formed by *isdA, isdB, isdH, isdI* and the transcriptional unit *isdCDEF-srtB-isdG* (11, 17). Like many other organisms, *S. aureus* encodes two heme oxygenases, IsdG and IsdI, which share approximately 70% amino acid identity and which bind and degrade heme to produce iron and staphylobilin (13, 18).

In this work, we investigated how *S. aureus* controls intracellular heme levels. We show that the heme oxygenase, IsdG, provides a link between the heme biosynthesis and uptake pathways in *S. aureus* and that this protein prevents excessive formation of toxic heme inside bacterial cells.

## 5.3. Materials and Methods

### Strains and growth conditions

The strains used in this work are listed in Table 1 and were grown under aerobic conditions, at 37 °C and 150 rpm. *S. aureus* was cultured in tryptic soy broth (TSB), with the exception of the cells that were used for RNA extraction that were cultured in Roswell Park Memorial Institute (RPMI) medium supplemented with 1% casamino acids. *E. coli* strains were grown in Luria-Bertani (LB), except *E. coli* expressing the pWhiteWalker plasmid that was grown in Brain Heart Infusion (BHI) medium. Selection was achieved by addition of the indicated antibiotics, namely kanamycin (50 μg $ml^{-1}$), erythromycin (20 μg $ml^{-1}$ or 400 μg $ml^{-1}$ for FRET experiments) and ampicillin (100 μg $ml^{-1}$).

**Table 1**. Strains used in this work

| Strains | Description | Reference |
|---|---|---|
| ***E. coli*** | | |
| XL1-Blue | Host strain used for genetic manipulation | Laboratory stock |
| BL21(DE3)Gold | Recombinant protein expression strain | Novagen |
| BL21$^{STAR}$DE3pLysS | Recombinant protein expression strain | Novagen |
| Δ*visA* | *E. coli* K12 *hemH* mutant strain | Mark O'Brian Lab |
| ***S. aureus*** | | |
| RN4220 | Restriction-deficient derivative of NCTC8325 | Laboratory stock |
| Newman | Clinical isolate used as wild type strain | Mariana Pinho Lab |
| Δ*hemH* | *hemH* mutant constructed in the Newman strain | (7) |
| Δ*hemQ* | *hemQ* mutant constructed in the Newman strain | (7) |

## RNA isolation and quantitative real-time RT-PCR assays

Overnight cultures of *S. aureus* were diluted to an optical density at 600 nm ($OD_{600}$) of 0.1 on RPMI containing 1% casamino acids or RPMI containing 1% casamino acids supplemented with hemin (2 μM). Cells at an $OD_{600}$ = 1 were treated with an ice-cold ethanol/phenol RNA protective solution (5%), centrifuged at 2000 *x g* for 5 min, and the pellets flash frozen in liquid nitrogen. For RNA isolation, pellets were thawed on ice, resuspended in 10 mM Tris pH 8 and lysed with 2 mg $ml^{-1}$ lysozyme and 30 μg $ml^{-1}$ lysostaphin at 37 °C, for 30 min. The lysates were transferred to Aurum RNA Binding Mini Columns and total RNA was extracted using Aurum™ Total RNA Mini Kit (Bio-Rad), following the manufacturer´s instructions. Contaminating DNA was removed using Ambion® TURBO DNA-free™DNase kit (Life Technologies), and RNA concentration and purity were evaluated in a Nanodrop ND-1000 UV–visible spectrophotometer (Thermo Fisher Scientific).

For the cDNA synthesis, 800 ng of RNA was reverse transcribed with the Transcriptor High Fidelity cDNA Synthesis Kit (Roche) using the Anchored-oligo (dT)18 and Random Hexamer primers. Quantitative real-time RT-PCR assays were done in a LightCycler® 480 (Roche) using the oligonucleotides listed in Table 2 and the LightCycler® 480 SYBR Green I Master kit (Roche). Relative quantification of each gene is shown in relation to the 16S rRNA reference gene, whose expression does not vary under the tested conditions, and using the comparative $C_T$ method. Assays were done for two independent biological samples analyzed in triplicate.

**Table 2**. List of oligonucleotides used in this work

| Primer | Oligonucleotide sequence (5´- 3´) | Restriction sites |
|---|---|---|
| **Cloning** | | |
| SaisdG_F | GGGCTAGCATGAAATTTATGGCAGAAAATAG | NheI |
| SaisdG_R | CACTCGAGTTATTTCATGTAACTATAGCC | XhoI |
| SaisdI_F | GAGCTAGCATGTTTATGGCAGAAAATAGATTAC | NheI |
| SaisdI_R | CACTCGAGTTATTTTTGATAGTGGTAGCCAATATC | XhoI |
| SaisdGLaL_R | CAACTCGAGTAAACTAGTTTATTTCATTAACTATAGCCTATATC | Spe/XhoI |
| SaisdILaL_R | CTAGCTCGAGTTAACTAGTTTATTTTTGATAGTGGTAGCC | Spe/XhoI |
| SaisdGpWW_F | GAATTCACAGGAGGGAGGATAATTATGAAATTTATG | EcoRI |
| SaisdGpWW_R | GGTACCCAACCTCTTTAAATTCAAATATTTCATG | KpnI |
| pWWblock_F | CGCGGATAACAATTAAGC | EcoRI |
| pWWblock_R | GTCAAAGTAGTGACAAGTGTTG | NcoI |
| EchemH_F | CGATAAGAGGCGCATATGCGTCAGACTAAAAC | NdeI |
| EchemH_R | CTCACTCGAGGCGATACGCGGCAACAAG | XhoI |
| hemHpbcb1_F | GGAAGGCATGCTCAATGACTAA | SphI |
| hemHpbcb1_R | AATAGCCACTGAACTAGTCACAACG | SpeI |
| hemQpbcb1_F | GCATGCAACATGAGTCAAGCAGCCG | SphI |
| hemQpbcb1_R | ACTAGTAACGTACCAATGTATTAAGAAATCG | SpeI |
| hemQpbcb7_F | GATTTTTGAAAAGGTACCATAAACATGAGTC | KpnI |
| hemQpbcb7_R | CGTACCAATGCTAGCAGAAATCGCAAAG | NheI |
| isdGpbcb7_F | AATAATTAAGGTAAGGTACCCAGAAAAG | KpnI |
| isdGpbcb7_R | TCTTTAAATTGCTAGCTTTCATGTA | NheI |
| isdIpbcb7_F | CATAAAATAGGGTACCGATTGCCCAT | KpnI |

**Table 2**. continued.

| Primer | Oligonucleotide sequence (5´- 3´) | Restriction sites |
|---|---|---|
| isdIpbcb7_R | GTTTTTAATAGCTAGCTTTTTGATAG | NheI |
| hemHpbcb7_F | GAAGGTGGTACCAATGACTAAAAAAATGGG | KpnI |
| hemHpbcb7_R | CACAAGCTAGCACGCTTCTTTCGTAATGAAAATATAG | NheI |
| **qReal-time RT-PCR** | | |
| hemART_F | GGTGCAGGGGAAATGAGTG | |
| hemART_R | CTCGAGGAACTGCAATATCAATC | |
| hemERT_F | GGGGCACCATTTACATTAGCGTC | |
| hemERT_R | CCTCGACATTTAATGCACCTACCC | |
| hemQRT_F | CGCATTGCTGACTTCCTAATC | |
| hemQRT_R | GGTCATACATTAATTTTTGGCG | |
| isdGRT_F | ATTTTACACGAGACATGGGATTG | |
| isdGRT_R | GGGCTACTTTCATCTTCATTTTTAC | |
| isdIRT_F | CAGTGCGGAAGAAACGATTGAAC | |
| isdIRT_R | GACTTTGCTGTCCATCGTCATCAC | |
| isdART_F | GGATGACTATATGCAACACCCTGG | |
| isdART_R | CATTGTTTGGTTTTGCTGCGTC | |
| isdBRT_F | CATAGCGCACCAACTCTCGTC | |
| isdBRT_R | CCGTTTGATACAGAGAAGCGAATG | |
| isdERT_F | CTTAACCAGCTGTCAATCTTCCAGTTCTCA | |
| isdERT_R | AACATTCGGCTCCATTGGTTGACC | |
| isdCRT_F | GTAAAAACACTGCCAAAGATGAACGC | |
| isdCRT_R | GCACCTGCTACATCAGTTGGTCCAT | |
| hrtBRT_F | GCGCATAGTTCCATTGTGCTATTGAA | |
| hrtBRT_R | GCTTGCTCTGCTTGATAACTCGCA | |
| htsART_F | GCTAAAGCTTTAAATAAAGAAAAAGAAGGCG | |
| htsART_R | GTTCGTTTAAAAATTGTCCAACATATGAATAG | |

## Gene cloning

The genes encoding *S. aureus* Newman IsdG and IsdI were amplified, by standard PCR reactions, from genomic DNA using the Phusion High-Fidelity DNA Polymerase (Thermo Fischer) and the oligonucleotides

described in Table 2. DNA fragments were cloned into either pET-23b or pET-28a vectors (Novagen) to produce wild type proteins and N-terminal His-Tag fused proteins, respectively. All plasmids were confirmed for gene integrity by DNA sequencing.

For the complementation experiments, plasmid pET-23b containing combinations of *hemH*, *hemQ*, *hemY*, *isdG*, *isdI* of *S. aureus* (*Sa*), namely pET-23b-S*ahemYHQisdG*, pET-23b-*SahemYHQisdI,* were generated by the link and lock methodology (19).

For the Förster Resonance Energy Transfer (FRET) studies, the *isdG*, *isdI*, *hemH* and *hemQ* genes amplified from *S. aureus* genomic DNA, as described above, were cloned into pBCB plasmids, which were kindly provided by Mariana Pinho (ITQB-NOVA, Portugal).

HemH and HemQ proteins fused at the N-terminal to GFP were generated by cloning the respective genes into SphI/SpeI-pBCB1-*gfp* vector whereas IsdG, IsdI, HemH and HemQ were fused at the C-terminal to mCherry (mCh) by cloning into the KpnI/NheI-pBCB7-*mCh* vector. After confirmation of the correct sequence of the fusion genes, BL21(DE3)Gold cells were used as recipient for the generated plasmids and analyzed by FRET.

For the flow cytometry experiments, the *S. aureus isdG* gene was cloned into the EcoRI/KpnI restriction sites of pWhiteWalker3 (kind gift of Simon Foster, University of Sheffield, UK) to generate the in-frame fusion *isdG-gfp* (pWW-*isdG-gfp*). Plasmid pWhiteWalker3 that expresses only GFP (pWW-*gfp*) was also constructed to be used as control. For this purpose, a gBlock gene fragment of 244 bp that includes a ribosomal binding site and the N-terminal sequence of GFP (Integrated DNA Technologies) was cloned into EcoRI/NcoI-pWW-*isdG-gfp*. The correct sequence of the two recombinant plasmids was confirmed, and after electroporation into *S. aureus* the fluorescence level of GFP was analyzed by flow cytometry.

**Complementation experiments**

Plasmid pET-23b harboring combinations of genes of *S. aureus hemY*, *hemH*, *hemQ*, *isdG*, *isdI,* and *E. coli hemH* were transformed into competent cells of *E. coli* ferrochelatase mutant Δ*visA* (kind gift from Mark O'Brian State, University of New York at Buffalo, New York, USA) (20). Overnight cultures were grown in LB supplemented with ampicillin and 5 μM hemin and 1 ml aliquots of cells were centrifuged at 1700 *x g* for 5 min and washed three times with LB. These pellets were used to inoculate LB-ampicillin, and growth was monitored for 8 h by measuring the optical density at 600 nm ($OD_{600}$) in a spectrophotometer (Multiskan™ GO, ThermoFisher Scientific). Assays were done for two independent biological samples.

**Infection assays**

Murine macrophages J774A.1 (5 x $10^5$ cells/ml) (LGC Promochem) were cultured in Dulbecco's modified Eagle's medium (DMEM) supplemented with 10% of fetal bovine serum, 100 μM of non-essential amino acids (Gibco), 50 U $ml^{-1}$ of penicillin (Gibco), and 50 μg $ml^{-1}$ of streptomycin (Gibco) in 24-well plates, at 37°C in a 5% CO2-air atmosphere. Prior to infection, macrophages were activated with 5 μg $ml^{-1}$ LPS (Sigma) and 1 μg $ml^{-1}$ IFN-Y (Sigma), for 5 h. *S. aureus* wild type and Δ*hemH* mutant were inoculated, separately, in TSB medium and grown overnight. The cultures were re-inoculated in TSB, and 4 ml of cells grown to an $OD_{600}$= 0.4 were centrifuged at 4300 *x g* for 5 min and washed three times with PBS. Cells were then resuspended in DMEM, diluted to OD=0.05 (~$10^7$ $CFU.ml^{-1}$) and used to infect the murine macrophages. After 30 min of infection, at 37 °C, cells were washed twice with PBS and incubated with 50 μg $ml^{-1}$ of gentamycin, at 37 °C, for 10 min, to prevent extracellular bacterial growth. Immediately after the addition of DMEM (time zero) and 2 and 4 h later, macrophages were collected, lysed with 2% of saponin and the number of

intracellular bacteria was determined by CFU counting on TSB agar plates, which also contained 4 μM hemin to allow for the growth of the ferrochelatase mutant strain. Experiments were done for three independent biological samples assayed in duplicate.

**Production of recombinant proteins**

For the purification of *S. aureus* ferrochelatase HemH, pET-23b-*SahemH* was transformed into BL21STAR(DE3) pLysS (Novagen) competent cells that were grown in LB medium at 37 °C and 150 rpm. Cells at an $OD_{600}$ of 0.6 were induced by addition of 400 μM of isopropyl β-D-1-thiogalactopyranoside (IPTG) in the presence of 8 mg $ml^{-1}$ of $FeSO_4$ and grown for an additional 16-20 h, at 20 °C. For the production of *S. aureus* IsdG and IsdI, plasmids pET-23b-*SaisdG* and pET-23b-*SaisdI* were transformed, separately, in competent cells of *E. coli* BL21(DE3)Gold. Cells were grown in LB medium until reaching an $OD_{600}$=0.7, and the protein expression was induced by addition of 1 mM of IPTG to the medium, and cells grown at 30°C for 3 h. Cells were harvested by centrifugation (10000 *x g*, 15 min, 4 °C), and the pellets were resuspended in 50 mM Tris-HCl pH 7.5 (Buffer A). Cells were disrupted in a French press operating at 1000 Psi, and centrifuged at 27216 *x g*, at 4°C, for 15 min. The supernatant was applied onto a $Ni^{2+}$ Sepharose fast flow column (GE Healthcare), previously equilibrated with buffer A supplemented with 10 mM of imidazole, and the proteins were eluted at 400 mM of imidazole and dialysed against buffer A. Proteins with level of purity >95%, as judged by SDS-PAGE, were concentrated in an Amicon Stirred Ultrafiltration Cell using a 10 kDa membrane (Millipore) and frozen until use.

## Enzymatic activities

*Catalase activity*

Overnight cultures of *S. aureus* wild type, Δ*hemH* mutant were grown in TSB only or supplemented with 4 μM hemin to an $OD_{600}$ of 1. Cells were pelleted by centrifugation (10000 *x g*, 10 min), resuspended in buffer A and incubated with 7 μg of lysostaphin for 45 min, at 37 °C. The protein concentration of the cell lysates was determined using the Pierce Bicinchoninic acid Protein Assay (Thermo Scientific) and Sigma protein standards. For the catalase activity assays, approximately 26 μg of cells lysate proteins were added to buffer A containing 10 mM $H_2O_2$. The catalase activity was measured by following the decrease in absorbance at 240 nm for the formation of $H_2O_2$ ($\varepsilon_{240nm}$ = 43.6 $M^{-1}cm^{-1}$) in a Shimadzu UV-1700 spectrophotometer. Assays were done in triplicate.

*Ferrochelatase activity*

The assays were performed under anaerobic conditions in a Coy model A-2463 and Belle Technology chamber equipped with a Shimadzu UV-1800 spectrophotometer. For the preparation of coproporphyrin III (copro III) solution, 1–2 drops of 25% $NH_4OH$ was added to 1-3 mg of copro III powder followed by addition of 1 ml of water. Copro III concentration was determined spectrophotometrically in 0.1 M HCl ($\varepsilon_{548}$ = 16.8 mM−1 $cm^{-1}$). For the ferrochelatase assay, HemH (10 μg) was pre-incubated with IsdI (1:10 molar ratio) or IsdG at room temperature, for 10 min. Next, these proteins were added to the reaction mixture that contained copro III (10 μM) and $(NH4)_2Fe(SO_4)_2$ (50 μM). The IsdG titration experiments, where performed using IsdG concentrations of 0.6, 1.2, 3 and 6 mM, which correspond to 1:1, 1:2, 1:5 and 1:10 stoichiometry relative to the concentration of HemH. The chelatase activity was measured by following

the decrease in absorbance of copro III, measured at 392 nm ($\varepsilon_{392nm}$ = 0.115 $\mu M^{-1}cm^{-1}$). Assays were done in triplicate.

**Heme abundance assays**

*S. aureus* wild type and Δ*isdG* mutant cells were grown for 8h and then diluted in TSB in the presence of 400 μM of aminolaevulinic acid. Cells were harvested by centrifugation (8000 x g, 5 min, 4 $^{o}$C), washed and resuspended in buffer A, and incubated with lysostaphin, at 37 $^{o}$C, for 45 min. The supernatant was collected by centrifugation and the intracellular heme was quantified essentially as previously described (21, 22). Cell extracts (250 μL) were mixed with the same volume of a solution containing 0.5 M NaOH and 2.5 % Triton-X-100, and the haemetine formation was determined measuring the absorbance at 575 nm in a spectrophotometer Shimadzu UV-1700. Hemin from Frontier Scientific was used as standard.

**Mass spectrometry of tetrapyrrole products**

The plasmids pET-23b containing combinations of *hemY*, *hemH*, *hemQ*, *isdG* and *isdI* were inserted into *E. coli* ferrochelatase mutant Δ*visA*. Cells were prepared as described above for the complementation experiments, and inoculated in LB medium to an $OD_{600}$~0.05 and grown for 7 h. Cells were harvested by centrifugation at 10000 *x g* for 10 min, resuspended in buffer A, disrupted at 900 Psi in a French press, and centrifuged at 17000 *x g* for 30 min, at 4 °C. Protein content of the cell-free lysates was quantified using a Nanodrop ND-2000C (Thermo Scientific). Lysates with the equal protein concentration were treated for heme extraction. Briefly, proteins were precipitated by incubation of lysates with an acetone:HCl (19:1 vol/vol) mixture for 20 min, at room temperature, and removed by centrifugation at 14000 *x g* for 2 min. Following addition to supernatants of 1 ml of cold water, few milligrams of $(NH_4)_2SO_4$ (Panreac)

and 300 µl of pure ethyl acetate (Sigma), heme was extracted from the organic phase after centrifugation at 14000 *x g* for 2 min. Samples were resolved by HPLC-MS on an Ace 5 AQ column attached to an Agilent 1100 series HPLC, equipped with a diode array detector and coupled to a micrOTOF-Q II (Bruker) mass spectrometer. Separation of the products was achieved by applying a gradient composed by 0.1% TFA and acetonitrile, at a flow rate of 0.2 ml $min^{-1}$. The column was first equilibrated with 20% solvent B, and after sample injection the concentration of solvent B was increased up to 100% during 50 min. Heme quantification was done by measuring the area of absorbance peak at 400 nm for m/z 616 (heme).

**Flow cytometry**

Overnight cultures of *S. aureus* RN4220 transformed with pWW-*isdG-gfp,* pWW-*isdI-gfp* or pWW-*gfp* were grown in TSB to an $OD_{600}$~1.5, diluted to an $OD_{600}$ of 0.1 in TSB supplemented with 10 µM of IPTG, and grown for one extra hour. At this stage, cells were divided in 10 ml aliquots and grown for 4 h in the absence and in the presence of 5 µM hemin or 400 µM of aminolaevulinic acid. Cells (1 ml) were collected by centrifugation at 11400 *x g* for 1 min, and the pellets were washed 3 times with PBS, diluted in PBS to an $OD_{600}$ of 0.1 and analyzed in a Cell Sorter S3e™ (Biorad). For each sample, at least, 300,000 cells were collected and analyzed with the FlowJo software (Tree Star), and three biological samples were measured for each condition.

**Fluorescent labelling of HemH**

*S. aureus* HemH was covalently labelled with 5-dimethylaminonaphthalene-1-sulfonyl chloride (dansyl chloride) according to the manufacturer´s instructions (Invitrogen). Briefly, recombinantly produced and purified *S. aureus* HemH (7.5 $mg.ml^{-1}$), solubilized in 0.1 M sodium

bicarbonate pH 8.6, was incubated in a 1:1 ratio with dansyl chloride (10 mg $ml^{-1}$ in dimethylformamide) for 1 h at 4°C, in the dark and under continuous stirring. The reaction was quenched by the addition of hydroxylamine (1.5 M, pH 8.5), and the mixture was then loaded onto a PD-10 column (GE Healthcare) equilibrated with buffer A in order to remove the excess of free dye by gel filtration. The HemH:dansyl labelling ratio was determined by spectrophotometric quantification of the dye ($\varepsilon_{331nm}$ = 4,000 $M^{-1}$ $cm^{-1}$) (23) and of HemH ($\varepsilon_{280nm}$ = 47,700 $M^{-1}$ $cm^{-1}$) (24), and estimated to be 0.97.

**Steady-state fluorescence anisotropy measurements**

Dansyl-labeled HemH (0.67 µM) was incubated with variable concentrations of IsdG or IsdI in buffer A.

The steady-state fluorescence anisotropy of each sample, <*r*>, was calculated according to:

$$< r >= \frac{I_{\mathrm{VV}} - G \cdot I_{\mathrm{VH}}}{I_{\mathrm{VV}} + 2\,G \cdot I_{\mathrm{VH}}} \qquad (1$$

where $I_{VV}$ and $I_{VH}$ are the fluorescence intensities (blank subtracted) of the vertically and horizontally polarized emission, when the sample is excited with vertically polarized light, respectively. The *G* factor ($G = I_{HV}/I_{HH}$) is an instrument correction factor which takes into account the transmission efficiency of the monochromator to the polarization of the light. Measurements were performed at 25 °C on a Fluorolog-3-21 spectrofluorometer (Horiba Jobin Yvon) with automated dual polarizers using 5-mm path length quartz cuvettes. The excitation wavelength was 340 nm with a bandwidth of 6 nm, and the fluorescence emission was recorded at 530 nm with 5 nm bandwidth. *Kd* and $<r>_B$ parameters were obtained by fitting the experimental data (steady-state fluorescence anisotropy, <*r*>

versus $[\mathrm{P2}]_t$, the total concentration of the binding partner 2 (dimeric IsdG or IsdI) using the equation:

$$< r >=< r >_f + \frac{([\mathrm{P1}]_t+[\mathrm{P2}]_t+K_\mathrm{d})-\sqrt{([\mathrm{P1}]_t+[\mathrm{P2}]_t+K_\mathrm{d})^2-4[\mathrm{P1}]_t\cdot[\mathrm{P2}]_t}\cdot(<r>_b-<r>_f)}{2[\mathrm{P2}]_t}$$

Where $[P1]_t$ represents the total concentration of the binding partner 1. The concentration of HemH was fixed to 0.67uM during the non-linear regression and assumed that the fluorescently-labeled protein is monomeric in solution; $[P2]_t$ is the total concentration of the binding partner 2. Binding stoichiometry was considered 1:1; $< r >_f$ represents the steady-state fluorescence anisotropy of the free protein. $<r>_F$= 0.165 (fixed during the analysis); and $< r >_b$ the steady-state fluorescence anisotropy of the bound protein.

**Förster Resonance Energy Transfer (FRET) and Fluorescence Lifetime Imaging Microscopy (FLIM)**

*E. coli* BL21(DE3)Gold were co-transformed with plasmids that express combinations of HemH, HemQ, IsdI and IsdG fused to GFP and mCherry (mCh) fluorophore proteins, namely pBCB-*hemH-gfp* and pBCB-*isdG-mCh*; pBCB-*hemH-gfp* and pBCB-*isdI-mCh*; pBCB-*hemQ-gfp* and pBCB-*isdG-mCh*; and pBCB-*hemQ-gfp* and pBCB-*isdI-mCh* (Table 3). Cells grown overnight in LB were sub-cultured into LB medium to an $OD_{600}$ of 0.15, supplemented with 1 mM IPTG and grown for 4 h. Cells (2 ml) were centrifuged at 4300 *x g* for 3 min, and fixed by incubation with 4% formaldehyde (vol/vol) in PBS, at room temperature, for 30 min and 90 rpm, washed with PBS and immobilized on 8 well µ-slides (Ibidi, slides, Germany) for FRET-FLIM experiments.

**Table 3.** List of plasmids used in this work

| Plasmid | Plasmid description | Phenotype | Reference |
|---|---|---|---|
| pET-23b-*SahemH* | *S. aureus hemH* cloned into pET-23b | $Amp^r$ | (7) |
| pET-23b-*SahemY* | *S. aureus hemY* cloned into pET-23b | $Amp^r$ | (7) |
| pET-23b-*SahemQ* | *S. aureus hemQ* cloned into pET-23b | $Amp^r$ | (7) |
| pET-23b-*SahemYHQ* | *S. aureus hemH*, *hemY* and *hemQ* cloned into pET-23b | $Amp^r$ | (7) |
| pET-23b-*SahemYHQisdG* | *S. aureus hemH*, *hemY*, *hemQ* and *isdG* cloned into pET-23b | $Amp^r$ | This study |
| pET-23b-*SahemYHQisdI* | *S. aureus hemH*, *hemY*, *hemQ* and *isdI* cloned into pET-23b | $Amp^r$ | This study |
| pET-23b-*SaisdG* | *S. aureus isdG* cloned into pET-23b | $Amp^r$ | This study |
| pET-23b-*SaisdI* | *S. aureus isdI* cloned into pET-23b | $Amp^r$ | This study |
| pET-23b-*EchemH* | *E. coli hemH* cloned into pET-23b | $Amp^r$ | This study |
| pET-23b-*EchemH-SaisdG* | *E. coli hemH* and *S. aureus isdG* cloned into pET-23b | $Amp^r$ | This study |
| pET-23b-*EchemH-SaisdI* | *E. coli hemH* and *S. aureus isdI* cloned into pET-23b | $Amp^r$ | This study |
| pBCB1-*gfp* | pMutin derivative vector for N- and C-terminal GFP fusions | $Amp^r$ $Ery^r$ | (25) |
| pBCB7-*mCH* | pMutin derivative vector for N- and C-terminal mCherry fusions | $Amp^r$ $Ery^r$ | (25) |
| pBCB-*hemHgfp* | *S. aureus hemH* cloned into pBCB1-GE | $Amp^r$ $Ery^r$ | This study |
| pBCB-*hemQgfp* | *S. aureus hemQ* cloned into pBCB1-GE | $Amp^r$ $Ery^r$ | This study |
| pBCB-*isdGmCH* | *S. aureus isdG* cloned into pBCB7-ChK | $Amp^r$ $Kan^r$ | This study |
| pBCB-*isdImCH* | *S. aureus isdI* cloned into pBCB7-ChK | $Amp^r$ $Kan^r$ | This study |
| pBCB-*hemHmCH* | *S. aureus hemH* cloned into pBCB7-ChK | $Amp^r$ $Kan^r$ | This study |
| pBCB-*hemQmCH* | *S. aureus hemQ* cloned into pBCB7-ChK | $Amp^r$ $Kan^r$ | This study |
| pWhiteWalker | pCQ11 derivative for C-terminal GFP and mCherry fusions | $Amp^r$ $Ery^r$ | (26) |
| pWW-*gfp* | pWhiteWalker containing the *gfp* gene | $Amp^r$ $Ery^r$ | This study |
| pWW-*isdGgfp* | *S. aureus isdG* fused to *gfp* and cloned into pWhiteWalker | $Amp^r$ $Ery^r$ | This study |

All measurements were acquired in a Leica TCS SP5 (Leica Microsystems CMS GmbH, Mannheim, Germany) inverted confocal microscope (DMI6000). A 63x apochromatic water immersion objective with a NA of 1.2 (Zeiss, Jena Germany) was used for all experiments. GFP and mCherry were excited respectively with the 476 nm and 514 nm lines from an Argon laser, and fluorescence emission was collected in the 485-540 nm range for GFP, and 580-700 nm for mCherry. In these conditions, spectral bleed-through was negligible.

Fluorescence lifetime imaging microscopy (FLIM) measurements were performed by time correlated single photon counting (TCSPC) using the confocal microscope coupled to a multiphoton Titanium: Sapphire laser (Spectra-Physics Mai Tai BB, Darmstadt, Germany) as the excitation source. FLIM data was acquired during 90-180 seconds to achieve reasonable photon statistics. The excitation wavelength was set to 840 nm and emission light was selected with a dichroic beam splitter with an excitation SP700 short-pass filter and an emission 525±25 nm band-pass filter inserted in front of the photomultiplier. Images were acquired using a Becker and Hickl SPC 830 module. Fluorescence decays for each cell were calculated by integrating the FLIM data for all pixels of each individual cell. Fluorescence lifetimes were obtained by analysing the fluorescence decays through a least square iterative re-convolution of decay functions with the instrument response function (IRF) using the software SPCImage (Becker and Hickl, Berlin, Germany). Intensity-weighted mean fluorescence lifetime ($\langle\tau\rangle$) of multiexponential decays were calculated as $\langle\tau\rangle = \sum_i \alpha_i \tau_i$, were $\alpha_i$ are the pre-exponential factors and $\tau_i$ are the individual lifetime values. Average FRET efficiencies in each cell can be determined from $<E> = 1- \langle\tau\rangle_{DA}/\langle\tau\rangle_D$, where $\langle\tau\rangle_{DA}$ and $<\tau>_D$ are the donor intensity-weighted mean fluorescence lifetime in the presence of acceptor and in the absence of acceptor, respectively. Assays were done for two independent biological samples and FRET efficiencies were determined for several cells.

## Genomic analysis

A dataset composed of 5060 complete prokaryotic genomes was downloaded from RefSeq (June 2016) (27). These correspond to all complete genomes available at the time in RefSeq. Taxonomic information was retrieved from NCBI and genomes were grouped by phylum or class. Homologous proteins involved in the several steps of heme biosynthesis and uptake (Urogen III synthesis: HemALBCD; PPD heme biosynthesis HemE(F/N)(Y/G/J)H; alternative heme biosynthesis: AhbABCD; S. aureus heme biosynthesis variant: HemEYHQ; *Staphylococcus* heme uptake and degradation: HstABC, IsdABCDEFGHI-SrtB, *B. subtilis* heme uptake: IsdCEDFGX1X2-Hal; heme oxygenases IsdG-type: MhuD, HmuQ/D; other heme oxygenases: HemO, HmuO, HmuS, HugZ, ChuS; heme transporters: HmuTUV, IsdEFD, HtsABC, Rv2002c-Rv2003-Rv2006c) were identified by BLAST (28) (E-value smaller than $10^{-10}$ and local amino acid identity of at least 25%). To distinguish between heme transporters systems from siderophores and/or cobalamin importers, sequences from biochemically-characterized transporters were used as queries as well. All query proteins are listed in Supplementary Data 1. When relevant, PFAM-A domain annotations were obtained by using the HMM approach as available at PFAM (29). Query coverage, gene fusions and genomic organization were also used for the identification of true positive hits. Due to their small length, to distinguish between the different IsdG homologous, an all versus all blast of putative IsdGs and query sequences and an alignment were performed. Hits were classified according to their best hit based on sequence identity, conservation of the catalytic triad (for HmoA) and sequence length. Selected IsdG-type homologous identified by Blast were aligned with ClustalO (30) and a maximum likelihood tree reconstructed with IQTree (Best-model selection WAG+G4)(31).

To distinguish between “bona fide” HemN from highly similar non-functional HemNs, all genomes were also queried for the presence of non-functional HemN in a similar way as in Dailey *et al* 2015 (8). To distinguish between HemQ and chlorite dismutases, sequences were aligned with ClustalO and a phylogenetic tree performed. Sequences corresponding to chlorite dismutases were discarded based on the conservation of the catalytic residues and position within a phylogenetic tree. A heme biosynthesis pathway was only considered to be present in a genome if: 1) 80% of its genes were identified and 2) if the characteristic proteins were present, HemN and/or HemF for classical heme pathway and HemQ for *S. aureus* variant. Cases in which a variant of the canonical pathways above described were present and/or missing one gene were assigned as hybrid or incomplete. Due to the high sequence similarity between genes involved in heme *d1* biosynthesis with genes from the heme alternative pathway (5), in organisms containing $cd_1$ nitrite reductase, the heme alternative pathway identified genes were considered to be involved in heme $d_1$ synthesis instead.

**Statistical analysis**

In all figures, error bars represent the standard deviation of at least two biological samples. Statistical differences were calculated by the two-tailed Student's t-test using GraphPad Prism (GraphPad Software).

## 5.4. Results

### The heme oxygenase IsdG interferes with heme formed via the heme biosynthesis pathway

To analyze the role of the two heme oxygenases of *S. aureus*, the *S. aureus* CPD pathway was reconstituted in a hemin auxotrophic strain of the Gram-negative bacteria *E. coli* that is deficient in protoporphyrin ferrochelatase (Δ*visA*). As *E. coli* does not take up exogenous heme through an Isd system, this host represents a good model to study the role of IsdG/I enzymes without the interference of an endogenous heme acquisition system, thus avoiding the use of *S. aureus* strains containing multiple mutations. The genes encoding the last three enzymes of the *S. aureus* CPD pathway, *hemYHQ*, were cloned by the Link and Lock method (19), expressed in the presence of either IsdG or IsdI in *E. coli* Δ*visA*, and growth of the complemented strain was monitored. The results showed that expression of HemYHQ alone abolished the heme auxotrophy of the strain. However, in the presence of either IsdG or IsdI, the growth of the strain was impaired (Fig. 5.2A).

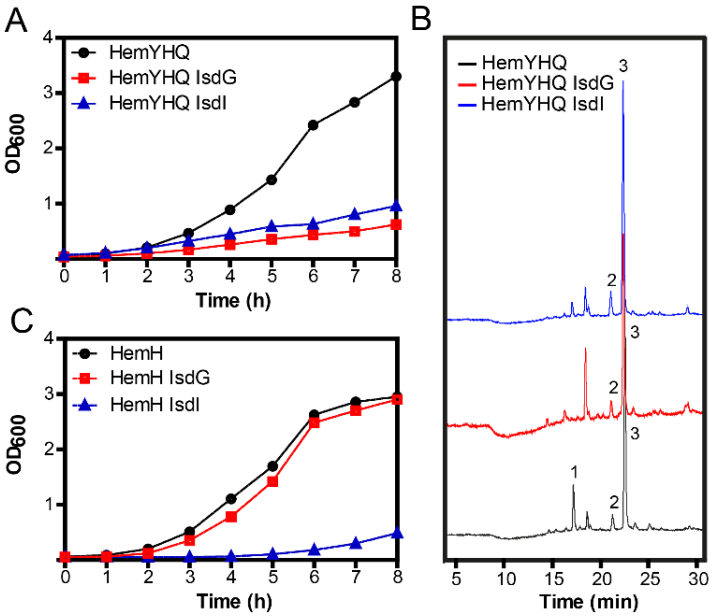


**Figure 5.2.** *S. aureus* IsdG and IsdI impair heme formation. (A) Growth of *E. coli* Δ*visA* cells complemented with *S. aureus* HemYHQ alone, or HemYHQ and *S. aureus* IsdG (HemYHQ IsdG) or HemYHQ and *S. aureus* IsdI (HemYHQ IsdI). (B) HPLC-MS profile of cells depicted in (A), with peaks corresponding to heme (m/z = 616; peak 1), iron-coproporphyrin III (m/z = 708; peak 2), and protoporphyrin IX (m/z = 553; peak 3). (C) Growth of *E. coli* Δ*visA* cells complemented with *E. coli* HemH alone or HemH and *S. aureus* IsdG (HemH IsdG) or HemH and *S. aureus* IsdI (HemH IsdI). Experiments were performed for two independent biological samples.



In order to understand the growth behavior of the complemented strains, the tetrapyrrole products formed during the expression of *S. aureus hemYHQ* genes in the presence of IsdI or IsdG were analyzed by HPLC-MS. As expected, cells expressing *S. aureus* HemYHQ exhibited a peak with a mass-to-charge ratio (*m/z*) of 616, confirming their ability to produce heme. However, this peak significantly decreased when IsdG or IsdI were also expressed (Fig. 5.2B), with cells expressing *S. aureus* HemYHQ-IsdI containing approximately 3 times less heme, and cells expressing HemYHQ together with IsdG showing no detectable peak corresponding to heme.

These results suggest that the heme oxygenases interfere with the heme formation *in vivo*.

To investigate whether the lack of heme formation promoted by *S. aureus* IsdG/IsdI was due to degradation of the heme formed or by inhibition of the CPD pathway, we repeated the experiments in an *E. coli* strain that synthesizes heme via the PPD pathway. To this end, the growth of an *E. coli* ferrochelatase mutant Δ*visA*, complemented with its own ferrochelatase was analyzed after expression of the *S. aureus* IsdG or IsdI.

Expression *in trans* of *E. coli ppfC* alone and in the presence of IsdG fully restored the heme auxotrophy of the Δ*visA* mutant strain. In contrast, growth impairment was observed when IsdI was present (Fig. 5.2C). These results show that only IsdI is able to degrade the heme formed through the PPD pathway.

Collectively, from these results we can infer that IsdI promotes the degradation of heme, whether it is biosynthesized by either the PPD or CPD branches, or acquired exogenously, as recovery of heme auxotrophy is not observed when IsdI is present. In marked contrast, IsdG was only observed to prevent recovery of heme auxotrophy when it was expressed together with the enzymes of the CPD pathway.

**IsdG decreases the ferrochelatase activity of HemH**

To understand how the *S. aureus* IsdG and IsdI constrain the CPD pathway, we tested whether they interfere with the activity of the *S. aureus* HemQ enzyme that catalyzes the last step of the CPD branch promoting the conversion of iron-coproporphyrin III into heme in the presence of its electron acceptor (7). Thus, *S. aureus* HemQ was incubated with iron-coproporphyrin III in the presence of either IsdG or IsdI and hydrogen peroxide. However, control experiments performed in the absence of HemQ showed that hydrogen peroxide activates the inherent peroxidase activity in IsdG and IsdI,

leading to degradation of the iron-coproporphyrin III substrate (Fig. S5.1). We therefore shifted our attention to the penultimate enzyme of the CPD branch, the ferrochelatase HemH, which plays an important role in the survival of *S. aureus* (Fig. 5.3), as also shown for the HemA and HemB enzymes involved in the first steps of the CPD pathway (32, 33)

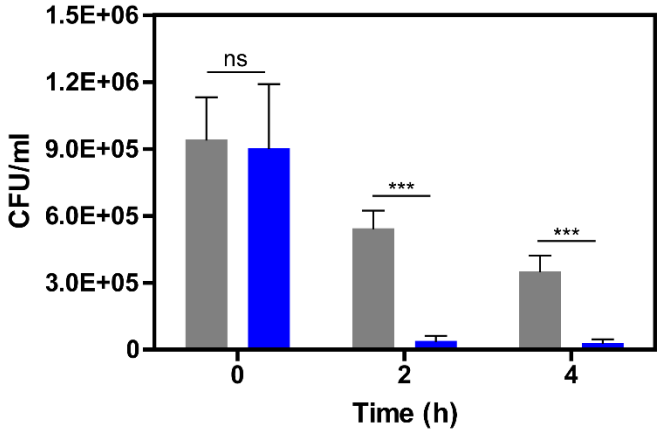


**Figure 5.3.** Importance of ferrochelatase for *S. aureus* survival. Activated murine macrophage J774 A.1 cells were incubated with *S. aureus* wild type (dark grey) and ferrochelatase *ΔhemH* mutant (blue) and bacterial survival was evaluated 2 h and 4 h post-infection. While immediately after infection similar survival rates were observed for the wild type and *ΔhemH* mutant strains, the viability of the *ΔhemH* mutant significantly decreased after 2 h and 4 h. Data represent the mean and standard deviation of three independent experiments, using the two-tailed unpaired Student's t-test (*** $p < 0.001$).

In *S. aureus* and other Gram-positive operating via the CPD pathway, the ferrochelatase incorporates iron into coproporphyrin III to form iron-coproporphyrin III, which is then sequentially decarboxylated by HemQ to yield protoheme. We observed that the cell lysate of *S. aureus hemH* mutant contained very low levels of cellular catalase activity, which was restored to wild type level upon addition of external hemin (Fig. 5.4). It was previously reported that the total cellular catalase activity was lower in *S. aureus hemB* and *hemQ* defective strains (34).

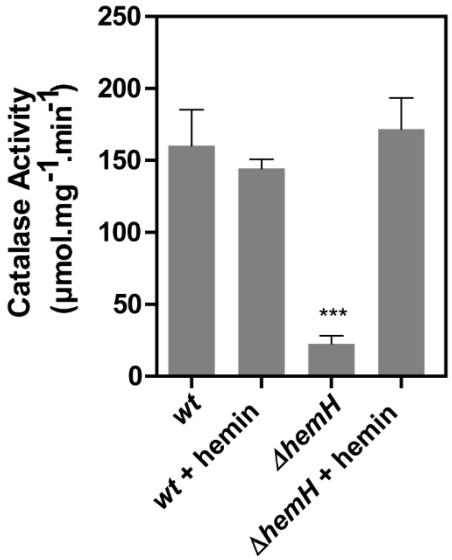


**Figure 5.4** – Inactivation of ferrochelatase lowers cellular catalase activity. Catalase activity of cell extracts from *S. aureus* wild type (*wt*) and Δ*hemH* mutant cells. Cells were grown in TSB and, where indicated, supplemented with 4 µM hemin.

We next tested whether the heme oxygenases impaired ferrochelatase activity. *S. aureus* HemH, IsdG and IsdI were recombinantly produced and purified, yielding stable proteins that had the expected molecular masses of approximately 35 and 12.5 kDa, respectively. *S. aureus* ferrochelatase activity was determined by following the formation of iron-coproporphyrin III, which yielded a specific activity of 61.6 ± 4.1 $nmol.min^{-1}mg^{-1}$. While addition of IsdI to the reaction mixture caused no significant alteration (Fig. 5.5A), the presence of IsdG led to a ~50% decrease in ferrochelatase activity. Furthermore, the activity of the enzyme decreased with increasing concentration of IsdG (Fig 5.5B).

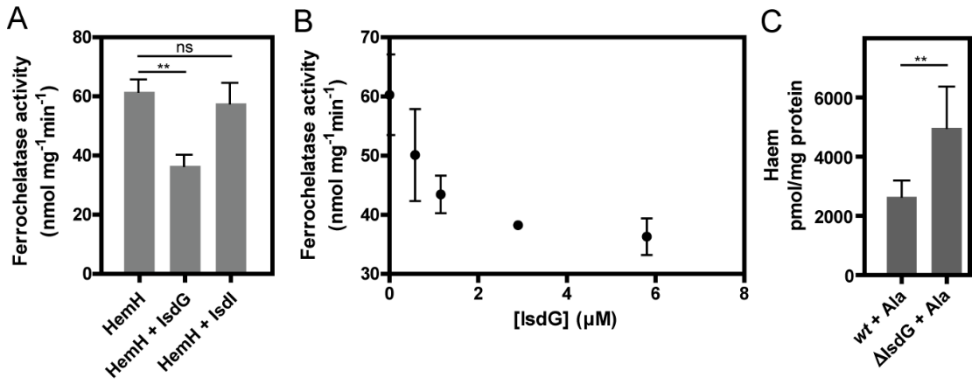


**Figure 5.5.** Influence of *S. aureus* IsdG on the CPD pathway. (A) IsdG decreases the ferrochelatase activity of *S. aureus* HemH while IsdI does not impair the activity. (B) Inhibition of *S. aureus* HemH ferrochelatase activity increases with IsdG concentration. (C) Intracellular heme quantification of *S. aureus* wild type and Δ*isdG* mutant for cells grown in the presence of 400 μM of aminolaevulinic acid (Ala).

In (A) and (B), activities were measured in reaction mixtures containing HemH alone, or with the addition of IsdG or IsdI, using coproporphyrin III (10 μM) and $(NH4)_2Fe(SO4)_2$ (50 μM) as substrates. In (B), IsdG was used in the following concentrations: 0.6, 1.2, 3.0 and 6.0 mM. Data depict the mean and standard deviation of three samples using a two-tailed unpaired Student's t-test (** $p < 0.01$).



These results show that IsdG, but not IsdI, attenuates the activity of the *S. aureus* HemH. Therefore, we next determined the heme cellular content in cells forming heme by the CPD pathway in the presence and absence of IsdG. For this purpose, *S. aureus* wild type and Δ*isdG* mutant cells were grown in the presence of aminolaevulinic acid, the first stable precursor of the heme biosynthesis pathway. Figure 5.5C shows that the IsdG inactivated strain has significantly higher heme content. Therefore, we conclude that IsdG impairs HemH lowering the amount of heme formed by the CPD pathway.

**Protein-protein interaction studies between IsdG and HemH**

We reasoned that the inhibition of the *S. aureus* HemH activity by IsdG is most likely to result from a direct interaction between the two proteins. To study this interaction *in vivo* fluorescence lifetime imaging based Förster resonance energy transfer (FLIM-FRET) was used. Additionally, interactions among the various CPD pathway protein components and *S. aureus* heme oxygenases were also evaluated. In order to do this, we constructed *S. aureus* HemH and hemQ proteins fused to a GFP donor molecule and IsdG, IsdI, HemQ and HemH fused to a mCherry acceptor molecule (Table 3).

The interaction between IsdG and HemH was analyzed in bacterial cells expressing *S. aureus* HemH-GFP and IsdG-mCherry. HemH-GFP exhibited a mono-exponential fluorescence decay with a lifetime $\tau_{HemH\text{-}EGFP}$ = 2.2 ± 0.1 ns (Fig S5.2). In the presence of IsdG-mCherry, the fluorescence decay of HemH-GFP was no longer accurately described by a single exponential and a shorter component had to be included in the fit, indicating the presence of FRET and thus an interaction between the two proteins (Fig. 5.6 and Fig S5.2). The FRET efficiencies (E) were dependent on the concentration of IsdG, according to the plots of E against mCherry/GFP fluorescence intensity ratios (Fig. 5.6), obtained from the confocal fluorescence measurements of each construct (see Methods).

Although some degree of interaction between HemH-GFP and IsdI-mCherry was also detected (Fig. 5.6A and 5.6C), the FRET efficiencies determined for this protein pair were much lower than those measured for IsdG and HemH (Fig. 5.6B), suggesting a much less efficient interaction. Furthermore, an interaction between HemQ and IsdG, but not HemQ and IsdI, was also observed (Fig. 5.6D and 5.6E).

Together, these data reveal that IsdG interacts with the last two enzymes of the CPD pathway, namely HemH and HemQ.

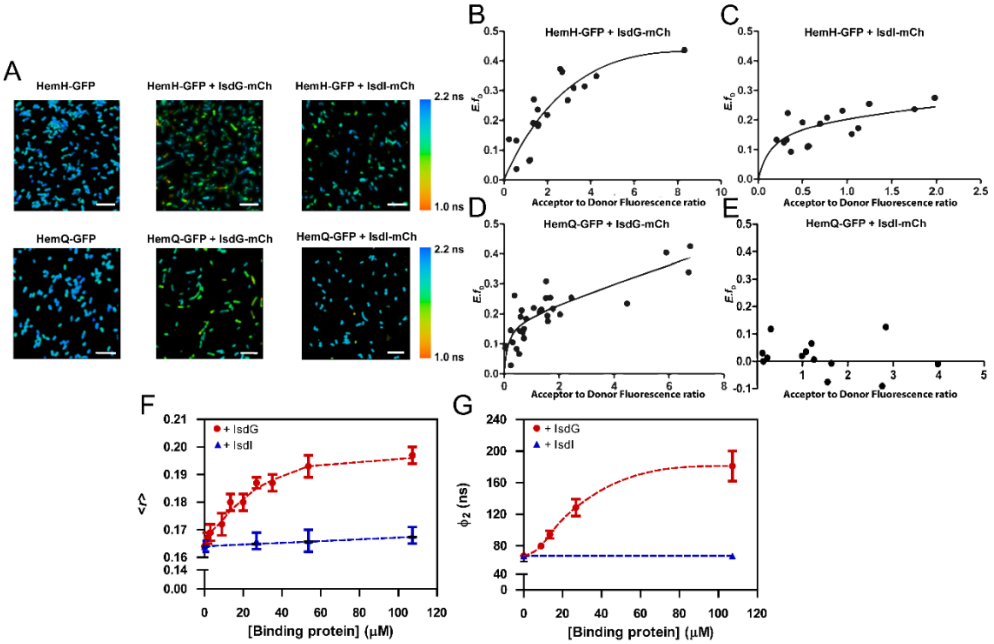


**Figure 5.6**. *S. aureus* HemH and IsdG interact *in vivo*. (A) Representative FLIM-FRET data of *E. coli* cells co-expressing HemH-GFP or HemQ-GFP with IsdG-mCherry or IsdI-mCherry, shown as false color lifetime images. Average fluorescence lifetime (<τ>) was rendered as color according to the color index indicated on the right. Scale bar represents 10 μm. For each cell in (A), the calculated average FRET efficiency (*E*) is plotted against the ratio of fluorescence (as measured by confocal microscopy) from the acceptor (mCherry) construct over donor (GFP), for HemH-GFP/IsdG-mCherry (B), HemH-GFP/IsdI-mCherry (C), HemQ-GFP/IsdG-mCherry (D), and HemQ-GFP/IsdI-mCherry (E). Lines are drawn as a guide to the eye. Data are from one representative sample. (F) Steady-state and (G) time-resolved fluorescence polarization binding assay between dansylated HemH and IsdG or IsdI. (F) The steady-state fluorescence anisotropy, <*r*>, and (G) long correlation fluorescence lifetime, $\phi_2$, of dansylated HemH are plotted as a function of IsdG (red circles) and IsdI (blue triangles) concentrations expressed as monomers. Conditions consisted of 0.7 μM dansyl-labeled HemH in 50 mM Tris-HCl buffer pH 8.0, at 25 ˚C. Dansyl fluorescence was monitored at 530 nm with excitation at 340 nm. The cuvette path length was 5 mm. Data represent the mean values of three independent measurements and error bars represent the standard deviation.

The FLIM-FRET protein-protein interaction studies were complemented with an *in vitro* homogeneous fluorescence polarization binding assay to monitor macromolecular complex formation between the two recombinant *S. aureus* proteins, HemH and IsdG. For this purpose, *S. aureus* HemH was covalently conjugated to dansyl chloride, a long-lived fluorescent probe, in order to evaluate its binding to IsdG using both steady-state and time-resolved fluorescence anisotropy measurements (35). The dansyl-labeled HemH gave a high steady-state fluorescence anisotropy in solution ($\langle r \rangle = 0.164 \pm 0.002$; Fig. 5.6F and Fig. S5.3). Upon increasing the concentration of dimeric IsdG in solution, the steady-state fluorescence anisotropy of dansyl-HemH steadily augmented (Fig. S5.4) reaching a plateau level of $\langle r \rangle \sim 0.20$ (Fig. 5.4F). In contrast, there was negligible binding observed between IsdI and HemH. Upon binding of dimeric IsdG to dansyl-labeled HmeH, the hydrodynamic volume of the protein complex increased, slowing down the overall rotational tumbling of dansyl-labeled HemH in solution during its excited-state fluorescence lifetime and ultimately producing an increase in its steady-state fluorescence anisotropy (20, 21). These data were further corroborated by time-resolved polarized fluorescence measurements of dansyl-labeled HemH during its titration with IsdG. The fluorescence anisotropy decay of dansyl-labeled HemH was greatly affected by addition of IsdG to the solution (Fig. S5.4). In particular, the longer rotational correlation time, $\phi_2$, assigned to the overall rotational motion of dansyl-labeled HemH in solution, increased significantly from $\phi_2 \sim$ 67 ns for dansyl-labeled HemH free in solution to $\phi_2 \sim$ 180 ns for dansy-labeled HemH in the presence of 107 μM IsdG (Fig. 5.6G and Table S5.1). A binding $K_d$ of 14.3 ± 2.6 μM and a $\langle r \rangle_B$ of 0.207 ± 0.003 was determined. These results clearly demonstrate that IsdG has the ability to bind to HemH in solution at physiological pH.

## Hemin increases IsdG expression

In order to assess the impact of heme uptake by the host to its endogenous heme biosynthesis, we determined the expression of the heme biosynthesis genes in *S. aureus* cells grown in medium supplemented with hemin (2.5 µM)**.** Addition of external hemin slightly modified the transcription of *hemA*, *hemE* and *hemQ* (Fig. 5.7A). A similar change was observed with the genes encoding the iron-regulated surface determinants *isdA*, *isdB* and *isdI*, while *hrtB* and *htsA* were strongly upregulated (Fig. 5.7A). Treatment with exogenous hemin also caused a significant induction of the *isdCDEG* operon, (Fig. 5.7A).

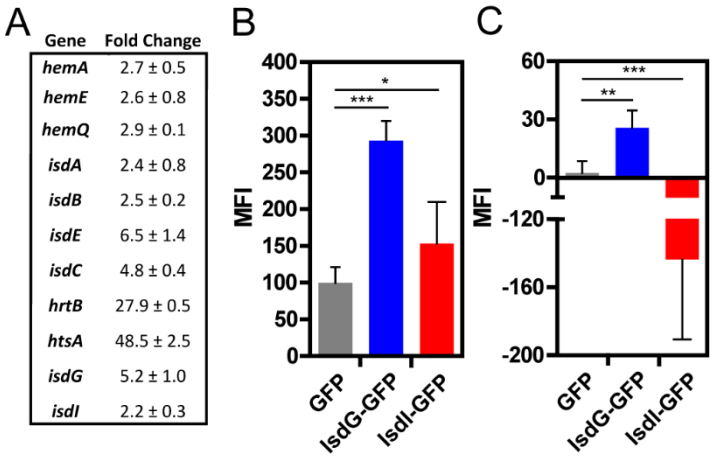


**Figure 5.7.** The cellular content of IsdG in *S. aureus* increases upon incubation with hemin. (A) Fold change in abundance of genes coding for enzymes involved in the heme biosynthesis and uptake pathways upon exposure to hemin. (B) Difference of the median GFP fluorescence intensity (MFI) between hemin-treated (5 µM) and untreated cells. (C) Difference of the median GFP fluorescence intensity between aminolaevulinic acid-treated (400 µM) and untreated cells. Fluorescence was measured in a flow cytometer and over 300,000 cells were counted. Data represent the mean and standard deviation of four measurements, using the two-tailed unpaired Student's t-test (*** $p < 0.001$, **p=0.005 *p=0.04).

The pronounced change in *isdG* gene expression led us to analyze the amount of IsdG protein in cells containing excess heme, which was either

added exogenously to the medium or produced endogenously through supplementation with aminolaevulinic acid. For this purpose, an IsdG-GFP fusion protein was constructed and the amount of IsdG was determined by the direct measurement of the fluorescence derived from the construct by flow cytometry. For comparative purposes, an IsdI-GFP fusion protein was also constructed. *S. aureus* expressing GFP, IsdG-GFP or IsdI-GFP were grown in either TSB supplemented with hemin or TSB containing an excess of aminolaevulinic acid. Addition of hemin increased the levels of IsdG, which was evidenced by the higher fluorescence of *S. aureus* cells expressing IsdG-GFP compared to cells expressing GFP alone (Fig. 5.7B). Cells expressing IsdI-GFP showed slightly higher fluorescence than cells expressing GFP alone, however at a much lower extent than cells containing IsdG-GFP (Fig. 5.7B). Interestingly, addition of aminolaevulinic acid caused an increase in fluorescence, revealing that internally produced heme also augments the cellular content of IsdG (Fig. 5.7C). In contrast, supplementation with aminolaevulinic acid produced a strong decrease of fluorescence in cells expressing IsdI-GFP. Therefore, the increase in the intracellular content of IsdG promoted by heme may trigger the interaction of IsdG with HemH with a consequential impairment of the CPD pathway.

**Distribution of IsdG-like proteins across genomes**

IsdG and IsdI are both IsdG-type heme degrading oxygenases, a family of proteins characterized by the presence of an antibiotic biosynthesis oxygenase (ABM) domain followed by a loop region. The loop region is proposed to be a target for degradation in *S. aureus* IsdG (37). To date, several members of this family have been studied, including *S. aureus* IsdI and IsdG (13), *S. lugdunensis* IsdG (38), *B. antracis* IsdG (39), *Mycobacterium tuberculosis* MhuD (40), *Bradyrhizobium japonicum* HmuQ and HmuD (41) and *Brucella melitensis* (41). Our analysis of the distribution

of IsdG-type homologues shows that such proteins are present in 1137 (22%) of the 5060 complete and annotated genomes surveyed (Supplementary Data 1). Organisms containing IsdG-type enzymes belong to several Bacilli genera, including Actinobacteria, Deinococcus-Thermus, Chloroflexi, Nitrospiraea, and Proteobacteria (mainly Alphaproteobacteria) taxa. IsdI enzymes are only present in genomes belonging to the *S. aureus* group that contain the IsdABCDEFH system. In contrast, canonical IsdG enzymes are present in several *Bacillus* and *Listeria* taxa while HmuD/Q are mainly Proteobacterial specific and MhuD Actinobacterial specific (Fig. 5.8A, Supplementary Data 1).

In a second study conducted with the genomes containing IsdGs homologues, an organism was considered to have a *de novo* heme biosynthesis ability if the full pathway was encoded in its genome (see Methods). Within this dataset, heme biosynthesis pathways were found in the genomes of many pathogenic bacteria from the *Bacillus*, *Staphylococcus* and Actinobacteria groups as well as *Chloroflexi*, *Nitrospira* and *Deinoccus-Thermus* bacteria and several Proteobacteria. No siroheme heme synthesis occurring through the alternative pathway was found in organisms containing IsdG, indicating an association of IsdG only with the protoporphyrin and coproporphyrin biosynthesis pathways (Fig. 5.8A, Supplementary Data 1). Interestingly, this search revealed the presence of a potential HemQ-CPD pathway in several halophilic archaea, where HemQ is fused with an ABM domain characteristic of IsdG-type enzymes. This fusion may represent in-built control system.

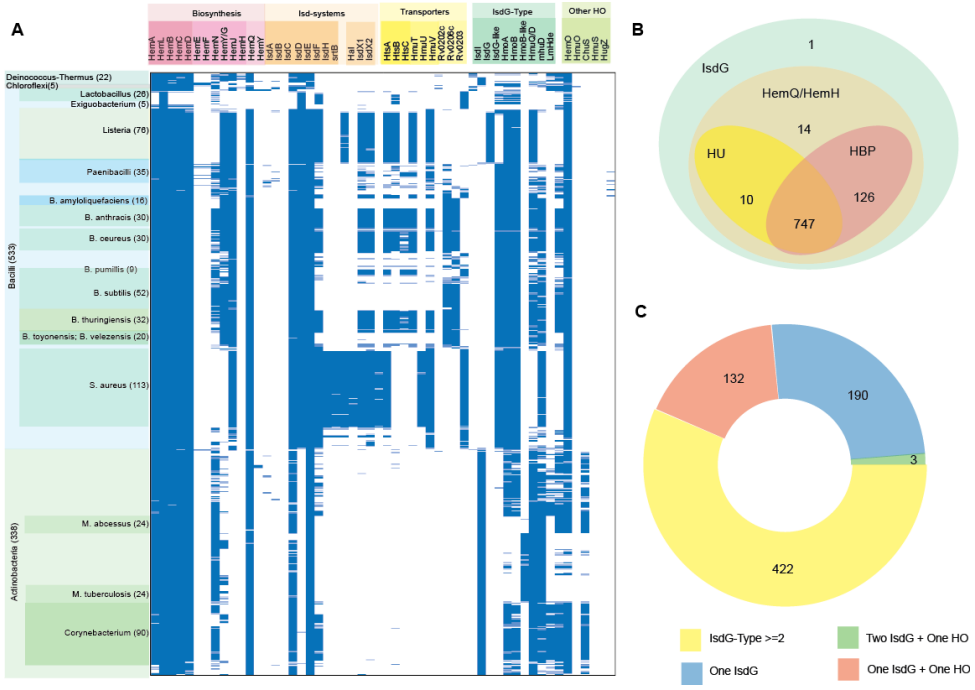


**Figure 5.8**. Distribution of heme metabolism and related genes across Gram-positive organisms containing IsdG-type enzymes. (A) Heat map representing the presence (blue ticks) or absence (white) of genes (columns) involved in heme biosynthesis, Isd systems, heme uptake and degradation in the 898 genomes (rows) containing IsdG-type enzymes. The full list is given in Supplementary Data 1. (B) Co-occurrence of IsdG-like enzymes (green) with heme biosynthesis pathway HBP (red), heme uptake system (yellow) and HemQ/H (brown). (C) Co-occurrence of additional heme oxygenases in the 747 Gram-positive organisms able to uptake and de novo synthesise heme and that contain one or more than one IsdG-type enzymes.

We used the IsdG-type dataset to classify organisms according to their ability to take up environmentally available heme. Similarity searches were performed for the most common ABC-type of heme transport modules present in Gram-positive organisms, such as the IsdEFG-like, HtsABC and HmuTUV systems (Fig. 5.8A, Supplementary Data 1). In addition, the mycobacterial heme acquisition system was included in this search (42). An organism was considered to be able to perform heme uptake if its genome encoded a complete transport system with at least one heme binding protein

(HmuT, IsdE or RV2003). In total, 806 (70%) genomes were found to encode ABC-type heme uptake systems. Heme uptake systems were found in *Deinococcus-Thermus*, *Chloroflexi*, *Rhizobiales* and several marine Alphaproteobacteria, indicating that the ability to acquire heme from external sources is more widespread than initially thought, as exemplified by the experimental characterization of the heme uptake system in phytoplankton-associated *Roseobacter* bacteria (43).

The IsdG-type dataset, which contains information from 1137 genomes, is composed of 898 (79%) Gram-positive (monoderms or transitional taxa) and 239 (21%) Gram-negative organisms. Within Gram-positives, 747 organisms (83%) encode complete (or almost complete) heme biosynthesis and uptake systems, 126 (14%) genomes encode genes for only a heme biosynthesis pathway, and 10 genomes encode genes for only a heme uptake system (Fig. 5.8B). In the remaining 15 genomes, no complete heme biosynthesis or uptake systems were found. However, in 14 of these, HemQ and/or HemH are encoded in addition to IsdG homologues. Several reasons might explain this observation: i) these 15 putative IsdGs may have a different biological role; ii) the detection of HemQ and/or HemH might indicate an as yet unidentified heme biosynthesis pathway; or iii) a different heme uptake system not surveyed in this study is present in the genomes of those 15 organisms (e.g., Ton-dependent heme uptake) with HemQ/HemH assisting IsdG in heme-degradation. Fourteen of these 15 organisms belong to *Lactobacillus plantarum* or *Lactobacillus reitti*, species that are unable to perform heme biosynthesis, but when grown with heme (and menaquinone), couple their heme-independent fermentative metabolism with aerobic respiration (44).

Within the 747 Gram-positive organisms able to access heme by both biosynthesis and uptake, 422 (~56%) contained two or more genes coding for IsdG-type heme degrading oxygenases. Apart from the *S. aureus* and *B. anthracis* strains that contain the Isd-like systems, Actinobacteria are

also represented. In the remaining genomes, although only one IsdG-type enzyme is present, genes coding for additional heme oxygenases belonging to the HemO, HmuO, ChuS/HmuS or HugZ families of heme oxygenases are also present in 135 cases (Fig. 5.8C). In Gram-negative bacteria, IsdG-type enzymes are present in 108 species that are able to access heme by both biosynthesis and uptake, whilst 131 organisms have just heme biosynthesis pathways but not uptake mechanisms. The presence of two heme oxygenases in organisms with both biosynthesis and uptake systems that contain IsdG-type enzymes is also observed in Gram-negative bacteria, where within the 108 organisms with IsdG-type enzymes, 88 (81%) have one additional heme oxygenase.

The wider distribution of IsdG-like enzymes is in contrast to IsdIs that are mainly present in *S. aureus* species that contain Isd-type uptake systems, and the occurrence of IsdG-like proteins in organisms that only obtain heme by protoporphyrin and coproporphyrin heme biosynthesis pathway strengthen the hypothesis that interactions between IsdG-type enzymes and HemH and/or HemQ may control and regulate endogenously produced heme. This is an example of how nature has adapted the same structural domain to perform similar functions, although IsdG-type enzyme regulation appears to be different between Gram-positives and Gram-negatives.

## 5.5. Discussion

We have investigated the way in which prokaryotes that obtain heme through heme biosynthesis and uptake pathways balance their high heme needs with the toxicity associated with free heme. We have shown that IsdG, one of the heme oxygenases in the *S. aureus* heme uptake pathway, controls intracellular heme content through a protein-protein interaction with ferrochelatase that results in inhibition of iron-coproporphyrin chelatase

activity. A comprehensive bioinformatics analysis showed that IsdG-like proteins are present in a significant number of prokaryotes that contain only the heme biosynthesis pathway. Altogether, the data allows us to propose that the IsdG protein family is not only the missing link between the two pathways, but also acts as the brake that avoids production of undesirably high intracellular heme levels.

In several microorganisms, IsdG-type heme oxygenases, including the *S. aureus* IsdG and IsdI, have been assigned a hemin-degradation role *in vitro* (13), and are required for growth when hemin is the only available iron source (45). We observed that IsdI impairs growth when heme is formed through PPD or CPD pathways, which is consistent with the heme degrading activity of IsdI. In contrast, IsdG inhibited growth only when heme was generated by the CPD pathway, which suggests that IsdG may interfere with the heme synthesis pathway. It is interesting to note that previous studies reported that *S. aureus* IsdG has a much lower heme degradation activity than IsdI (46).

Experimentally, we have demonstrated that strains containing IsdG have lower amounts of intracellular heme formed via the heme biosynthesis route and IsdG has the ability to decrease the iron-coproporphyrin chelatase activity of *S. aureus* HemH. Furthermore, we showed by *in vivo* FLIM-FRET and fluorescence polarization binding assays that the two proteins interact and have generated a model for this interaction.

Under our conditions, addition of heme did not repress expression of the *S. aureus* CPD pathway linked genes, as has been reported previously for several organisms. The only exception to this observation is with the *Corynebacterium diphtheriae gtrR*, which is repressed under heme replete conditions (47). Thus, in general, heme does not serve as a feedback factor to repress its own synthesis at the transcriptional level. Heme toxicity *in S. aureus* has previously been associated with induction of the heme regulator transporter HrtAB (48). In agreement with this, when we treated cells with

hemin, they exhibited induction of the first gene of the *hrtBA* operon. More significantly, we observed that expression of *isdG* was highly upregulated, indicating that IsdG may play a role in heme regulation. Furthermore, this upregulation translated into an increase of the IsdG protein abundance, as shown by FACS. Consistent with our results, IsdG, but not IsdI, has been reported to be regulated at the post-transcriptional level such that it is stabilized in the presence of heme and undergoes proteolytic degradation in the absence of heme (31, 22). We observed a higher abundance of IsdG in *S. aureus* when it was grown in iron-replete medium, while other authors have reported that IsdG is expressed more upon addition of exogenous hemin to iron-starved cultures of *S. aureus* (45). These differences are most probably due to the experimental conditions used in the two assays.

The bioinformatics analysis reported in this work estimates that among bacteria that only synthesize heme endogenously approximately one third contain IsdG-like proteins. Even in organisms with a less well-defined heme biosynthesis pathway, IsdG-type enzymes coexist with HemQ and/or HemH enzymes (Fig. 5.8B). This is in agreement with previous studies that have shown that the presence of IsdG is not restricted to organisms that have both the heme biosynthesis and acquisition machineries (49). However, in many cases the genes encoding for IsdG-like enzymes are co-localised with genes for protoporphyrin PPD and coproporphyrin CPD pathways. Hence, IsdG may regulate both these routes for endogenous biosynthesis of heme. Our data support the proposal that in *S. aureus* this control occurs through the interaction of IsdG with HemH, as the presence of IsdG strongly decreases ferrochelatase activity and the intracellular heme abundance. Although at this stage the interaction at the molecular level between IsdG and HemH cannot be fully described due to the lack of detailed structural information, we hypothesize that this interaction may block the access of the substrate to the porphyrin binding cleft of HemH.

Until now there has been a great deal of focus on the mechanisms of heme uptake as a source of iron, whilst ignoring the question of how microbes prevent unwanted heme toxicity by fine tuning exogenously acquired heme with heme synthesized endogenously. The scheme depicted in Fig. 5.9 summarises our current proposal for bacteria to maintain their intracellular free heme pool below hazardous levels. Organisms with both heme biosynthesis and uptake systems use external heme in two different ways. External heme is transported into the cytoplasm through dedicated systems, including those of the Isd-type, where it is either directly incorporated into apo-hemeproteins or degraded by IsdI, HemO, HmuO, ChuS/HmuS or HugZ- like proteins to release iron. On the other hand, heme also increases the abundance of IsdG to levels that are sufficient to interact with HemH blocking its function, i.e, impairing the heme biosynthesis pathway. Hence, one of the heme oxygenase enzymes would likely be dedicated to heme degradation to provide a source for iron whilst the other would act to restrain internal heme biosynthesis. Moreover, in systems that only synthesize heme via an internal heme biosynthesis pathway and contain IsdG-like proteins, IsdG may play an important role in preventing excessive production of heme.

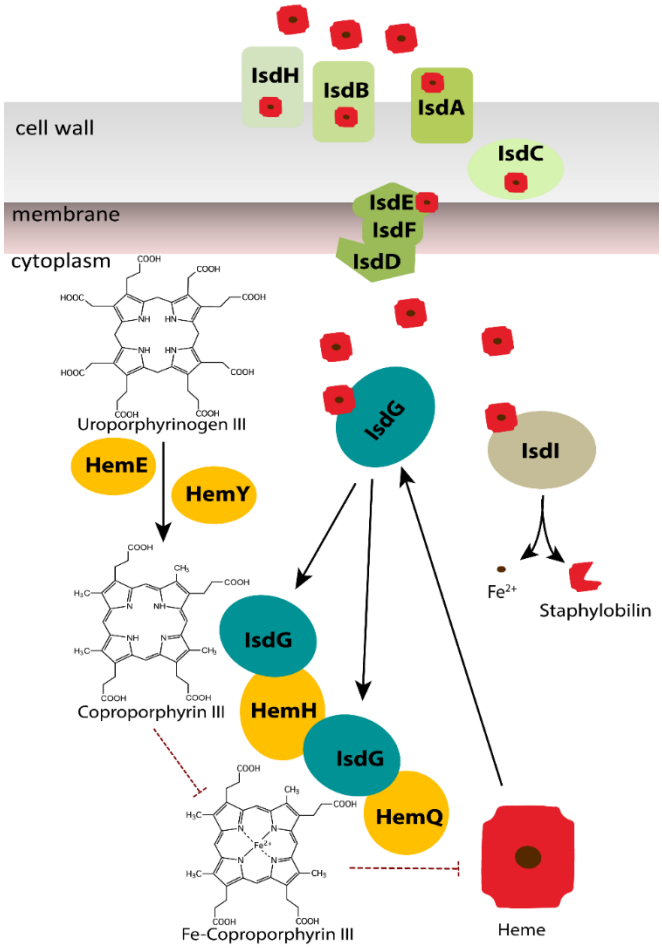


**Figure 5.9.** Proposed scheme for the role of IsdG-like proteins in the control of heme production through crosstalk between heme biosynthesis and uptake systems. *S. aureus* CPD is represented proceeding from uroporphyrinogen III to heme via the HemE, HemY, HemH and HemQ enzymes. *S. aureus* heme uptake is represented by the Isd system. In this scheme, IsdH and IsdB scavenge hemeoglobin heme which enters into the cell through IsdA, IsdC and IsdEFD. In the cytoplasm, heme is mainly degraded by IsdI to staphylobilin, iron and formaldehyde. Increase of heme content augments the IsdG abundance to levels that allow its interaction with HemH, resulting in the inhibition of CPD pathway.

Collectively, our results show that the heme uptake and biosynthesis are not independent processes, and that IsdG-like proteins have a role in the crosstalk between these two systems which allow bacteria to adapt to a

range of environments while avoiding heme toxicity. Therefore, we predict that the design of inhibitory drugs targeting the IsdG family of proteins will have a significant therapeutic benefit for the treatment of pathogenic infections.

### 5.6. Acknowledgements

The work was funded by Fundação para a Ciência e Tecnologia (FCT, Portugal) under grants PTDC/BBB-BQB/5069/2014, SFRH/BD/95912/2013 (MAMV) and SFRH/BD/118545/2016 (LSOS).

### 5.7. References

1. Choby JE, Skaar EP (2016) Heme synthesis and acquisition in bacterial pathogens. *J Mol Biol*:16–18.
2. Anzaldi LL, Skaar EP (2010) Overcoming the heme paradox: heme toxicity and tolerance in bacterial pathogens. *Infect Immun* 78(12):4977–4989.
3. Dailey HA, Dailey TA, Gerdes S, Jahn D, Jahn M, O'Brian MR, Warren MJ (2017) Prokaryotic heme biosynthesis: multiple pathways to a common essential product. *Microbiol Mol Biol Rev* 81(1):e00048-16.
4. Heinemann IU, Jahn M, Jahn D (2008) The biochemistry of heme biosynthesis. *Arch Biochem Biophys* 474(2):238–251.
5. Bali S, Lawrence AD, Lobo SA, Saraiva LM, Golding BT, Palmer DJ, Howard MJ, Ferguson SJ, Warren MJ (2011) Molecular hijacking of siroheme for the synthesis of heme and *d1* heme. *Proc Natl Acad Sci U S A* 108(45):18260–5.
6. Lobo SAL, Warren MJ, Saraiva LM (2012) Sulfate-reducing bacteria reveal a new branch of tetrapyrrole metabolism. *Adv Microb Physiol* 61:267–295.
7. Lobo SAL, Scott A, Videira MAM, Winpenny D, Gardner M, Palmer

MJ, Schroeder S, Lawrence AD, Parkinson T, Warren MJ, Saraiva LM (2015) *Staphylococcus aureus* haem biosynthesis: characterisation of the enzymes involved in final steps of the pathway. *Mol Microbiol* 97(3):472–487.

8. Dailey HA, Gerdes S, Dailey TA, Burch JS, Phillips JD (2015) Noncanonical coproporphyrin-dependent bacterial heme biosynthesis pathway that does not use protoporphyrin. *Proc Natl Acad Sci U S A* 112(7):2210–5.
9. Wang LY, Brown L, Elliott M, Elliott T (1997) Regulation of heme biosynthesis in *Salmonella typhimurium*: Activity of glutamyl-tRNA reductase (HemA) is greatly elevated during heme limitation by a mechanism which increases abundance of the protein. *J Bacteriol* 179(9):2907–2914.
10. McNicholas PM, Javor G, Darie S, Gunsalus RP (1997) Expression of the heme biosynthetic pathway genes *hemCD*, *hemH*, *hemM* and *hemA* of *Escherichia coli*. *FEMS Microbiol Lett* 146(1):143–148.
11. Mazmanian SK, Skaar EP, Gaspar AH, Humayun M, Gornicki P, Jelenska J, Joachmiak A, Missiakas DM, Schneewind O (2003) Passage of heme-iron across the envelope of *Staphylococcus aureus*. *Science* 299(5608):906–9.
12. Skaar EP, Humayun M, Bae T, DeBord KL SO (2004) Iron-source preference of *Staphylococcus aureus* infections. *Science* 305(5690):1626–8.
13. Skaar EP, Gaspar AH, Schneewind O (2004) IsdG and IsdI, heme-degrading enzymes in the cytoplasm of *Staphylococcus aureus*. *J Biol Chem* 279(1):436–443.
14. Thöny-Meyer L (1997) Biogenesis of respiratory cytochromes in bacteria. *Microbiol Mol Biol Rev* 61(3):337–76.
15. Stauff DL, Bagaley D, Torres VJ, Joyce R, Anderson KL, Kuechenmeister L, Dunman PM, Skaar EP (2008) *Staphylococcus*

*aureus* HrtA Is an ATPase required for protection against heme toxicity and prevention of a transcriptional heme stress response. *J Bacteriol* 190(10):3588–3596.

16. Tarai B, Das P, Kumar D (2013) Recurrent challenges for clinicians: emergence of methicillin-resistant *Staphylococcus aureus*, vancomycin resistance, and current treatment options. *J Lab Physicians* 5(2):71.
17. Skaar EP, Schneewind O (2004) Iron-regulated surface determinants (Isd) of *Staphylococcus aureus*: Stealing iron from heme. *Microbes Infect* 6(4):390–397.
18. Reniere ML, Ukpabi GN, Harry SR, Stec DF, Krull R, Wright DW, Bachmann BO, Murphy ME, Skaar EP (2010) The IsdG-family of haem oxygenases degrades haem to a novel chromophore. *Mol Microbiol* 75(6):1529–1538.
19. McGoldrick HM, Roessner CA, Raux E, Lawrence AD, McLean KJ, Munro AW, Santabarbara S, Rigby SEJ, Heathcote P, Scott AI, Warren MJ (2005) Identification and characterization of a novel vitamin B12 (cobalamin) biosynthetic enzyme (CobZ) from *Rhodobacter capsulatus*, containing flavin, heme, and Fe-S cofactors. *J Biol Chem* 280(2):1086–1094.
20. Frustaci JM, O'Brian MR (1993) The *Escherichia coli visA* gene encodes ferrochelatase, the final enzyme of the heme biosynthetic pathway. *J Bacteriol* 175(7):2154–2156.
21. Wolf H, Lang W, Zander R (1984) Alkaline haematin D-575, a new tool for the determination of haemoglobin as an alternative to the cyanhaemiglobin method. I. Description of the method. *Clin Chim Acta* 136(1):95–104.
22. Levicán G, Katz A, de Armas M, Núñez H, Orellana O (2007) Regulation of a glutamyl-tRNA synthetase by the heme status. *Proc Natl Acad Sci U S A* 104(9):3135–3140.

23. Gustiananda M, Liggins JR, Cummins PL, Gready JE (2004) Conformation of prion protein repeat peptides probed by FRET measurements and molecular dynamics simulations. *Biophys J* 86(4):2467–2483.
24. Gasteiger E, Hoogland C, Gattiker A, Duvaud S, Wilkins MR, Appel RD, Bairoch A (2005) Protein Identification and Analysis Tools on the ExPASy Server. *The Proteomics Protocols Handbook*, pp 571–607.
25. Pereira PM, Veiga H, Jorge AM, Pinho MG (2010) Fluorescent reporters for studies of cellular localization of proteins in *Staphylococcus aureus*. *Appl Environ Microbiol* 76(13):4346–4353.
26. García-Lara J, Weihs F, Ma X, Walker L, Chaudhuri RR, Kasturiarachchi J, Crossley H, Golestanian R, Foster SJ (2015) Supramolecular structure in the membrane of *Staphylococcus aureus*. *Proc Natl Acad Sci U S A* 112(51):15725–30.
27. Pruitt KD, Tatusova T, Maglott DR (2004) NCBI Reference Sequence (RefSeq): a curated non-redundant sequence database of genomes, transcripts and proteins. *Nucleic Acids Res* 33(Database issue):D501–D504.
28. Altschul SF, Madden TL, Schäffer AA, Zhang J, Zhang Z, Miller W, Lipman DJ (1997) Gapped BLAST and PSI-BLAST: a new generation of protein database search programs. *Nucleic Acids Res* 25(17):3389–402.
29. Finn RD, Coggill P, Eberhardt RY, Eddy SR, Mistry J, Mitchell AL, Potter SC, Punta M, Qureshi M, Sangrador-Vegas A, Salazar GA, Tate J, Bateman A (2016) The Pfam protein families database: towards a more sustainable future. *Nucleic Acids Res* 44(D1):D279-85.
30. Sievers F, Wilm A, Dineen D, Gibson TJ, Karplus K, Li W, Lopez R, McWilliam H, Remmert M, Söding J, Thompson JD, Higgins DG (2011) Fast, scalable generation of high-quality protein multiple

sequence alignments using Clustal Omega. *Mol Syst Biol* 7:539.

31. Nguyen LT, Schmidt HA, Von Haeseler A, Minh BQ (2015) IQ-TREE: A fast and effective stochastic algorithm for estimating maximum-likelihood phylogenies. *Mol Biol Evol* 32(1):268–274.
32. Hammer ND, Reniere ML, Cassat JE, Zhang Y, Hirsch AO, Hood MI, Skaar EP (2013) Two heme-dependent terminal oxidases power *Staphylococcus aureus* organ-specific colonization of the vertebrate host. *MBio* 4(4):1–9.
33. Hammer ND, Cassat JE, Noto MJ, Lojek LJ, Chadha AD, Schmitz JE, Creech CB, Skaar EP (2014) Inter- and intraspecies metabolite exchange promotes virulence of antibiotic-resistant *Staphylococcus aureus*. *Cell Host Microbe* 16(4):531–537.
34. Mayfield J a., Hammer ND, Kurker RC, Chen TK, Ojha S, Skaar EP, DuBois JL (2013) The chlorite dismutase (HemQ) from *Staphylococcus aureus* has a redox-sensitive heme and is associated with the small colony variant phenotype. *J Biol Chem* 288(32):23488–23504.
35. Valeur B, Berberan-Santos MN (2012) *Molecular Fluorescence: Principles and Applications, Second Edition*.
36. Jameson DM, Ross JA (2010) Fluorescence Polarization/Anisotropy in Diagnostics and Imaging. *Chem Rev* 110(5):2685–2708.
37. Reniere ML, Haley KP, Skaar EP (2011) The flexible loop of *Staphylococcus aureus* IsdG is required for its degradation in the absence of heme. *Biochemistry* 50(31):6730–7.
38. Haley KP, Janson EM, Heilbronner S, Foster TJ, Skaar EP (2011) *Staphylococcus lugdunensis* IsdG liberates iron from host heme. *J Bacteriol* 193(18):4749–4757.
39. Skaar EP, Gaspar AH, Schneewind O (2006) *Bacillus anthracis* IsdG, a heme-degrading monooxygenase. *J Bacteriol* 188(3):1071–80.
40. Nambu S, Matsui T, Goulding CW, Takahashi S, Ikeda-Saito M (2013)

A new way to degrade heme: the *Mycobacterium tuberculosis* enzyme MhuD catalyzes heme degradation without generating CO. *J Biol Chem* 288(14):10101–9.

41. Puri S, O'Brian MR (2006) The hmuQ and hmuD genes from *Bradyrhizobium japonicum* encode heme-degrading enzymes. *J Bacteriol* 188(18):6476–6482.
42. Tullius M V, Harmston CA, Owens CP, Chim N, Morse RP, McMath LM, Iniguez A, Kimmey JM, Sawaya MR, Whitelegge JP, Horwitz MA, Goulding CW (2011) Discovery and characterization of a unique mycobacterial heme acquisition system. *Proc Natl Acad Sci U S A* 108(12):5051–6.
43. Shane L. Hogle, Bianca Brahamsha KAB (2017) Direct heme uptake by phytoplankton-associated *Roseobacter* bacteria. *mSystems* 2(1):1–15.
44. Brooijmans R, Smit B, Santos F, van Riel J, de Vos WM, Hugenholtz J (2009) Heme and menaquinone induced electron transport in lactic acid bacteria. *Microb Cell Fact* 8:28.
45. Reniere ML, Skaar EP (2008) *Staphylococcus aureus* haem oxygenases are differentially regulated by iron and haem. *Mol Microbiol* 69(5):1304–1315.
46. Loutet SA, Kobylarz MJ, Chau CHT, Murphy MEP (2013) IruO is a reductase for heme degradation by IsdI and IsdG proteins in *Staphylococcus aureus*. *J Biol Chem* 288(36):25749–25759.
47. Bibb LA, Kunkle CA, Schmitt MP (2007) The ChrA-ChrS and HrrA-HrrS signal transduction systems are required for activation of the *hmuO* promoter and repression of the *hemA* promoter in *Corynebacterium diphtheriae*. *Infect Immun* 75(5):2421–2431.
48. Torres VJ, Stauff DL, Pishchany G, Bezbradica JS, Gordy LE, Iturregui J, Anderson KL, Dunman PM, Joyce S, Skaar EP (2007) A *Staphylococcus aureus* regulatory system that responds to host heme

and modulates virulence. *Cell Host Microbe* 1(2):109–19.

49. Sousa FL, Thiergart T, Landan G, Nelson-Sathi S, Pereira IAC, Allen JF, Lane N, Martin WF (2013) Early bioenergetic evolution. *Philos Trans R Soc B Biol Sci* 368(1622):20130088–20130088.

## 5.8. Supplementary data

**Supplementary Table 1.** Analysis of the fluorescence anisotropy decays obtained for dansyl-labelled HemH in the absence and in the presence of the IsdG/IsdI. Conditions consisted of 0.67 μM dansyl-labelled HemH in 50 mM Tris-HCl buffer pH 8.0, at 25 ºC. $\beta_i$ and $\phi_i$ are the amplitude and the rotational correlation time of the $i^{th}$ decay component. The 95% confidence intervals of the fitted rotational correlation times are indicated within square brackets ($\lambda_{ex}$= 340 nm; $\lambda_{em}$= 530 nm).

| **Binding protein** | **[Protein] (μM)** | **$\beta_1$** | **$\phi_1$ (ns)** | **$\beta_2$** | **$\phi_2$ (ns)** | **$\chi^2$** |
|---|---|---|---|---|---|---|
| | 0 | 0.06 | 2.2 [1.8; 2.6] | 0.18 | 67 [64; 70] | 1.25 |
| | 9 | 0.06 | 2.6 [2.2; 3.1] | 0.18 | 80 [77; 84] | 1.10 |
| IsdG | 13.4 | 0.06 | 2.8 [2.3; 3.2] | 0.18 | 94 [89; 100] | 1.12 |
| | 26.8 | 0.05 | 3.7 [3.0; 4.4] | 0.18 | 128 [118; 140] | 1.07 |
| | 107.2 | 0.04 | 2.2 [2.0; 3.7] | 0.19 | 181 [162; 207] | 1.16 |
| IsdI | 107.2 | 0.04 | 2.4 [1.8; 3.1] | 0.18 | 67 [64; 73] | 1.18 |

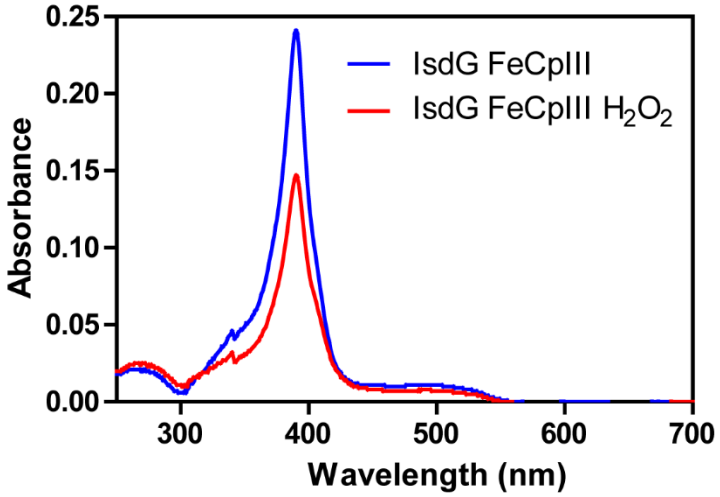


**Supplementary Figure 5.1.** *S. aureus* IsdG peroxidase activity in the presence of $H_2O_2$. UV-visible spectra of iron-copro III (FeCpIII) incubated with IsdG in the absence (blue) and in the presence of $H_2O_2$ (red), and recorded after 7 h of incubation.

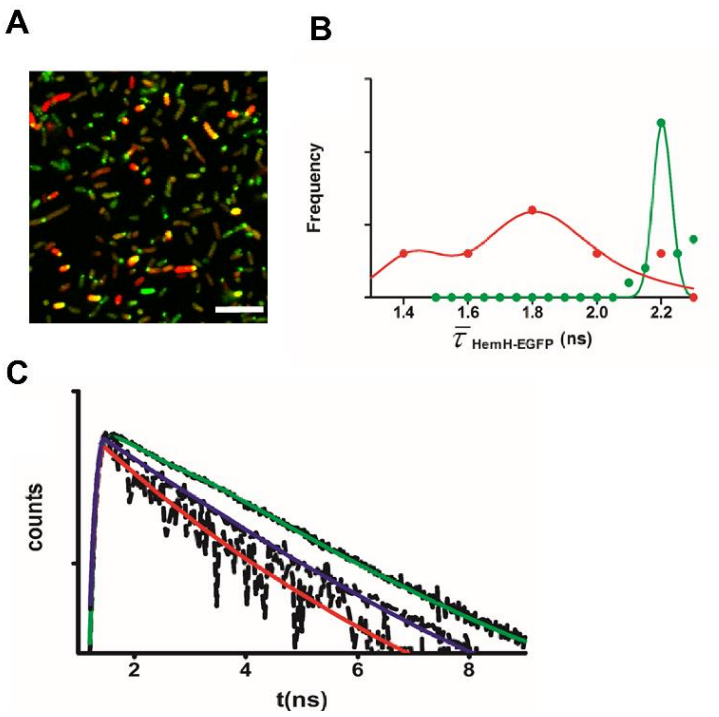


**Supplementary Figure 5.2.** Interaction between *S. aureus* ferrochelatase HemH and IsdG proteins (A) Overlay of confocal fluorescence microscopy images of HemH-GFP (green) and IsdG-mCherry (red) fluorescence. Scale bar of 10 μm. (B) Histogram of average fluorescence lifetimes of HemH-GFP from individual cells in the absence (green) and in the presence of IsdG-mCherry (red). (C) Comparison of normalized TCSPC decays obtained for: cells expressing only HemH-GFP (fitted with a mono-exponential decay of $\tau$ = 2.20 ns – shown in green), cells co-expressing HemH-GFP and IsdG-mCherry (fitted with a bi-exponential decay of $<\tau>$= 1.93 ns – depicted in purple). A bi-exponential decay was also fitted to the isolated fluorescence decay of a single cell co-expressing HemH-GFP and higher levels of IsdG-mCherry ($<\tau>$= 1.79 ns – depicted in red).

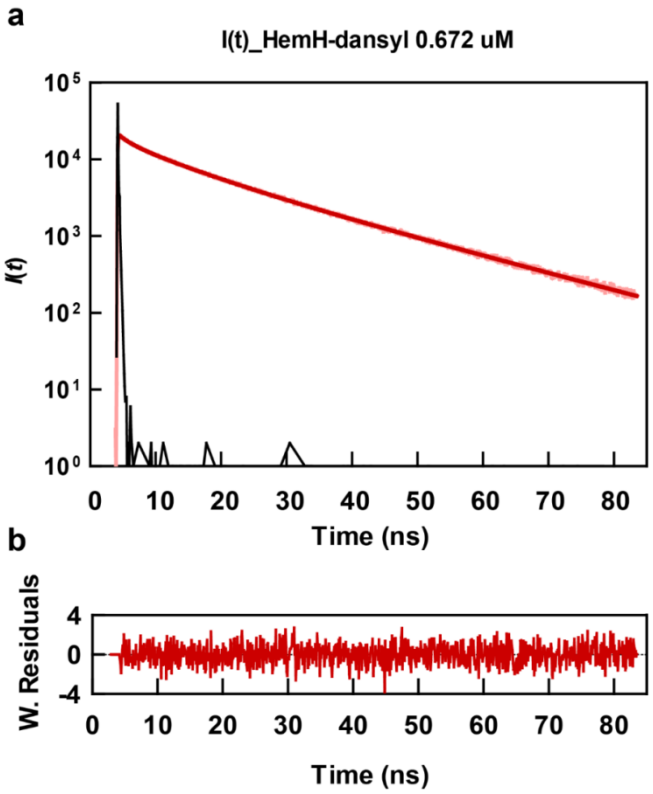


**Supplementary Figure 5.3.** Representative fluorescence intensity decay of dansyl-labelled *S. aureus* ferrochelatase HemH. (A) The depicted curves correspond to the instrument response function (IRF, black), experimental fluorescence intensity decay (light red), and fitted intensity decay (dark red). The corresponding weighted residuals of the fit are presented in panel (B). Conditions consisted of 0.67 μM dansyl-labelled HemH in 50 mM Tris-HCl buffer pH 8.0, at 25 °C. The excitation and emission wavelengths used were 340 and 530 nm, respectively. The fitted parameters were: $\alpha_1$= 0.15, $\tau_1$= 0.17 [0.13; 0.21] ns, $\alpha_2$= 0.14, $\tau_2$= 1.87 [1.73; 1.98] ns, $\alpha_3$= 0.32; $\tau_3$= 8.7 [8.7; 8.8] ns, $\alpha_4$= 0.39; $\tau_4$= 19.4 [19.2; 19.8] ns and the intensity-weighted mean fluorescence lifetime was $<\tau>$= 16 ns ($\chi^2$= 1.1.0). The 95% confidence intervals of the fitted fluorescence lifetimes are indicated within square brackets.

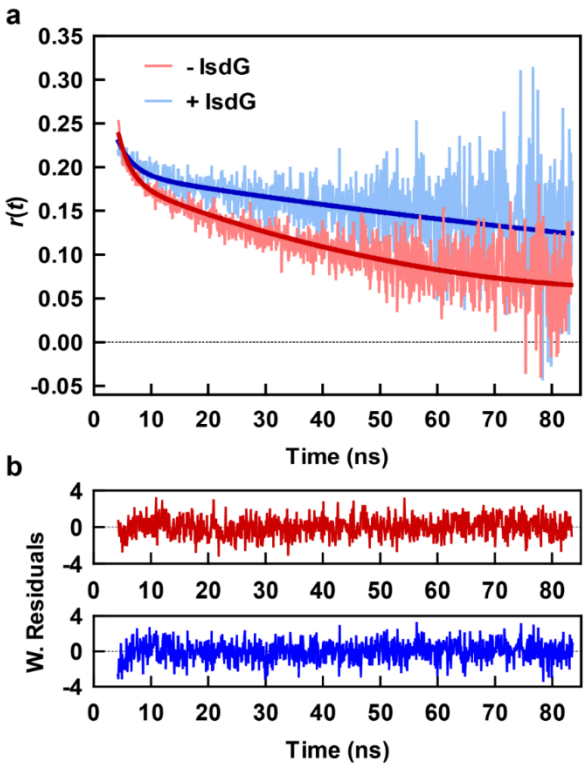


**Supplementary Figure 5.4.** Influence of *S. aureus* IsdG on the fluorescence anisotropy decay of dansyl-labelled *S. aureus* HemH. In A, the light and dark curves shown correspond to the experimental and fitted anisotropy decays for 0.67 μM dansyl-labelled HemH in the absence (red curves) and in the presence of 107 μM IsdG (blue curves). The corresponding weighted residuals of the fits are presented in panel B. The reactions were done in 50 mM Tris-HCl buffer pH 8.0, at 25 °C. The excitation and emission wavelengths used were 340 and 530 nm, respectively.

# Chapter 6

## Characterization of siroheme biosynthesis in *Staphylococcus aureus*

**Manuscript in preparation:**

**Videira MAM**, Família C, Lobo SAL and Saraiva LM (2018) Characterization of siroheme synthesis in *Staphylococcus aureus*.

MAMV designed the research, interpreted the data, performed all the *in silico* analysis, complementation experiments, enzymatic activities and wrote the manuscript.

## 6.1. Summary

Siroheme is a modified tetrapyrrole and the prosthetic group in enzymes involved in life dependent processes such as nitrogen and sulfur assimilation. Analysis of the *Staphylococcus aureus* genome revealed the presence of two genes annotated as *cysG* which are putatively involved in siroheme biosynthesis. These genes were cloned, overproduced and the purified proteins were used in *in vitro* assays to analyze their function in siroheme synthesis. The two genes were shown to encode two distinct enzymes: one involved in the transformation of uroporphyrinogen III to precorrin-2 (uroporphyrinogen III methyltransferase, SirA), and another that performs the conversion of precorrin-2 to sirohydrochlorin (precorrin-2 dehydrogenase, SirC). Further analysis of the *S. aureus* genome revealed the presence of a third gene encoding a protein that shares 25% sequence identity with *Bacillus megaterium* SirB. However, this gene was annotated as *nirR* and predicted to encode a nitrite reductase transcriptional regulator. Nevertheless, the gene was cloned and its function was investigated by *in vivo* complementation. The recombinant protein was expressed and biochemically characterized. The complementation assays, performed in an *E. coli* strain unable to produce siroheme showed that when NirR was expressed together with SirA and SirC, the cells produced siroheme. These results proved that the *nirR* gene encodes a sirohydrochlorin ferrochelatase. Therefore, the gene annotation was corrected as the gene was *sirB*. Altogether, the pathway and the enzymes that transform uroporphyrinogen III into siroheme were identified in this work.

## 6.2. Introduction

*Staphylococcus aureus* is one of the leading causes of nosocomial infections and a major health concern due to the increase in the number of antibiotic resistant strains. *S. aureus* is a facultative anaerobe that is usually grown in the laboratory in the presence of oxygen. However, upon host invasion, *S. aureus* faces environments with low oxygen concentrations (*e.g.* abscesses) (1). To grow under near anaerobic conditions, *S. aureus* uses fermentation or performs respiration on the account of electron acceptors such as nitrate or nitrite (1–4). As mentioned in chapter 1, *S. aureus* reduces nitrate to nitrite by means of nitrate reductase (NarGHI), and the accumulated nitrite is reduced to ammonia by nitrite reductase (NirBD) (5, 6). NirBD contains a siroheme cofactor that transfers six electrons from nicotinamide adenine dinucleotide (NADH) to nitrite, which is reduced to ammonia.

In general, bacteria synthesize siroheme from uroporphyrinogen III in a three step pathway that includes methylation of uroporphyrinogen III, oxidation of precorrin-2, and insertion of iron into sirohydrochlorin (7, 8) (Figure 6.1).

In *Escherichia coli* and *Salmonella enterica*, the three reaction steps are accomplished by a single multifunctional enzyme called siroheme synthase CysG (7). The protein (of 457 amino acid residues) is composed by a N-terminal region with dehydrogenase and ferrochelatase activities ($CysG^{B}$), and a C-terminal region with S-adenosyl-l-methionine (SAM)-dependent uroporphyrinogen III (uro´gen III) methyltransferase (SUMT) activity ($CysG^{A}$), that converts uro´gen III to precorrin-2 (8).

In *Saccharomyces cerevisiae*, two enzymes are required for the synthesis of siroheme, encoded by *MET1* and *MET8* genes (9). The product of *MET1* (Met1p) is a protein that shares amino acid sequence similarity to the C-terminal region of the *E. coli* CysG, and like CysG, it has SUMT activity

(10). Met8p protein encoded by the *MET8* is a bifunctional enzyme that as the N-terminal region of *E. coli* CysG has $NAD^+$-dependent precorrin-2 dehydrogenase and sirohydrochlorin chelatase activities (10). In the Gram-positive *Bacillus megaterium*, the synthesis of siroheme occurs via three proteins, namely SirA, SirB and SirC that are genetically organized in the gene cluster *sirABC*. These proteins exhibit SUMT activity (SirA), precorrin-2 dehydrogenase activity (SirC) and sirohydrochlorin ferrochelatase activity (SirB) (11, 12).

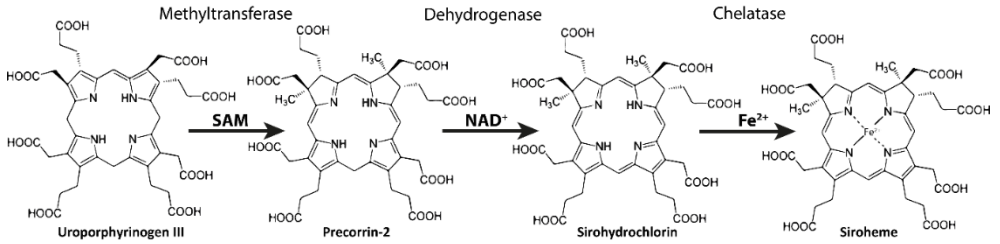


**Figure 6.1.** Outline of the three reactions necessary for the synthesis of siroheme.

In this work, we have investigated the siroheme biosynthetic pathway of *S. aureus* and shown that three gene products are required for the conversion of uro´gen III to siroheme, which were named SirA, SirB and SirC. It is also reported that the gene annotated as *nirR* in the genome of *S. aureus*, putatively encoding a nitrite reductase transcriptional regulator, is in fact the gene that encodes the enzyme that inserts iron into sirohydrochlorin, acting in last step of siroheme biosynthesis, and therefore it was renamed *sirB*.

## 6.3. Materials and Methods

### Bacterial strains and growth conditions

Strains and plasmids used in this work are described in Table 1. *E. coli* XL1-Blue was used as host strain for genetic manipulation, *E. coli* BL21(DE3)Gold and *E. coli* BL21STAR DE3 pLysS were used for protein

expression, and *E. coli* 302Δa (cysteine auxothrophic *cysG* mutant strain) was used for the complementation experiments. All strains were grown aerobically in Luria-Bertani (LB) at 37 °C and 150 rpm. Exception was made for the *E. coli* 302Δa strain, which for the complementation experiments was grown on minimal medium composed of M9Salts (12.8 g/L $Na_2HPO_4$, 3 g/L $KH_2PO_4$, 0.5 g/L NaCl, 1 g/L $NH_4Cl$) plus 20 mM glucose, 2 mM $MgSO_4$, 0.1 mM $CaCl_2$ and 1.5% agar. Antibiotic resistance was selected using, chloramphenicol (35 μg.ml$^{-1}$) and ampicillin (100 μg.ml$^{-1}$). Competent cells were prepared essentially as described previously (13). *E. coli* XL1-Blue, *E. coli* BL21(DE3)Gold, *E. coli* BL21STAR DE3 pLysS and *E. coli* 302Δa were grown overnight in LB, at 37 °C and 150 rpm. The cells were diluted in LB at an $OD_{600}$=0.1 and grown to an $OD_{600}$=0.6. At this point, the flask was left on ice for 10 min and the culture was centrifugated (1087 *x g*, 10 min, 4°C). The pellet was resuspended in ice-cold TB buffer (10 mM Pipes; 55 mM MnCI2; 15 mM $CaCl_2$ and 250 mM KCI), incubated on ice for 10 min and centrifuged again as described above. Cells were resuspended in TB buffer with 7% DMSO and frozen in liquid nitrogen.

**Table 6.1.** Strains and plasmids used in this work

| Strain | Genotype | Description | Resistance | Reference |
|---|---|---|---|---|
| *E. coli* BL21(DE3)Gold | $F^-$ *ompT hsdS*$_B$($r_B^-$ $m_B^-$) *gal dcm* | Recombinant protein expression | | Novagen |
| *E. coli* BL21STAR DE3 pLysS | $F^-$ *ompT hsdS*$_B$($r_B^-$ $m_B^-$) *gal dcm* | Recombinant protein expression | $Cm^R$ | Novagen |
| *E. coli* 302Δa | $Nir^S$, $Lac^{+}$,$Cys^-$; *cysG*$^-$ | cysG$^-$ strain used in complementation experiments | | Cole 1987 |
| *E. coli* XL1-Blue | *recA1 endA1 gyrA96 thi-1 hsdR17 supE44 relA1 lac [F´ proAB lacI*$^q$ *ZΔM15 Tn10 (Tet*$^R$*)* | Host strain used for genetic manipulation | $Tet^R$ | Laboratory strain |
| **Plasmid** | **Inserted genes** | **Description** | **Resistance** | **Reference** |
| pETcoco-2*ABCD* | *M. barkeri cobA, M. thermautotrophicus hemB, B. megaterium hemC and hemD* | Plasmid used for the production of precorrin-2 | $Amp^R$ | M.J Warren´s lab |
| pETcoco-2*ABCDC* | Same as pETcoco-2*ABCD* plus *M. thermautotrophicus sirC* | Plasmid used for the production of sirohydrochlorin | $Amp^R$ | (14) |
| pET-23b-*SacysG1* | *S. aureus cysG1* | *S. aureus cysG1* cloned in pET-23b | $Amp^R$ | This study |
| pET-23b-*SanirR* | *S. aureus* nirR | *S. aureus nirR* cloned in pET-23b | $Amp^R$ | This study |
| pET-23b-*SacysG2* | *S. aureus cysG2* | *S. aureus cysG2* cloned in pET-23b | $Amp^R$ | This study |
| pET-14b-*DvhemC* | *D. vulgaris hemC* | *D. vulgaris hemC* cloned in pET-14b | $Amp^R$ | (15) |
| pET-14b-*DvhemD*$^d$ | *D. vulgaris hemD*$^d$ | *D. vulgaris hemD*$^d$ cloned in pET-14b | $Amp^R$ | (15) |
| pET-14b-*DvsirC* | *D. vulgaris sirC* | *D. vulgaris sirC* cloned in pET-14b | $Amp^R$ | (15) |
| pKK223.2-*cysG* | *E. coli cysG* | Used as positive control in complementation experiments | $Amp^R$ | (16) |
| pCIQ-*sirCcobA* | *M. thermoautotrophicus sirC and P. denitrificans cobA* | *M. thermoautotrophicus sirC and P. denitrificans cobA* cloned in pACYC | $Cm^R$ | (16) |
| pACYC-SacysG1SacysG2 | *S. aureus cysG1 and cysG2* | *S. aureus cysG1 and cysG2* cloned in pACYC | $Cm^R$ | This study |

**Cloning procedures**

*S. aureus* genes *cysG1*, *cysG2* and *nirR* were PCR amplified using genomic DNA of *S. aureus* Newman strain and the primers described in Table 2. The DNA fragments were digested with the restriction enzymes indicated in Table 2 and ligated to pET-23b (Novagen), which was previously digested with enzymes so that non-tag, N-terminal or C-terminal His-tag fused proteins could be produced. For all genes, integrity was confirmed by DNA sequencing. For the complementation assays, *S. aureus cysG1* and *cysG2* were cloned into pACYCDuet plasmid previously digested with Bgl II/XhoI and NcoI/HindIII, respectively, to generate plasmid pACYC-*SacysG1SacysG2*.

**Table 6.2.** Oligonucleotides used in this work

| Gene | Putative enzyme | Oligonucleotides 5´-> 3´ | Restriction Sites |
|---|---|---|---|
| ***cysG1*** | Uroporphyrin III methyltransferase | GAGCTAGCCACCACCACCACCACCACATGTCTGTAGAGGAATATG | NheI |
| | | CAAAGCTTTTTACTAGTTTAGTGACATAACACTGTATTAG | HindIII |
| ***nirR*** | Sirohydrochlorin ferrochelatase | CACAAAGCTAGCATGATTTGGTATACAATAC | NheI |
| | | CGTTAGTGCTCGAGTATTTTCATTGGAATC | XhoI |
| ***cysG2*** | Precorrin-2 dehydrogenase | AAGGAGCTAGCTCAACATGAATATGCCATTAATG | NheI |
| | | CGCTACTCGAGTCTTACATCCAACCACGCTA | XhoI |
| **Complementation experiments** | | | |
| ***cysG1*** | Uroporphyrin III methyltransferase | GAACGTAGATCTATGTCTGTAGAGGAATATG | Bgl II |
| | | TTATTCTCGAGAAATTAGTGACATAACACTG | XhoI |
| ***cysG2*** | Precorrin-2 dehydrogenase | AAGGACCATGGTCAACATGAATATGCCATTAATG | NcoI |
| | | CAAAGCTTCCGACTAGTTTATCTTACATCCAACCACGC | HindIII |

**Protein expression and purification**

CysG1 (N-terminal-His-tag), NirR (C-terminal-His-tag) and CysG2 (C-terminal-His-tag) proteins from *S. aureus* and HemC, HemD$^{d}$ (HemD domain that contains uro´gen III synthase activity) and SirC His-tagged proteins from *Desulfovibrio vulgaris* were purified as described previously (17) (Tables 1 and 2). Plasmids pET-23b-*SacysG1*, pET-23b-*SanirR*, pET-23b-*SacysG2*, pET-14b-*DvhemC*, pET-14b-*DvsirC* and pET-14b-*DvhemD$^{d}$* were transformed, separately, in *E. coli* BL21STAR(DE3) pLysS competent cells and grown in LB medium to an $OD_{600}$=0.6. At this stage, cells were induced with 400 μM of isopropyl β-D-1-thiogalactopyranoside (IPTG) and grown for 16-20 h, at 20 °C. Cells were harvested by centrifugation (11000 *x g*, 10 min, 4°C), resuspended in 20 mM Tris-HCl buffer pH 8 and lysed in a French press at 1000 psi. Cells were centrifuged twice (48300 *x g*, 10 min, 4°C), and the soluble fraction was applied onto a $Ni^{2+}$ Sepharose fast flow column (GE Healthcare), previously equilibrated with 20 mM Tris-HCl buffer pH 8, 500 mM NaCl and 10 mM imidazole. *S. aureus* CysG1, NirR, CysG2 proteins were eluted in 50 mM Tris-HCl buffer pH 8, 500 mM NaCl and containing 500 mM imidazole. The *D. vulgaris* HemC, HemD$^{d}$ and SirC proteins were eluted in the same buffer that contained 400 mM imidazole. Protein fractions were concentrated in an Amicon Stirred Ultrafiltration Cell using a 10 kDa membrane (Millipore) and buffer exchanged against 50 mM Tris-HCl buffer pH 8 in PD-10 columns (GE Healthcare). This last step was done under anaerobic conditions (Coy model A-2463 and Belle Technology) to avoid the inactivation of the enzymes. Proteins were judged pure by SDS-PAGE, and protein concentration was determined spectrophotometrically, at 280 nm, using the following theoretical extinction coefficient (ExPASy software) (18), $\varepsilon_{280nm}$=22920 $M^{-1}$ $cm^{-1}$ SaCysG2, $\varepsilon_{280nm}$=31665 $M^{-1}$ $cm^{-1}$ SaCysG1 and $\varepsilon_{280nm}$=8480 $M^{-1}$ $cm^{-1}$ DvSirC.

## Enzymatic assays

The enzymatic assays were performed under anaerobic conditions in a Shimadzu UV-1800 spectrophotometer in the anaerobic chamber mentioned above. All reactions were done in 50 mM Tris-HCl buffer pH 8 and at room temperature. Kinetic parameters were obtained by fitting the activity and substrate concentration values to a Michaelis-Menten equation and using GraphPad Prism (GraphPad Software, La Jolla, CA, USA).

*Uroporphyrinogen III methyltransferase activity*

Due to its commercial unavailability, the uro´gen III substrate was produced anaerobically by incubation of 5 mg of the *D. vulgaris* His-tagged enzymes HemC and $HemD^{d}$ with 1 mg of porphobilinogen (PBG) (Frontier Scientific) in a reaction volume of 2 ml. Uro´gen III was separated from the His-tagged *D. vulgaris* enzymes using a $Ni^{2+}$ Sepharose fast flow column. Uro´gen III was diluted in 1 M HCl and its concentration was determined spectrophotometrically at 405 nm ($\varepsilon_{405}=5.4\times10^{5}\ M^{-1}\ cm^{-1}$).

So far, precorrin-2 has not been characterized regarding its extinction coefficient, and the quantification of the generated precorrin-2 is evaluated indirectly through the conversion to sirohydrochlorin (19). Therefore, the uro´gen III methyltransferase activity of CysG1 was coupled to precorrin-2 dehydrogenase activity of *D. vulgaris* SirC as described previously (15). The reaction mixture consisted of 31 µg of *S. aureus* CysG1, 8 µg *D. vulgaris* SirC, 125 µM S-adenosyl-L-methionine (SAM), 100 µM $NAD^{+}$ and uro´gen III (0.4-7 µM) in a final reaction volume of 1 ml and the formation of sirohydrochlorin was observed by following an increase of absorbance at 376 nm ($\varepsilon_{376}=2.4\times10^{5}\ M^{-1}\ cm^{-1}$).

*Precorrin-2 dehydrogenase activity*

Since the precorrin-2 substrate is also not commercially available, the porphyrin was produced using the recombinant plasmid pETcoco-2*ABCD* (Table 2), which expresses a His-tagged form of the following enzymes required for the formation of precorrin-2 from δ-aminolevulinic acid (δ-Ala): *Methanosarcina barkeri* uro´gen III methyltransferase (CobA), *Methanothermobacter thermautotrophicus* porphobilinogen synthase (HemB), *Bacillus megaterium* porphobilinogen deaminase (HemC) and uro´gen III synthase (HemD). To this end, plasmid pETcoco-2*ABCD* was transformed into *E. coli* BL21(DE3)Gold competent cells that were grown ,in LB medium supplemented with 0.2% (w/v) glucose and ampicillin, to an $OD_{600}$ of 0.5. At this stage, the medium was further supplemented with L-arabinose (0.02% w/v), grown for two extra hours, and after addition of 400 μM IPTG the cells were cultured overnight, at 20°C. Following expression, cells were harvested by centrifugation (11000 *x g*, 10 min, 4°C), the cell pellet was resuspended in 50 mM Tris-HCl buffer pH 8, 100 mM NaCl and disrupted in a French Cell, at 1000 psi. The soluble fraction was buffer exchanged under anaerobic conditions against 50 mM Tris-HCl buffer pH 8 using a PD-10 column (GE Healthcare). Precorrin-2 was produced by an overnight incubation of a reaction mixture that contained 3 ml of the cell lysate, 2 mg SAM and 2 mg δ-Ala followed by passage through a $Ni^{2+}$ Sepharose fast flow column, to separate the His-tagged proteins from precorrin-2.

Precorrin-2 dehydrogenase activity was measured by incubation of precorrin-2 (2.5 μM) (quantified as described above) with several concentrations of $NAD^+$ (0.05-2 mM) and *S. aureus* CysG2 (4 μg), in a final reaction volume of 1 ml. The activity was measured by following the appearance of sirohydrochlorin,

*Sirohydrochlorin ferrochelatase activity*

The sirohydrochlorin substrate was also prepared enzymatically by transforming the recombinant pETcoco-2*ABCDC*, which contains the same genes as in pETcoco-2*ABCD* plus the *M. thermautotrophicus sirC* (Table2) (14), into *E. coli* BL21(DE3)Gold competent cells. Cell growth, protein expression and preparation of cell fraction was done essentially as described in the previous section where pETcoco-ABCD was used. Sirohydrochlorin was produced by mixing 3 ml of the soluble fraction resultant from pETcoco-2*ABCDC* expression, 3 mg $NAD^+$, 2 mg δ-Ala and 3 mg SAM in an overnight incubation done under anaerobic conditions, and the sirohydrochlorin formed was determined spectrophotometrically. Siroheme was produced by anaerobic incubation of sirohydrochlorin (4 µM), $(NH4)_2Fe(SO4)_2$ (100 µM) and *S. aureus* NirR (15 µg), in a 1 ml reaction mixture, and its formation was followed by the UV–Visible spectroscopy.

**Complementation experiments**

Plasmid pACYC-*SacysG1SacysG2* was introduced into a strain lacking *cysG,* namely *E. coli* 302Δa, that is unable to synthesize siroheme. Siroheme is the cofactor of sulfite reductase and therefore the strain is also unable to reduce sulfite to sulfide requiring a source of sulfide or cysteine to grow, as sulfide is a precursor of cysteine synthesis (20). Plasmid pKK223.2-*cysG* (16), that was used as a positive control for the synthesis of siroheme, and pCIQ-*sirCcobA*, harboring *Methanothermobacter thermoautotrophicus sirC* and *Pseudomonas denitrificans cobA* genes (16), were also transformed into *E. coli* 302Δa competent cells and used in the complementation experiments. pET-23b-*SasirB* was transformed into *E. coli* 302Δa harboring pCIQ-*sirCcobA* or pACYC-*SacysG1SacysG2* and used to test *in vivo* the ferrochelatase activity. *E. coli* 302Δa colonies expressing the desired plasmids were diluted in PBS to an $OD_{600}$ of 0.1 and grown in plates that

contained minimal medium supplemented with or without cysteine (0.05 mg $ml^{-1}$) and appropriated antibiotics. The plates were incubated, at 37°C, for 20 h to 48 h.

## 6.4. Results

The amino acid sequences of the enzymes known to perform the synthesis of siroheme were used to search homolog proteins in *S. aureus* genome by means of BLAST (21). Two genes were identified as *cysG*, which encode a hypothetical uro´gen III methyltransferase and a precorrin-2 dehydrogenase/sirohydrochlorin ferrochelatase (Figure 6.2). In order to establish how siroheme is biosynthesized in *S. aureus*, these genes that were named *cysG1* and *cysG2* were cloned, and the proteins were recombinantly produced and biochemically characterized.

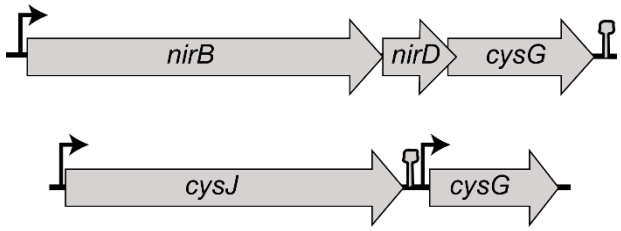


**Figure 6.2.** Genomic organization of genes encoding putative enzymes involved in siroheme synthesis in *S. aureus* Newman. Putative uro´gen III methyltransferase is located downstream of the genes encoding nitrite reductase large subunit (NirB) and nitrite reductase small subunit (NirD). The putative precorrin-2 dehydrogenase/sirohydrochlorin ferrochelatase is located downstream of a gene encoding a putative sulfite reductase flavoprotein CysJ.

## The uroporphyrinogen III methyltransferase of *S. aureus*

The CysG1 protein contains 325 amino acids and a molecular mass of approximately 40 kDa. This protein shows the highest amino acid sequence identity and similarity with the *B. megaterium SirA* (Table 3), although the latter contains several extra residues at the C-terminal (Figure 6.3).

**Table 6.3.** Amino acid sequence identity and similarity of homologs of *S. aureus* CysG1, NirR and CysG2 enzymes. Accession numbers: SirA/CobA proteins: *S. aureus* CysG1 (WP_000109968.1), *B. megaterium* SirA (AAA22317.1), *Pseudomonas (P.) denitrificans* CobA (AAA25773.1), *E. coli* CysG C-terminal 216-457 (WP_000349855.1), *Paracoccus (Pa.) denitrificans* CobA (WP_011748768.1). SirB/CbiX proteins: *S. aureus* NirR (YP_001333335), *B. megaterium* SirB (CAD48922), *Synechocystis sp.* CbiX (BAA10794.1), *Archaeoglobus (A.) fulgidus* CbiX (WP_010878224.1), *Paracoccus (Pa.) pantotrophus* CbiX (A0A023GPI5). SirC proteins: *S. aureus* CysG2 (YP_001333335), *B. megaterium* SirC (CAD48923) *E. coli* CysG N-terminal 1-223 (WP_000349855.1), *Desulfovibrio (D.) vulgaris* SirC (YP_010682), *Saccharomyces (Sac) cerevisae* Met8p (NP_009772.1).

| | Identity (%) | Similarity (%) | Query cover (%) |
|---|---|---|---|
| **SirA (uro´gen III methyltransferase)** | | | |
| *B. megaterium* | 44 | 62 | 76 |
| *P. denitrificans* | 37 | 54 | 72 |
| *E. coli* | 38 | 55 | 95 |
| *Pa. denitrificans* | 37 | 52 | 73 |
| **SirB (sirohydrochlorin ferrochelatase)** | | | |
| *B. megaterium* | 25 | 43 | 81 |
| *Synechocystis sp.* | 23 | 40 | 76 |
| *A. fulgidus* | 29 | 53 | 19 |
| *Pa. pantotrophus* | 25 | 42 | 72 |
| **SirC (precorrin-2 dehydrogenase)** | | | |
| *B. megaterium* | 35 | 61 | 97 |
| *E. coli* | 27 | 50 | 95 |
| *D. vulgaris* | 23 | 42 | 91 |
| *Sac. cerevisae* | 22 | 37 | 68 |

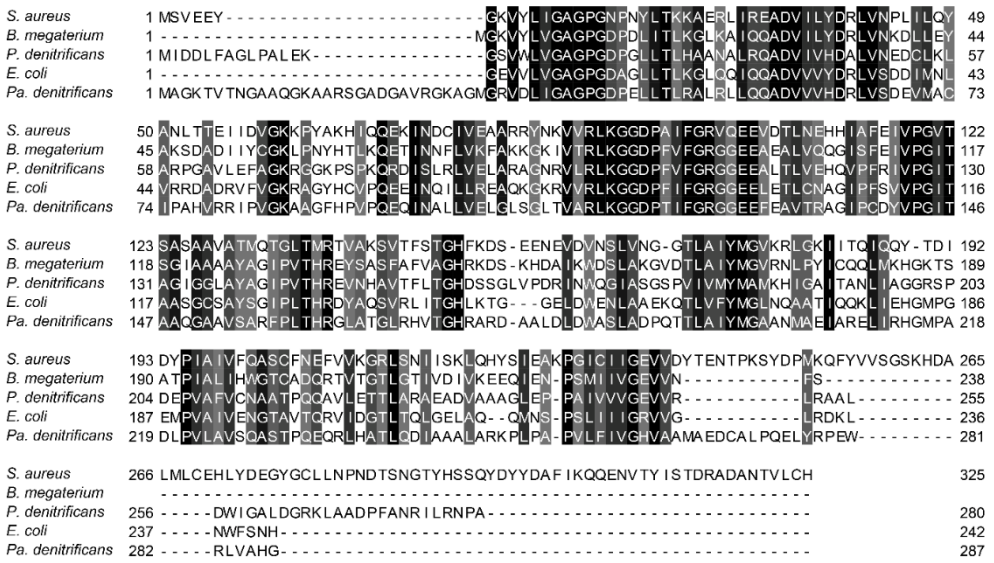


**Figure 6.3**. Sequence alignment of *S. aureus* CysG1 with selected bacterial SUMT proteins. The colors represent the conservation of residues from black (high) to light grey (low). Accession numbers*: S. aureus* CysG1 (WP_000109968.1); *B. megaterium* SirA (AAA22317.1); *P. denitrificans* CobA (AAA25773.1.); *E. coli* CysG C-terminal 216-457 (WP_000349855.1); *Pa. denitrificans* CobA (WP_011748768.1). Proteins were aligned using MUSCLE (22).

To investigate whether *S. aureus cysG1* encodes a protein able to function as uro´gen III methyltransferase, the purified protein was incubated with uro´gen III and SAM *in vitro*. The reaction generated a yellow product with a UV-Visible spectrum typical of precorrin-2 (Figure 6.4A) (19). The kinetic parameters were obtained by coupling the CysG1 activity with the *D. vulgaris* SirC activity, as described in the methods section. *S. aureus* CysG1 converts uro´gen III to precorrin-2 with a specific activity of 7.0 ± 0.6 nmol.mg$^{-1}$min$^{-1}$ and a $K_M$ for uro´gen III of 0.3 ± 0.15 µM (Figure 6.4B). As CysG1 functions as a uro´gen III methyltransferase enzyme we decided to rename it as SirA.

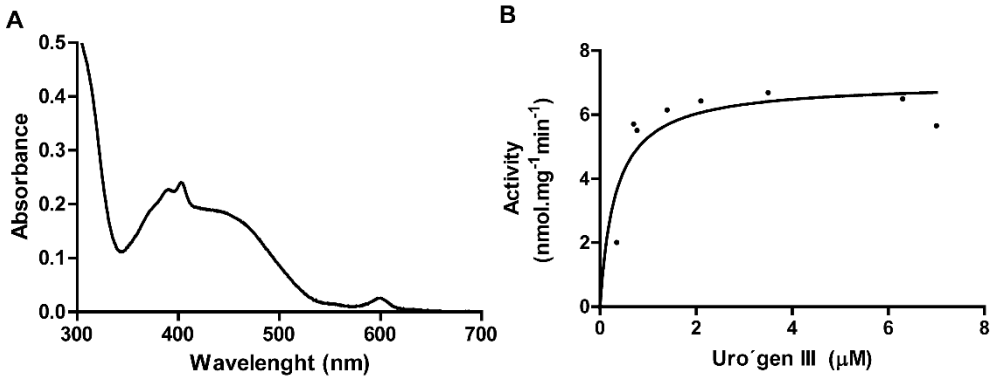


**Figure 6.4.** *S. aureus* CysG1 uroporphyrinogen III methyltransferase activity. (A) UV-Visible spectrum of precorrin-2 generated after incubation of uro´gen III with SAM and *S. aureus* CysG1. (B) *S. aureus* CysG1 activity was observed by coupling its reaction with the reaction for precorrin-2 dehydrogenase activity, using *D. vulgaris* SirC, $NAD^+$, SAM and uro´gen III.

### *S. aureus* CysG2 is a precorrin-2 is dehydrogenase

The putative *S. aureus* precorrin-2 dehydrogenase CysG2 was overproduced and purified as described in the materials and methods. It is a 201 amino acid protein with a molecular mass of approximately 25 kDa. The protein exhibits low sequence identity with other known precorrin-2 dehydrogenases, namely those of *E. coli*, *D. vulgaris*, *S. cerevisiae* and the highest identity with the *B. megaterium* SirC (Table 3). *S. aureus* CysG2 contains a sequence that in other proteins constitutes the $NAD^+$ binding site; nevertheless, in the *S. aureus* enzyme the last glycine of this motif is substituted by a valine ($GlyxGlyxxAlaxxxAlax_6Val$) (Figure 6.5).


**Figure 6.5.** Amino acid sequence alignment of *S. aureus* CysG2 with selected bacterial precorrin-2 dehydrogenases. The $NAD^+$ binding motif is marked with asterisks. The colors represent the conservation of residues from black (high) to light grey (low). Accession numbers: *S. aureus* CysG2 (YP_001333335); *B. megaterium* SirC (CAD48923); *E. coli* CysG N-terminal 1-223 (WP_000349855.1; *D. vulgaris* SirC (YP_010682); and *Sac. cerevisae* Met8p (NP_009772.1). Proteins were aligned using MUSCLE (22).

The activity of the *S. aureus* CysG2 was tested by incubation of the purified protein with precorrin-2, which was previously prepared in a reaction containing *S. aureus* SirA and $NAD^+$. Formation of sirohydrochlorin was deduced by the change in color of the reaction mixture from yellow to purple, and further confirmed by the presence of a maximum peak at 376 nm in the UV-Visible spectrum (Figure 6.6A), which is a characteristic of this compound (19). The catalytic parameters of the $NAD^+$-dependent precorrin-2 dehydrogenase activity of *S. aureus* CysG2 were determined. The measurements were done using as substrates, precorrin-2, generated by the enzymes expressed from pET-coco2-ABCD, and $NAD^+$, and following the appearance of sirohydrochlorin peak at 376 nm. The *S. aureus* CysG2 has a specific activity of 62 ± 2 $nmol.mg^{-1}min^{-1}$ and a $K_M$ for $NAD^+$ of 340 ± 44 µM (Figure 6.6B). Therefore, CysG2 was renamed SirC as their homologues in *B. megaterium* and *D. vulgaris*.

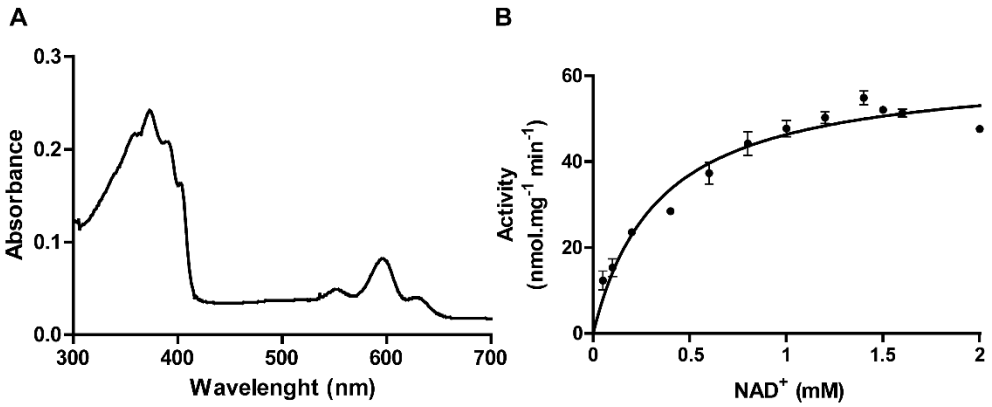


**Figure 6.6.** *S. aureus* CysG2 precorrin-2 dehydrogenase activity (A) UV-Visible spectrum of sirohydrochlorin generated after the incubation of precorrin-2 with $NAD^+$ and *S. aureus* CysG2. (B) Activity of the *S. aureus* CysG2 activity evaluated in the reaction containing precorrin-2 and several concentrations of $NAD^+$ (0.05-2 mM) as substrates.

### The sirohydrochlorin ferrochelatase of *S. aureus*

BLAST search of the *S. aureus* Newman genome did not retrieve a gene encoding a sirohydrochlorin ferrochelatase (SirB). Since *S. aureus* SirA and SirC showed the highest amino acid sequence identity and similarity to *B. megaterium* (Table 3), a more extensive BLAST search was done using *B. megaterium* sirohydrochlorin ferrochelatase SirB. The new search retrieved *nirR* gene annotated as nitrite reductase regulator (NirR). This gene is located upstream of *nirBD* that encodes the nitrite reductase large subunit (NirB) and the nitrite reductase small subunit (NirD) (Figure 6.7). *S. aureus* NirR shares 25% sequence identity and 43% similarity to the *B. megaterium* SirB (Table 3). The *nirR* gene has 732 bp and its initiation codon is annotated as GTG, which encodes a valine amino acid instead of a methionine. Therefore, we searched in the upstream region of this erroneously annotated initiation codon for nucleotides encoding a methionine amino acid, which was

found 39 bp apart creating a gene with 771 bp. After cloning this gene into pET-23b, the protein was expressed and purified for further analysis.


**Figure 6.7.** Genomic organization of *nirR* gene upstream genes encoding nitrite reductase large subunit (NirB) and nitrite reductase small subunit (NirD) in *S. aureus* Newman.

The expression of NirR generated a poorly soluble protein of 255 amino acid with a molecular mass of approximately 29 kDa. To test if *S. aureus* NirR works as a sirohydrochlorin ferrochelatase, an *in vitro* reaction was performed in the presence of $Fe^{2+}$ and sirohydrochlorin, which was generated by the proteins expressed from pETcoco-2*ABCDC*. Incubation of *S. aureus* NirR with sirohydrochlorin and ferrous iron produced a significant change in the sirohydrochorin UV-Visible spectrum towards the formation of a spectrum characteristic of siroheme (Figure 6.8) (23). We therefore concluded that NirR has sirohydrochlorin ferrochelatase activity, and the protein was renamed SirB as it homolog protein in *B. megaterium*.

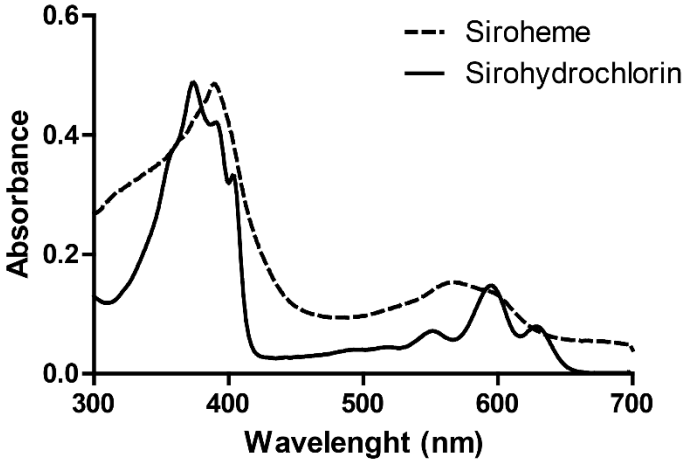


**Figure 6.8.** UV–Visible spectra of siroheme (dashed line) after the incubation of sirohydrochlorin (solid line) with $(NH_4)_2Fe(SO_4)_2$ and *S. aureus* NirR/SirB.

Despite the low sequence identity (around 25%) to other known SirB/CbiX proteins (Table 3), the amino acid sequence alignment of *S. aureus* SirB with orthologues reveals conservation of the histidine residues essential for sirohydrochlorin ferrochelatase activity. His22 (*S. aureus* numbering) present in all aligned sequences, His86 (*S. aureus* numbering), are conserved in *B. megaterium* and *Archeoglobus fulgidus*, and His145 (*S. aureus* numbering) is found in the amino acid sequences of *D. vulgaris* and *P. pantotrophus* (Figure 6.9). The conservation of these histidine residues corroborates the role of *S. aureus* SirB as a sirohydrochlorin ferrochelatase enzyme.

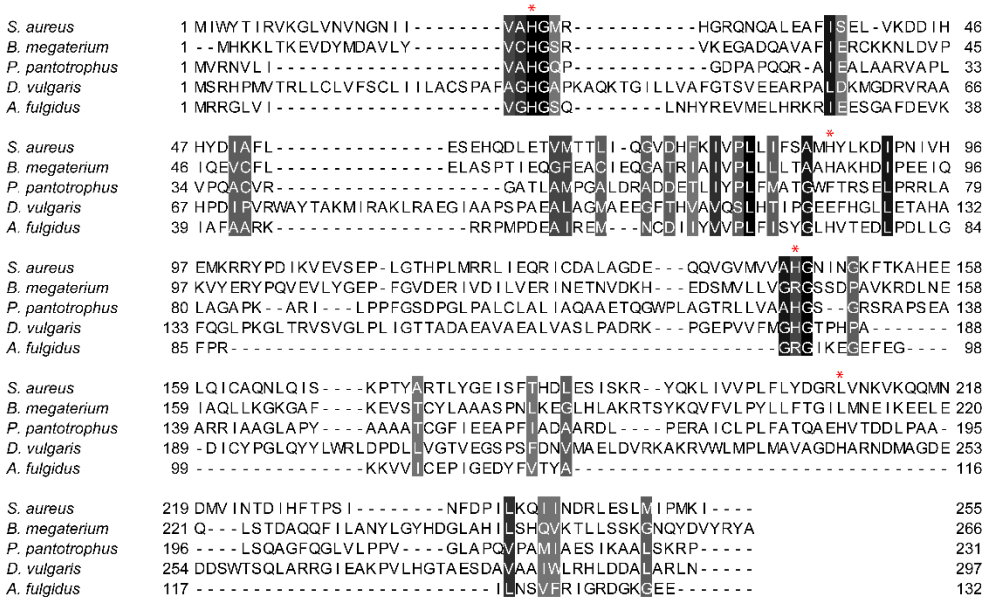


**Figure 6.9.** Amino acid sequence alignment of *S. aureus* SirB with selected bacterial SirB/CbiX enzymes. The colors represent the conservation of residues from black (high) to light grey (low). Asterisks represent histidine amino acids required for sirohydrochlorin ferrochelatase acitivity in selected SirB/CbiX homologs. Accession numbers: *S. aureus* SirB (YP_001333335); *B. megaterium* SirB (CAD48922); *P. pantotrophus* cbiX (A0A023GPI5); *D. vulgaris* CbiK$^{P}$ (WP_010937953.1); and *A. fulgidus* cbiX (WP_010878224.1). Proteins were aligned using MUSCLE (22).

## *In vivo* role of *S. aureus* SirA, SirB and SirC enzymes

The *E. coli cysG* deletion mutant Δ302a is unable to synthesize siroheme and can only grow in minimal medium when supplemented with cysteine, sulfide or when transformed with plasmids carrying genes that encode proteins that perform the biosynthesis of siroheme (20).

To investigate whether *S. aureus* SirA, SirB and SirC proteins produce siroheme *in vivo*, we have done complementation experiments using the strain described above. First, the *S. aureus* SirB was tested for its sirohydrochlorin ferrochelatase activity *in vivo*. The *S. aureus sirB* gene was

transformed into *E. coli* Δ302a together with *M. thermoautotrophicus sirC* and *P. denitrificans cobA* and grown in minimal medium without cysteine. We observed that the presence of the three genes in *E. coli* Δ302a allowed the growth of the strain in the absence of cysteine supplementation (Figure 6.10A), thus confirming the role of *S. aureus* SirB as a sirohydrochlorin ferrochelatase.

The three proteins of *S. aureus*, SirA, SirC and SirB were also tested together in *E. coli* Δ302a to infer their role in siroheme biosynthesis *in vivo*. After the transformation of the three genes, the growth of this strain was assessed in a minimal medium that did not contain cysteine. We observed that *E. coli* Δ302a carrying *S. aureus sirA*, *sirB* and *sirC* genes relieved the cysteine auxotrophy phenotype (Figure 6.10B). Therefore, we conclude that in *S. aureus* three consecutive steps are required for siroheme synthesis which are performed by the newly renamed SirA, SirB and SirC.

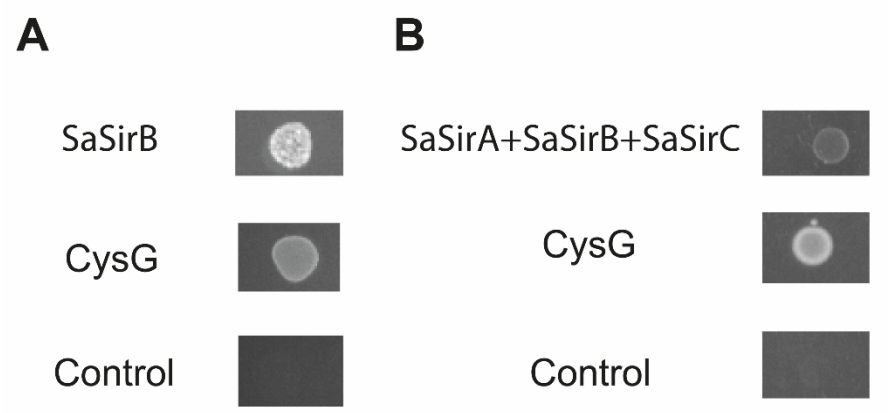


**Figure 6.10.** *S. aureus* produces siroheme using SirA, SirB and SirC. CysG represents the growth of *E. coli* 302Δa strain carrying pKK223.2-*cysG*, used as positive control, and control represents the growth of *E. coli* 302Δa strain carrying an empty pET-23b, used as negative control. All strains were grown in the absence of cysteine. (A) *E. coli* 302Δa strain expressing *M. thermoautotrophicus* SirC and *P. denitrificans* CobA (pCIQ-*sirCcobA*) plus *S. aureus* SirB (pET-23b-*SanirR*). (B) *E. coli* 302Δa strain expressing *S. aureus* SirA and SirC (pACYC-*SacysG1SacysG2*) plus *S. aureus* SirB (pET-23b-*SanirR*).

## 6.5. Discussion

In this work, we have identified and characterized for the first time the proteins that are required to perform the biosynthesis of siroheme in *S. aureus*. These genes were named *sirA*, *sirB* and *sirC,* as their *B. megaterium* counterparts, and encode a uroporphyrinogen III methyl-transferase, a sirohydrochlorin ferrochelatase and a precorrin-2 dehydrogenase, respectively. Contrary to *B. megaterium*, these genes are not organized in a single operon (11), but instead are widespread in the genome of *S. aureus*, with *sirA* and *sirB* being relatively closely located: *sirA* is part of the *nirBD* operon which is located downstream of *nirD*, while *sirB* is located upstream of the *nirBD* operon (Figure 6.2 and 6.7). The *sirC* gene is found in a different region of the genome (Figure 6.2).

Although *S. aureus sirA* and *sirC* were annotated as *cysG*, which in *E. coli* encodes a single siroheme synthase that is capable of performing all the steps involved in siroheme synthesis, we have demonstrated that these two gene products are required to perform the uroporphyrinogen III methyl-transferase and precorrin-2 dehydrogenase, respectively. The kinetic parameters obtained for uroporphyrinogen III methyl-transferase activity of *S. aureus* SirA (7.0 $nmol.mg^{-1}min^{-1}$ and a $K_M$ of 0.3 µM for uro´gen III) are similar to those reported for *D. vulgaris* CobA (3 $nmol.mg^{-1}min^{-1}$ and a $K_M$ of 0.4 µM for uro´gen III) (15).

Despite the high amino acid sequence identity between the *S. aureus* and *B. megaterium* SirA (Table 3), the first has 87 extra amino acids residues in the C-terminal. Although the role of these residues are not known, it is possible that they are required for the correct folding of the protein.

Unlike the $CysG^B$ of *E. coli*, the *S. aureus* SirC does not have ferrochelatase activity and only acts as a precorrin-2 dehydrogenase. This protein has a specific activity of 62 ± 2 $nmol.mg^{-1}min^{-1}$ which in the same order of magnitude of activity reported for *B. megaterium* SirC (60

nmol.mg$^{-1}$min$^{-1}$) (11). On the other hand, *S. aureus* SirC has a much lower activity and also lower affinity for $NAD^+$ (340 ± 44 µM) when compared to *D. vulgaris* SirC (700 nmol.mg$^{-1}$min$^{-1}$ and $K_M$ for $NAD^+$ of 70 µM) (15).

The genome of *S. aureus* does not describe a homolog protein of SirB, which is probably due to low sequence identity of the protein with the other bacterial homolog proteins. This first led us hypothesize that *S. aureus* SirC would have a dehydrogenase/chelatase activity similar to what was observed for $CysG^B$ of *E. coli* and Met8p of *Sac. cerevisiae* (8, 10). However, *S. aureus* SirC shows no ferrochelatase activity. A suitable candidate was found in the gene annotated as *nirR*, which was shown to encode a functional sirohydrochlorin ferrochelatase as attested by the generation of siroheme when the enzyme is incubated with sirohydrochlorin and ferrous iron (Figure 6.8).

Overall, this work revealed that *S. aureus* has a functional pathway to produce siroheme that involves three independent enzymes, which has enlarged our knowledge on the metabolism of tetrapyrrole biosynthesis in this important pathogen.



## 6.6. Acknowledgements

The work was funded by Fundação para a Ciência e Tecnologia (FCT, Portugal) under grants PTDC/BBB-BQB/5069/2014 and SFRH/BD/95912/2013 (MAMV).

## 6.7. References

1. Fuchs S, Pané-Farré J, Kohler C, Hecker M, Engelmann S (2007) Anaerobic gene expression in *Staphylococcus aureus*. *J Bacteriol* 189(11):4275–4289.

2. Burke KA, Lascelles J (1975) Nitrate reductase system in *Staphylococcus aureus* wild type and mutants. *J Bacteriol* 123(1):308–316.
3. Götz F, Bannerman T, Schleifer K (2006) The Genera *Staphylococcus* and *Macrococcus*. *The Prokayotes*, pp 5–75.
4. Evans JB (1975) Uracil and pyruvate requirements for anaerobic growth of staphylococci. *J Clin Microbiol* 2(1):14–17.
5. Neubauer H, Götz F (1996) Physiology and interaction of nitrate and nitrite reduction in *Staphylococcus carnosus*. *J Bacteriol* 178(7):2005–2009.
6. Pantel I, Lindgren PE, Neubauer H, Götz F (1998) Identification and characterization of the *Staphylococcus carnosus* nitrate reductase operon. *Mol Gen Genet* 259(1):105–114.
7. Spencer JB, Stolowich NJ, Roessner CA, Scott AI (1993) The *Escherichia coli* cysG gene encodes the multifunctional protein, siroheme synthase. *FEBS Lett* 335(1):57–60.
8. Warren MJ, Bolt EL, Roessner CA, Scott AI, Spencert JB, Woodcock SC (1994) Gene dissection demonstrates that the *Escherichia coli cysG* gene encodes a multifunctional protein. *Biochem J* 302:837–844.
9. Hansen J, Muldbjerg M, Chérest H, Surdin-Kerjan Y (1997) Siroheme biosynthesis in *Saccharomyces cerevisiae* requires the products of both the *MET1* and *MET8* genes. *FEBS Lett* 401(1):20–24.
10. Raux E, McVeigh T, Peters SE, Leustek T, Warren MJ (1999) The role of *Saccharomyces cerevisiae* Met1p and Met8p in sirohaem and cobalamin biosynthesis. *Biochem J* 338 ( Pt 3:701–708.
11. Raux E, Leech HK, Beck R, Schubert HL, Santander PJ, Roessner CA, Scott AI, Martens JH, Jahn D, Thermesr C, Rambach A, Warren MJ (2003) Identification and functional analysis of enzymes required for precorrin-2 dehydrogenation and metal ion insertion in the

biosynthesis of sirohaem and cobalamin in *Bacillus megaterium*. *Biochem J* 370:505–516.

12. Leech HK, Raux-Deery E, Heathcote P, Warren MJ (2002) Production of cobalamin and sirohaem in *Bacillus megaterium*: an investigation into the role of the branchpoint chelatases sirohydrochlorin ferrochelatase (SirB) and sirohydrochlorin cobalt chelatase (CbiX). *Biochem Soc Trans* 30:610–613.
13. Inoue H, Nojima H, Okayama H (1990) High efficiency transformation of *Escherichia coli* with plasmids. *Gene* 96(1):23–28.
14. Frank S, Deery E, Brindley AA, Leech HK, Lawrence A, Heathcote P, Schubert HL, Brocklehurst K, Rigby SEJ, Warren MJ, Pickersgill RW (2007) Elucidation of substrate specificity in the cobalamin (vitamin B12) biosynthetic methyltransferases. Structure and function of the C20 methyltransferase (CbiL) from *Methanothermobacter thermautotrophicus*. *J Biol Chem* 282(33):23957–23969.
15. Lobo SAL, Brindley A, Warren MJ, Saraiva LM (2009) Functional characterization of the early steps of tetrapyrrole biosynthesis and modification in *Desulfovibrio vulgaris* Hildenborough. *Biochem J* 420(2).
16. Lobo SAL, Brindley AA, Romão C V., Leech HK, Warren MJ, Saraiva LM (2008) Two distinct roles for two functional cobaltochelatases (CbiK) in *Desulfovibrio vulgaris* Hildenborough. *Biochemistry* 47(21):5851–5857.
17. Lobo SAL, Scott A, Videira MAM, Winpenny D, Gardner M, Palmer MJ, Schroeder S, Lawrence AD, Parkinson T, Warren MJ, Saraiva LM (2015) *Staphylococcus aureus* haem biosynthesis: characterisation of the enzymes involved in final steps of the pathway. *Mol Microbiol* 97(3):472–487.
18. Tools D, Mirrors S, Contact A (2010) ExPASy Proteomics Server. *Search*:1–2.

19. Schubert HL, Raux E, Brindley AA, Leech HK, Wilson KS, Hill CP, Warren MJ (2002) The structure of *Saccharomyces cerevisiae* Met8p, a bifunctional dehydrogenase and ferrochelatase. *EMBO J* 21(9):2068–2075.
20. Kolko MM, Kapetanovich LA, Lawrence JG (2001) Alternative pathways for siroheme synthesis in *Klebsiella aerogenes*. *J Bacteriol* 183(1):328–335.
21. Altschul SF, Madden TL, Schäffer AA, Zhang J, Zhang Z, Miller W, Lipman DJ (1997) Gapped BLAST and PSI-BLAST: a new generation of protein database search programs. *Nucleic Acids Res* 25(17):3389–402.
22. Edgar RC (2004) MUSCLE: Multiple sequence alignment with high accuracy and high throughput. *Nucleic Acids Res* 32(5):1792–1797.
23. Murphy MJ, Siegel LM, Tove SR, Kamin H (1974) Siroheme: a new prosthetic group participating in six-electron reduction reactions catalyzed by both sulfite and nitrite reductases. *Proc Natl Acad Sci* 71(3):612–616.

# Discussion

# Chapter 7

## General discussion

## 7.1. The coproporphyrin-dependent pathway of *Staphylococcus aureus*

For several years, bacteria were known to synthesize heme through the protoporphyrin-dependent (PPD) pathway, but this notion was challenged upon the discover of the siroheme-dependent (SHD) pathway (1), that is currently considered to be the more ancient route for the synthesis of heme. The work presented here also uncovered a third route used by *S. aureus* to synthesize heme, namely the coproporphyrin-dependent (CPD) pathway. This route involves the decarboxylation of uro´gen III to copro´gen III, oxidation of the latter to coproporphyrin III, insertion of iron into coproporphyrin III yielding iron-coproporphyrin III or coproheme and, in the last step, the decarboxylation of iron-coproporphyrin III to heme. Dailey and co-workers have proposed that this pathway is active in Gram-positive bacteria, mostly in Firmicutes and Actinobacteria (2). Hence, it is now known that heme may be synthetized through three pathways that share the common intermediate uro´gen III but differ at the stage at which the ferrous iron is inserted into the porphyrin, and in the type of the intermediates that are formed along the route.

The CPD and the PPD pathways have a common first enzymatic reaction in which uro´gen III is converted to coproporphyrinogen III, and that is catalyzed by the uro´gen III decarboxylase enzyme (HemE). In the next step of the CPD pathway, copro´gen III is oxidized to copro III by the coproporphyrin synthase or copro´gen oxidase HemY (Chapter 4). Similarly, the penultimate step of the PPD pathway is carried out by proto´gen oxidase HemY that promotes the oxidation of protoporphyrinogen IX to protoporphyrin IX (proto IX). The overall structure of the HemY´s that operate in the CPD and PPD pathways is similar and the major differences between the two structures occur at the active site. The CPD HemYs present a substrate pocket that is larger and more positively charged than that of the PPD HemYs, and this difference is most likely due to the need to

accommodate the two extra propionate side chains of copro´gen III (3). Nevertheless, the similarity of the overall structures suggests that the two families of enzymes use a similar reaction, which consists in a six-electron oxidation where oxygen acts as electron acceptor and that generates $H_2O_2$. Interestingly, while in *B. subtilis*, that uses the CPD route, the HemY enzyme is also capable of oxidizing proto´gen IX (4), the *S. aureus* HemY cannot perform this reaction (Chapter 4).

In the CPD pathway, the insertion of iron into the copro III substrate occurs in the penultimate step, whereas in the PPD pathway the insertion of iron into proto IX occurs in the last step. In the SHD pathway, iron is inserted into sirohydrochlorin to yield siroheme that is then converted to heme in three additional and consecutive steps catalyzed by the enzymes AhbA and AhbB, AhbC and AhbD. In spite of these differences, the copro III and proto IX ferrochelatases have resembling structures differing mainly by the presence of an extra loop in the active site of the protoporphyrin ferrochelatases. The absence of this loop in the active site of coproporphyrin ferrochelatases is proposed to allow the housing of the bulkier coproporphyrin substrate (2).

The last reaction of the CPD pathway is the decarboxylation of the two propionate side chains of coproheme to yield heme catalyzed by HemQ. In the SHD pathway a similar reaction also occurs that is promoted by AhbD (1). Although both proteins decarboxylate coproheme by two consecutive steps, the proteins are structurally and mechanistically different. While HemQ is a homopentamer in a donut-shape structure that does not require any cofactor but uses an electron acceptor for the reaction, AhbD is a monomeric protein arranged in a Triosephosphate Isomerase (TIM) barrel-like motif that harbors two iron-sulfur clusters and promotes the cleavage of S-adenosyl methionine to perform the decarboxylation reaction (5). In *S. aureus*, HemQ firstly decarboxylates the ring A of coproheme forming monovinyl, in a reaction that requires one molar equivalent of $H_2O_2$, and then promotes the decarboxylation of ring B generating heme. This last reaction

is slower and requires, at least, five molar equivalents of $H_2O_2$ (Figure 4.6/Chapter 4). In contrast, HemQ of *Listeria* requires 2 molar equivalents of $H_2O_2$ for the complete decarboxylation of both propionates (6). Although, *in vitro* HemQ enzymes use FMN and $H_2O_2$ as acceptors (7), the *in vivo* electron acceptor of this decarboxylation reaction is not yet know.

Some of the genomes of bacteria predicted to synthesize heme via the CPD pathway encode two coproheme descarboxylases, HemQ and AhbD (2). We speculate that HemQ will be active under aerobic conditions, while AhbD would function under anaerobic conditions. Similarly, some Gram-negative bacteria with the PPD pathway contain two coprogen oxidases, namely HemF and HemN, which are active under aerobically and anaerobic conditions, respectively.

In prokaryotes, the PPD pathway is the most used route and occurs frequently in Proteobacteria and Cyanoacteria (8). The CPD branch is largely present in Firmicutes and Actinobacteria, but also exists in monoderm to diderm transition organisms such as *Deinococcus* (7). A significant number of Firmicutes and few representatives of Actinobacteria also encode a SHD pathway, which is mainly present in the Archaea and the denitrifying and sulfate-reducing bacteria (8). It is interesting to note that although the SHD pathway is considered to be the more ancient route, it seems to be the less represented of the heme biosynthetic pathways among bacteria (8).



## 7.2. *Staphylococcus aureus* regulates the heme biosynthesis pathway by crosstalk with the heme uptake system

The *de novo* heme biosynthesis pathway and the heme uptake system are two ways which *S. aureus* uses to obtain heme. However, the simultaneous utilization of the two pathways for the same purpose could be energetically costly. Therefore, we hypothesized the existence of a crosstalk mechanism between the two pathways that could regulate the intracellular

heme levels. Furthermore, and as mentioned in Chapter 2, high heme levels are extremely toxic for the bacterium and mechanisms are expected to exist to tightly regulate the intracellular content of this essential molecule.

The heme translocated into the cell by the *S. aureus* Isd system has two fates: i) direct incorporation of heme into apo-hemeproteins; and/or ii) heme degradation by IsdI and IsdG proposed to yield nutritional iron. However, in this work we observed that elevated heme concentrations increased the abundance of the IsdG protein (Figure 5.7/Chapter 5), that interacts with the coproporphyrin ferrochelatase (Figure 5.6/Chapter 5). Moreover, we showed that the interaction of IsdG with HemH decreases the coproporphyrin ferrochelatase activity, in a concentration dependent mode (Figure 5.5/Chapter 5).

Although we have shown by FLIM-FRET that IsdG also interacts with HemQ (Figure 5.6/Chapter 5), more experiments are required to further understand the implication of this interaction on the heme biosynthesis pathway. Interestingly, the HemQ protein of *Haloferax volcanii* was previously reported to be fused to a monooxygenase protein (9) which suggests that these proteins may function together. Also, in *Propionobacterium acnes*, HemH is fused to HemQ (10). Taking to account these observations, and the fact that HemQ catalyzes the enzymatic step that follows the reaction promoted by HemH, is tempting to speculate that the three proteins HemH/IsdG/HemQ may form an active complex for a tighter regulation or better operation of the heme synthesis process. This would explain the co-occurrence of IsdG with HemH/HemQ proteins even in the absence of an operational heme biosynthesis pathway, as accessed by the bioinformatic analysis (Figure 5.8/Chapter 5). Additionally, a complex between these proteins would also explain the presence of copro III rather than coproheme in the *hemQ* mutant strain (11), as copro III is the substrate for HemH and not for HemQ.

IsdG-type proteins are widely distributed across prokaryotic genomes and present in both monoderm and diderm bacteria. IsdG-type proteins are also found in organisms that only contain heme uptake systems, thus suggesting that they may act as heme oxygenases. Nevertheless, differences may exist among IsdG-type proteins of Gram-positive and Gram-negative bacteria as *S. aureus* IsdG impairs CPD heme biosynthesis pathway but not the PPD pathway (Figure 5.2/Chapter 5), which is the more common pathway occurring in Gram-negative bacteria.

Altogether, we show that in *S. aureus* there is a crosstalk between the two heme supply systems that is promoted by IsdG.

Other examples of heme regulation involving ferrochelatases have been reported. Previous studies have shown that in *Bradyrhizobium japonicum* and in *Alphaproteobacteria* mainly of the Rhizobiales order, the iron response regulator (Irr) modulates heme biosynthesis through the interaction with ferrochelatase (12). Irr senses iron indirectly by interaction with ferrochelatase upon insertion of iron into proto IX, which occurs in the last step of the PPD pathway (12, 13). In iron-replete cells, ferrochelatase is active due to the presence of the substrates, protoporphyrin IX and iron, and promotes the formation of heme. Irr responds to the iron status of heme biosynthesis and forms a complex with ferrochelatase that leads to its inactivation. Irr is subsequently degraded upon binding of the heme formed through the ferrochelatase activity. Under iron-limiting conditions, the lack of iron bound to ferrochelatase activates Irr, which represses the heme biosynthesis gene *hemB* and prevents the accumulation of toxic porphyrins (13, 14).

The control of heme synthesis by Irr differs from what we observed in *S. aureus*. In *B. japonicum* Irr inhibits heme biosynthesis through the repression of heme biosynthetic genes when ferrochelatase is not producing heme. In *S. aureus*, the increase of the IsdG levels triggered by heme promote the interaction of IsdG with hemH and the consequent inhibition of

the ferrochelatase activity. Although both mechanisms to control heme biosynthesis involve ferrochelatase, they are opposed since the regulation by Irr requires the disassembling of the ferrochelatase-Irr complex while in *S. aureus* it requires the formation of the ferrochelatase-IsdG complex.

In humans, frataxin delivers iron to ferrochelatase. It was reported that lower concentrations of human frataxin promoted the activity of the human ferrochelatase while high concentrations frataxin impairs the ferrochelatase activity (15).

More recently, a new mechanism of regulation via protein interaction with ferrochelatase was described for the purple photosynthetic *Rhodobacter sphaeroides* (16). PufQ regulates the switch between the formation of heme and the formation of bacteriochlorophylls, as both products are synthetized from protoporphyrin IX in the tetrapyrrole synthesis pathway. Under oxygen-limited conditions, the PufQ protein interacts with ferrochelatase to impair heme synthesis and favors the insertion of magnesium into protoporphyrin IX by magnesium chelatase, towards the formation of bacteriochlorophyll (16). In this case, PufQ sequesters ferrochelatase thus restricting the availability of the protoporphyrin IX substrate.

Although only three mechanisms to control heme synthesis via protein interaction are described so far, it is curious to note that all have in common the involvement of ferrochelatase.

### 7.3. *Staphylococcus aureus* synthesizes siroheme

It was previously suggested that *S. aureus* harbors genes encoding proteins putatively involved in siroheme synthesis (17, 18), but the organization and characterization of this pathway was never addressed.

We have shown that *S. aureus* owns a fully operational siroheme biosynthesis pathway, that converts uro´gen III into siroheme in three

consecutive reaction steps, carried out by three proteins, namely SirA, SirB and SirC.

*S. aureus* SirA has uro´gen III methyltransferase activity and catalyzes the bis-methylation of uro´gen III into precorrin-2. (Figure 6.4/Chapter 6). This activity was previously reported to be associated with the $CysG^A$ domain of the multifunctional CysG enzyme of *E. coli* (19) and the Met1p protein of *Sac. cerevisae* (20). The amino acid sequence similarity observed between *S. aureus* SirA, the $CysG^A$ domain of *E. coli* and CobA of *P. denitrificans* (Table 3/Chapter 6) suggests for SirA a kidney-like shape overall structure, formed by a homodimer with two sequential α/β domains (21, 22).

*S. aureus* SirC is involved in the second step of the siroheme synthesis catalyzing the oxidation of precorrin-2 to sirohydrochlorin (Figure 6.4/Chapter 6). This $NAD^+$-dehydrogenase activity was previously reported for the $CysG^B$ and Met8p proteins of *E. coli* and *Sac. cerevisae*, respectively (19, 20). The crystal structure of these proteins comprises three domains: i) an N-terminal Rossmann fold that binds $NAD^+$; ii) a central dimerization domain; and iii) a C-terminal helical domain (21, 23, 24). The high amino acid sequence similarity between *S. aureus* SirC and $CysG^B$ and Met8p and the presence of $NAD^+$ binding motif at the N-terminal region suggests that *S. aureus* SirC may adopt a similar structure. However, $CysG^B$ and Met8p have dual activity and perform the insertion of iron into sirohydrochlorin, the last step of the pathway, a feature that was not observed for *S. aureus* SirC.

In *S. aureus*, the final step of the pathway is achieved by the sirohydrochlorin ferrochelatase SirB that generates siroheme *in vitro* and *in vivo* (Figure 6.8 and 6.10/Chapter 6). Although $CysG^B$ of *E. coli* and Met8p of *Sac. cerevisae* also have sirohydrochlorin ferrochelatase activity, the biochemical properties of *S. aureus* SirB are more similar to the type-II chelatases, such as the protoporphyrin IX ferrochelatase and the bacterial CbiK/CbiX (25) including the SirB of *B. megaterium* (26).

The comparison of the amino acid sequence of several sirohydrochlorin chelatases (Figure 6.9/Chapter 6) shows the conservation of several histidine residues that were previously reported to modulate the chelatase activity and/or being involved in metal binding. For example, two of the residues that in *A. fulgidus* CbiX$^{S}$ (His10 and His75) are proposed to be involved in metal binding (27), are also present in *S. aureus* SirB (His22 and His86).

*D. vulgaris* contains two types of cobaltochelatases, CbiK$^{C}$ and Cbik$^{P}$, that are both able to insert iron into sirohydrochlorin (28). Cbik$^{P}$ has higher iron chelatase activity and it was demonstrated that His182 is the most important residue for iron chelation into sirohydrochlorin (29). In *P. pantotrophus* CbiX, the equivalent His127 is proposed to be involved in substrate and metal binding (30). This histidine residue is conserved (His145) in *S. aureus* SirB. Interestingly, and in spite of the high amino acid sequence similarity between *S. aureus* and *B. megaterium* SirB proteins (Table 6.3/Chapter6), the latter does not contain this residue.

The chelatase activity is also proposed to rely on another histidine residue that is present in *D. vulgaris* CbiK$^{P}$ (His244) and *P. pantotrophus* CbiX (His187) (29, 30). In *S. aureus* SirB, this amino acid is replaced by the positively charged Lys209, suggesting that this lysine residue could be important for the chelatase activity.

Therefore, the catalytic site of *S. aureus* SirB is predicted to accommodate residues His22, His86, His145 and possibly Lys209 that are expected to be involved in metal/substrate binding and/or chelatase activity.

Type II chelatases are monomers or homodimers with a mixed α/β architecture. Larger type II chelatases, such as SirB, CbiX$^{L}$, CbiK and HemH, are proposed to have evolved from CbiX$^{S}$ by a gene duplication and fusion event (25, 27) and the residues forming the active site are either located in the N-terminal or C-terminal regions (25). In *B. megaterium* SirB and CbiX$^{L}$, the residues that form the active site are present in the N-terminal region

(25), while in *D. vulgaris* CbikP, *Salmonella enterica* CbiK and *P. pantotrophus*, these residues are located in the C-terminal region (27, 30). This pattern is not observed in *S. aureus* SirB, as the enzyme contains conserved histidine residues, which are proposed to form the catalytic site, in the N and the C-terminal regions. Although the importance of His145 in the catalytic activity of *S. aureus* SirB remains to be established, these observations may suggest that this protein represents an evolutionary later-branch point.

## 7.4. Final remarks

At the beginning of this work, little information was available on the metabolism of porphyrins in *S. aureus*. The data obtained in this dissertation have shown how *S. aureus* builds up the tetrapyrrole molecules and controls the heme biosynthesis pathway. In Figure 7.1 it is schematized the tetrapyrrole related pathways of *S. aureus* which are important for the adaptation of the bacteria to different host environments.

During infection, *S. aureus* has to survive in the iron-restricted environment of the host and faces fluctuating concentrations of $O_2$. *S. aureus* uses the Fur protein to sense iron and under iron starvation conditions Fur no longer represses *isd* genes (31), which triggers the uptake of exogenous heme from the host hemeproteins into the cytoplasm. Internalized heme is either degraded by *S. aureus* heme oxygenases, which we proposed to mainly occur via IsdI, or is directly incorporated into hemeproteins. Nevertheless, under iron-replete conditions, the import of heme still occurs and heme is directly incorporated into membrane cytochromes (32, 33).

In parallel to heme uptake, *S. aureus* synthesizes heme *de novo* through the heme biosynthesis pathway via coproporphyrin III, using HemE, HemY, HemH and HemQ to catalyze the final steps of the route (Chapter 4).

The increase of intracellular heme content, resultant from the two pathways, elevates the amount of IsdG in the cell (Chapter 5), which promotes the interaction with the HemH protein of the CPD pathway. This interaction causes the inhibition of HemH ferrochelatase activity and therefore impairs the formation of heme through this pathway as shown in Chapter 5.

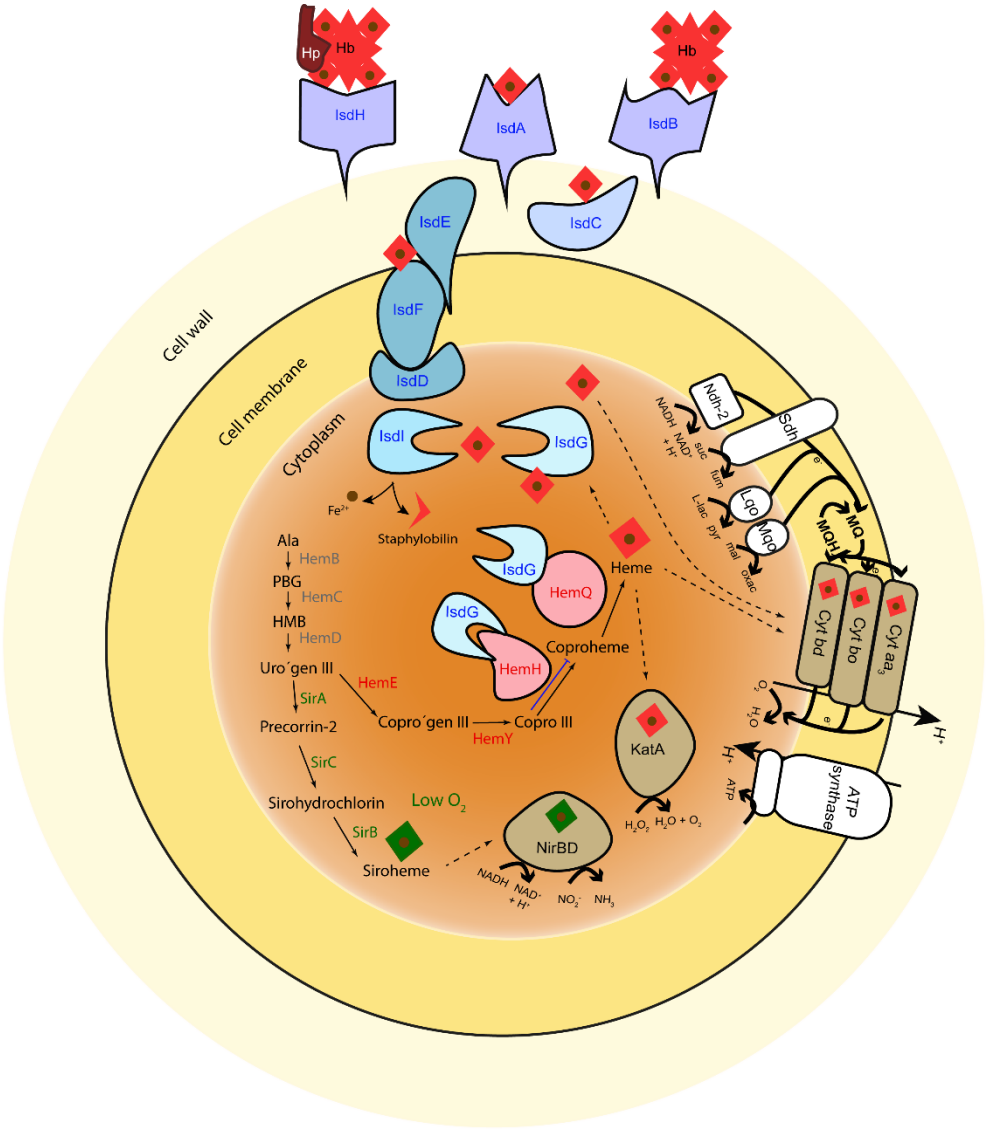


**Figure 7.1** Overview of the metabolic heme pathways of *S. aureus* studied in this dissertation. The scheme shows the relationship of *S. aureus* heme pathways, the heme uptake system (proteins in blue), the heme biosynthesis (proteins involved in early steps in grey and the CPD pathway in red) and the siroheme pathway (proteins in green). Under low iron conditions, the heme uptake system imports heme, which is degraded in the cytoplasm mainly by IsdI. Heme biosynthesis provides heme to hemeproteins, KatA (Catalase) and Cyt (cytochrome oxidases). On the other hand, HemH and HemQ of the heme biosynthesis are inhibited by the IsdG protein of the heme uptake system. Under low oxygen environments, siroheme is synthesized and is incorporated into NirBD (nitrite reductase). L-lactate (Lqo), succinate (Sdh) and malate (Mqo) dehydrogenases; suc, succinate; fum, fumarate; L-lac, L-lactate; pyr, pyruvate; mal, malate; oxac, oxaloacetate. H+, proton. Ala, aminolevulinic acid. PBG, porphobilinogen. HMB, hydroxymethylbilane. Uro´gen III, uroporphyrinogen III. Copro´gen III, coproporphyrinogen III. Copro III, coproporphyrin III. Hp, haptoglobin. Hb, hemoglobin.

*In vivo*, *S. aureus* faces different oxygen tensions which are critical for its growth (34). The energy requirements in these different environments are in part accomplished by heme, which is synthesized aerobically and anaerobically to replenish cytochromes operative in aerobic and anaerobic respiration. When colonizing $O_2$-restricted environments, which can be found in the abscesses, bone and bone marrow, intestinal lumen and during *S. aureus* biofilm formation (35), *S. aureus* uses nitrate or nitrite as electron acceptors, and in the absence of these electron acceptors the bacteria shifts to fermentative metabolism (36). When nitrate is available during anaerobic growth, the NreABC regulator induces the expression of nitrate and nitrite reductase genes, as well as the *sirB* gene, now shown to be involved in siroheme synthesis (Chapter 6) (18). As mentioned in Chapter 1, the respiratory nitrate reductase (NarGHI) reduces nitrate to nitrite, which is further reduced to ammonia by nitrite reductase (NirBD). The latter contains a siroheme cofactor that was demonstrated here to be synthesized from uroporphyrinogen III via *S. aureus* SirA (Uro´gen III methyltransferase), SirC (Precorrin-2 dehydrogenase) and SirB (Sirohydrochlorin ferrochelatase) (Chapter 6). *In vivo*, the nitrite reductase operon, that includes the *sirA* gene was shown to be upregulated in early adaptation to the mouse lung (37). This observation could reflect the accumulation of nitrite in sites infections due to the oxidation of nitric oxide produced by phagocytic cells (38).

*S. aureus* pathogenesis is commonly associated with small colony variants (SCV), which have been frequently isolated from infected patients (39). These metabolically inactive persister cells have deficient respiration and are known to be more resistant to antibiotics (39). Several heme biosynthesis mutants have a SCV phenotype (11, 40, 41), as is the case of *S. aureus* HemH mutant (Figure S4.3/Chapter 4). As shown for other genes involved in heme synthesis (40–42), the *hemH* gene is important for *S. aureus* survival (Figure 5.3/Chapter 5).

As persister cells are generally found in biofilms (43), which are quasi-anaerobic environments, NarGHI, NirBD and proteins for siroheme synthesis are expected to play an important role in the dormant phase of the bacteria. In agreement, nitrate and nitrite reductase genes are upregulated in *S. aureus* biofilms (44) and the *nirA* of *Mycobacterium tuberculosis*, which encodes a siroheme containing sulfite reductase, was found to be upregulated in cells at the dormant state (45).

Humans synthesize heme via a PPD pathway (46); moreover, the enzymes participating in heme biosynthesis pathway of *S. aureus* are apparently different or absent from the human genome, such as HemQ. We also showed that *S. aureus* HemY resists acifluorfen inhibition contrarily to the human HemY homolog (Chapter 4). Therefore, this protein is a possible candidate for drug targeting and can contribute to the urgent requirement of novel antibiotics to fight *S. aureus* infections, which has a significant negative socioeconomic impact.

To conclude, this thesis provides novel insights into *S. aureus* physiology and metabolism. It elucidates on how these bacteria synthesize heme and siroheme, a knowledge that can be extended to other pathogens. Additionally, a crosstalk between two heme providing pathways in *S. aureus* was uncovered, a mechanism that is important to maintain non-toxic intracellular heme levels. Future studies are required to comprehend all biological aspects of this entanglement. Hopefully, the outcomes of this work will aid to deal with the urgent problem associated with the infections caused by this “superbug”.

## 7.5. References


1. Bali S, Lawrence AD, Lobo SA, Saraiva LM, Golding BT, Palmer DJ, Howard MJ, Ferguson SJ, Warren MJ (2011) Molecular hijacking of siroheme for the synthesis of heme and *d1* heme. *Proc Natl Acad Sci U S A* 108(45):18260–5.
2. Dailey HA, Gerdes S, Dailey TA, Burch JS, Phillips JD (2015) Noncanonical coproporphyrin-dependent bacterial heme biosynthesis pathway that does not use protoporphyrin. *Proc Natl Acad Sci U S A* 112(7):2210–5.
3. Qin X, Sun L, Wen X, Yang X, Tan Y, Jin H, Cao Q, Zhou W, Xi Z, Shen Y (2010) Structural insight into unique properties of protoporphyrinogen oxidase from *Bacillus subtilis*. *J Struct Biol* 170(1):76–82.
4. Hansson M, Hederstedt L (1994) *Bacillus subtilis* HemY is a peripheral membrane protein essential for protoheme IX synthesis which can oxidize coproporphyrinogen III and protoporphyrinogen IX. *J Bacteriol* 176(19):5962–5970.
5. Lobo SAL, Lawrence AD, Romão C V., Warren MJ, Teixeira M, Saraiva LM (2014) Characterisation of *Desulfovibrio vulgaris* haem b synthase, a radical SAM family member. *Biochim Biophys Acta - Proteins Proteomics* 1844(7):1238–1247.
6. Hofbauer S, Mlynek G, Milazzo L, Pühringer D, Maresch D, Schaffner I, Furtmüller PG, Smulevich G, Djinović-Carugo K, Obinger C (2016) Hydrogen peroxide-mediated conversion of coproheme to heme b by HemQ-lessons from the first crystal structure and kinetic studies. *FEBS J* 283(23):4386–4401.
7. Dailey HA, Gerdes S (2015) HemQ: An iron-coproporphyrin oxidative decarboxylase for protoheme synthesis in Firmicutes and Actinobacteria. *Arch Biochem Biophys* 574:27–35.

8. Dailey HA, Dailey TA, Gerdes S, Jahn D, Jahn M, O'Brian MR, Warren MJ (2017) Prokaryotic heme biosynthesis: multiple pathways to a common essential product. *Microbiol Mol Biol Rev* 81(1):e00048-16.
9. Bab-Dinitz E, Shmuely H, Maupin-Furlow J, Eichler J, Shaanan B (2006) *Haloferax volcanii* PitA: an example of functional interaction between the Pfam chlorite dismutase and antibiotic biosynthesis monooxygenase families? *Bioinformatics* 22(6):671–675.
10. Dailey T, Boynton T, Albetel A, Gerdes S, Johnson M, Dailey H (2010) Discovery and Characterization of HemQ: An essential heme biosynthetic pathway component. *J Biol Chem* 285(34):25978–25986.
11. Mayfield J a., Hammer ND, Kurker RC, Chen TK, Ojha S, Skaar EP, DuBois JL (2013) The chlorite dismutase (HemQ) from *Staphylococcus aureus* has a redox-sensitive heme and is associated with the small colony variant phenotype. *J Biol Chem* 288(32):23488–23504.
12. O'Brian MR (2015) Perception and homeostatic control of iron in the rhizobia and related bacteria. *Annu Rev Microbiol* 69(1):229–245.
13. Qi Z, O'Brian MR (2002) Interaction between the bacterial iron response regulator and ferrochelatase mediates genetic control of heme biosynthesis. *Mol Cell* 9(1):155–162.
14. Hamza I, Chauhan S, Hassett R, O'Brian MR (1998) The bacterial Irr protein is required for coordination of heme biosynthesis with iron availability. *J Biol Chem* 273(34):21669–21674.
15. Yoon T, Cowan JA (2004) Frataxin-mediated iron delivery to ferrochelatase in the final step of heme biosynthesis. *J Biol Chem* 279(25):25943–25946.
16. Chidgey JW, Jackson PJ, Dickman MJ, Hunter CN (2017) PufQ regulates porphyrin flux at the haem/bacteriochlorophyll branchpoint of tetrapyrrole biosynthesis via interactions with ferrochelatase. *Mol Microbiol* 106(6):961–975.

17. Götz F, Bannerman T, Schleifer K (2006) The Genera *Staphylococcus* and *Macrococcus*. *The Prokayotes*, pp 5–75.
18. Schlag S, Fuchs S, Nerz C, Gaupp R, Engelmann S, Liebeke M, Lalk M, Hecker M, Götz F (2008) Characterization of the oxygen-responsive NreABC regulon of *Staphylococcus aureus*. *J Bacteriol* 190(23):7847–7858.
19. Warren MJ, Bolt EL, Roessner CA, Scott AI, Spencert JB, Woodcock SC (1994) Gene dissection demonstrates that the *Escherichia coli cysG* gene encodes a multifunctional protein. *Biochem J* 302:837–844.
20. Hansen J, Muldbjerg M, Chérest H, Surdin-Kerjan Y (1997) Siroheme biosynthesis in *Saccharomyces cerevisiae* requires the products of both the *MET1* and *MET8* genes. *FEBS Lett* 401(1):20–24.
21. Stroupe ME, Leech HK, Daniels DS, Warren MJ, Getzoff ED (2003) CysG structure reveals tetrapyrrole-binding features and novel regulation of siroheme biosynthesis. *Nat Struct Biol* 10(12):1064–73.
22. Vévodová J, Graham RM, Raux E, Schubert HL, Roper DI, Brindley AA, Ian Scott A, Roessner CA, Stamford NPJ, Elizabeth Stroupe M, Getzoff ED, Warren MJ, Wilson KS (2004) Structure/function studies on a S-adenosyl-L-methionine-dependent uroporphyrinogen III C methyltransferase (SUMT), a key regulatory enzyme of tetrapyrrole biosynthesis. *J Mol Biol* 344(2):419–433.
23. Schubert HL, Raux E, Brindley AA, Leech HK, Wilson KS, Hill CP, Warren MJ (2002) The structure of *Saccharomyces cerevisiae* Met8p, a bifunctional dehydrogenase and ferrochelatase. *EMBO J* 21(9):2068–2075.
24. Schubert HL, Rose RS, Leech HK, Brindley AA, Hill CP, Rigby SEJ, Warren MJ (2008) Structure and function of SirC from *Bacillus megaterium*: a metal-binding precorrin-2 dehydrogenase. *Biochem J* 415(2):257–63.

25. Brindley AA, Raux E, Leech HK, Schubert HL, Warren MJ (2003) A story of chelatase evolution: Identification and characterization of a small 13-15-kDa “ancestral” cobaltochelatase (CbiXs) in the archaea. *J Biol Chem* 278(25):22388–22395.
26. Raux E, Leech HK, Beck R, Schubert HL, Santander PJ, Roessner CA, Scott AI, Martens JH, Jahn D, Thermesr C, Rambach A, Warren MJ (2003) Identification and functional analysis of enzymes required for precorrin-2 dehydrogenation and metal ion insertion in the biosynthesis of sirohaem and cobalamin in *Bacillus megaterium*. *Biochem J* 370:505–516.
27. Romão C V, Ladakis D, Lobo SAL, Carrondo MA, Brindley AA, Deery E, Matias PM, Pickersgill RW, Saraiva LM, Warren MJ (2011) Evolution in a family of chelatases facilitated by the introduction of active site asymmetry and protein oligomerization. *Proc Natl Acad Sci* 108(1):97–102.
28. Lobo SAL, Brindley AA, Romão C V., Leech HK, Warren MJ, Saraiva LM (2008) Two distinct roles for two functional cobaltochelatases (CbiK) in *Desulfovibrio vulgaris* Hildenborough. *Biochemistry* 47(21):5851–5857.
29. Lobo SAL, Videira MAM, Pacheco I, Wass MN, Warren MJ, Teixeira M, Matias PM, Romão C V., Saraiva LM (2017) *Desulfovibrio vulgaris* CbiK P cobaltochelatase: evolution of a haem binding protein orchestrated by the incorporation of two histidine residues. *Environ Microbiol* 19(1):106–118.
30. Bali S, Rollauer S, Roversi P, Raux-Deery E, Lea SM, Warren MJ, Ferguson SJ (2014) Identification and characterization of the “missing” terminal enzyme for siroheme biosynthesis in α-proteobacteria. *Mol Microbiol* 92(1):153–163.
31. Mazmanian SK, Skaar EP, Gaspar AH, Humayun M, Gornicki P, Jelenska J, Joachmiak A, Missiakas DM, Schneewind O (2003)

Passage of heme-iron across the envelope of *Staphylococcus aureus*. *Science* 299(5608):906–9.

32. Skaar EP, Humayun M, Bae T, DeBord KL SO (2004) Iron-source preference of *Staphylococcus aureus* infections. *Science* 305(5690):1626–8.
33. Haley KP, Skaar EP (2012) A battle for iron: host sequestration and *Staphylococcus aureus* acquisition. *Microbes Infect* 14(3):217–227.
34. Park MK, Myers RA, Marzella L (1992) Oxygen tensions and infections: modulation of microbial growth, activity of antimicrobial agents, and immunologic responses. *Clin Infect Dis* 14(3):720–40.
35. Balasubramanian D, Harper L, Shopsin B, Torres VJ (2017) *Staphylococcus aureus* pathogenesis in diverse host environments. *Pathog Dis* 75(1):1–13.
36. Somerville GA, Proctor RA (2009) At the crossroads of bacterial metabolism and virulence factor synthesis in staphylococci. *Microbiol Mol Biol Rev* 73(2):233–248.
37. Chaffin DO, Taylor D, Skerrett SJ, Rubens CE (2012) Changes in the *Staphylococcus aureus* transcriptome during early adaptation to the lung. *PLoS One* 7(8):e41329.
38. Ignarro LJ, Fukuto JM, Griscavage JM, Rogers NE, Byrns RE (1993) Oxidation of nitric oxide in aqueous solution to nitrite but not nitrate: comparison with enzymatically formed nitric oxide from L-arginine. *Proc Natl Acad Sci U S A* 90(17):8103–8107.
39. Proctor RA, von Eiff C, Kahl BC, Becker K, McNamara P, Herrmann M, Peters G (2006) Small colony variants: a pathogenic form of bacteria that facilitates persistent and recurrent infections. *Nat Rev Microbiol* 4(4):295–305.
40. von Eiff C, Heilmann C, Proctor RA, Woltz C, Peters G, Götz F (1997) A site-directed *Staphylococcus aureus hemB* mutant is a small-colony variant which persists intracellularly. *J Bacteriol* 179(15):4706–12.

41. Hammer ND, Reniere ML, Cassat JE, Zhang Y, Hirsch AO, Hood MI, Skaar EP (2013) Two heme-dependent terminal oxidases power *Staphylococcus aureus* organ-specific colonization of the vertebrate host. *MBio* 4(4):1–9.
42. Hammer ND, Cassat JE, Noto MJ, Lojek LJ, Chadha AD, Schmitz JE, Creech CB, Skaar EP (2014) Inter- and intraspecies metabolite exchange promotes virulence of antibiotic-resistant *Staphylococcus aureus*. *Cell Host Microbe* 16(4):531–537.
43. Lewis K (2007) Persister cells, dormancy and infectious disease. *Nat Rev Microbiol* 5(1):48–56.
44. Beenken KE, Dunman PM, McAleese F, Macapagal D, Murphy E, Projan SJ, Blevins JS, Smeltzer MS, Jon S, Smeltzer MS, Blevins JS (2004) Global gene expression in *Staphylococcus aureus* biofilms. *J Bacteriol* 186(14):4665–4684.
45. Schnell R, Sandalova T, Hellman U, Lindqvist Y, Schneider G (2005) Siroheme- and [Fe4-S4]-dependent NirA from *Mycobacterium tuberculosis* is a sulfite reductase with a covalent Cys-Tyr bond in the active site. *J Biol Chem* 280(29):27319–27328.
46. Layer G, Jahn D, Deery E, Lawrence AD, Warren MJ (2010) Biosynthesis of Heme and Vitamin B12. *Comprehensive Natural Products II* (Elsevier), pp 445–499.